

DAVIDE TRAPANI

**A MONITORING METHOD
FOR AFTER – EARTHQUAKE
DAMAGE EVALUATION OF BUILDINGS**

TUTOR: PROF. DANIELE ZONTA

2015

UNIVERSITA' DEGLI STUDI DI TRENTO

Scuola di Dottorato in Ingegneria dei Sistemi Strutturali Civili e Meccanici

XXVII Ciclo

Esame finale: 22 04 2015

Commissione esaminatrice:

Prof. Jiri Maca, Czech Technical University in Prague

Prof. Maria Rosaria Pecce, Università del Sannio

Prof. Daniele Zonta, Università degli Studi di Trento

Dott. Paolo Clemente, UTPRA – ENEA CRE Casaccia

Dott. Loris Vincenzi, Università di Modena e Reggio Emilia

Abstract

After-earthquake assessment of buildings in terms of usability and safety is nowadays performed by in-charge technicians which are called to give their judgment basing mainly on in-field surveys and visual inspections. This necessarily implies additional inconvenience for residents and economic losses in the affected area, being often large the time required for conducting the surveys and being the judgment on the safe side in absence of objective data. A near real-time assessment based on objective data related to the seismic response of the structures is possible though the use of a monitoring systems capable of providing information on the state of the monitored structure inferring observations of its dynamic response. One of the most reliable parameter which can be correlated to the state of condition of a structure after an earthquake is the ductility demand expressed in terms of interstory drift. The use in monitoring systems of this indicator is examined in this thesis through case studies on reinforced concrete framed buildings and precast industrial buildings. In the design process of the systems I proposed a capacity-demand approach, through the prior formal definition of the requirements of accuracy and the calculation of the actual accuracy of the designed monitoring system. In particular I investigated in detail the uncertainties, both instrumental and related to model, to be combined in order to obtain the overall uncertainty of the information provided by the monitoring system, when using the method of double integration of the acceleration measurements. I have found that in general the instrumental uncertainties have less importance to the uncertainties of the model, in particular in presence of residual displacements at the end of the seismic motion. Aiming to reduce uncertainties in the presence of residual displacements and to cancel the need of high-pass filtering acceleration signals, I proposed a sensing bar prototype instrumented with accelerometers and inclinometers.

Sommario

La verifica post-sismica degli edifici in termini di agibilità e sicurezza avviene attualmente per mezzo del giudizio, basato su indagini prevalentemente visive o su analisi approfondite ma a posteriori, di tecnici incaricati dalle Amministrazioni competenti. Ciò implica necessariamente ulteriori disagi e perdite economiche nell'area colpita dal sisma, essendo spesso notevole il tempo richiesto per l'esecuzione delle verifiche e a favore di sicurezza gli esiti delle indagini stesse in mancanza di dati oggettivi. Una verifica in tempo quasi reale basata su dati oggettivi relativi risposta sismica delle strutture è possibile attraverso l'utilizzo di un sistema di monitoraggio in grado di fornire un'informazione relativa allo stato della struttura monitorata dedotta dall'osservazione della sua risposta dinamica. Uno degli indicatori più affidabili per la deduzione dello stato di condizione di una struttura colpita dal sisma è la domanda di duttilità espressa in termini di spostamento massimo di

interpiano. L'utilizzo di questo indicatore viene studiato in questa tesi attraverso casi studio relativi a edifici intelaiati in cemento armato ed edifici industriali prefabbricati. Viene adottato un approccio domanda-capacità, attraverso una definizione formale a priori dei requisiti di accuratezza e il calcolo dell'accuratezza effettiva del sistema di monitoraggio progettato. In particolare vengono studiate in dettaglio le incertezze, sia strumentali che di modello, che influiscono sull'incertezza complessiva dell'informazione fornita dal sistema di monitoraggio quando si utilizza il metodo della doppia integrazione delle misure di accelerazione. Si evidenzia in particolare come le incertezze strumentali abbiano un'importanza minore delle incertezze di modello, in particolare in presenza di spostamenti residui al termine del moto sismico. Viene quindi proposto un prototipo di asta strumentata in grado di misurare accelerazioni e inclinazioni dalle quali è possibile calcolare lo spostamento relativo tra due piani secondo tre diversi approcci.

Acknowledgments

This research was partially funded in the context of MEMSCON project (EC Seventh Framework Programme Grant Agreement n. CP-TP 212004-2) and by Area Prefabbricati S.p.A. I wish to thank in particular: Manthos Bimpas, Angelos Amditis, Nicolas Saillen, Matteo Pozzi, Manos & Dimitris Bairaktaris, Tom Torfs and Juan Santana for their precious contribution to the activities related to MEMSCON Project, and Emanuel Mandredini, Moreno Manfredini, and Antonello Gasperi for their support in the development of the monitoring system prototype for precast buildings. I wish to thank also Dott.sa Monica Mattevi, Mayor of Stenico, for allowing our start-up company to install in the Elementary School the prototype of the seismic monitoring system I developed in the last period of my research.

I wish mention also Daniele Zonta, Emiliano Debiasi, Giacomo Cigognetti, Daniele Coato, Luca Perolo, Mattia Montanari, Cristiano Bazzoli, Andrea Anselmo and Andrea Maroni, all people collaborating in the research group at the University of Trento for their important contribution to the development of this research.

1	INTRODUCTION	1
1.1	PROBLEM STATEMENT	1
1.2	OBJECTIVES	3
1.3	OVERVIEW OF THE THESIS	4
1.4	LIMITATIONS	5
2	STATE OF THE ART OF SEISMIC STRUCTURAL HEALTH MONITORING OF BUILDINGS.....	7
2.1	INTRODUCTION	7
2.2	MOTIVATION FOR SEISMIC STRUCTURAL HEALTH MONITORING.....	7
2.3	THE EXPERIENCE OF THE STRONG MOTION INSTRUMENTATION PROGRAMS	12
2.4	MONITORING SYSTEMS BASED ON CHANGES OF STRUCTURAL PARAMETERS	15
2.5	MONITORING SYSTEMS BASED ON RESPONSE MONITORING DURING THE EARTHQUAKE.....	17
2.6	TECHNOLOGY FOR SEISMIC STRUCTURAL HEALTH MONITORING	20
2.7	INDUSTRIAL DEPLOYMENTS	21
2.8	DEFINITION AND PURPOSES OF A SEISMIC STRUCTURAL HEALTH MONITORING SYSTEM.....	22
2.9	CONCLUSIONS	24
3	A LOGICAL FRAMEWORK FOR SEISMIC STRUCTURAL HEALTH MONITORING DESIGN	25
3.1	INTRODUCTION	25
3.2	ACTIVITIES RELATED TO STRUCTURAL HEALTH MONITORING OF STRUCTURES.....	25
3.2.1	Design of the monitoring system	26
3.2.2	Installation of the monitoring system.....	26
3.2.3	System management	27
3.2.4	Data management	27
3.2.5	Shutting down of the monitoring system	27
3.3	STRUCTURAL MONITORING DESIGN	28
3.3.1	Principles	28
3.3.2	Analogy between monitoring system design and structural design	30
3.3.3	Information as a state variable	31
3.3.4	Accuracy of the information	32
3.3.5	Choice of the monitoring strategy.....	33
3.3.6	Comparison between capacity and demand	33
3.4	CHOICE OF THE STATE VARIABLE.....	34
3.4.1	Reliability of the state variable to be provided	34

3.4.2	Seismic damage in RC buildings	36
3.4.3	Damage indices for RC structures	37
3.4.4	Displacement-based damage assessment	40
3.5	AN EXAMPLE: DESIGN OF SEISMIC STRUCTURAL HEALTH MONITORING SYSTEMS	42
3.5.1	Objective	43
3.5.2	Choice of the information or state variable	43
3.5.3	Definition of the accuracy demand	43
3.5.4	Choice of the monitoring strategy	43
3.5.5	Computation of the uncertainties related to instrumental errors	43
3.5.6	Computation of the uncertainties related to the model	44
3.5.7	Computation of the accuracy capacity	44
3.5.8	Capacity < Demand: how to modify the monitoring strategy	44
3.6	CONCLUSIONS	44
4	UNCERTAINTY ANALYSIS OF DRIFT ESTIMATION USING ACCELERATION MEASUREMENTS	47
4.1	INTRODUCTION	47
4.2	THE CONCEPT OF UNCERTAINTY IN MEASUREMENTS	47
4.3	DISPLACEMENTS COMPUTATION FROM ACCELERATION MEASUREMENTS	50
4.3.1	Displacement estimations at instrumented locations	51
4.3.2	Story displacement calculation	53
4.4	INSTRUMENTAL UNCERTAINTIES IN DISPLACEMENT ESTIMATION FROM ACCELERATION MEASUREMENTS	54
4.4.1	Bias error	54
4.4.2	Calibration error	55
4.4.3	Temperature dependent errors	56
4.4.4	Ratiometricity	56
4.4.5	Misalignment error	56
4.4.6	Mounting error	57
4.4.7	Cross-axis sensitivity	57
4.4.8	Noise	58
4.4.9	Summary of instrumental uncertainties and their combination	62
4.5	NUMERICAL ANALYSIS OF THE MODEL UNCERTAINTIES	63
4.5.1	Methodology	63
4.5.2	Newmark's method	64
4.5.3	Double integration	64
4.5.4	Results on linear system	65
4.5.5	Effect of residual displacements	68
4.6	CONCLUSIONS	70

5	MEMSCON EU PROJECT	73
5.1	INTRODUCTION	73
5.2	DESCRIPTION OF MEMSCON EU PROJECT.....	73
5.3	TECHNOLOGY	77
5.3.1	Phase I accelerometer	77
5.3.2	Phase II.1 accelerometer	80
5.3.3	Phase II.2 accelerometer	83
5.3.4	Phase II.2 strain gauges.....	83
5.4	LABORATORY EVALUATION OF MEMSCON TECHNOLOGY	84
5.4.1	Phase I accelerometer evaluation & calibration tests	84
5.4.2	Phase II.1 accelerometer evaluation & calibration tests.....	94
5.4.3	Earthquake simulation on small-scale metal frame.....	101
5.4.4	Test on full-scale 3D frame.....	104
5.5	DISCUSSION ON LABORATORY EVALUATION.....	124
5.5.1	Phase I accelerometers	124
5.5.2	Phase II accelerometers.....	124
5.5.3	System evaluation on full-scale 3D frame	125
5.6	CONCLUSIONS	126
6	CASE STUDY: SEISMIC MONITORING OF PRECAST BUILDINGS	127
6.1	INTRODUCTION	127
6.2	SCOPE OF APPLICATION	127
6.3	OBJECTIVES	130
6.4	MONITORED LIMIT STATE	131
6.5	CHOICE OF THE INFORMATION PROVIDED BY THE SYSTEM AND TARGET ACCURACY	132
6.6	CHOICE OF THE PHYSICAL QUANTITY TO BE OBSERVED	133
6.7	THE INFERRING MODEL.....	133
6.7.1	Displacement time histories estimation	133
6.7.2	Numerical example	135
6.8	ANALYSIS OF UNCERTAINTIES	137
6.8.1	Instrumental uncertainties	137
6.8.2	Model uncertainties.....	137
6.9	DESCRIPTION OF THE HARDWARE	141
6.9.1	Accelerometers and cables.....	141
6.9.2	Controller and Data acquisition modules.....	143
6.9.3	Host Pc.....	144
6.9.4	Communication devices.....	144
6.9.5	Power supply device	144
6.10	DESCRIPTION OF THE SOFTWARE.....	145

6.10.1	Software modules	145
6.10.2	RT Application	147
6.10.3	Client Application.....	149
6.10.4	Pre-processor	150
6.11	EVALUATION OF THE SYSTEM IN LABORATORY CONDITIONS	153
6.11.1	List of experimental tests	153
6.11.2	Test equipment.....	153
6.11.3	Calibration tests	156
6.11.4	Noise evaluation	157
6.11.5	Accuracy evaluation in terms of acceleration measurements	160
6.11.6	Accuracy evaluation in terms of displacement	163
6.12	CONCLUSIONS	169
7	A MONITORING METHOD BASED ON ACCELERATION AND TILT MEASUREMENTS	173
7.1	INTRODUCTION	173
7.2	MOTIVATION	173
7.3	THE SENSING BAR	175
7.4	REAL-TIME MONITORING OF TILT.....	177
7.4.1	Arrangement with two accelerometers and one inclinometer	177
7.4.2	Arrangement with three inclinometers.....	179
7.4.3	Preliminary tests	179
7.5	ITERATIVE BASELINE CORRECTION METHOD.....	182
7.5.1	Theoretical background	183
7.5.2	Algorithm of the method.....	186
7.5.3	Simplified approach	187
7.6	PROTOTYPE OF THE SYSTEM	188
7.7	CONCLUSIONS	192
8	CONCLUSIONS AND FUTURE WORK	195
8.1	CONCLUSIONS	195
8.2	FUTURE WORK.....	200
	REFERENCES	202

List of figures

FIGURE 1-1 – LOGICAL FRAMEWORK OF SEISMIC STRUCTURAL HEALTH MONITORING	2
FIGURE 1-2 – TECHNOLOGICAL FRAMEWORK FOR SEISMIC STRUCTURAL HEALTH MONITORING	3
FIGURE 2-1 – USABILITY INSPECTIONS FOLLOWING THE EARTHQUAKE IN EMILIA (ITALY) REGION IN 2012 (DOLCE 2013)	8
FIGURE 2-2 – GREEN, YELLOW AND RED PLACARDS AS FOR ATC-20 (ATC 20-1 2005).....	9
FIGURE 2-3 - TYPICAL LAYOUT OF STRONG MOTION INSTRUMENTATION PROGRAM MONITORING SYSTEMS (BUILDING RESEARCH INSTITUTE 2009).....	13
FIGURE 2-4 - NSMP STATIONS MAP (USGS 2014)	14
FIGURE 3-1 – FLOWCHART OF THE DESIGN OF A MONITORING SYSTEM.....	30
FIGURE 3-2 – ENERGY-DISSIPATING MECHANISM. FROM (PAULEY AND PRIESTLEY 1992).....	35
FIGURE 3-3 – PERFORMANCE LEVELS AND LIMIT STATES, FROM (MPAMPATSIKOS 2008)	35
FIGURE 4-1 – STEPS OF THE ALGORITHM FOR INTERSTORY DRIFT CALCULATION	51
FIGURE 4-2 . STORY DISPLACEMENT CALCULATION	53
FIGURE 4-3 - MODELED NOISE IN ACCELERATION MEASUREMENTS.....	60
FIGURE 4-4 - DISPLACEMENT TIME HISTORIES DUE TO NOISE	61
FIGURE 4-5 – UNCERTAINTY DUE TO NOISE IN FUNCTION OF NOISE AMPLITUDE AND HIGH-PASS FREQUENCY CUT	62
FIGURE 4-6 - ERROR BETWEEN MAX NEWMARK DISPLACEMENT AND DOUBLE INTEGRATION DISPLACEMENT ($F_{\text{CUT}} = 0.6 \text{ Hz}$).....	67
FIGURE 4-7 - ERROR BETWEEN MAX NEWMARK DISPLACEMENT AND DOUBLE INTEGRATION DISPLACEMENT ($F_{\text{CUT}} = 1.2 \text{ Hz}$).....	67
FIGURE 4-8 - ERROR BETWEEN MAX NEWMARK DISPLACEMENT AND DOUBLE INTEGRATION DISPLACEMENT ($F_{\text{CUT}} = 2.0 \text{ Hz}$).....	68
FIGURE 4-9 – EXAMPLE OF FORCE-DISPLACEMENT TIME HISTORY.....	69
FIGURE 4-10 - ERROR BETWEEN MAX NEWMARK DISPLACEMENT AND DOUBLE INTEGRATION DISPLACEMENT VARYING AT VARYING RESIDUAL DISPLACEMENT	70
FIGURE 5-1 – PARTNERS OF MEMSCON EU PROJECT.....	75
FIGURE 5-2 – LAYOUT OF THE MEMSCON MONITORING SYSTEM: STRAIN SENSORS ARE PLACED AT THE LOWEST LEVEL OF THE BUILDING WHILE ACCELEROMETERS ARE PLACED IN PAIRS AT EACH FLOOR (FROM WWW.MEMSCON.COM).....	75
FIGURE 5-3 - OVERVIEW OF THE MEMSCON METHODOLOGY, FROM (RISA AND TECNIC 2011)	76
FIGURE 5-4 – PROPOSED SECTIONAL STIFFNESS, FROM (DBA AND TECNIC 2009)	76
FIGURE 5-5 – STRUCTURAL ASSESSMENT RESULT	77
FIGURE 5-6 - PHASE I BASE STATION AND ACCELEROMETER	79
FIGURE 5-7 - SCHEME OF THE SOFTWARE WAKE-UP PROCEDURE.....	79
FIGURE 5-8 – FORMAT OF THE TRANSMITTED DATA	80

FIGURE 5-9 – THE PHASE II.1 ACCELEROMETER: OUTSIDE (A) AND INSIDE (B)	81
FIGURE 5-10 – SCREENSHOT OF VIEWER SOFTWARE AND DATA ACQUISITION PROCESS.....	82
FIGURE 5-11 – PHASE II.2 MEMSCON ACCELEROMETER	83
FIGURE 5-12 – PHASE II.2 MEMSCON FRONT-END STRAIN SENSOR	84
FIGURE 5-13 – PHASE II.2 MEMSCON WIRELESS UNITS FOR STRAIN SENSOR	84
FIGURE 5-14 - TESTING SCHEME.....	85
FIGURE 5-15 - SENSOR ARRANGEMENT: (LEFT) TESTS ON X AXIS; (CENTER) TESTS ON Y AXIS; (RIGHT) TESTS ON Z AXIS	85
FIGURE 5-16 – ORIGINAL TIME HISTORIES OF THE SAMPLE TEST	86
FIGURE 5-17 – REFERENCE AND WIRELESS SIGNALS NOT IN SYNC AT T = 25 SEC	87
FIGURE 5-18 - SPECTRA OF REFERENCE SIGNALS	88
FIGURE 5-19 – SPECTRA OF WIRELESS SIGNALS	89
FIGURE 5-20 – PHASE I CALIBRATION CURVES (X AXIS)	90
FIGURE 5-21 - PHASE II CALIBRATION CURVES (Y AXIS).....	90
FIGURE 5-22 – PHASE I CALIBRATION CURVES (Z AXIS).....	91
FIGURE 5-23 - SENSORS ARRANGEMENT (TESTS ON X AXIS).....	95
FIGURE 5-24 – ORIGINAL OUTPUT (Z DIRECTION, 3 HZ, HIGH AMPLITUDE TEST).....	96
FIGURE 5-25 - SPECTRA OF REFERENCE SIGNALS	97
FIGURE 5-26 - SPECTRA OF WIRELESS SIGNALS	97
FIGURE 5-27 - HIGH AMPLITUDE SWEEP TEST ALONG X AXIS TIME HISTORIES	101
FIGURE 5-28 – STEEL/ALUMINUM FRAME	102
FIGURE 5-29 – SWEEP TEST ON FRAME TIME HISTORIES	103
FIGURE 5-30 - EARTHQUAKE SIMULATION TEST TIME HISTORIES	104
FIGURE 5-31 – SCHEME OF THE CONSTRUCTION	105
FIGURE 5-32 - PLANE VIEW OF THE CONSTRUCTION	106
FIGURE 5-33 – MODEL FOR SEISMIC ANALYSIS	106
FIGURE 5-34 - 3D FRAME - PLANE VIEW	107
FIGURE 5-35 - 3D FRAME - LATERAL VIEW	107
FIGURE 5-36 - 3D FRAME - FRONT VIEW	108
FIGURE 5-37 – COLUMN CROSS SECTION	108
FIGURE 5-38 – LONGITUDINAL FOUNDATION BEAMS CROSS SECTION.....	109
FIGURE 5-39 - TRANSVERSE FOUNDATION BEAMS CROSS SECTION	109
FIGURE 5-40 – BEAM AT THE TOP CROSS SECTION	110
FIGURE 5-41 - TRANSVERS BEAM AT THE TOP CROSS SECTION	110
FIGURE 5-42 – CONCRETE SLAB CROSS SECTION	110
FIGURE 5-43 – ANCHORAGE OF THE FRAME TO THE STRONG FLOOR.....	111
FIGURE 5-44 – LOAD DISTRIBUTION SYSTEM.....	112
FIGURE 5-45 – TEST SETUP	112
FIGURE 5-46 –ARRANGEMENT OF THE ACCELEROMETERS ABOVE THE SLAB	113

FIGURE 5-47 – LVDTs TRANSDUCERS COORDINATES	114
FIGURE 5-48 – ACCELEROGRAM OF CHENOVA EARTHQUAKE	114
FIGURE 5-49 – RESPONSE IN TERMS OF DISPLACEMENT RESPECT TO THE GROUND	115
FIGURE 5-50 – DISPLACEMENTS PROFILE - COLUMN C1	119
FIGURE 5-51 – DISPLACEMENT PROFILE – COLUMN C2	120
FIGURE 5-52 – FORCE – DISPLACEMENT BACKBONE CURVE.....	120
FIGURE 5-53 – LONGITUDINAL ACCELERATION AT THE TOP OF COLUMN C3	121
FIGURE 5-54 – TRANSVERSE ACCELERATION AT THE TOP OF COLUMN C3	122
FIGURE 5-55 - ESTIMATION OF DISPLACEMENT TIME HISTORIES: TRANSVERSE DIRECTION (TOP) AND LONGITUDINAL DIRECTION (BOTTOM).....	123
FIGURE 5-56 – COMPARISON BETWEEN ESTIMATED DISPLACEMENTS AND DISPLACEMENTS INDUCED BY THE HORIZONTAL ACTUATOR.....	123
FIGURE 6-1 – LOSS OF SEATING OF THE BEAM AND SHEAR FAILURE DUE TO RESULTANT REDUCED SEATING DIMENSION (SAVOIA, BACCI, AND VINCENZI 2012).....	129
FIGURE 6-2 – CLADDINGS COLLAPSE DUE TO INSUFFICIENT DISPLACEMENT CAPACITY AND STRENGTH OF THE CONNECTIONS BETWEEN CLADDINGS AND STRUCTURAL ELEMENTS (SAVOIA, BACCI, AND VINCENZI 2012)	129
FIGURE 6-3 – EXAMPLE OF THRESHOLD VALUES DEFINITION	131
FIGURE 6-4 – EXAMPLE STRUCTURE (IN RED, MEASURED NODE DISPLACEMENTS; LABELS 0-8 DISPLACEMENTS IN THE X DIRECTION, LABELS 9-15 DISPLACEMENTS ALONG Y DIRECTION; EVEN LABELS DISPLACEMENTS AT THE GROUND LEVEL, ODD LABELS DISPLACEMENTS AT THE ROOF LEVEL).....	136
FIGURE 6-5 – STRUCTURAL MODELS USED FOR THE NUMERICAL ANALYSIS	139
FIGURE 6-6 – MEAN ERROR AGAINST NUMBER OF MODES AND SENSORS	140
FIGURE 6-7 – MEAN ERROR AGAINST NUMBER OF MODES AND SENSORS	140
FIGURE 6-8 – ACCELEROMETER MODEL PCB 3711 (LABEL S1).....	142
FIGURE 6-9 – ACCELEROMETER MODEL CXL04GP1 (LABEL S2).....	142
FIGURE 6-10 – POWER UNIT FOR SENSORS	143
FIGURE 6-11 - MASTER UNIT (A) AND SLAVE UNIT (B)	144
FIGURE 6-12 – NI 9205 MODULE.....	144
FIGURE 6-13 – FRONT PANEL (LEFT) AND BLOCK DIAGRAM OF A SIMPLE APPLICATION PRODUCING THE SUM OF TWO NUMBERS.....	145
FIGURE 6-14 - COMPACTRIO ARCHITECTURE (FROM WWW.NI.COM).....	146
FIGURE 6-15 – PRODUCER-CONSUMER ARCHITECTURE.....	147
FIGURE 6-16 - RT APP BLOCK DIAGRAM	148
FIGURE 6-17 – MINIMUM NUMBER OF “NEGATIVE” PACKETS TO BE CONSIDERED AS RELATIVE TO THE SAME EVENT.....	149
FIGURE 6-18 - CLIENT APPLICATION.....	150
FIGURE 6-19 – MAIN WINDOW OF THE PRE-PROCESSOR.....	151

FIGURE 6-20 - $[\Phi]$ MATRIX AND LED INDICATORS OF THE MONITORED NODES	151
FIGURE 6-21 - $[\Phi]$ MATRIX, LED INDICATORS OF THE MONITORED NODES AND $[M]$ MATRIX	152
FIGURE 6-22 – DEFINITION OF THE NUMBER OF CONDITIONS TO BE MONITORED AND OF THRESHOLDS	152
FIGURE 6-23 – GENERATION OF $[D]$ (CYAN) AND $[T]$ MATRICES.....	153
FIGURE 6-24 – APS 400 ELECTRO SEIS	154
FIGURE 6-25 – SETUP OF THE SHAKING TABLE	154
FIGURE 6-26 - BRYSTON 7B-SST (ADAPTED FROM HTTP://BRYSTON.COM).....	155
FIGURE 6-27 - AGILENT 33220AW (ADAPTED FROM HTTP://WWW.HOME.AGILENT.COM).....	155
FIGURE 6-28 – LASER DISPLACEMENT TRANSDUCER OPTONCDT 1605	156
FIGURE 6-29 – CALIBRATION CURVES OF SENSORS S11, S12, S21, S22.....	157
FIGURE 6-30 - BACKGROUND NOISE: TIME DOMAIN (LEFT) AND FREQUENCY DOMAIN (RIGHT) RELATIVE TO THE UNFILTERED SIGNAL	159
FIGURE 6-31 – BACKGROUND NOISE: TIME DOMAIN (LEFT) AND FREQUENCY DOMAIN (RIGHT) RELATIVE TO THE FILTERED SIGNAL	159
FIGURE 6-32 – SPURIOUS DISPLACEMENTS: TIME DOMAIN (LEFT) AND FREQUENCY DOMAIN (RIGHT)	159
FIGURE 6-33 – RECORD OF FIVIZZANO	162
FIGURE 6-34 – RECORD OF MIRANDOLA IN HORIZONTAL DIRECTION	162
FIGURE 6-35 - RECORD OF COPPARO	162
FIGURE 6-36 - RECORD OF MIRANDOLA IN VERTICAL DIRECTION.....	163
FIGURE 6-37 – RECORDS USING SINUSOIDAL WAVES AS INPUT (ESTIMATED DISPLACEMENTS ARE IN CONTINUOUS LINE; MEASURED DISPLACEMENT ARE IN DOTTED LINE)	164
FIGURE 6-38 – DEPENDENCY OF MEAN VALUE AND STANDARD DEVIATION ON DISPLACEMENT AMPLITUDE	165
FIGURE 6-39 – WAVES COMBINATION TESTS: 1, 1.1, AND 1.5 HZ	165
FIGURE 6-40: WAVES COMBINATION TESTS: 2, 2.1, 2.3 HZ.....	166
FIGURE 6-41 - WAVES COMBINATION TESTS: 2, 2.1, 2.3 HZ.....	166
FIGURE 6-42 – SEISMIC WAVE TESTS: L’AQUILA 1 RECORD	167
FIGURE 6-43 – SEISMIC WAVES TESTS: L’AQUILA 2 RECORD.....	167
FIGURE 6-44 - SEISMIC WAVES TESTS: FIVIZZANO RECORD	168
FIGURE 6-45 - SEISMIC WAVES TESTS: MIRANDOLA RECORD	168
FIGURE 6-46 - EXAMPLE OF TRESHOLDS.....	170
FIGURE 7-1 – EFFECT OF RESIDUAL INTERSTORY DRIFT (RID) ON PEAK INTERSTORY DRIFT (PID) ESTIMATION FROM ACCELERATION DATA ONLY	174
FIGURE 7-2 - SCHEMA OF THE SENSING BEAM (UN-DEFORMED CONFIGURATION).....	175
FIGURE 7-3 - SCHEMA OF THE SENSING BEAM (RESIDUAL DEFORMED CONFIGURATION)	176
FIGURE 7-4 - SENSING BEAM (MECHANICAL PART)	176
FIGURE 7-5 - UPPER CONNECTION TO THE FLOOR	176

FIGURE 7-6 - LOWER CONNECTION TO THE FLOOR.....	176
FIGURE 7-7 - FORCES APPLIED TO THE INCLINOMETER	177
FIGURE 7-8 – MEASURED ANGLES (TEST 0.5 HZ).....	181
FIGURE 7-9 – DISPLACEMENTS (TEST 0.5 HZ).....	181
FIGURE 7-10 - MEASURED ANGLES (TEST 1.0 HZ)	182
FIGURE 7-11 – DISPLACEMENTS (TEST 1.0 HZ).....	182
FIGURE 7-12 – ACCELERATION, VELOCITY AND DISPLACEMENT TIME HISTORIES RECORDED BY TCU068 STATION IN THE NS DIRECTION DURING THE 1999, CHI-CHI EARTHQUAKE, ADAPTED FROM (AKKAR AND BOORE 2009).....	184
FIGURE 7-13 – PARAMETERS OF THE MODEL FOR BASELINE CORRECTION, ADAPTED FROM (AKKAR AND BOORE 2009).....	185
FIGURE 7-14 - . DISPLACEMENT TIME HISTORIES OBTAINED BY DOUBLE INTEGRATION OF THE CORRECTED ACCELERATION TIME HISTORIES. DIFFERENT CURVES CORRESPOND TO DIFFERENT T2 VALUES (ASSUMING T1 = 20 SEC JUST BEFORE STRONG SHAKING). FROM (DAVID M. BOORE 2001)	186
FIGURE 7-15 – MODEL ERROR ON PDI ESTIMATION ADDING RID VALUE.....	188
FIGURE 7-16 – STENICO ELEMENTARY SCHOOL.....	188
FIGURE 7-17 – COMPONENTS OF SAFEQUAKE SYSTEM.....	189
FIGURE 7-18 – GEMAC IS2D90P24 INCLINOMETER	190
FIGURE 7-19 – RION AKE19T ACCELEROMETER	190
FIGURE 7-20 – MAIN SCREEN OF THE APPLICATION	191
FIGURE 7-21 – DETAIL OF THE CONNECTION OF THE SENSING BEAM TO THE 1° FLOOR.....	191
FIGURE 7-22 - RACK.....	191
FIGURE 7-23 – LOCATION OF THE BEAM AT THE FIRST FLOOR (BEHIND A FINISHING)	192
FIGURE 7-24 – SENSING BEMA COVERED BY THE PLASTIC PROTECTIVE INVOLUCRE.....	192

List of tables

TABLE 2-1 – AFTER-EARTHQUAKE DAMAGE ASSESSMENT ACTIVITIES9

TABLE 2-2 - DAMAGE CLASSIFICATION FOR COLUMNS AND SHEAR WALLS IN JAPAN, ADAPTED FROM
(KAMINOSONO, KUMAZAWA, AND NAKANO 2002)..... 10

TABLE 2-3 – DAMAGE DESCRIPTION FOR RC COLUMNS AND SHEAR WALLS IN ITALY, ADAPTED FROM
(BAGGIO ET AL. 2009)..... 11

TABLE 2-4 – DAMAGE DESCRIPTION FOR RC BUILDINGS IN GREECE, ADAPTED FROM
(ANAGNOSTOPOULOS AND MORETTI 2008) 11

TABLE 3-1 – ACTIVITIES RELATED TO SEISMIC MONITORING28

TABLE 3-2 – EQUIVALENCE BETWEEN STRUCTURAL DESIGN AND MONITORING SYSTEM DESIGN31

TABLE 3-3 – PARK & ANG DAMAGE INDEX THRESHOLDS39

TABLE 3-4 – PEAK DRIFT RATIOS LIMITATIONS FOR RC STRUCTURES AS REPORTED IN (SULLIVAN,
PRIESTLEY, AND CALVI 2012)..... 41

TABLE 3-5 – RESIDUAL DRIFT RATIOS LIMITATIONS FOR RC STRUCTURES AS REPORTED IN
(SULLIVAN, PRIESTLEY, AND CALVI 2012) 41

TABLE 4-1 – NOISE BANDWIDTH OF BUTTERWORTH FILTER59

TABLE 4-2 – SOURCES OF INSTRUMENTAL UNCERTAINTIES (* WHEN A HIGH-PASS FILTER IS APPLIED)
..... 62

TABLE 4-3 – ERROR BETWEEN MAX NEWMARK DISPLACEMENT AND DOUBLE INTEGRATION
DISPLACEMENT ($F_{CUT} = 0.6$ Hz)..... 65

TABLE 4-4 - ERROR BETWEEN MAX NEWMARK DISPLACEMENT AND DOUBLE INTEGRATION
DISPLACEMENT ($F_{CUT} = 1.2$ Hz)..... 66

TABLE 4-5 - ERROR BETWEEN MAX NEWMARK DISPLACEMENT AND DOUBLE INTEGRATION
DISPLACEMENT ($F_{CUT} = 2.0$ Hz)..... 66

TABLE 5-1 – PROPOSED RELATION BETWEEN DAMAGE RATIO AND DAMAGE STATES, ADAPTED FROM
(RISA AND TECNIC 2011) 77

TABLE 5-2 – PHASE I ACCELEROMETER CHARACTERISTICS 78

TABLE 5-3 – PHASE 2 ACCELEROMETER CHARACTERISTICS 81

TABLE 5-4 – ACTUAL SAMPLING RATE OF PHASE I DEVICES87

TABLE 5-5 – PHASE I ACCELEROMETER SENSITIVITY (X AXIS) 89

TABLE 5-6 - PHASE I ACCELEROMETER SENSITIVITY (Y AXIS)89

TABLE 5-7 - PHASE I ACCELEROMETER SENSITIVITY (Z AXIS)..... 89

TABLE 5-8 - X AXIS SCATTERS (LOW AMPLITUDE TESTS)92

TABLE 5-9 - Y AXIS SCATTERS (LOW AMPLITUDE TESTS)92

TABLE 5-10 - Z AXIS SCATTERS (LOW AMPLITUDE TESTS).....92

TABLE 5-11 - X AXIS SCATTERS (HIGH AMPLITUDE TESTS) 92

TABLE 5-12 - Y AXIS SCATTERS (HIGH AMPLITUDE TESTS)92

TABLE 5-13 - Z AXIS SCATTERS (HIGH AMPLITUDE TESTS).....	93
TABLE 5-14 – STD OF ACCELERATION ERROR VECTOR (Y AXIS)	94
TABLE 5-15 – ACTUAL SAMPLING RATE OF PHASE II.1 DEVICES	95
TABLE 5-16 – SENSITIVITY OF PHASE II.1 ACCELEROMETERS (X AXIS)	97
TABLE 5-17 - SENSITIVITY OF PHASE II.1 ACCELEROMETERS (Y AXIS).....	97
TABLE 5-18 – SENSITIVITY OF PHASE II.1 ACCELEROMETERS (Z AXIS).....	98
TABLE 5-19 - X AXIS SCATTERS (LOW AMPLITUDE TESTS)	98
TABLE 5-20 - Y AXIS SCATTERS (LOW AMPLITUDE TESTS)	98
TABLE 5-21 - Z AXIS SCATTERS (LOW AMPLITUDE TESTS).....	99
TABLE 5-22 - X AXIS SCATTERS (HIGH AMPLITUDE TESTS)	99
TABLE 5-23 – Y AXIS SCATTERS (HIGH AMPLITUDE TESTS).....	99
TABLE 5-24 – Z AXIS SCATTERS (HIGH AMPLITUDE TESTS)	99
TABLE 5-25 – BACKGROUND NOISE OF MEMSCON AND REFERENCE ACCELEROMETERS	100
TABLE 5-26 - STD ERROR (SWEEP TESTS).....	103
TABLE 5-27 – STD OF EARTHQUAKE SIMULATION TESTS ERROR.....	104
TABLE 5-28 – TESTS SEQUENCE	115
TABLE 6-1 - $[\Phi]^T$ MATRIX FOR THE EXAMPLE STRUCTURE (IN GREY ARE THE MEASURED NODE DISPLACEMENTS)	135
TABLE 6-2 - $[\Phi_{Xm}]^T$ MATRIX FOR THE EXAMPLE STRUCTURE.....	136
TABLE 6-3 - $[\Phi_{Xu}]^T$ MATRIX FOR THE EXAMPLE STRUCTURE.....	136
TABLE 6-4 – MEAN ERROR AGAINST NUMBER OF MODES AND SENSORS	140
TABLE 6-5 – MEAN ERROR AGAINST NUMBER OF SENSORS (M =3)	140
TABLE 6-6 – S1 SENSOR SPECIFICATIONS	142
TABLE 6-7 – S2 SENSOR SPECIFICATIONS	142
TABLE 6-8 – DIFFERENCE BETWEEN DECLARED AND ACTUAL SENSITIVITY OF THE SENSORS	157
TABLE 6-9 - RMS NOISE VALUES FOR DIFFERENT CABLE LENGTHS WITH AND WITHOUT THE APPLICATION OF A 4-TH ORDER BUTTERWORTH FILTER	158
TABLE 6-10 – EFFECTIVE VALUE OF THE DIFFERENCE BETWEEN RESPONSE OF SENSORS S1 AND S2 AND OF REFERENCE ACCELEROMETERS.....	161
TABLE 6-11 – MEAN AND STANDARD DEVIATION OF THE DIFFERENCE BETWEEN THE RESPONSE OF SENSOR S1 AND OF REFERENCE ACCELEROMETER TO 4 SEISMIC EVENTS	163
TABLE 6-12 – DIFFERENCE BETWEEN MEASURED AND ESTIMATED PEAK DISPLACEMENTS (SINE TESTS)	165
TABLE 6-13 - DIFFERENCE BETWEEN MEASURED AND ESTIMATED PEAK DISPLACEMENTS (WAVES COMBINATION TESTS)	166
TABLE 6-14 - DIFFERENCE BETWEEN MEASURED AND ESTIMATED PEAK DISPLACEMENTS (SEISMIC WAVES TESTS).....	169
TABLE 6-15 – MAXIMUM AND MINIMUM VALUES OF MEASURED (Δ_M) AND ESTIMATED (Δ_E) DISPLACEMENTS.....	169

1 Introduction

1.1 Problem statement

Many structures were designed prior to the adoption of seismic design standards. The costs required to bring all the structures up to modern standards are not sustainable, and their need are difficult to justify to an owner who has never experienced seismic damage (M. Celebi et al. 2004). In the vulnerability assessment process, the potential damage may be very difficult to quantify and it should be expressed in the form of probability statements only (Porter, Mitrani-Reiser, and Beck 2006).

Damage indices provide a way to quantify numerically the seismic damage sustainable or sustained by a structure (Williams and Sexsmith 1995; Kappos 1997). Damage indices can be based on the results of non-linear dynamic analysis, on the measured response of the structure during the earthquake or on a comparison of the physical properties before and after the earthquake.

The last two methodologies are related to seismic structural health monitoring of structures. Seismic structural health monitoring systems represent today an important available tool for after-earthquake damage assessment of civil structures, allowing for the identification in near real-time of the structures which are safe, or not safe, with regard to possible aftershocks (Mehmet Celebi 2007). In the near future this tool will probably support or even substitute the currently damage assessment methodology, based on visual inspection of structures damaged by the earthquake, mitigating economic losses related to seismic events. Time is in fact a critical aspect in buildings damage assessment procedure, because buildings cannot attend their regular purpose until they are judged as

safe. The speed with which evaluations are conducted determines the duration for which the potentially damaged buildings remain unusable (Kamat and El-Tawil 2007). The elapsed time directly translates into significant economic losses and to circumstances in which humans are exposed to precarious working and living conditions.

A seismic structural monitoring system is defined in this thesis as a system which allows automated after-earthquake damage classification of a structure by means of a backward analysis. This analysis is based on the collection of a set of observations, on the extraction from the set of values of one or more state variables representing the state of condition of the structure, and on a model, depending on the prior knowledge about the structure and linking observations to state variable (Figure 1-1). Purposes of such a system are assessing building usability and aiding the surveyors in damage localization during visual inspection of damaged structures in the emergency phase, and providing the detailed building response data in the following exhaustive damage evaluation phase.

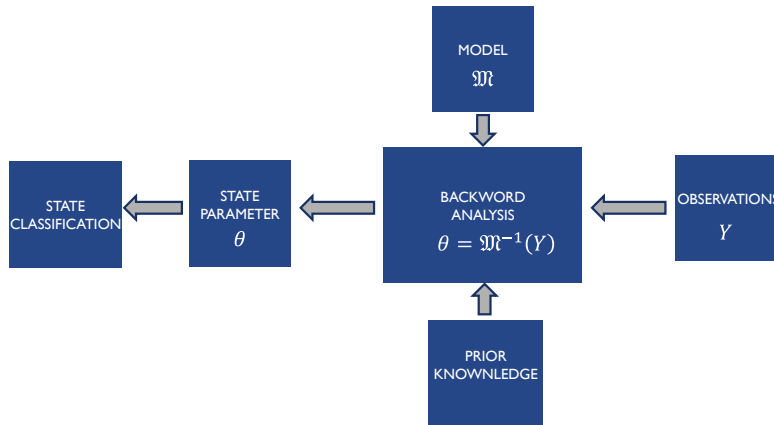


Figure 1-1 – Logical framework of seismic structural health monitoring

From a technological point of view, the realization of the logical framework depicted in Figure 1-1 implies the arrangement of a network of sensors in the monitored building for the collection of a set of observations Y of a mechanical quantity q . The sensors may transduce the mechanical quantity in an electrical or optical transmittable quantity. Data transmission typology (wired or wireless) from sensors to a data acquisition (DAQ) unit is one of the aspect which monitoring system design process deals with. The DAQ converts the electrical or optical quantity received from sensors into a digital form. Data in digital form is then used by an artificial intelligence included in an automatic software to extract one or more features, or state variables, which can be related to structural damage. Raw data and processed data can then be transmitted to people involved in the damage assessment process and to a remote database for data storage (Figure 1-2).

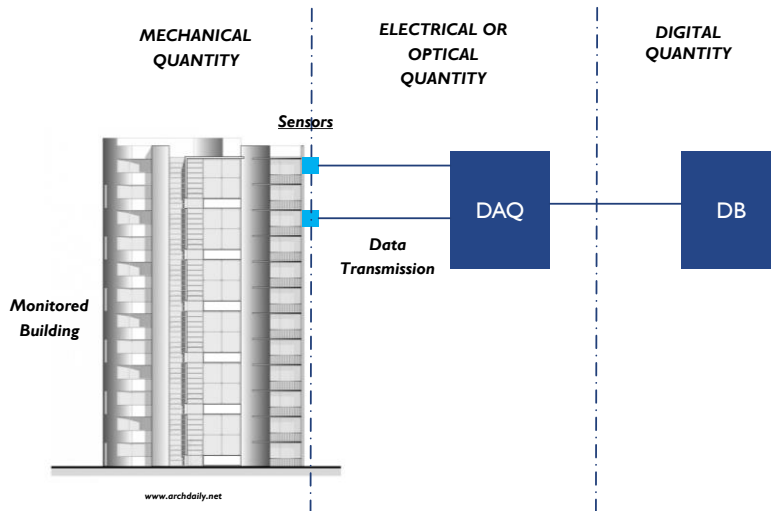


Figure 1-2 – Technological framework for seismic structural health monitoring

Despite the great importance that seismic structural health monitoring can have in the assessment of earthquake-induced damage, to my knowledge there is a lack in the literature and in international standards of comprehensive guidelines for the conception, design, management and maintenance of structural health monitoring systems, in particular in the matter of seismic monitoring systems. Most of the systems seems in fact currently in the form of prototypes and demonstrators.

In this thesis, I investigate therefore how the problem of seismic structural health monitoring is currently faced and I propose a rational framework which can be used in the design process of such a system. In this context, I study the instrumental and model uncertainties involved in structural drift estimation based on acceleration measurements only, believing this parameter one of the best correlated to structural and non-structural damage. Then I apply the proposed framework to the design of a system for industrial precast buildings. The laboratory evaluation of an innovative monitoring system based on MEMS technology and wireless data transmission is also discussed in detail. At last, I propose a new monitoring method supposed to overcome limitations of the current procedure used for the extraction of state variables in ductility-based monitoring systems.

1.2 Objectives

In this thesis I want to investigate how the problem of after-earthquake damage assessment of reinforced concrete buildings is currently faced by researchers and people involved in monitoring activities, and to investigate and to define formally the main limitations of the methods currently adopted. Recognizing a lack of comprehensive guidelines or standards for the conception, design, management and maintenance of seismic structural health monitoring systems for after-earthquake damage assessment, I have as an objective the definition of a rational framework which can be used

to design such a seismic monitoring system for buildings. Being the precision and the accuracy of the system a central aspect of the proposed framework, I want to investigate formally the accuracy of the currently most used ductility-based method for damage assessment, which is the interstory drift estimation from acceleration measurements only. In particular I want to demonstrate that the method implies a substantial decrease of accuracy in the estimation of the maximum drift in case of inelastic residual displacements at the end of the motion. Then I want to demonstrate how the proposed framework can be applied differently to case studies concerning seismic monitoring of framed reinforced concrete buildings and precast industrial buildings. In closing, I want propose a new monitoring method based on acceleration and tilt measurements, able not only to provide automatically the value of the residual interstory drift just after the earthquake, but also to increase the accuracy of the estimation of the maximum interstory drift. The possible industrial deployment of the method is also discussed.

1.3 Overview of the thesis

In Chapter 2 I show the general framework and main principles of the currently adopted visual-based after-earthquake damage assessment methodology. I clarify how a seismic structural health monitoring can support or even substitute this methodology. Then I report a state of the art on seismic structural health monitoring systems describing especially strong motion instrumentation programs currently active in the world and categorizing the monitoring systems described in the literature into vibration-based and ductility-based systems. Recognizing the future importance of wireless instrumentation I briefly report also some experiences on this topic.

Chapter 3 contains the proposed rational framework for seismic structural health monitoring systems design. First, different phases and involved actors in the process of seismic monitoring are described. Then, the similarities between monitoring system design and structural design are highlighted, proving that a demand-capacity approach in terms of accuracy is suitable to drive the design process of a monitoring system. This Chapter deals also with the seismic behaviour of ductile reinforced concrete buildings and on limit states and damage indices used in the literature to express the condition state of a building after a seismic event. This discussion has the aim to guide the reader to the choice of the information to be obtained by a seismic monitoring system and of its use. A qualitative example is also reported in this Chapter.

Chapter 4 deals with the uncertainty analysis of structural drift estimation based on acceleration measurements only. First, the process is fully described. For each step of the process, related uncertainties are listed and their propagation from acceleration measurements to structural drift estimation is studied. In particular, the error induced by signal processing required to perform double integration of acceleration measurements is investigated by means of a parametric analysis. The aim here is to find the limits of applicability of the method.

In Chapter 5 I report my experience within Memsccon research project. It was a European Research Project aiming to develop a structural monitoring system, to be installed in new RC framed buildings, based on MEMS technology and wireless data transmission, for their protection against seismic events and settlements. As deeply illustrated in this Chapter, my task in the Project was the laboratory evaluation of Memsccon technology, performed on both small scale specimens and on a full scale 3D frame tested dynamically. The Chapter contains a brief description of the Project, the detailed description of the laboratory tests and a discussion on the results.

In Chapter 6 I apply the proposed framework and the method of structural drift estimation based on acceleration measurements only on a case study regarding the seismic monitoring of precast industrial buildings. In particular in this Chapter I investigate the peculiarities of these buildings defining monitored limit states and monitoring strategy, which is different from the case of framed RC structures when the assumption of rigid diaphragm behaviour of the floor is not valid. The monitoring system is then illustrated from the technological point of view, in particular system components and software that I developed are described. Results of the evaluation of the system in laboratory conditions are also reported in this Chapter.

Recognizing the limits of applicability of the methods of structural drift estimation based on acceleration measurement only, in Chapter 7 I describe a new monitoring method based on acceleration and tilt measurements, which decreases the uncertainties related to Peak Interstory Drift estimation. The method is described both from a theoretical point of view and from a technological point of view. A case study concerning the seismic monitoring of a school building is also presented in this Chapter.

Some concluding remarks are made in Chapter 8.

1.4 Limitations

This thesis explicitly deals with the problem of seismic structural health monitoring of reinforced concrete structures compliant to the current design practice in seismic prone areas. These structures include new reinforced concrete buildings and recently retrofitted buildings. In these type of structures failure mechanisms are ductile, and brittle failure of structural components is avoided by applying principles of hierarchy of strength. The monitoring strategy studied in detail in this thesis, which is the real-time monitoring of ductility demand, can be used reliably to link monitoring data to state of condition of the monitored building only if the structure satisfies the requisites above. Otherwise, the monitoring system provides only the response of the building, to be used in a following analysis by an expert user, but no information about the state can be provided automatically.

In this thesis I propose a logical framework for the design process of a monitoring system. The most important aspect of the framework is that it is possible to use a capacity-demand approach in terms of accuracy or probability of misclassification of the state of condition when designing a system. In the second case the most suitable approach in the comparison between capacity and demand is

probabilistic, taking into account the randomness of both capacity and demand. I only touched on this problem, assuming then the classification process as deterministic and suggesting to take into account the uncertainty of the classifier by means of safety factors.

In closing, despite not studied in this thesis, the content of this work can be extended to buildings made of different construction materials, such as steel and woods, when failure mechanism are ductile and it is possible to relate structural damage to displacement demand.

2 State of the art of seismic structural health monitoring of buildings

2.1 Introduction

In this chapter the motivation for seismic structural health monitoring is investigated. I report here briefly the currently adopted methodology for after-earthquake damage assessment in different countries in the world. I clarify how seismic structural health monitoring can improve damage assessment activities both in the emergency phase and in the reconstruction and rehabilitation, helping to mitigate economic losses due to seismic events. Definition and purposes of a seismic monitoring system are also stated in this Chapter. State of the art on seismic monitoring system is started introducing strong motion instrumentation programs, which are structural monitoring frameworks currently managed by public agencies for research activities. Monitoring systems based on vibration measurements are introduced and their limitation are briefly investigated. Then I focus my attention to the ductility-based monitoring systems from both the theoretical and technological point of view.

2.2 Motivation for seismic structural health monitoring

After-earthquake damage assessment is a critical aspect in civil engineering, being central identifying as soon as possible which structures are safe and which are not safe for occupancy, in particular with

regard to possible aftershocks, with the aim to protect public safety and estimate the economic losses due to an earthquake (M. Celebi et al. 2004). Damage identification in the emergency phase following an earthquake is not an easy task and further high economic impact on society is often related to unnecessary evacuation and downtime, in particular for critical facilities such as schools and hospitals or industrial facilities (Günay and Mosalam 2013). The reason for this may be ascribed to the current way to perform damage assessment in structures. In the emergency phase following an earthquake, damage assessment is typically performed on-site by volunteer qualified inspectors, with the goals to quickly evaluate the usability of structures struck by the seismic event and to preserve public safety. Despite guidelines and usability forms detailing the inspection procedure are provided to the inspectors, commonly the final judgment about structure usability is competence and responsibility of the surveyor squad (JRC 2007), and subjectivity is always introduced in the judgment, often overestimating damage for safety reasons. Damage assessment and usability evaluation is performed almost completely by visual inspection procedure and usually it requires a number of weeks due to the high number of buildings to be inspected and the limited number of available inspectors. Figure 2-1 reports for example the number of usability inspections over time after the earthquake occurred in Emilia region in 2012. The time needed for usability assessment of the whole building stock in a region can cause additional costs (indirect costs of the earthquake) on the society, in particular related to downtime of industrial and critical facilities.

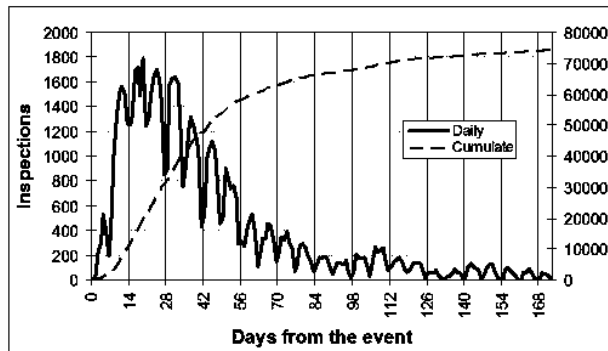


Figure 2-1 – Usability inspections following the earthquake in Emilia (Italy) region in 2012 (Dolce 2013)

Studying the literature (Kaminosono, Kumazawa, and Nakano 2002; ATC 20-1 2005; New Zealand Society for Earthquake Engineering 2009; Baggio et al. 2009) I can observe that the activities related to post-seismic visual-based damage assessment is similar in almost all seismic prone areas. Assessment procedure is commonly subdivided in four or more phases (Table 2-1) and the building usability assessment actually interests the second and the third only.

The first phase (*Overall damage evaluation*) is usually conducted within hours after an earthquake by Authorities and public agencies, and has the purpose to identify areas and buildings requiring in-site damage evaluation. The second phase (*Level 1 rapid assessment*) is conducted within days by appointed volunteers which identify by visually inspection from exterior most critical areas and

buildings, which are usually tagged following the concept stated below. The third phase (*Level 2 rapid assessment*), also conducted by appointed volunteers, is the detailed visual inspection of the buildings tagged as “yellow” or “red” in the previous phase. The fourth phase (*Detailed engineering evaluation*) is the engineering evaluation of the “yellow” and “red” buildings, conducted in order to numerically quantify structural damage and restore structural safety, being this problem strictly related to the evaluation of residual strength and stiffness to lateral actions.

Table 2-1 – After-earthquake damage assessment activities

Purpose	Timing	Description	Performed by
Overall Damage Evaluation	Within hours	Assessment of aggregate damage in the affected area	Authorities
Level 1 Assessment	Rapid Within days	Assess most critical areas (“red” areas” are cordoned off)	Volunteers from the building industry
Level 2 Assessment	Rapid Within months	Assess building safety and decide level of occupancy	Volunteers from the building industry
Detailed Engineering Evaluation	Longer-term	Quantify structural and non-structural damage and design remedial works	Contracted engineers

The aim of the first three phases (especially of the second and the third) is to categorize the building in the immediate into one of the possible classes related to the structural safety against potential aftershocks. Commonly there are three possible classifications: “*Inspected*” class means that no damage or slight damage is found during the inspection, original lateral resistance is not degraded and occupancy is allowed; “*Limited Entry*” class means that damage to structural and/or non-structural elements is found and use is not allowed unless repair is made; “*Unsafe*” class corresponds to severe damage found and limited or none safety of the structure against aftershocks. These three classes typically correspond to different colours (green, yellow, and red respectively, Figure 2-2) of placards or other signs posted on the inspected buildings.



Figure 2-2 – Green, yellow and red placards as for ATC-20 (ATC 20-1 2005)

Inspections are usually carried out and damage assessment is performed following guidelines and inspection forms provided by public agencies. Methodologies adopted in several seismic prone areas are briefly described in the following.

As reported in (Kaminosono, Kumazawa, and Nakano 2002) in Japan a quick damage inspection of buildings is performed immediately after a severe event with the aim to preserve public safety from aftershocks and to organize civil defense activities (e.g. number of temporary houses required). Temporary classification of the structures is performed by sticking on the buildings colored placards, which indicate “unsafe” (red placard), “limited entry” (yellow placard) or “inspected” (green placard). In all the cases, including green placard, no judgment about long-term structural performance is done, being all the possible classification related to structural safety to aftershocks only (Kaminosono, Kumazawa, and Nakano 2002). Following the emergency stage, first a detailed quantitative damage assessment and then a seismic capacity evaluation of the building stock are performed (Nakano, Kuramoto, and Murakami 2004). For reinforced concrete buildings, in particular, structural damage is classified basing on observed damage in vertical elements only, following damage classification reported in Table 2-2.

Table 2-2 - Damage classification for columns and shear walls in Japan, adapted from (Kaminosono, Kumazawa, and Nakano 2002)

Level	Description
I	Crack widths in vertical elements less than 0.2 mm
II	Crack widths in vertical elements range from 0.2 to 1.0 mm
III	Crack widths in vertical elements range from 1.0 to 2.0 mm; Crushing of concrete cover
IV	Crack widths in vertical elements more than 2.0 mm Exposed reinforced bars Spalling of concrete cover
V	Buckling of reinforcing bars Cracks in concrete core Visible leaning of vertical elements

The same concept is adopted in California, USA (ATC 20-1 2005) and in New Zealand (New Zealand Society for Earthquake Engineering 2009). In the first level evaluation, buildings are categorized after the seismic event after a quick visual inspection as “No Apparent Hazard” and green tagged if no restrictions on entry are needed, as “Restricted Use” if damage makes the building dangerous to enter, and “Unsafe” if major damage is present and no entry is allowed. The class “Restricted Use”, in particular, implies that safety issues can be solved only after a detailed in-site evaluation performed by an engineer in the second level evaluation. There is then a third level requested when the structural safety cannot be assessed by visual method alone, which is performed in accordance to procedures

like the ones reported in FEMA 306 (Applied Technology Council (ATC)-43 1998). Similar approaches are currently applied also in Greece (Anagnostopoulos and Moretti 2008), Spain (Vidal, Feriche, and Ontiveros 2009), Turkey (Taskin et al. 2012), and Italy (Baggio et al. 2009).

Table 2-3 – Damage description for RC columns and shear walls in Italy, adapted from (Baggio et al. 2009)

Level	Description
D0	No damage. Crack widths about 0.2-0.4 mm
D1	Slight damage. Hairline cracks in columns. Crack widths up to 1.0 mm in beams. Diagonal cracks in partition walls.
D2-D3	Moderate or Severe damage. Cracks widths up to 4.0-5.0 mm on beams. Cracks widths up to 2.0-3.0 mm on columns and shear walls. Spalling of concrete cover. Clear damage on infills and partition walls. Small leaning of vertical elements.
D4-D5	Crack widths higher than 5.0 mm on beams. Cracks widths higher than 3.0 mm on columns and shear walls. Leaning of vertical elements about 1.0-2.0%.

Table 2-4 – Damage description for RC buildings in Greece, adapted from (Anagnostopoulos and Moretti 2008)

Level	Description
1	Very light non-structural damage. Fine cracks in few infill walls. Light spalling of concrete.
2	Crack widths less than 3.0 mm in a few infill or partition walls. Horizontal crack width in beams and columns less than 2.0 mm (horizontal cracks) and 0.5 mm (diagonal cracks). Cracking or partial failure of parapets and chimneys.
3	Extended diagonal cracks in infills and partition walls. Spalling and crushing of concrete. Crack widths up to 4.0-5.0 mm (horizontal cracks) and 2.0 mm (diagonal cracks) in beams and columns. Dislocation or partial collapse of parapets and chimneys. Visible inclination of the building.
4	Partial or total collapse. Failure of infills and partition walls. Exposure and buckling of reinforcing bars. Collapse of parapets and chimneys. Considerable residual drift of the building. Failure of foundations.

From Table 2-2, Table 2-3 and Table 2-4 it can be seen that damage is evaluated in site referring to the existence and magnitude of cracks in reinforced concrete members for the assessment of structural damage, and in infills and partition walls for the assessment of non-structural damage. It should be noted, however, that crack detection in structural members is not easy to handle, in particular when the members are covered by architectural finishes and claddings, which in principle should be removed to assess the presence of damage, this increasing hugely the costs also for structures not damaged by the seismic event (Mahin 1998). There is therefore a need for monitoring systems

including technologies and methods which may support, or even replace in some aspects, the damage evaluation phase of buildings and structures struck by seismic motion.

Seismic structural health monitoring has been an important research topic during last decades and still a number of researches is being performed. In fact, there is not yet a broadly accepted definition of the technologies, methods and scopes for seismic monitoring systems. To my knowledge, there is not even a widely accepted definition of seismic structural health monitoring system.

The aim of a monitoring system is give an information about the building. This information can be a characteristic of the response (in this case the monitoring system is a measuring instrument only) or a parameter or variable related to the state of condition of the building. In order to provide real-time information about building usability, the latter type of information should be provided by the system, while for post-seismic engineering evaluation also a response parameter is adequate. The first step is therefore collecting observations of a physical quantity through sensors, transducing the physical quantity in electrical or optical transmissible signals, and the computation of the parameter or variable related or not to the state of condition of the building. In the following section, some experiences reported in the literature are briefly discussed.

2.3 The experience of the strong motion instrumentation programs

Currently, seismic monitoring is mainly performed within strong motion instrumentation programs performed by several agencies in the world, mainly in the United States and in Japan. A strong motion instrumentation program is a rational framework for the collection of earthquake data, including ground shaking and structural responses, in a specific region. Typical layout of monitoring systems used for strong motion recording consists of at least two sensors located at the base and the top of a building, recording accelerations in three orthogonal directions, being dense arrays of sensors needed in case of high-rise buildings or when torsional component of building response is expected (Shakal and Huang 2013).

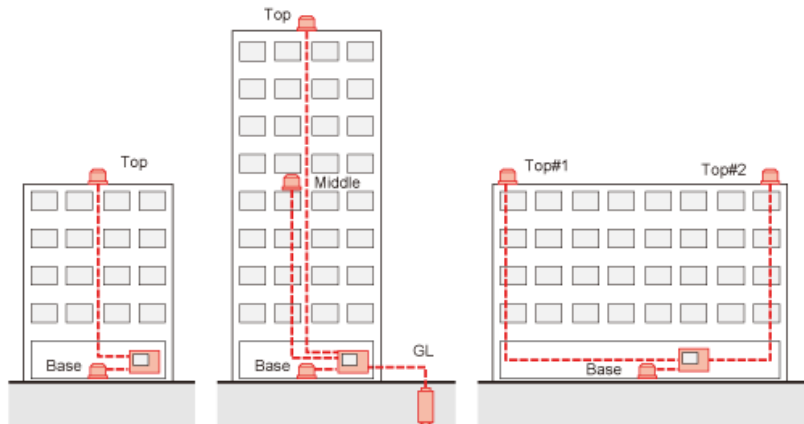


Figure 2-3 - Typical layout of strong motion instrumentation program monitoring systems (Building Research Institute 2009)

In United States, CSMIP (California Strong Motion Instrumentation Program) provides earthquake data related to ground shaking and structural response. According to the information available at the website of Department of Conservation's California Geological Survey (constrv.ca.gov), there are currently 650 ground-response stations and 170 buildings, 20 dams and 60 bridges monitored. For the structural monitoring task, CSMIP adopts monitoring units produced by Kinemetrics Inc. and Refraction Technology Inc., consisting of a tri-axial accelerometer and a 18-bit recorder. Accelerometers are force-balance accelerometers characterized by a ± 4 g acceleration range, 0.01-50 Hz bandwidth, < 0.03 mg acceleration noise in the range 0.01-50 Hz. The 18-bit recorder is activated on triggering or manually. On-board memory allows up to 60 minutes data recording per channel. The selected sampling rate is 200 samples per second. These and others system characteristics are reported in (CSMIP 2007) while an up to date review about the status of the CSMIP is reported in (Shakal and Huang 2013). With the same technology, the National Strong Motion Project (NSMP) of United States Geological Survey (USGS) currently manage the monitoring from 1214 stations (126 buildings). An example of the monitoring systems for buildings of the NSMP array can be found in the UCLA Factory Building Seismic Array website (USGS 2005), where data are available for download. As in CSMIP systems, accelerometers are force-balance Kinemetrics accelerometers with ± 4 g measurement range and 0.01-50 Hz bandwidth. A description of the NSMP instrumentation can be found in (Ulusoy, Kalkan, and Banga 2013), where the instrumentation of Veteran Affairs hospital buildings is detailed. In these buildings, every floor has at least three mono-axial accelerometers oriented horizontally in two orthogonal directions and another tri-axial accelerometer is located on the ground floor.



Figure 2-4 - NSMP stations map (USGS 2014)

In Japan, strong motion observations are performed by Building Research Institute (BRI). In BRI website (Building Research Institute 2009) it is stated that 74 stations are currently in operation, one third of them located in Tokyo. Most of the buildings are monitored with accelerometers located at the floor level and the top of the building. The BRI Urban Disaster Mitigation Research Centre is the only densely instrumented building with 33 channels (21 channels in the surrounding ground, 12 channels in the main building). Most of accelerometers used by BRI are force-balance accelerometers with similar characteristics to the ones adopted in the US.

In Italy, structural response of public facilities (45% of schools, 21% public offices, 17% hospitals and 17% others) is currently being monitored by DPC within the OSS program (DPC 2014). The typical system consists of an array of 15-32 mono-axial force-balance accelerometers and a 24-bit recorder transmitting data to a central unit in Rome via ADLS or UMTS when acceleration is higher than a threshold set at 0.01g. Ground motion intensity factors (PGA, duration, Arias intensity factor) and building response is calculated and a finite element model of the building based on detailed inspection and Operational Modal Analysis (OMA) procedures is used to estimate structural damage. Parameters and data are available for download at <http://www.mot1.it/ossdownload/index.php?evid=1419421210>.

The analysis of the literature about strong motion instrumentation programs allows me to make a few comments about them. These systems are conceived to provide seismic input (i.e. accelerations of the ground) and structural seismic response (i.e. accelerations measured at few points of the structures and in some cases displacements) with the aim of research and data collection only. The use of the collected data is choice and responsibility of the final user (i.e. who downloads data from online database). Examples of use are the generation of response spectra for linear and non-linear analysis, studies about ground displacements, verification of models and methods for damage assessment. No information about buildings' usability or structural safety are provided by these systems. Strong motion instrumentation programs' systems should be therefore classified as seismic measuring systems rather than as seismic structural health monitoring systems.

2.4 Monitoring systems based on changes of structural parameters

Damage detection methods based on changes of modal parameters of the structure require vibration-based identification techniques for the identification of the modal parameters of the structure (natural frequencies, mode shapes, and damping ratios) before and after the seismic event. It is well known that the dynamic behavior of a structure can be expressed as a combination of modes characterized by a set of parameters depending on structure's physical parameters (Rainieri and Fabbrocino 2014). The basic idea of seismic monitoring based on changes of modal parameters is that the presence of damage, included the damage induced by an earthquake, can be assessed by means of a comparison between the dynamic characteristics of the structure before and after the seismic excitation and the subsequent extraction of a state variable or damage feature sensitive to damage extension and possibly its location. The topic was studied by many author both from a theoretical point of view and by means of practical implementations on real structures, particularly on bridges. A comprehensive state of the art about these methods can be found in (Sohn, Farrar, and Hemez 2004) and here only a brief introduction is provided, also because I did not work in this topic during my research.

The simplest way to obtain a state variable basing on modal identification methods is defining the state variable as a function of natural frequencies variations due to damage (Salawu 1997). The basic idea of this type of monitoring is that a variation $\delta\omega_i$ of the i -th natural frequency of a structure is a function of stiffness reduction δK due to damage and damage location p (forward problem):

$$\delta\omega_i = f(\delta K, p) \tag{2.1}$$

The inverse problem is the estimation of the value of stiffness reduction and its localization based on natural frequency estimations. A number of techniques was proposed in the literature for the identification of natural frequencies from structural vibration response (Salawu and Williams 1995; Salawu 1997). Despite the series of publications about damage detection from natural frequencies changes, this approach presents two main challenges, being the first the fact that often local damage does not influence global response of the structure and the second the influence of environmental conditions on dynamic response, which can mask structural changes induced by damage. For example, frequency shifts, due to changes in ambient conditions within a single day, exceeding 5% were observed in (Sohn 2001). Moreover, it is noted that if it is true that the presence of damage implies a frequency change, a frequency change does not necessarily imply the presence of damage, being possible other sources for this variation, such as environmental effects or not-stochastic ambient noise. In this type of monitoring, therefore, reliable results are obtained only in case of severe structural damage and of high accuracy of measurements.

Another possible approach is the monitoring of mode shape variations. One possible state variable related to the state of the structure, hence to the presence of damage, is the relative difference between mode shapes in terms of displacements (Sohn, Farrar, and Hemez 2004):

$$\{RD\}_i^j = \frac{\{\phi_0\}_i^j - \{\phi_D\}_i^j}{\{\phi_0\}_i^j} \quad (2.2)$$

where $\{RD\}_i^j$ is the relative difference between $\{\phi_0\}_i^j$ which is the value of eigenvector $\{\phi\}_i$ at point j in the undamaged state and $\{\phi_D\}_i^j$ which is the value of eigenvector $\{\phi\}_i$ at point j in the damaged state. Another possible state variable is Modal Assurance Criterion (MAC). It indicates the correlation between two sets of modal vectors, for example those from damaged and undamaged states. The MAC index is a scalar value assuming values between 0 (sets of modal vectors are uncorrelated) and 1 (sets of modal vectors are perfectly correlated) and is defined as (Ewins 2000):

$$MAC = \frac{|\phi_{ui}^T \phi_{di}|^2}{(\phi_{ui}^T \phi_{ui})(\phi_{di}^T \phi_{di})} \quad (2.3)$$

where ϕ_{ui} is the i -th mode shape of the undamaged structure and ϕ_{di} is the corresponding mode shape of the damaged structures. It is worth pointing out that damage detection is not the unique application of RD and MAC (and others similar quantities) and that at most they can give a perception about a possible damage state.

In principle, most of these and other methods not reported here can be used to infer the presence of damage into a building after a seismic event. However, to accomplish the task required by a seismic structural health monitoring system listed in section 2.8 only a few of the methods can be automatically executed by the system in quasi real-time, without the interaction with an expert user. Therefore in the following only some of the methods which can be easily implemented in seismic monitoring systems for automatic execution are reported. Most of them are related to Operational Modal Analysis (OMA) techniques. Contrary to Experimental Modal Analysis, which requires the knowledge of both the input excitation and the output response to obtain a transfer function describing the structure, Operational Modal Analysis only requires measurement of the output of the structure excited by ambient vibration sources such as wind and traffic. The basic assumption is that the set of measured data is the response of the structure to a stochastic input which can be modeled as white Gaussian noise. The techniques for the identification of modal parameters can be classified in parametric methods and non-parametric methods (Bindi et al. 2014). In the parametric methods modal parameters are identified basing on model updating approach. In the non-parametric methods modal parameters are identified directly from measured data. Obviously, only the latter methods are suitable for automatic identification. The former, in fact, require extensive interaction from an expert user, and cannot be automated in a stand-alone monitoring system. OMA techniques can be further classified in OMA in the time domain and OMA in the frequency domain (Rainieri and Fabbrocino 2014). Most important OMA techniques in the time domain are NExT, ARMA and SSI-based techniques. Most important methods in the frequency domain are PP, FDD and its enhancement EFDD, RD. Most of these techniques have been applied in monitoring systems for large structures, in particular for bridges, but there are also experiences of their application on building monitoring.

(Zimmerman et al. 2008) investigate the possibility of implementation of three different OMA techniques in the frequency domain (PP, FDD and RD), modified for a parallel processing environment, on a network of wireless nodes attached to MEMS accelerometers, with the goal of the modal identification (modal frequencies, mode shapes and modal damping ratios) of a balcony of an historic theatre in Detroit. In (Bindi et al. 2014) non-parametric identification methods, namely the PP method and FDD method, are applied to perform OMA and extract frequencies and mode shapes of an 8-story RC building located in northern Greece. In the same paper, seismic interferometry, which is based on the correlation of waves recorded at different receivers, is used to locate structural damage.

A comparison between the performance of different techniques was performed by University of Naples (Rainieri, Fabbrocino, and Cosenza 2010). 4 different OMA techniques namely Cov-SSI (covariance driven Stochastic Subspace Identification), DD-SSI (Data Driven Stochastic Subspace Identification), EFDD (Enhanced Frequency Domain Decomposition), SOBI (Second Order Blind Identification) were implemented in a seismic monitoring system (integrated to a seismic early warning system) in the main building of the School of Engineering in Naples. Results of the carried out both in operational conditions and during the Aquila earthquake are that operational modal analysis techniques allow to monitor the building dynamic parameters before and after an earthquake. (Ulusoy, Kalkan, and Banga 2013) describes the monitoring system currently under development by USGS and installed inside VA hospital buildings in California. Four algorithms able to both detect and localize damage are implemented in the system to compute (i) shear-wave travel time; (ii) modal parameters, (iii) base shear force, (iv) interstory drift ratio. The algorithms were validated using data from full-scale shake table test at the University of California, San Diego. Results of the tests are (1) frequency shifts obtained by OMA technique in operational conditions are consistent with visually observed damage (2) OMA is not reliable during the earthquake (3) mode shape curvatures correctly identify damaged zone in the building (4) interstory drift estimation is the most practical approach for damage detection but it is recognized the critical role of the accuracy of the drift computation from acceleration measurements.

2.5 Monitoring systems based on response monitoring during the earthquake

The second family of seismic monitoring systems includes these systems able to monitor in real-time or in quasi real-time (being the difference the time needed to compute dynamic response of the structure) the dynamic response of a structure to an earthquake and, in particular, displacement and deformation demands. It is well known from displacement-based design theory, in fact, that structural damage can be related to seismic displacement demand and in particular to interstory drift ratios (Calvi 1999; Priestley, Calvi, and Kowalsky 2007; Sullivan, Priestley, and Calvi 2012).

In (M. Celebi et al. 2004) the authors present a monitoring system for buildings which records acceleration and computes displacements and drift ratios to measure the performance of the building

during an earthquake. In absence of data related to an earthquake, the system can be used to record ambient vibration data used to monitor modal parameters of the building. More recently, (Mehmet Celebi 2007) presents a state of the art of the methodologies to obtain structural displacements and drift ratios for damage assessment purposes. The approach of monitor drift ratios was applied to three steel frame buildings in California. Two possibilities are investigated, one using GPS and the other using accelerometers. Qualitative results of the application are reported. In (Porter, Mitrani-Reiser, and Beck 2006) the Authors propose an integrated system which is able to estimate damage (existence and location) and loss after the earthquake. The system is based on acceleration measurements at the building's base, a stochastic model of the structure, the execution of a non linear time history analysis to estimate probabilistic seismic demands. Structural response is input for fragility functions. Results of the study are that the method is suitable to quantify damage but it is not able to localize damage. The only relevant accelerometer (for loss estimation) is the one placed at the base level. (Ponzo et al. 2010) presents a simplified method based on a statistical approach that uses the data recorded at the top of the building to extract the maximum interstory drift, used as damage indicator. Three parameters are considered in the statistical approach: (i) maximum the top acceleration (ii) first modal frequency variations (iii) equivalent viscous damping variation. The approach was investigated through small-scale RC models (research projects TREMA and POP) and numerical simulations. Results of the experimental tests are that analytically obtained interstory drift is the same ($R^2 = 1$) of experimentally observed interstory drift and that maximum acceleration at the top of the building is the predominant parameter for low intensity excitation (up to 0,20 g). Numeric simulations confirm the experimental results.

Other structural monitoring methods involve the use of Global Position System (GPS). GPS is a navigation satellite system which has recently emerged as a possible measurement technology for displacement measurements both statically and dynamically (Mehmet Celebi 2007). The main advantage of GPS-based methods respect to accelerometer-based methods is the possibility to monitor structural response at frequencies lower than 0.5 Hz, and the ability to retrieve also residual displacements at the end of the motion. The typical arrangement of a monitoring system based on GPS consists of one or more GPS receivers installed on the structure and a base station (Real-time Kinematic arrangement). The typical upper limit of the sampling rate of GPS technology is about 25 Hz while currently the maximum sampling rate of GPS receivers available on the market is 100 Hz (Im, Hurlbaeus, and Kang 2013). Due to this limit, at the moment GPS is able to detect deformation of long period structures only, with an accuracy reported by (Mehmet Celebi and Sanli 2002; Nickitopoulou, Protopsalti, and Stiros 2006) as equal to ± 10 mm in the horizontal direction and to ± 20 mm in the vertical direction. Recently, other sensors, mainly accelerometers, have been combined by researchers with GPS in order to improve their monitoring range and accuracy. Accelerometers and GPS are in fact in some way dual: accelerometers exhibit best performance at higher frequencies while GPS at very low frequencies. Several algorithms were proposed to integrate accelerometers and GPS data and applied mainly to bridge monitoring, with the aim of removing drifts from integrated

velocities and displacements. (Roberts, Meng, and Dodson 2004; Chan et al. 2006; Kim, Kim, and Sohn 2014).

University of Michigan (Kamat and El-Tawil 2007) proposes a remote sensing technique based on augmented reality (AR) for post-earthquake damage assessment. The method is comparing, in an AR device, a previously stored baseline view of the undamaged structure to the view of the structure after the event. Damage in the building is automatically assessed measuring through image processing the permanent interstory drift ratio as the differences between the two views. Tested in laboratory conditions, the error in drift estimation done by the system is between 2.8% and 7.2% for drift values between 83 mm and 275 mm (being the higher value of the error relative to the lower value of the drift) and is higher up to 181% for smaller drift values around 40 mm).

As reported in the literature, vision-based methods have often sufficient accuracy and resolution for post-seismic damage evaluation based on residual displacement estimation. These methods require the installation of dense arrays of target panels or points on the structure's surface. Main limitation of these methods is the need for protection of the targets in order to ensure their performance over time. Augmented reality methods does not require the installation of target on the structure, but the accuracy is limited. Laser scanning is a promising method for residual displacement detection, but the accuracy is similar to augmented reality methods and laser scanning equipment is still very expensive. All the previous methods, anyway, does not allow for transient displacements monitoring.

GPS systems are currently used to monitor the deformation of long-period structures such as bridges and high-rise buildings. GPS typical sampling rate is of the order of 25 Hz and GPS accuracy is of the order of 10-20 mm. Accuracy is affected by a number of factors (such as sampling rate, satellite visibility, location of the monitored structure, etc.) and it is not an easy task to define the uncertainties of the measurement. Recently, several researchers proposed new algorithms to integrate GPS data with accelerometers data. These algorithms were tested in bridge structures and high-rise buildings, while no information are available in the literature about their performance in low-rise structures.

Currently, the method of displacement estimation from acceleration data only is the most used and appears to be the only valid one, in particular for low-rise buildings. As highlighted in section... displacement calculation from acceleration data only presents two fundamental issues, being the first one the total loss of information about structural residual displacements thus about residual interstory drift (RID) and the second the underestimate of peak deformation thus of peak interstory drift (PID). The state variable proposed in (A Cheung and Kiremidjian 2013) is residual drift, which is related by the Authors to damage using the approach reported in FEMA 356 (ASCE 2000). The choice of this state variable reflects the need to adopt a simple damage detection algorithm to be embedded into microprocessor of wireless sensor nodes. Residual drift is estimated from rotation observations recorded at the end of the structural motion by one or more tri-axial MEMS accelerometers placed along the columns. The algorithm was validated through experimental tests conducted on reinforced concrete columns by University of California and University of Nevada, with the aim to define optimal sensor number and location and (Balafas and Kiremidjian 2013; Balafas and Kiremidjian 2014).

While for structures with acceptable ductile behavior approaches based on ductility demand estimation are proved to be suitable for structural seismic-induced damage estimation, when brittle failure of structural components is expected different techniques can be used. The approach used by Goel (Goel 2011) is to use as state variable the ratio between the inertial base shear value, defined as sum of all floor inertial forces above the base of the building, and the structural base shear value, which is the shear capacities of the total number of columns at the base level. Inertial base shear is estimated monitoring accelerations at each floor of the building and is calculated as:

$$V_{bl} = \sum_{j=1}^{NF} m_j \ddot{u}_j \quad (2.4)$$

Limongelli (Limongelli 2011) proposes as state variable the interpolation error which is done using cubic spline functions to interpolate the profile of the FRF along the height of the structure, being the structure a multistory frame with a beam-like behavior. The interpolation error at the point z_i is defined as:

$$\Delta H(z_i, f) = \left| H_R(z_i, f) \right| - \left| H_S(z_i, f) \right| \quad (2.5)$$

being $H_R(z_i, f)$ the magnitude value of the frequency response function at point z_i calculated from recorded signals and $H_S(z_i, f)$ is the magnitude value of the frequency response function at point z_i interpolated through a spline function of magnitude values of frequency response function at all instrumented point except point z_i . In order to remove the dependency on the frequency, (Limongelli 2011) suggest to take the norm of the function $\Delta H(z_i, f)$ over the frequency range:

$$E(z_i) = \sqrt{\sum_{i=1}^N \Delta H^2(z_i, f)} \quad (2.6)$$

being N the number of discrete frequencies of the FRF. Damage induces an increase in flexibility hence an increase of $E(z_i)$. Damage index is positive in damage state and negative in undamaged state and is defined as:

$$D(z) = \frac{E(z) - \mu_{E_0}(z)}{\sigma_{E_0}(z)} - Z \quad (2.7)$$

where $\mu_{E_0}(z)$ is the mean value of $E(z)$ distribution in undamaged state, $\sigma_{E_0}(z)$ is the standard deviation of $E(z)$ distribution in undamaged state and Z is a damage threshold value.

2.6 Technology for seismic structural health monitoring

An important research topic is the one related to the transmission of data from sensors to recorders, in particular to the possibility to use wireless technology in structural health monitoring (J. P. Lynch

2006). In fact, it is well known that instrumentation wiring is a relevant component of a monitoring system total cost. Moreover, noise in data increases with the distance between sensor and A/D converter. Wireless nodes can significantly decrease the costs of monitoring and cancels the distance between sensors and recorders. In fact they can be defined as electronic components including into the same package sensors, ASIC, low power microprocessor and A/D converter, batteries and antenna (Torfs et al. 2013).

Reliability of wireless structural health monitoring is proven for static parameters monitoring (e.g. temperature, humidity, strain) or for modal testing applications (Jerome P Lynch et al. 2003), being currently the most important issue the one related to battery duration and replacement. In dynamic monitoring of critical parameters such as the real-time response monitoring of a building during a seismic event, the adoption of wireless instrumentations is still discouraged because data loss, difficult in time synchronization between different nodes, energy consumption and different clock rates between different nodes. Both for static and dynamic applications, wireless monitoring requires the implementation of techniques and damage detection algorithms which minimize energy consumption (Torfs et al. 2013). The system initially proposed in (A Cheung and Kiremidjian 2013), in this moment in the status of patent pending (Allen Cheung et al. 2014) implements wireless nodes based on MEMS accelerometers as sensing components to estimate post-seismic residual drift of instrumented columns. In this case a reliable synchronization between different channels is unnecessary because de facto this system belongs to the family of systems for static monitoring of structures. The simple damage detection algorithm entails low energy consumption of the embedded microprocessor and of the transmission task: rotation is calculated by the microprocessor starting from a set of acceleration measurements, and a single value of rotation is transmitted. The system was successfully tested during experimental tests performed by University of California and University of Nevada on real-scale reinforced concrete columns (Balafas and Kiremidjian 2013; Balafas and Kiremidjian 2014).

2.7 Industrial deployments

The market related to seismic monitoring system design, production and management is still in an early stage and typically components originally conceived for diverse applications (e.g. for aerospace, defense, or industrial markets) or for general purpose are used to develop a monitoring system. On the contrary, often products (i.e. sensors and data acquisition components, software) specifically designed for the seismic application are homemade components developed internally in the academia in order to satisfy cost requirements or to investigate the performance of new technologies. To my knowledge, there are no companies working on the market providing seismic monitoring services including system conception and design, installation, management and, in particular, the sharing of information related to the state of condition of the monitored structure.

In the last few years, a few patents concerning structural health monitoring have been presented. Most of them concerns the invention of sensor nodes or the development of data transmission networks, while very few documents can be found disclosing complete monitoring systems. This is particularly true of seismic monitoring systems. Most important patents about seismic monitoring of structures are briefly reported below. The object of the invention in (Straser, Kiremidjian, and Meng 2001) is a monitoring system consisting of sensor nodes based on MEMS accelerometers with wireless transmission capability, providing structural condition assessment both for extreme events (being response parameters Arias Intensity and Interstory Drift) and service conditions (using a set of methods for structural modal analysis). Patent by (Allen Cheung et al. 2014) adopts one or more sensor nodes, consisting of multi axis MEMS accelerometer, a digital processor, a memory and a radio, attached to columns of the building to measure point rotations, wirelessly transmitted to a central unit. The central unit estimates residual drifts of the columns from rotation measurements, using a model of plastic deformation of the columns. The damage of the columns is estimated using a relation between residual drift to damage (e.g. FEMA 356). Patent by (Duron, Wiesmann, and Pranger 2004) discloses an invention directed to the detection of imminent collapse of a building, due to earthquake events or fire, based on detection of changes in ambient response levels. Invention disclosed in (Lichtenwalner et al. 1999) relates to a system, conceived for aerospace industry but adaptable to civil engineering, which assesses damage in the structure monitoring changes in transfer functions between pairs of piezoelectric actuator/sensor located in the structure.

(Iwan, Radulescu, and Radulescu 2013) reports a system that provides continuous real time monitoring of interstory hysteretic behavior by means of the production of interstory Hysteresis Loops. The system consists of a set of accelerometers located at the ground and the floors of a building. A central unit automatically calculates for each floor displacement time histories via numerical double integration of acceleration measurements \ddot{y}_i and estimates restoring forces at floor j . Observation of Hysteresis Loops allows for damage detection and localization. This patent is currently adopted in R-SHAPE seismic monitoring system (<http://earthquake.usgs.gov/monitoring/nsm/structures/la.php>).

2.8 Definition and purposes of a seismic structural health monitoring system

The analysis of the state of the art about seismic structural health monitoring allows me to find a definition of such a system. In principle, the collection of a set observation is related to the activity of monitoring the structural response. In the strict sense, the structural response is the dynamic response (e.g. accelerations, velocities and displacements) of the structure to the earthquake. In a broader sense, the structural response is a set of effects of the earthquake on the structure, including changes on structural parameters from before to after the earthquake. I adopt the latter definition of structural response, which allows to classify most of the systems discussed in the state of the art as seismic

monitoring systems, therefore both the systems able to monitor structural dynamic response and the systems able to monitor changes on structural parameters.

The definition of seismic structural health monitoring system used in this thesis is the following.

A seismic structural health monitoring system is a system permitting to obtain information on the monitored structure after an earthquake, by means of a backward analysis based on: (a) the collection of a set of observations; (b) a prior knowledge of the structure; (c) a model relating observations and information. The obtained information can be related or not to the state of condition of the structure. If it is, the information is a state variable. If it is not, the information is a response parameter.

The purposes of a seismic structural health monitoring systems are the following.

In the emergency phase, to assess building usability and to aid the surveyors in damage localization during visual inspection of damaged structures; in the engineering evaluations phase, to provide the detailed building response data.

In particular a network of seismic structural health monitoring systems can mitigate the impact of seismic events on society both in the emergency phase and in the engineering evaluation phase.

In the immediate it can:

- (i) advise the Authorities about the most damaged areas and structures in a region, this allowing an optimization of the available resources in the emergency phase (this may support or potentially replace *Overall evaluation* and *Level I Assessment* activities);
- (ii) advise the users about the usability of the structure and in particular to inform them about the fact that the structure is safe to be occupied again after the first probable evacuation, without the need of an in-site inspection (this may support *Level II Assessment* activities);
- (iii) aid the inspector providing reliable information about most important building areas and members (e.g. floors) to be inspected first, that is the areas which experienced maximum seismic demand (this also may support *Level II Assessment* activities);

In the evaluation phase it can:

- (iv) provide the detailed building response data to the engineer in-charge for the complete damage and economic losses estimation of the damaged building, in particular giving an estimate of the residual strength of the building to lateral loads.

2.9 Conclusions

After-earthquake damage assessment is a critical aspect in civil engineering, being central identifying as soon as possible which structures are safe and which are not safe for occupancy, in particular with regard to possible aftershocks, with the aim to protect public safety and estimate the economic losses due to an earthquake. Usual methodology for after-earthquake damage assessment is in-field, visual-based, time consuming, and often subjective. There is a need of systems capable to automatically detect structural damage after an earthquake, giving immediate advice about usability and providing quantitative information about structural response to be used in the process of detailed engineering evaluation and retrofitting design. After studying how the problem of after-earthquake automatic damage assessment is currently faced, it is possible to classify methods for damage assessment in two classes: (i) methods in which the damage is assessed through the comparison between a prior and a following state of the structure (e.g. methods based on changes of modal parameters); (ii) methods in which the damage state of the structure is inferred through the real-time monitoring of the structural response of the structure during the earthquake (e.g. methods based on ductility demand). A definition of seismic structural health monitoring encompassing both the categories is a system permitting to obtain information on the monitored structure after an earthquake, by means of a backward analysis based on: (a) the collection of a set of observations; (b) a prior knowledge of the structure; (c) a model relating observations and information. The obtained information can be related or not to the state of condition of the structure. If it is, the information is a state variable. If it is not, the information is a response parameter. This definition is used in the following of this thesis.

3 A logical framework for seismic structural health monitoring design

3.1 Introduction

The objective of a seismic structural health monitoring is to get an information which can be related to the state of the monitored structure after the seismic event in terms of structural damage. This information should be obtained with an adequate level of confidence. The level of confidence of the information provided by the system relies not only on the performance of the system itself, but also on the knowledge of the designer of the structure to be monitored.

In this chapter I first discuss, basing on my experience, the activities related to structural monitoring in order to give an overview of the main aspects which must be taken into account in this field. Then, I propose a logical framework for the design process of a monitoring system, showing also conceptual similarities between structural design and system design. A qualitative example with the application of the framework to the particular case of seismic monitoring is finally discussed in this Chapter.

3.2 Activities related to structural health monitoring of structures

The process of design, installation, and management of a seismic structural health monitoring is a complex process which implies different tasks and involves different individuals, namely a customer,

a designer, technicians, testers and a managing professional or company. Basing on my own experience and on (Glisic, Inaudi, and Casanova 2010) I propose in the following a classification of the most important tasks related to seismic monitoring, which is: a) design of the monitoring system; b) installation of the monitoring system; c) management of the monitoring system; d) data management; e) shutting down of the monitoring system. Each of these tasks are briefly discussed in the following.

3.2.1 *Design of the monitoring system*

The activity of design of the monitoring system starts from the definition of the scope of the monitoring activity, which is the definition of the reason because the system has to be designed and of the boundary conditions of the activity (needs of the customer, social and economic issues related to the monitoring activity, etc.). For example, a customer may be interested in a monitoring system able to assess with a high degree of confidence the building usability after an earthquake, taking into account damage to both structural and non-structural components. An artificial intelligence is thus required in such a system. Another customer may be interested in a monitoring system able to monitor structural dynamic response in terms of displacement of a single control point of the building during the earthquake and to send data to a structural engineer in charge of non-linear structural analysis and damage assessment. In this case, the system is only a measuring instrument and no algorithms for damage detection are required.

The second stage is the definition of the state variable (i.e. the quantity which is related to state condition of the structure) which has to be extracted by the monitoring system. The choice of the state variable depends on the scope of the monitoring activity. For example the state variable may be the decrease in stiffness of the structure due to the seismic input, the residual displacements at the end of the motion, the interstory drift ratio and so on.

The selection of type and number hardware components is strictly related to building characteristics, selected state variable and desired accuracy of the state variable estimation. For example, for a system based on OMA techniques relating structural damage to modal properties of the building, a dense network high-sensitivity piezoelectric seismic accelerometers for the observation of structural response to ambient vibration are probably the best choice. On the other hand, if the selected state variable for the monitoring of a shear-type framed building is the mean interstory drift ratio, a pair of low-cost capacitive accelerometers at the base and at the top of the building may be appropriate.

The following stages are the design of the physical sensor network, the definition of the monitoring scheduling, and the selection of the use of monitoring data. Lastly, an economic estimation of the monitoring system must be performed and basing on this, the process can be iterative.

3.2.2 *Installation of the monitoring system*

The installation of the monitoring system implies physical installation of equipment (sensor, cables, acquisition units, and accessories such as electrical conduits) and software installation (modules for system management, state variable extraction from data, user interface (UI) and so on). Physical installation of equipment is usually performed by a technician, with the supervision of the system's designer. Software installation is usually performed by the system's designer.

3.2.3 *System management*

A monitoring system requires a management and maintenance plans in order to guarantee its functionality during time. For example, depending on their quality sensors may be need of replacement after several year. The design of the plans is usually performed by the system's designer, while the operational management is conducted by the system supplier or by the customer itself.

3.2.4 *Data management*

Basic data management consists of automatic or on-demand execution of measurements, data storage and data access. Commonly in the past data was stored locally on more or less structured acquisition files, which needed to be processed manually by in charge technicians in order to extract useful information. Today, the state-of-the-art is a monitoring system which automatically store raw data locally and transmit automatically processed data to a remote database. Client web-applications give the access to processed data. In particular, these applications allow for data visualization, data export, further data analysis and eventually data interpretation..

3.2.5 *Shutting down of the monitoring system*

Depending on a number of factors (contracts between involved counterparts, economic issues, emergence onto the market of new technologies) the monitoring system can be interrupted (from management activities interruption only, to powering interruption) and eventually dismantled. Dismantling activities are generally conducted by the customer or by an appointed technician.

Table 3-1 – Activities related to seismic monitoring

System Design	System Installation	System Management	Data Management	Shutting down
Scope definition	Sensors installation	Maintenance plan	Data storage	Monitoring interruption
Parameters selection	DAQ units installation	Repair service	Data access	System dismantlement
Hardware selection	Accessories installation		Data visualization	
Sensor network design	Software installation		Data export	
Selection of powering strategy	UIs installation		Data Analysis	
Selection of data communication strategy			Data Interpretation	
Scheduling selection				
Data use selection				

3.3 Structural monitoring design

3.3.1 Principles

Seismic structural monitoring is a particular branch of structural health monitoring. Structural health monitoring can be seen as a inferential process through which information (related or not to state of condition) on a structure are obtained, basing on a set of periodic or continue observations of physical parameters, a prior knowledge of the structure, and a model between observations and information to be obtained (Zonta 2014). Information can be one or more parameters or variables related to the state of condition of the structure, or an estimation of a physical quantity of interest. Being the objective of monitoring obtaining information, the precise definition of information to be obtained is a critical requisite of system design.

A monitoring system consists of a network of sensors measuring physical quantities, a data acquisition unit, a storage unit, and a set of procedures aiming to infer information. When the information is related to state of condition (for example when the system is expected to provide damage state or to highlight on-going degradation phenomena), algorithms based on which a Decision Support System (DSS) or Expert System software packages are developed, are also logically included in the system. Sensors can be embedded into structural elements (e.g. strain gauges or fiber optic sensors embedded

in concrete columns), fixed to their surface (e.g. accelerometers above a concrete slab) or also be remote respect to the monitored structure (e.g. displacement monitoring through GPS measurements). The physical quantities to be measured depend on the application and include quantities related to the environment hence to ambient actions (temperature, humidity, vibrations, etc.), quantities related to applied actions (static and dynamic actions), and quantities related to the structural response (accelerations, static and dynamic displacements, deformations, strains and so on). In general, all quantities which are expected to influence the information that the system is supposed to provide should be measured.

Measurements recorded by the sensors can be transmitted to data acquisition unit through electrical or optical wires, or wirelessly. The inferential process may be performed locally (i.e. inside or in the proximity of the monitored building) or remotely, automatically or manually, in real-time or in non-real time. All of these aspects, and others not explicitly mentioned here, must be taken into account in the design process of the monitoring systems.

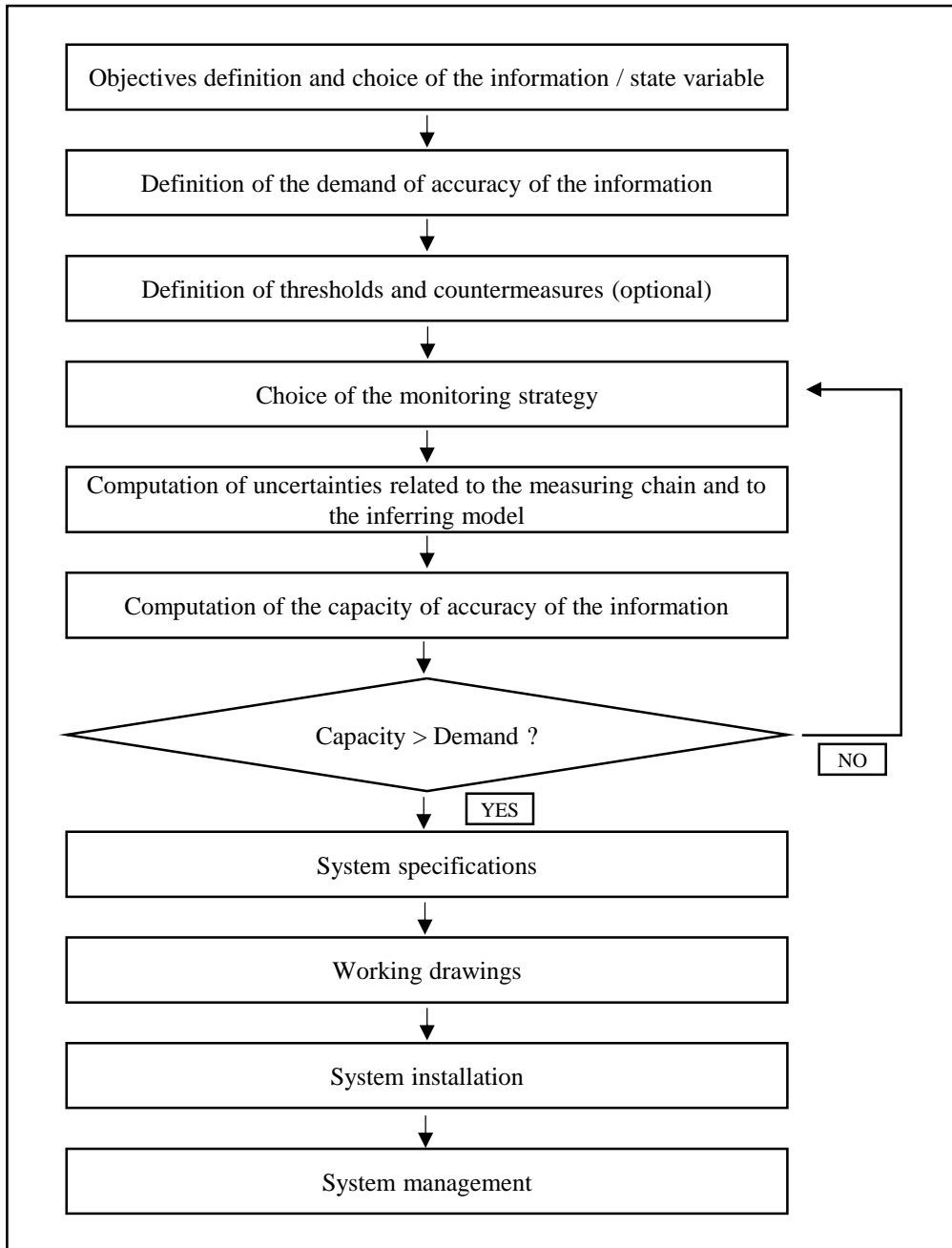


Figure 3-1 – Flowchart of the design of a monitoring system

3.3.2 Analogy between monitoring system design and structural design

The monitoring system design is in some way similar to structural design, as showed in Table 3-2 below.

While the objective of structural design it is nothing other than ensure structural stability with an adequate level of safety against applied actions, the objective of monitoring system design is the knowledge of a certain information about the monitored structure with an adequate level of confidence or, in other terms, with an adequate accuracy. The effectiveness of a monitoring system depends in fact on the reliability of the information provided.

Monitoring system design can be driven by a relation between demand and capacity like structural design. In structural design we compare for each structural member the demand (e.g. a bending moment, a displacement, a deformation, etc.) to the capacity of the member. In monitoring system we can follow the same approach comparing the demand, which in this is case is the requested accuracy of information provided, and the capacity, which is the accuracy of the information actually obtained. Alternatively, this comparison can be done in terms of sensor accuracy (demand and capacity) instead of information accuracy. The choice of system components can be therefore based on this comparison. In both structural design and monitoring system design a model must be introduced. In structural design the model links actions and, for example, stress or deformation. In monitoring system design, the model links observations (i.e. measurements of the physical quantities) to information.

The limit state approach of design can be therefore used also in monitoring system: actually a comparison between capacity and demand is performed, being the performance of the designed system expressed in terms of probability of information, or state, misidentification (e.g. probability of occurrence of false positives and false negatives).

Table 3-2 – Equivalence between structural design and monitoring system design

	Structural design	Monitoring system design
Objective	Structural stability with adequate safety	Knowledge of structural state with adequate confidence
Design target	Actions	State knowledge accuracy
Demand	Stress/deformation	Measurement accuracy
Model	Relationship between stress and actions	Relationship between state variables and measurements
Capacity	Resistance/deformation capacity	Sensor accuracy
Limit state	Stress/deformation < resistance/deformation capacity	Measurement accuracy demand < sensor accuracy
Performance metric	Probability of failure	Probability of state misidentification

3.3.3 *Information as a state variable*

Information provided by a monitoring system can be related or not to the state of condition of the structure. In the former case, the state of the structure must be represented by the system quantitatively and univocally by a state variable or parameter. A state variable is defined here as a logical or numerical representation of the state of the structure provided by the system.

A state variable can assume:

- (i) a binary form, that is the state variable can assume only two values. Examples: yielded or not yielded, cracked or uncracked, maximum load exceeded or not exceeded;
- (ii) a discrete form, that is the state variable can assume a set of discrete numerical or descriptive values. Example: slight, moderate, or severe damage;
- (iii) the value of a response parameter. Examples: maximum displacement, maximum interstorey drift, forces, strains, deflection;
- (iv) the value of indicators highlighting the variations of structural parameters induced by the earthquake, such as flexibility-based damage indices;
- (v) the value of indicators taking into account a set of response parameters and structural parameters, such as cumulative damage indices.

3.3.4 *Accuracy of the information*

The most important design requirement is the accuracy of the information provided by the system. The effectiveness of a monitoring system depends in fact on the reliability of the information provided. Aiming to the design of a system, it is necessary to specify the accuracy in which the information has to be provided. It is worth noting that the defined accuracy must take into account all uncertainties involved in the process linking the observations and the information. In other terms, also the uncertainties related to the model must be considered, being the model related or not to the monitored structure. This concept can be clarified by an example. Assume the information to be the displacement of the roof of a building over time and observations to be the displacements of the same point collected by a GPS station. In this case, accuracy of the information (the point displacement) depends on the model, possibly including environmental effects, linking GPS raw data and the point displacement. On the other hand, assuming the information to be the bending moment at the bottom end of a column of the same building, the model linking the observations to the information shall include also a formula, with its uncertainty, linking displacement of the roof to the bending moment. The accuracy can be expressed in different terms depending on the nature of the information. When the information is a classification (binary form, discrete form) the simplest method to describe the accuracy is the probability of misclassification, which is the maximum passable frequency of wrong state identifications, expressed in form of a confusion matrix (Mitchell 2010). For the particular case of the binary classification, an alternative method is the probability of “false positives” (or errors of the first kind, the probability of identifying the structure as “unsafe” when it is “safe”) and “false

negatives” (or errors of the second kind, the probability of identifying the structure as “safe” when it is “unsafe”).

For a parameter, the uncertainty can be defined in terms of the maximum variance between the estimated value of the parameter and its true value, of the percentage error between the estimated value of the parameter and its true value, or of the standard deviation of the parameter.

3.3.5 *Choice of the monitoring strategy*

Having defined the requirements on the accuracy of the information provided by the monitoring system, the following task in system design is the choice of the measurement strategy. The measurement strategy is the set of techniques and methods we use to estimate the value of the information from the set of observations recorded by the sensors. The accuracy of the information provided depends in fact on the instrumental uncertainties (i.e. related to the sensors and to measuring chain) and on the uncertainties of the model (e.g. numerical errors, incompleteness of the model, uncertainties of the classifier, etc.).

The choice of the measurement strategy depends therefore on the required accuracy and includes:

- the choice of the physical quantity to be observed, including number and location of the measurements and sampling frequency;
- the choice of the inferring model;
- the choice of the components of the system, including sensors, data transmission equipment, data acquisition devices.

3.3.6 *Comparison between capacity and demand*

Instrumental uncertainties including the whole measuring chain from physical quantity to digital values must be combined to uncertainties related to the model used to link observations to information. A prior knowledge of single uncertainties related to each system component can be obtained from data sheets or from laboratory evaluation following available guidelines, for example (JCGM 2008). These uncertainties must be combined to the model –related uncertainties. The resulting value represent the capacity, in terms of accuracy of the information, of the designed system. If the capacity is lower than the demand, that is the requested accuracy of the information, the measuring strategy must be modified. On the contrary, if the capacity is higher than the demand, specifications of the system can be compiled.

3.4 Choice of the state variable

3.4.1 *Reliability of the state variable to be provided*

The information provided by a seismic monitoring system can be related or not to the state condition of the monitored structure. In the latter case, the information is a state variable. A state variable is defined as a variable or parameter which can be used to estimate the state condition, commonly by means of a classification in terms of damage, of the monitored structure after a seismic event.

The whole design process of a seismic monitoring system and particularly the definition of the objectives and the choice of the state variable is strictly dependent on the knowledge of the designer about the structural behavior of the structure to be monitored and on the expected response of the building to the earthquake. In other words, the designer of the system must be aware of the possible failure mechanisms and of the possible damage location. These are particularly straightforward in the case of the design of monitoring systems to be installed in recent buildings or in recently retrofitted buildings.

According to the deformation-based approach of design, to the performance-based design, and to the principle of capacity design (Priestley, Calvi, and Kowalsky 2007), on which current design codes are based, the structures including reinforced concrete buildings cannot sustain seismic demand remaining in the elastic field. Rather, structures have to dissipate energy developing large inelastic deformations without collapse. This implies that also structures compliant to the seismic codes are expected to sustain a certain amount of damage during a strong earthquake. The design of a new reinforced concrete structure or the design of retrofitting for existing ones implies therefore the establishment of a global failure mechanism which has to be as much ductile as possible (Priestley, Calvi, and Kowalsky 2007). The capacity design principle implies moreover that inelastic deformations should occur in the highest possible number of ductile elements and not in brittle ones, and that overstrength to undesired failure mechanism should be provided (Pauley and Priestley 1992). These concepts entail a set of prescriptions such as providing members a shear strength higher than flexural strength in order to avoid brittle shear failure, or avoiding column-sway mechanism developing inelastic deformations in beams rather than in columns (Figure 3-2).

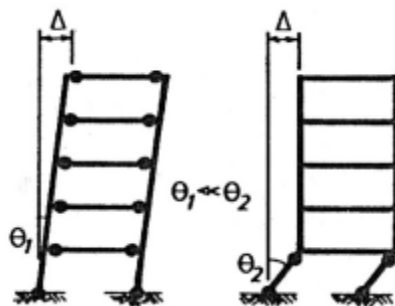


*Figure 3-2 – Energy-dissipating mechanism.
From (Pauley and Priestley 1992)*

Prescription are also provided to increase ductility capacity at material level, element level and structural level (Ricci 2010). At material level, for example, highest ductility is obtained increasing concrete confinement, this in turns achieved by an adequate design of transverse reinforcement in terms of spacing and detailing. At element level, an increase in ductility can be achieved by adequate construction detailing. A structural level, it is well known that a regular distribution of stiffness and mass is critical to avoid the concentration of inelastic demand.

The design of a seismic monitoring system for buildings should implies the knowledge of all these aspects concerning structural behaviour, when the objective of the system is providing an information related to the state of condition of the monitored. For example, a system providing an information related to safety (e.g. safe or not safe) based on ductility demand cannot be reliable (and usable) if shear failure or concentration of inelastic demand are possible but not taken into account.

Contextually to the design of seismic monitoring systems, a preliminary study of the structure performed in accordance with the principles on which seismic assessment of existing buildings is based should be performed. Eurocode 8-3 explicitly deals with this problem. The assessment is based on the fact that the building must satisfy different performance levels depending of the intensity of the earthquake. The code refers to the state of damage in the structure, defined through three Limit States (LS) namely: Near Collapse (NC) Significant Damage (SD) and Damage Limitation (DL).

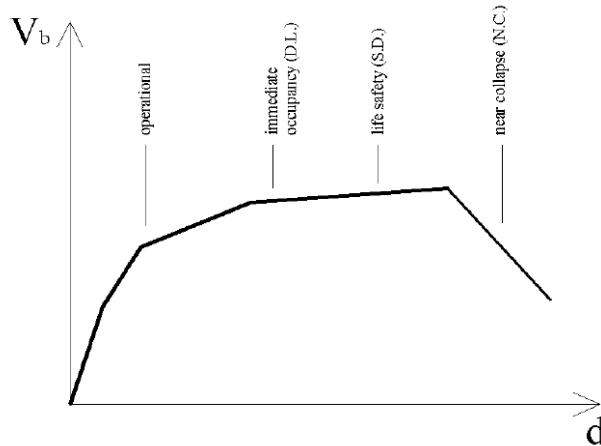


*Figure 3-3 – Performance levels and limit states, from
(MPampatsikos 2008)*

For the verification of the structural elements a distinction is made between ductile and brittle behaviour. Ductile elements are verified by checking that demand does not exceed the corresponding capacities in terms of deformations. Brittle elements are verified by checking that demand do not exceed the capacities in terms of strength. For the calculation of capacities, mean value properties of materials shall be used, appropriately divided by the confidence factors which depends on the

knowledge level. In the code it is stated that in assessing the resistance of existing structures the input data should be collected from: (i) available documentation specific to the building in question; (ii) generic data sources (iii) field investigations; (iv) in-situ and laboratory tests. All the following information should be obtained and should in my opinion be part of the monitoring system design process:

- a) identification of the structural system and of its compliance with regularity criteria from on-site investigation or from original design drawings;
- b) identification of the type of foundations;
- c) identification of the ground conditions;
- d) information about cross-sectional properties of structural elements and on materials;
- e) information about defects and detailing;
- f) information on the seismic design criteria;
- g) definition of the importance class of the building;
- h) information about past and present structural damage;

3.4.2 *Seismic damage in RC buildings*

Actual damage in the building varies as a continuous function of earthquake demand but commonly one of several damage states describing damage (for example slight, moderate, extensive and complete damage) and directly related to structure performance levels (for example fully operational, operational, life safe, near collapse) is used to express the state of a building after a seismic event. Damage induced by earthquakes can occur on structural elements (mainly beams and columns) and on non-structural elements (partition walls, claddings, content). Damage on structural elements is strictly related to casualties and catastrophic loss of functionality, while damage on non-structural elements induces mainly economic loss. Non-structural elements are sensitive to lateral displacement in general and to interstory drift or story drift ratio in particular (e.g. partition walls directly connected to the structure) or to acceleration (claddings and content).

Total damage in reinforced concrete structures and components depends on a number of factors such as the accumulation and distribution of damage, failure modes, number of sustained inelastic cycles and the ground motion characteristics. Given the uncertainties involved on post-seismic damage estimation, a probabilistic approach appears to be more consistent than a deterministic one. Introducing fragility functions it is possible to estimate the probability of damage function of the seismic demand. Fragility functions represent the probability of exceeding a damage limit state for a structure subjected to a seismic excitation and involve uncertainties associated with structural capacity, earthquake intensities and damage limit-state definition. The probability of being in a particular state of damage is calculated as the difference between fragility functions (Ruiz-Garcia and Miranda 2003).

3.4.3 *Damage indices for RC structures*

Damage in structural elements is generally related to cracking and subsequent crushing first of the concrete cover (spalling) and later of the confined core. Other failure modes can precede crushing of the concrete core, such as buckling or fracture of the longitudinal reinforcing bars, fracture of the stirrups or loss of anchorage. Anyway damage in reinforced concrete is typically related to inelastic deformations. For this reason, both state variables and damage index are often related to deformation quantities (strain, curvature, displacement) or dissipated energy. Damage and eventually failure in RC structures are due to the interaction between the failure mechanism related to peak deformation demand and the failure mechanism related to fatigue.

A damage index is a numerical value assuming zero value when no damage occurs and a value of 1 when failure of the element or of the structure occurs. Damage indices can be classified into local damage indices (damage in a single member or at a joint) and global damage indices (overall damage on the structure). Local damage indices can be further classified into non-cumulative indices and cumulative indices, the difference being to consider or not the effect of repeated cycles. Some of the most used damage indices are briefly reported in the following. Others damage indices were proposed in the literature. An extended state of the art review on damage indices for reinforced concrete structures is reported in (Williams and Sexsmith 1997) while concepts involved in defining damage indices for RC buildings are referenced in (Kappos 1997).

The first used damage index is ductility (Newmark and Rosenblueth 1974). Ductility can be expressed in terms of curvature, rotation or displacement and is defined as the ratio of the maximum curvature/rotation/displacement ($\theta_m, \phi_m, \delta_m$ respectively) by the yield value. In order to obtain a damage index which is equal to 1 at failure, maximum curvature/rotation/displacement values are normalized by the ultimate instead of the yield value ($\theta_u, \phi_u, \delta_u$ respectively):

$$\mu_\theta = \frac{\theta_m}{\theta_u} \quad (3.1)$$

$$\mu_\phi = \frac{\phi_m}{\phi_u} \quad (3.2)$$

$$\mu_\delta = \frac{\delta_m}{\delta_u} \quad (3.3)$$

Most of the times ductility is expressed in terms of peak ductility demand during the earthquake. An example of peak ductility demand is the value of peak interstory drift ratio. The interstory drift ratio is defined as the difference between the displacements of two consecutive floors, divided by the story height. It is also possible to express ductility in terms of residual drift or permanent deformation of structural members. It was proven in fact that residual drift value influences not only the costs related

to post-earthquake structural refurbishment, but also the safety perceived by the occupants, physical ailments, the ability to evacuate the structure, and structural functionality in general (McCormick et al. 2008). The advantage of using ductility as the damage index is its simplicity and the possibility to design a monitoring system able to provide ductility demand. The draw-back is that it totally neglects the effects of repeated cycles.

In (Banan and Veneziano 1982) it is proposed to consider in the damage indices both contributes of stiffness degradation and cumulative plastic rotations, defining a damage function as:

$$\begin{aligned}
D &= f(FDR, NCR) \\
FDR &= \frac{K_i}{K_r} \\
NCR &= \frac{\sum_{i=1}^{nc} |\theta_i|}{\theta_y}
\end{aligned} \tag{3.4}$$

being FDR the ratio between initial and secant stiffness, NCR the normalized cumulative rotation, θ_i the plastic rotation during the i -th cycle, θ_y the yield rotation and nc the number of cycles.

A different approach is to relate structural damage in a member to stiffness degradation, how proposed for example in (Roufaiel and Meyer 1987). In this paper a damage index named MFDR (Modified Flexural Damage Ratio) is defined as:

$$MFDR = \frac{\frac{\phi_x}{M_x} - \frac{\phi_y}{M_y}}{\frac{\phi_f}{M_f} - \frac{\phi_y}{M_y}} \tag{3.5}$$

where ϕ_x / M_x is the minimum secant stiffness reached during the earthquake, ϕ_y / M_y is the secant stiffness at yielding, ϕ_f / M_f is the secant stiffness at failure of the member. This index is equal to zero below yielding and equal to 1 at failure. Calculating this index for post seismic damage assessment based on structural health monitoring implies strain monitoring (to estimate curvatures) and the prior definition of the moment-curvature relationship for all members.

The damage index proposed in (Stephens and Yao 1987) considers the effects of cumulative plastic deformation occurred during the earthquake. In particular, the damage sustained by a member during each cycle of response is:

$$\Delta d_i = \left(\frac{\Delta \delta^+}{\Delta \delta_f} \right)^{1 - \frac{b \Delta \delta^-}{\Delta \delta^+}} \tag{3.6}$$

being $\Delta \delta^+$ the positive change in plastic deformation in cycle i , $\Delta \delta^-$ the negative change in plastic deformation in cycle i , $\Delta \delta_f$ the positive change in plastic deformation in a single cycle test to failure, b a constant. The total damage due to n cycles is:

$$D = \sum_{i=1}^n \Delta d_i \tag{3.7}$$

Tests on small scale RC frames, described in the paper, highlighted that up to damage classified as “light” the scatter of the damage index by Stephens and Yao is very low. For damage classified as “near-collapse” values of the index differ each other up to 600%. This was confirmed also with the application of the method to a real building. In principle, this method can be used for damage assessment based on structural health monitoring, but the high uncertainties related to b coefficient (dependent on the member) and on the value to be used for $\Delta\delta_f$ discourage its application.

The damage index proposed in (Park and Ang 1985) is certainly the most famous cumulative damage index in the literature and its parameters were calibrated by numerous researcher for various types of structures. It was proposed both as local damage index and as a weighted global damage index. It is defined as:

$$D = \frac{\delta_m}{\delta_u} + \beta \frac{\int dE}{F_y \delta_u} \tag{3.8}$$

The first term is the maximum deformation reached divided by the ultimate deformation capacity under static loading. The second term represents the effect of dissipated energy on the accumulated damage. In particular, the integral is the total hysteretic energy absorbed, while β is a coefficient taking into account the effect of cyclic loading. Typical classification for the thresholds between limit states is:

Table 3-3 – Park & Ang damage index thresholds

D	Damage
$D < 0.1$	No damage
$0.10 < D < 0.25$	Minor damage
$0.25 < D < 0.40$	Moderate damage
$0.40 < D < 1.00$	Severe damage
$D = 1.00$	Collapse

In (Di Pasquale and Cakmak 1987) is proposed a damage index which is independent from the ultimate characteristics of the structure, depending only on structural parameters which can be obtained by instrumental measurements. In particular, they propose a two-dimensional global damage space which takes into account peak deformation and fatigue contributes to damage, both relating to stiffness degradation. Stiffness degradation of some elements results in fact in a decrease of the global stiffness, which can be highlighted monitoring fundamental period over time of shaking. The approach is as follows: the interval of duration of the seismic event is divided into n windows and for each of these windows the fundamental period is estimated. Damage indices for the two contributes are calculated basing on fundamental period evolution. The contribution of the peak deformation named maximum softening is calculated as:

$$D_M = \max_{i=1,n} \frac{T_i - T_0}{T_0} \quad (3.9)$$

where T_i is the fundamental period computed in the i -th time window and T_0 is the initial fundamental period. The contribute of fatigue named cumulative softening is calculated as:

$$D_E = \sum_{i=1}^n \frac{T_i - T_0}{T_0} \frac{s_i}{T_i} \quad (3.10)$$

being s_i the amplitude of the cycle. Maximum softening parameter was compared to ductility index (in terms of displacements) and cumulative softening was compared to energetic terms of Park & Ang damage index demonstrating both a correlation factor close to the unity with the corresponding indices.

3.4.4 *Displacement-based damage assessment*

In performance-based structural health monitoring, drift values resulting from monitoring are used to estimate damage in structural and non-structural components (Porter, Mitrani-Reiser, and Beck 2006). Drift and interstory drift values are commonly used in structural design process to ensure an acceptable deformation and in order to limit P- Δ effects and damage to non-structural components (partition walls, windows, etc.). In linear elastic design procedures, drift values taking into account structural linear response are computed multiplying drift value obtained from elastic design by an amplification factor which depends on the structure (Priestley, Calvi, and Kowalsky 2007). Using non-linear procedures, the result of these is the maximum expected drift and no amplification is needed.

The most common format for the definition of limit states for earthquake resistant structures is as follows: (i) serviceability limit state mandates that the building remains elastic and very low damage occurs, in particular stress is less than yield and drifts are less than thresholds related to non-structural elements; (ii) damageability limit state entails that stresses are slightly higher than elastic limit, drifts are higher than thresholds related to non-structural elements, so limited damage to structural and non-structural elements occurs, but the structure is still repairable; (iii) ultimate limit state implies that severe structural damage occurs with plastic rotations at plastic hinges; thresholds on drift values are driven by stability check. In Italy (CNR-DT 212-2013), severe damage limit states implies that a drop of the lateral strength of the building occurs and that the entity of damage is high enough to make the structure not repairable; collapse prevention limit state implies that severe damage to structural elements occurs and that the residual lateral strength of the building is negligible. Eurocode 8 defines two limit states only. Damage limitation requirement is satisfied if interstory drift ratio is lower than (i) 0.005 for buildings having brittle non-structural elements (ii) 0.0075 for buildings having ductile non-structural elements (iii) 0.010 for buildings having non-structural elements not interfering with structural deformation or without non-structural elements. No-collapse requirement is considered to

be met if conditions on resistance (4.4.2.2.), ductility (4.4.2.3) and equilibrium (4.4.2.4) are met. Anyway no limits on drift or displacements are provided. The same limitations on interstory drift ratio reported on Italian standards (NTC 08) for the serviceability limit state. Slightly different limitations are provided in (Sullivan, Priestley e Calvi 2012) for the first two limit states (level 1, serviceability for which only insignificant damage is expected and level 2, damage control for which damage is still economically repairable):

Table 3-4 – Peak drift ratios limitations for RC structures as reported in (Sullivan, Priestley, and Calvi 2012)

Drift limit	Level 1	Level 2	Level 3
brittle NS elements	0.004	0.025	No limit (control P-D effects)
ductile NS elements	0.007	0.025	No limit (control P-D effects)
detailed NS elements	0.010	0.025	No limit (control P-D effects)

Table 3-5 – Residual drift ratios limitations for RC structures as reported in (Sullivan, Priestley, and Calvi 2012)

Residual drift limit	Level 1	Level 2	Level 3
Buildings	0.002	0.005	No limit

Anyway it is worth emphasising that the values reported above are in general conservative and in any case related to design. To relate measured lateral displacements to performance of the RC columns hence to their state, it is necessary to define threshold values of displacements corresponding to different performance levels. Current codes for seismic design report values of member stiffness which overestimates actual member stiffness, this being safe for force-based design but unsafe for displacement-based design or damage assessment. A number of studies, most of them concerning displacement based seismic design, were carried out to give engineers practical formulas for the estimation of deformation of reinforced concrete members corresponding to different performance levels, which is governed by limiting material strain (Priestley, Calvi, and Kowalsky 2007). In particular, fixing concrete and reinforcing steel limit stains ($\epsilon_{c,ls}$ and $\epsilon_{s,ls}$ respectively) it is possible to calculate corresponding limit state curvatures:

$$\phi_{ls,c} = \frac{\epsilon_{c,ls}}{c} \quad (3.11)$$

$$\phi_{ls,s} = \frac{\epsilon_{s,ls}}{(d-c)} \quad (3.12)$$

being c the neutral axis depth and d the effective depth of the section. The displacement can be estimated by the expression (Priestley, Calvi, and Kowalsky 2007):

$$\Delta_{d,ls} = \Delta_y + \Delta_p = \phi_y \frac{(H + L_{sp})^2}{3} + (\phi_{ls} - \phi_y) L_p H \quad (3.13)$$

where H is the column high, L_{sp} represents strain penetration effects, L_p is the plastic hinge length. It was demonstrated that yield curvature ϕ_y basically does not depend on reinforcement content and axial load level but only on yield strain and effective section depth. For rectangular concrete columns yield curvature can be estimated as (Priestley, Calvi, and Kowalsky 2007):

$$\phi_y = 2.10\epsilon_y / h_c \quad (3.14)$$

Yield curvature can be used to approximate displacement at yielding Δ_y of vertical cantilevers:

$$\Delta_y = \frac{\phi_y (H + L_{sp})^2}{3} \quad (3.15)$$

where L_b is the span.

Equation (3.15) does not take into account shear contribution to overall deflection and the effect of slippage. More adherent expressions for the deformation at yielding and, also, for the ultimate deformation capacity are reported in (Panagiotakos and Fardis 2001). These expressions are based on database comprised of 682 monotonic and cyclic tests of RC column members in uniaxial bending. The following relation for the chord rotation at yielding was statistically fitted to the results of the tests:

$$\theta_y = \frac{\phi_y L_s}{3} + 0.0025 + a_{sl} \frac{0.25\epsilon_y d_b f_y}{(d - d') \sqrt{f'_c}} \quad (3.16)$$

The expression takes into account in the second member the shear distortion of the shear span at flexural yielding, which can be considered as constant respect to the parameters. The third term is due to slippage, being a_{sl} a binary coefficient which is 1 if slippage of longitudinal steel is possible and 0 if it is not. The statistical distribution of the ratio between experimentally observed and calculated by Eq. (3.16) chord rotation at yielding shows a mean value of 1.06 (that is, Eq. (3.16) underestimates the observed value) and a coefficient of variation equal to 36%. It can be seen in the figures reported in the paper that extreme values of the ratio reach also 250% (i.e. 1% predicted, 2.5% observed or 1.5% predicted, 0.5% observed).

3.5 An example: design of seismic structural health monitoring systems

Two cases of monitoring system design are discussed qualitatively in order to clarify the concepts of the previous sections. The first is the design of a monitoring system where the objective is the

knowledge of the maximum displacement sustained by a generic columns. The second instead is a monitoring system where the objective is to know if the column is yielded or not at the end of the seismic motion.

3.5.1 *Objective*

- (1) To know the maximum displacement experienced by a column during an earthquake;
- (2) To know if the longitudinal reinforcement steel at the base of the column is yielded or not after the seismic motion.

3.5.2 *Choice of the information or state variable*

- (1) Maximum absolute value of the time history of displacement experienced by the column during the earthquake (response parameter);
- (2) Binary classification where one class represents the not-yielded state of the column and the other one its yielded state.

3.5.3 *Definition of the accuracy demand*

- (1) Accuracy of 1.0 cm in terms of standard deviation of the estimation of the maximum absolute value of displacement;
- (2) Accuracy of 10^{-2} in terms of probability of misclassification of the yielded state (i.e. the probability of classify the column as not-yielded when it is yielded is 10^{-2}).

3.5.4 *Choice of the monitoring strategy*

- (1) Real-time monitoring of accelerations at the top end of the column using an accelerometer and computation of displacement time history from numerical double integration. Computation of the maximum absolute value of the displacement time history;
- (2) Real-time monitoring of accelerations at the top end of the column using an accelerometer and computation of displacement time history from numerical double integration. Computation of the maximum absolute value of the displacement time history. Comparison between this value and the value of displacement at yielding resulting from a (chosen) structural model of the column;

3.5.5 *Computation of the uncertainties related to instrumental errors*

- (1) Computation of uncertainties related to the accelerometer, influenced by cables, and to the acquisition unit.
- (2) Same as above.

3.5.6 *Computation of the uncertainties related to the model*

- (1) Computation of uncertainties related to the model used to obtain the maximum displacement value from acceleration measurements (e.g. errors introduced by signal processing, numerical integration etc.);
- (2) Computation of uncertainties related to the model used to obtain the maximum displacement value from acceleration measurements and estimate of the uncertainty related to the structural model of the column (i.e. estimate of the reliability of the formula).

3.5.7 *Computation of the accuracy capacity*

- (1) Capacity is calculated considering uncertainties related to the measuring chain and to the model linking acceleration measurements to the maximum displacement;
- (2) Capacity is calculated considering uncertainties related to the measuring chain, to the model linking acceleration measurements to the maximum displacement, and to the structural model used to classify the state of the column.

3.5.8 *Capacity < Demand: how to modify the monitoring strategy*

- (1) Increase capacity by selecting system components with better performance and/or tuning the model used to estimate the maximum displacement value from acceleration measurements;
- (2) Increase capacity by selecting system components with better performance and/or tuning the model used to estimate the maximum displacement value from acceleration measurements and/or adopt a more refined structural model for the state classification.

3.6 Conclusions

The design of a structural health monitoring system is, like the design of a civil structure, a logical process consisting on the definition of a demand to be compared to a capacity. In monitoring design the demand can be expressed in terms of the accuracy of the information that the system is expected to provide, while the capacity is the accuracy of the information actually provided. In this Chapter I discussed a logical framework for the process of system design, identifying the following steps: (i) objective definition and choice of the information; (ii) definition of the demand of accuracy; (iii)

choice of the monitoring strategy, including choice of the system components, sensors number and location, sampling frequency, models linking observations and information; (iv) computation of all uncertainties involved in the process; (v) definition of the capacity of accuracy; (vi) comparison between demand and capacity. Then I applied qualitatively the framework to two examples of design of seismic monitoring systems, showing the different approach to be used when the objective of monitoring is, or it is not, the knowledge of a structural parameter or classification instead of a parameter independent to the structure. I remark here that the full knowledge of the real physical state is impossible to obtain from a monitoring system, due in particular to epistemic uncertainties involved in the assessment process. Factors as members' geometry and construction details may introduce high uncertainties in the state estimation and may imply also catastrophic consequences. For example, a monitored system based on ductility measurements would provide information on the damage state related to flexural capacity only, but no information are provided about a possible shear failure. Thus, when the objective of monitoring is the knowledge of a structural parameter or a state condition, one should remember that the information actually provided by the monitoring system is not related to the physical state of the monitored building, but rather to a set of conventional thresholds depending on the prior knowledge of the system designer of the structure.

4 Uncertainty analysis of drift estimation using acceleration measurements

4.1 Introduction

The process of estimate of structural drift values from acceleration measurements only is an error prone process involving uncertainties related to different sources.

In this chapter I carry out the analysis of uncertainties in the process of drift estimation from acceleration measurements only. First, general concepts of uncertainties of measurements are introduced and the formal steps needed to estimate drift values from acceleration measurements are reminded. Following the definition of the most important uncertainties related to the process, each of them are investigated. In particular I study how instrumental uncertainties propagate through double integration process and the dependence of uncertainty in the estimation of displacements on the ratio between frequency of the first mode of vibration and the low limit of the band-pass filter and on the residual displacement.

4.2 The concept of uncertainty in measurements

“Uncertainty of a measurement” may mean doubt about the validity of the result of a measurement (general concept) or may mean the quantitative measures of this concept (for example, standard deviation). The formal definition of uncertainty is (JCGM 2008):

“Parameter (for example a standard deviation or the half-width of an interval having a stated level of confidence), associated with the result of a measurement, that characterizes the dispersion of the values that could reasonably be attributed to the measurand”.

Therefore the concept of uncertainty is different from the concept of error. Measurement uncertainty is an estimate of the error in a measurement, that is, it represents a range of possible value that the error of a measurement can assume. Measurement error is instead the difference between the true value and the measured value (Dunn 2010).

Uncertainty of a measurement can be evaluated following two different methods (JCGM 2008). Type A evaluation of uncertainty is the method of evaluation of uncertainty by the statistical analysis of a series of observations. Uncertainty is thus obtained from a probability density function derived from an observed frequency distribution. In fact, in most cases the best estimate of the expected value μ_q of a quantity q varying randomly (i.e. a random variable) for which N independent observations q_k have been obtained from testing is the arithmetic mean \bar{q} of the observations (JCGM 2008):

$$\bar{q} = \frac{1}{N} \sum_{k=1}^N q_k \quad (4.1)$$

The experimental variance of the observations is instead the best estimate of the variance σ^2 , which represents the variability of the observations respect to the mean, of the probability distribution of q (JCGM 2008):

$$s^2(q_k) = \frac{1}{N-1} \sum_{j=1}^N (q_j - \bar{q})^2 \quad (4.2)$$

The best estimate of the variance of the mean $\sigma^2(\bar{q}) = \sigma^2 / N$ quantifies how well \bar{q} estimates the expectation of μ_q of q and is given by (JCGM 2008):

$$s^2(\bar{q}) = \frac{s^2(q_k)}{N} \quad (4.3)$$

Type B evaluation of uncertainty is instead the method of evaluation of uncertainty of quantities that has not been obtained from repeated observations. Uncertainty is obtained from an assumed probability density function based on the prior knowledge on the process of measure. In particular, the uncertainties are evaluated basing on previous measured data, previous experience, manufacture’s specifications, data provided in certificates, and so on.

In this Chapter both the methods are used; anyway often only Type B evaluation can be performed in the computation of uncertainties in the design process of a monitoring system.

Uncertainty is strictly related to the concept of error of measurement. Traditionally, errors have been classified in random errors and systematic errors (Morris and Langari 2011). Random errors arise from unpredictable or stochastic temporal and spatial variations of parameters influencing the measuring process. These variations are termed random effects, and cause variations in repeated observations of the measurand. The expected value (mean) of random errors is zero (JCGM 2008). Random errors affects the precision of a measurement (Dunn 2010). Systematic errors arise from systematic effects influencing the measuring process (Morris and Langari 2011). Systematic errors, if recognized through the process of calibration, can in principle be compensated applying a correction function or a correction factor to the measurement. Systematic error affects the accuracy of a measurement (Dunn 2010).

If all of the quantities on which the result of a measurement depends are varied performing in this way a sensitivity analysis, the uncertainty of the measurement can be evaluated by statistical means. This is however impossible in practice, so the uncertainty of a measurement result is evaluated using a mathematical model of the measurement and the law of propagation of uncertainty or using the Monte Carlo method). The mathematical model must be as complete as possible to fulfil the accuracy requirements. The mathematical model consists in general of a functional relationship between the measurand Y (not measured directly) and N other parameters:

$$Y = f(X_1, X_2, \dots, X_N) \quad (4.4)$$

The input quantities may themselves be measurands and may depend on other quantities. Further, f may be determined experimentally or may exist as an algorithm.

If the functional relationship f can be expressed explicitly that is f is a mathematical function, uncertainty on the measurement y of measurand Y can be estimated using the law of propagation of errors. When all input quantities are independent the standard uncertainty of y where y is the estimate of the measurand Y is obtained combining the standard uncertainties of the input estimates x_1, x_2, \dots, x_n . The combined standard uncertainty is the positive square root of the combined variance which is given by the law of propagation of uncertainty (JCGM 2008):

$$\sigma(y) = \sqrt{\sum_{i=1}^N \left(\frac{\partial f}{\partial x_i} \right)^2 \sigma^2(x_i)} \quad (4.5)$$

The partial derivatives are computed at $X_i = x_i$ (expected value) and are often called sensitivity coefficients describing how the output estimate y varies with changes in the value of the input estimates.

4.3 Displacements computation from acceleration measurements

The most common method to obtain displacements and interstory drift ratio values from seismic monitored buildings is the numerical double integration of acceleration data only.

The algorithm is not new, and it is also currently used by strong instrumentation program to provide structural displacements of monitored building (Consortium of Organizations for Strong-Motion Observation Systems 2009). There is however a lack of consensus in the literature about the formal steps needed to estimate displacements time histories starting from acceleration measurements only. In particular, differences between different approaches are related to the necessity of high-pass filtering velocity time histories. For example in (Paolucci et al. 2011) Italian ITACA procedure is described. It consists of the following steps:

1. Read acceleration time histories;
2. Detrend acceleration time histories;
3. Pad the beginning and end of acceleration time histories;
4. Apply band-pass acausal Butterworth filter to acceleration time histories;
5. Strip off the padded portions of acceleration time histories;
6. Integrate numerically the acceleration to obtain velocity;
7. Detrend velocity time histories;
8. Integrate numerically the velocity to obtain displacement;
9. Detrend displacement time histories.

In (D. M. Boore, Azari Sisi, and Akkar 2012) the PEER NGA Procedure is reported. In this procedure, a 6-th order polynomial is fitted to the displacement trace after double integration of acceleration time histories, the second derivative of the polynomial is subtracted to the acceleration time histories and the so corrected time histories are double integrated to obtain corrected velocity and displacement time histories.

In both case (Paolucci et al. 2011; D. M. Boore, Azari Sisi, and Akkar 2012) the goal of the procedures is to obtain PGA, PGV and PGD values and response spectra, and not a structural drift estimation.

The procedure of structural drift estimation when hypothesis of diaphragm behaviour of the floor is valid is described in (D. Skolnik and Wallace 2010) and in (D. A. Skolnik, Nigbor, and Wallace 2011). The procedure consists of the following steps (Figure 4-1):

1. Read acceleration time histories;
2. Acceleration signals processing (baseline correction, zero-padding signal ends, band-pass filtering);
3. Displacement time histories estimation from double numerical integration of processed acceleration time histories;

4. Computation of the floor displacements;
5. Computation of the interstory drift.

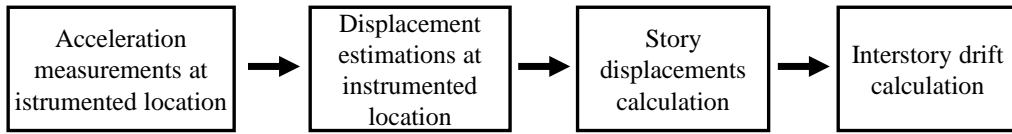


Figure 4-1 – Steps of the algorithm for interstory drift calculation

4.3.1 Displacement estimations at instrumented locations

In principle, numerical double integration of acceleration measurement is a simple task and can be performed calculating first velocity time histories and then displacement time histories performing numerical integration using for example the trapezoidal rule or other integration techniques. Discrete measurements of acceleration $a_i = a(t_i)$ are recorded by accelerometers at time t_i with a sampling interval Δt . Velocities $v_i = v(t_i)$ are computed by means of a first numerical integration and displacement $d_i = d(t_i)$ are estimated by means of a second numerical integration. Well-known expression relative to the trapezoidal rule for numerical integration are:

$$v_i = v_{i-1} + \frac{\Delta t}{2}(a_{i-1} + a_i) \quad (4.6)$$

$$d_i = d_{i-1} + \frac{\Delta t}{2}(v_{i-1} + v_i) \quad (4.7)$$

Indeed, displacement estimation at instrumented locations from acceleration measurements require a number of signal processing operations, such as baseline correction, zero-padding, low-pass filtering and high-pass filtering (D. Skolnik and Wallace 2010). These steps are briefly discussed below:

Baseline correction

Baseline correction of the acceleration measurements is required to the fact that often acceleration signals have an offset at their start, this due mainly to temperature fluctuations, instrument bias drift over time, and supply voltage drift over time. Baseline shift is an issue in monitoring systems where data is recorded on trigger (for example when acceleration measurements are higher than a threshold). In these system, an automatic periodic baseline cancelling is needed.

When a baseline correction is needed, this is performed by subtracting the pre-event mean of acceleration data to the whole signal. It is therefore important to always maintain in memory a data buffer of a few seconds to perform this task.

Low-pass filtering

Low-pass filtering is needed in order to increase signal-to-noise ratio (SNR) of the signal, which is to reduce the influence of noise (instrumental, environmental) on the signal's quality. This task is particularly important for low-cost noisy instruments and when the instruments are installed in a noisy environmental (for example an industrial building). Considering again the case of a monitoring system in which data is recorded on trigger, in order to set low values of threshold an high SNR value is required, minimizing so the probability of false alarms. Drawback of low-pass filtering is the loss of high frequency information on the signal, and a decrease of the signal amplitude.

High-pass filtering

Baseline correction briefly presented above removes constant baseline shift but does not remove varying baseline shift in acceleration signals, which are due to a number of factors (D. Skolnik and Wallace 2010), including electrical and mechanical effects, misalignment, cross-axis sensitivity and A/D conversion process. Whatever the source of varying baseline shift, the effect on displacement estimation procedure is a linear trend on the velocity signals and a quadratic trend in displacement signals, if equations (4.6) and (4.7) are directly applied.

Low-pass filtering

The low-pass filtering is the most important task in the process of displacement estimation from acceleration measurements. All acceleration and velocity signals must be processed using the same filter parameters in order to avoid to introducing phase delays between displacement signals. Displacement values are strictly dependant on the choice of filter's cut-off frequency, in particular for high-flexibility structures. Moreover, remove frequencies from DC to the cut-off frequency implies that all information about possible residual displacements at the end of the seismic motion are loss.

Zero padding

Zero padding refers to adding zeros at both the signal ends in order to accommodate filter (in particular high-pass ones) transients.

The process of estimate of structural drift values from acceleration measurements only is an error prone process involving uncertainties related to different sources. In accordance to the framework for the design of a monitoring system discussed in Chapter 3, two main sources of uncertainties must be computed for the determination of the capacity of accuracy of the system:

- (1) uncertainties related to the instrumental errors;
- (2) uncertainties related to the model linking observations and information.

Both these sources are investigated in the following sections.

4.3.2 Story displacement calculation

Assuming that floor diaphragm is rigid, its degrees of freedom are three (translation in x direction, translation in y direction, rotation θ around geometric center, Figure 4-2) and neglecting the importance of redundancy, only three sensors are necessary.

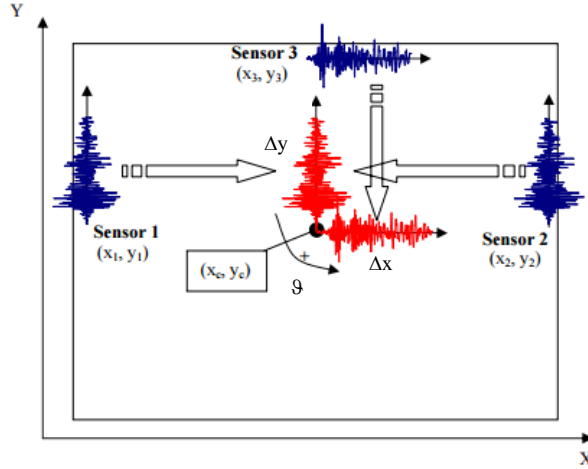


Figure 4-2 . Story displacement calculation, adapted from (Naeim et al. 2005)

Let assume that the floor in Figure 4-2 has three sensors with coordinates (x_1, y_1) , (x_2, y_2) and (x_3, y_3) which estimate displacement time histories $d_1(t)$, $d_2(t)$ and $d_3(t)$. Let assume also that the geometric center of the floor has coordinates (x_c, y_c) . The relation between displacements at sensor location and displacements and rotation at the geometric center is:

$$\begin{bmatrix} d_1(t) \\ d_2(t) \\ d_3(t) \end{bmatrix} = \begin{bmatrix} 0 & 1 & (x_1 - x_c) \\ 0 & 1 & (x_2 - x_c) \\ 1 & 0 & -(y_3 - y_c) \end{bmatrix} \begin{bmatrix} \Delta_x(t) \\ \Delta_y(t) \\ \theta(t) \end{bmatrix} \quad (4.8)$$

The displacements and rotation of the geometric center of the floor is therefore, from Eq. (4.8):

$$\begin{bmatrix} \Delta_x(t) \\ \Delta_y(t) \\ \theta(t) \end{bmatrix} = \begin{bmatrix} \frac{y_c - y_3}{x_2 - x_1} & \frac{y_3 - y_c}{x_2 - x_1} & 1 \\ \frac{x_2 - x_c}{x_2 - x_1} & \frac{x_c - x_1}{x_2 - x_1} & 0 \\ -\frac{1}{x_2 - x_1} & \frac{1}{x_2 - x_1} & 0 \end{bmatrix} \begin{bmatrix} d_1(t) \\ d_2(t) \\ d_3(t) \end{bmatrix} \quad (4.9)$$

The displacements of any point of the floor with coordinates (x_p, y_p) can be computed using the expressions:

$$\begin{cases} x_p(t) = \Delta_x(t) - (y_p - y_c)\theta \\ y_p(t) = \Delta_y(t) - (x_p - x_c)\theta \end{cases} \quad (4.10)$$

4.4 Instrumental uncertainties in displacement estimation from acceleration measurements

Most of the seismic structural health monitoring systems are based on observations collected by using accelerometers. For these reason, only errors related to this category of transducers is investigated in the following. The goal here is to determine how uncertainties related to acceleration measurements affect displacement estimation.

Uncertainties affecting acceleration measurements can be classified in systematic errors and random errors. Systematic errors are errors affecting in the same way all acceleration values of a time history of acceleration. In principle, most of them can be evaluated by Type A evaluation in laboratory conditions and removed by means of calibration of the instrument. In so doing, only random errors should be considered. However, actually calibration procedure is seldom performed by an engineer buying accelerometers for monitoring purposes, therefore both type of errors are considered in this analysis. In particular, the designer who wants to evaluate uncertainties shall use Type B evaluation methodology, usually adopting values of the parameters provided by manufactures in data sheets or certificates.

Definition of characteristic parameters of accelerometers and instrumental errors are reported in many white papers and application notes, available online, by accelerometer producers, for example (Kionix 2007), (Freescale Semiconductor 2007) and (STMicroElectronics) to name a few.

Most important characteristic parameters of accelerometers are accuracy and precision. Accuracy expresses how close it is a measured acceleration value to the actual acceleration value. Precision expresses how close repeated measurements of the same acceleration value are between each other. Most important instrumental errors affecting accuracy are bias error, calibration error, temperature dependent errors, ratiometric error, misalignment errors, cross sensitivity errors and mounting errors. Precision is instead affected basically by instrumental noise.

4.4.1 *Bias error*

Bias error is the difference between the ideal zero-g output and the zero-g output measured by the sensor. In other words, bias is the value of acceleration measured by the accelerometer when it is at rest. It is commonly due to tolerance in the sensor components or to thermal effects. The first cause, not varying in time, is not of concern because it is a constant value and it can be easily removed before sensor installation. The second dynamic cause it is of concern because is not easily predictable and implies a bias drift in time which can cause system triggering (false alarm). In drift

estimation procedure, however, bias error are removed simply subtracting the mean value of the pre-event part of the signal to the whole time history of accelerations.

Assuming that accelerometer is at rest and that noise value is equal to zero, acceleration time history expression is:

$$a_i = B \quad \forall i \quad (4.11)$$

Double integrating the acceleration time history using equation we obtain a time history of displacements which is the error due to bias:

$$e_b(t_i) = \frac{1}{2} B t_i^2 \quad (4.12)$$

that is the error due to the presence of bias is an absolute error increasing quadratically with time. As stated before, the static component of the bias can be removed simply subtracting the pre-event portion of the acceleration time history to the whole time history. The dynamic component cannot be removed in this way and it is the cause of linear trends in velocity time histories and quadratic trends in displacement time histories. These trend are commonly removed applying a band-pass filter to the acceleration time histories (actually they are the first justification to band-pass filtering, being the second the presence of low-frequency components in noise). In this case, it can be said that:

$$e_b(t_i) \approx 0 \quad (4.13)$$

4.4.2 Calibration error

Sensitivity is the parameter relating input (actual acceleration applied to the instrument) and output (voltage or current) and it is commonly provided by the manufacturer. In real life, the actual sensitivity value is slightly different from the one provided. In case it is not possible to perform device calibration, this error, named calibration error, must be considered in the analysis. A sensitivity error is usually expressed as a percentage of the nominal value of sensitive. For example in an instrument data sheet the following may be reported:

$$S = 1000 \pm 1\% [mV/g] \quad (4.14)$$

that is the actual sensitivity of the instrument can be each value between 990 mV/g and 1010 mV/g. Here, I assume that probability distribution of sensitivity parameter can be modelled as a triangular distribution with mean equal to the nominal value of the sensitivity and standard deviation (JCGM 2008):

$$e_s = \sqrt{\Delta S^2 / 6} [\%] \quad (4.15)$$

where ΔS is the half dimension of the interval and standard deviation is expressed in percentage.

It can be seen from the expressions for numerical integration that this error does not propagate in the process and that it affects in the same way acceleration and displacements time histories, that is, an error of ΔS % in the acceleration time history reflects itself in an error of ΔS % in displacement estimation.

4.4.3 *Temperature dependent errors*

Temperature dependent errors are due to the dependence of bias and sensitivity on temperature. Bias can vary by 1-3 mg/°C while sensitivity can vary by some hundredth of percent/°C, depending on the packaging of the accelerometer and on its quality. The effect of environment on bias and sensitivity values is a drift in time. While bias drift is of concern for triggering only, sensitivity drift can induce significant errors. Depending on environmental condition, accelerometers with suitable temperature coefficients should be selected. The error affecting sensitivity due to environmental effects can be managed as calibration error. That is, an error of ΔS_T % due to temperature in the acceleration time history reflects itself in an error of ΔS_T % in displacement estimation.

4.4.4 *Ratiometricity*

Ratiometric error affects mostly MEMS accelerometers and it is due to variable supply voltage: output voltage and input voltage are in fact proportional to each other. Ratiometricity affects both bias and sensitivity. Ratiometric error (in %) affecting bias (B_R) and sensitivity (S_R) can be expressed by the formulas:

$$B_R = \left(\frac{Bias @ V_{dd}}{Bias @ V_{nom}} - \frac{V_{dd}}{V_{nom}} \right) 100 \quad (4.16)$$

$$S_R = \left(\frac{S @ V_{dd}}{S @ V_{nom}} - \frac{V_{dd}}{V_{nom}} \right) 100 \quad (4.17)$$

being V_{dd} the supply voltage and V_{nom} the nominal supply voltage. Regulation of supply voltage is critical to obtain small measurement errors. Having knowledge about performance of the power supply, also the error affecting sensitivity due to ratiometricity can be managed as calibration error. That is, an error of ΔS_R % due to temperature in the acceleration time history reflects itself in an error of ΔS_R % in displacement estimation.

4.4.5 *Misalignment error*

Misalignment error is due to erroneous positioning of components inside instrument package. The result of this error on acceleration measurements is equivalent to the one of sensitivity error and is

managed in the same way in the propagation error analysis. In particular, the fact that the sensor component is not perfectly aligned to the instrument package reflects in an underestimation of acceleration proportional to $\cos \alpha_m$ where α_m is the misalignment angle between the two directions. Also for this error I assume the triangular distribution, obtaining the following standard deviation (JCGM 2008):

$$e_m = \sqrt{(1 - \Delta\alpha_m)^2} / 6 [\%] \quad (4.18)$$

being $\Delta\alpha_m$ the half dimension of the interval provided by the manufacturer and being the standard deviation expressed in percentage.

4.4.6 Mounting error

Mounting error is due to the installation procedure. In practice the instrumented is mounted on the structure on a direction which is different to the desired one (which in general corresponds to a principal axis of the building). This, from my own experience, can be due to errors in the mounting procedure itself or, more likely, to a discrepancy between the “structure in the design drawings” and the real structure, in particular due to construction tolerance. The result of this error on acceleration measurements is also equivalent to the one of sensitivity error. In particular, the fact that the installed instrument is not perfectly aligned to the desired measuring direction reflects in an underestimation of acceleration proportional to $\cos \alpha_p$ where α_p is the angle between the two directions. For this type error I assume that it is a random error with expected value equal to zero and a standard deviation equal to 2% but more detailed considerations can be done in presence of a good prior knowledge of the correspondence between design drawings and real building.

$$e_p = 2 [\%] \quad (4.19)$$

Also this error obviously reflects itself in an error of e_p % in displacement estimation

4.4.7 Cross-axis sensitivity

Cross-axis sensitivity error or transverse sensitivity error is due to the output induced on a sense axis of the accelerometers from an acceleration applied on a perpendicular axis, and it is mainly due to tolerances in placement components inside the sensor’s package. It is commonly expressed in data sheets as a percentage of instrument sensitivity. The measured acceleration along an axis is equal to the actual acceleration along the axis plus a spurious acceleration equal to the acceleration on the perpendicular axis multiplied by the cross-axis sensitivity. The standard deviation of the error due to cross-axis sensitivity can be obtained as the product of two Gaussian distribution. The first Gaussian is related to the cross-axis sensitivity coefficient. I assume that this coefficient is a random

variable with zero mean and standard deviation σ_{Sc} . The second Gaussian is related to the displacement value on the transverse direction when the displacement value on the measured direction is maximum. I assume that displacement time history along the transverse direction can be modelled as a zero-mean sine wave with amplitude $d_{T,max}$. The RMS value RMS_x of a sine wave is defined as:

$$RMS_x = \frac{1}{\sqrt{2}} d_{T,max} \quad (4.20)$$

where $d_{T,max}$ is the amplitude of the sine wave. If the signal is zero-mean, RMS value is equal to the standard deviation of the signal. The standard deviation of the value assumed by the displacement in the transverse direction when the displacement in the measuring direction is maximum is:

$$\sigma_{dc} = \frac{1}{\sqrt{2}} d_{T,max} \quad (4.21)$$

Being c a random variable result of the product of two Gaussian random variables a and b , the variance of c is expressed as (Frishman 1971):

$$\sigma_c^2 = \sigma_a^2 \sigma_b^2 + \sigma_a^2 \mu_b^2 + \sigma_b^2 \mu_a^2 \quad (4.22)$$

that is in case of zero-mean random variables, the variance of their product is equal to the product of their variances.

Therefore the standard deviation of the cross-axis sensitivity error is the product of the standard deviation of the cross-axis sensitivity parameter by the standard deviation of the value assumed by the displacement in the transverse direction when the displacement in the measuring direction is maximum:

$$\sigma_{c=Sc\sigma_{dc}} = \sigma_{Sc} \frac{1}{\sqrt{2}} d_{T,max} \quad (4.23)$$

4.4.8 Noise

Errors affecting precision of the acceleration measurements are typically expressed as noise. Noise in accelerometers is electronic noise (related to ASIC performance) and mechanical noise (thermos-mechanical noise and environmental vibrational noise). Noise is frequently reported in instrument data sheets in the form of noise density n_d ($\mu g / \sqrt{Hz}$). Noise can be modeled as white noise. The effects on the acceleration signal is therefore the superposition of a sequence of zero-mean uncorrelated random variables.

To calculate RMS (which is equal to standard deviation being the noise zero-mean) of the noise related to a noise bandwidth B the following expression can be used (Kionix 2007):

$$a_n = n_d \sqrt{B} \quad (4.24)$$

Most used digital filter for seismic applications is Butterworth filter because its amplitude linearity in the pass-band. Noise bandwidths of Butterworth as well of other filters are reported in many electronic textbooks, for example in (McClaning 2011), as the ratio between noise bandwidth and the 3dB cutoff frequency, functional of the filter’s order:

Table 4-1 – Noise Bandwidth of Butterworth filter

Order	[-]	1	2	3	4	5	6	7
B/f _{cut}	[-]	1.57	1.11	1.05	1.03	1.02	1.01	1.008

This formula can be used for the choice of filter’s order and cutoff frequency suitable for the application having fixed the value of instrumental noise, i.e. the sensor.

In order to determine the uncertainties in terms of displacements due to noise, I performed a parametric analysis varying noise amplitude in range 0.1-50 cm/s² (mg) and high-pass frequency cut in range 0.1-5 Hz. Noise was modelled as White Noise. Displacements time histories were obtained by the inverse Fourier transform of the spectra of accelerations divided by the frequency squared. Time histories of noise in accelerometer measurements are reported in Figure 4-3 while Figure 4-4 are displacement time histories when the standard deviation of the noise is equal 10 cm/s². Results of the analysis are illustrated in Figure 4-5. It can be seen that the uncertainty related to noise in terms of displacements is proportional to noise itself whilst it is inversely proportional to high-pass frequency cut, being typical values (noise 10-20 cm/s², f_{cut} 0.2-0.5 Hz) ranging between 0.1-1.0 mm

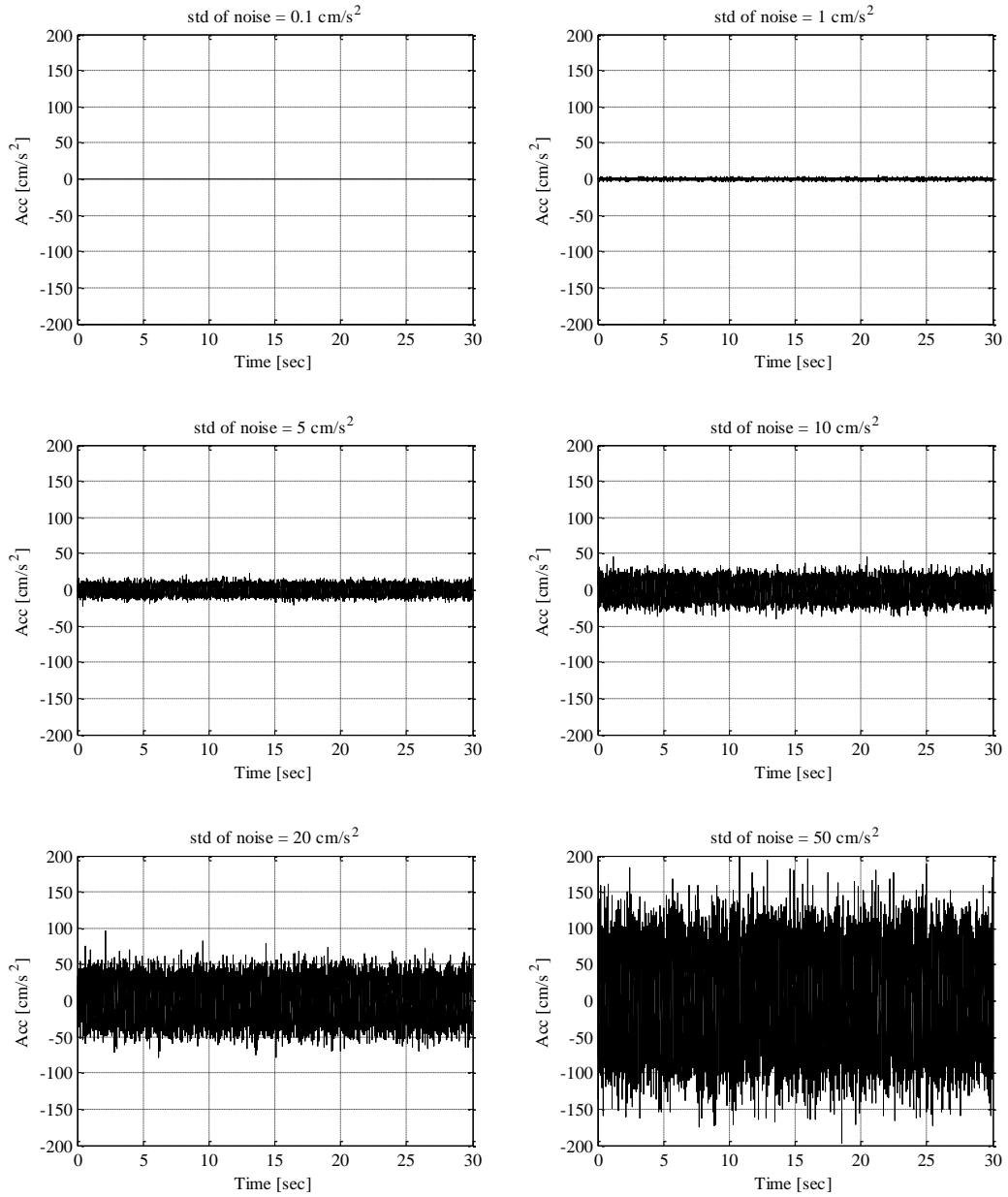


Figure 4-3 - Modeled noise in acceleration measurements

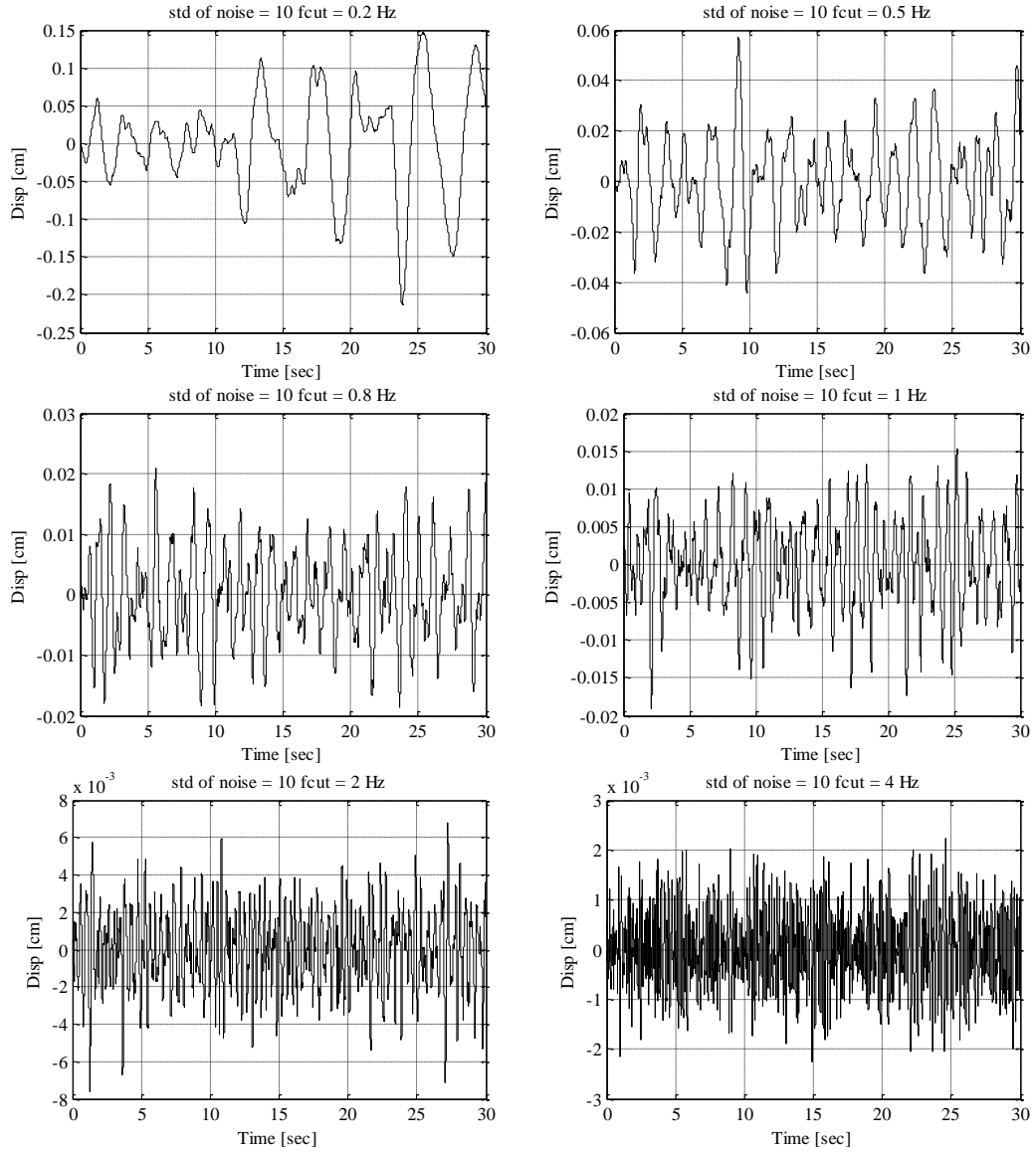


Figure 4-4 - Displacement time histories due to noise

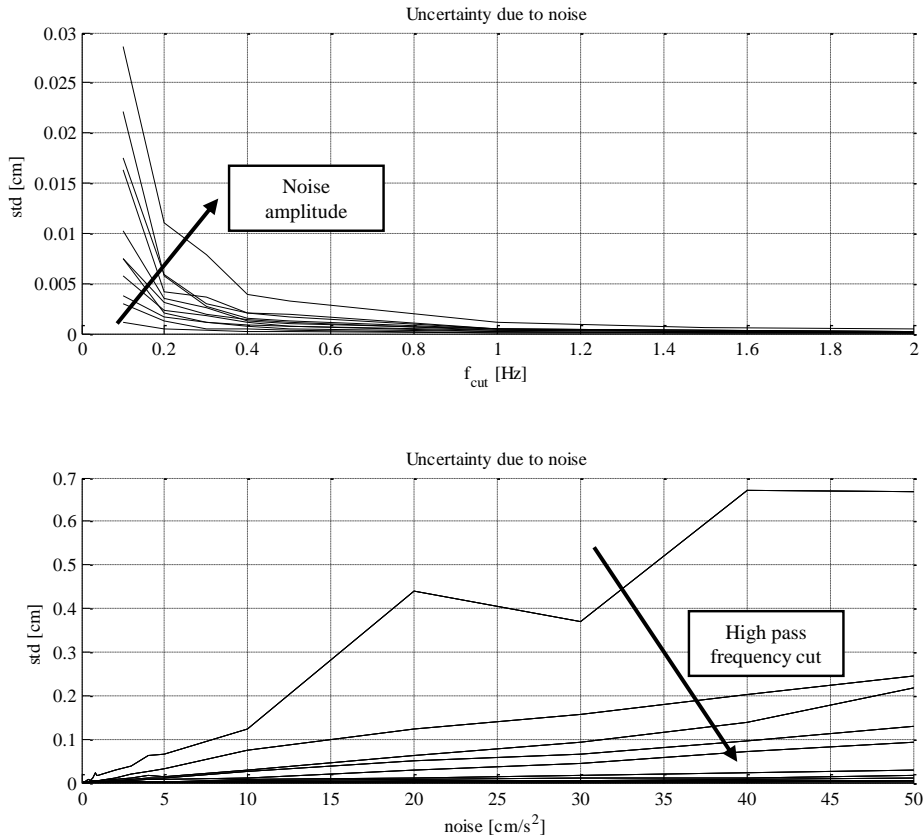


Figure 4-5 – Uncertainty due to noise in function of noise amplitude and high-pass frequency cut

4.4.9 Summary of instrumental uncertainties and their combination

In the following table instrumental uncertainties are summarized. Typical values were obtained from data sheets of MEMS capacitive accelerometers and on my personal experience.

Table 4-2 – Sources of instrumental uncertainties (* when a high-pass filter is applied)

Error	Symbol	Metric	Value (typ.)
Bias	e_b	cm	0.0*
Calibration	e_S	%	1 - 2
Environmental	e_{ST}	%	0.5 - 1
Ratiometricity	e_R	%	1 - 2
Misalignment	e_m	%	0.0
Mounting	e_p	%	2 - 3
Cross-axis sensitivity	e_c	%	2 - 3
Noise	e_n	cm	0.5

The total uncertainty in an estimate of displacement is therefore composed of different components that must be combined together. Uncertainties which metric is expressed in percentage can be combined using the root-sum-square method since it is unlikely that all error components would be at their maximum absolute value simultaneously if the error sources are statistically independent. The total uncertainty is therefore obtained as (Morris and Langari 2011):

$$E = \pm\sqrt{e_1^2 + e_2^2 + e_3^2 + \dots + e_n^2} \quad (4.25)$$

Applying this formula and using the values reported in Table 4-2, the overall instrumental uncertainty can be estimated as in the range 3-6% when evaluation is based on data sheets only (i.e. no calibration is carried out) and can be reduced at 2-3% when proper calibration of components is performed.

4.5 Numerical analysis of the model uncertainties

4.5.1 *Methodology*

The analysis presented here aims at finding a numerical estimation of model uncertainty in the computation of displacement (and the interstory drift too) with only measurement of accelerations. In order to have a large number of unprocessed data, many acceleration data (raw data) from ITACA database (Pacor et al. 2011) were analyzed. This type of data are ground acceleration recorded by accelerometers during the last strong earthquakes in Italy, chosen among those with magnitude greater than 4.5, as the earthquake of L'Aquila or the earthquake of Emilia.

These accelerograms were used to compute accelerations and displacements of a single degree of freedom structure by using two different methods, namely the Newmark's time stepped integration method and the double integration method presented in the previous part of this work.

The model uncertainty was in fact studied comparing the displacement of the sdof computed by Newmark's method (assumed as "true" value) and the displacement obtained by double integration. It is worth pointing out that the acceleration (and also displacement) time history provided by Newmark's method is relative respect to the ground.

The analysis was carried out by varying arbitrarily the parameters (e.g. input acceleration, structure frequency, cutoff frequency of the high-pass filter) to find how these changes influence the model uncertainty.

Two types of sdof systems were considered for the simulation, namely a linear system where the force-displacement relation is indefinitely linear elastic, and a nonlinear system where the force-displacement relation was assumed as elastic-perfectly plastic.

The first allows for the study of the uncertainty due to double integration method, in particular to the numerical integration itself and to the cutoff frequency of the high-pass filter.

The second allows for the study of uncertainty due to residual displacement at the end of the motion. The model error was computed in percentage as the ratio between the difference of maximum relative displacement obtained from the two methods and maximum relative displacement calculated by Newmark's method.

$$e = \frac{u_{\max} - \hat{u}_{\max}}{u_{\max}} \times 100 \quad (4.26)$$

where u_{\max} is the relative displacement obtained from Newmark's method and \hat{u}_{\max} is the displacement obtained from double integration.

4.5.2 *Newmark's method*

The analyzed structure is a simple structure that is composed by a reinforced concrete square column supporting the tributary area of a reinforced concrete and masonry roof. It is called simple structure because it can be idealized as a concentrated or lumped mass m supported by a massless structure with stiffness k in the lateral direction. The lumped mass m is equal to the mass of the roof and the lateral stiffness k is equal to the stiffness of the column. The height of the column was set to 6 meters and the dimension of the side of reinforced concrete column was assumed equal to 0.4 m for linear system but was varied from 0.4 m to 0.7 m for nonlinear system.

Newmark's method is a time-stepping method based on the following equations:

$$\dot{u}_{i+1} = \dot{u}_i + [(1-\gamma)\Delta t] \ddot{u}_i + (\gamma\Delta t) \ddot{u}_{i+1} \quad (4.27)$$

$$u_{i+1} = u_i + (\Delta t) \dot{u}_i + [(0.5-\beta)\Delta t^2] \ddot{u}_i + \beta\Delta t^2 \ddot{u}_{i+1} \quad (4.28)$$

The parameters β and γ define the variation of acceleration over a time step and determine the stability and accuracy characteristics of the method. Typical selection for γ is 0.5 and $1/6 < \beta < 1/4$ is satisfactory from all points of view, including that of accuracy. In this analysis the variation of acceleration over a time step was assumed constant, equal to the average value, assuming $\gamma = 0.5$ and $\beta = 0.25$. Implementing the algorithms reported in chapter 5 of (Chopra 2011) the differential equation of motion it was solved numerically, then acceleration, velocity and displacement of the lumped mass were known.

4.5.3 *Double integration*

The acceleration resulting from Newmark's method is relative to the ground. Therefore, the acceleration obtained with Newmark's method was added to acceleration data downloaded from ITACA database (which is the ground acceleration) to get the absolute acceleration of the lumped

mass, in order to simulate the measurement process. Absolute acceleration was the parameter to start computation of the second approach, the double integration method. Integration was performed using the trapezoidal rule. A 4th-order Butterworth high pass filter was implemented to filter acceleration before integration. The cutoff frequency was one of the parameters that were changed to understand the model error variation. After that, the mean of the velocity had been removed from the computed velocity before second integration to obtain displacements. A zero pads had been added at the beginning and at the end of time series before filtering in order to include the effect of the filter transients when performing operations such as integration to obtain displacements. The length of these pads was chosen equal to the signal length.

In order to obtain relative displacement, also the double integration of the ground acceleration was performed. The relative displacement from double integration was therefore:

$$\hat{u} = \hat{U} - \hat{u}_g \quad (4.29)$$

This formula is exactly the same that the one it is used when relative displacement or interstory drift ratio is computed from acceleration measurements at the top and bottom of a column member.

4.5.4 Results on linear system

The analysis performed on the linear system consists in varying the value of the natural frequency f of the system and the value of the cutoff frequency of the Butterworth filter f_{cut} . A total of 630 analysis were performed. In the next tables, only a few of them are reported.

Table 4-3 – Error between max Newmark displacement and double integration displacement ($f_{cut} = 0.6$ Hz)

f [Hz]	f/f_{cut}	ALF [%]	ALF [%]	MDC [%]	MDN [%]	MDN [%]	MRN [%]	MRN [%]	SRP [%]	MODE [%]	MODE [%]
0.3	0.50	82.8	84.3	90.2	74.8	76.3	69.1	55.1	62.8	75.1	75.1
0.6	1.00	35.9	30.7	46.2	37.5	28.2	28.6	37.3	33.0	30.4	24.4
1.0	1.67	-5.5	6.7	13.9	2.7	-1.7	3.8	15.4	11.2	-4.2	2.9
1.37	2.28	-2.6	3.0	5.3	1.2	8.4	-9.5	-2.3	0.8	-3.6	0.4
2.0	3.33	-7.2	0.6	-1.8	0.2	-9.4	15.9	8.8	-11.4	-6.8	-3.9
4.0	6.67	-5.6	-7.4	8.5	-5.4	0.4	5.2	0.0	-8.2	-6.6	4.2
8.0	13.33	-5.3	3.0	1.0	1.6	22.8	-7.4	0.3	18.3	0.8	3.4

Table 4-4 - Error between max Newmark displacement and double integration displacement ($f_{cut} = 1.2$ Hz)

f	f/f_{cut}	ALF	ALF	MDC	MDN	MDN	MRN	MRN	SRP	MODE	MODE
[Hz]		[%]	[%]								
0.3	0.25	91.3	92.8	94.4	90.4	91.1	86.8	82.0	82.5	91.9	90.3
0.6	0.50	81.3	83.8	79.8	79.4	82.0	86.1	82.8	83.8	83.3	70.9
1.0	0.83	37.2	32.1	36.2	47.9	55.4	52.9	56.8	57.3	47.0	54.1
1.37	1.14	16.3	16.0	19.3	12.4	29.5	11.0	17.0	17.2	19.1	17.1
2.0	1.67	2.3	7.4	0.8	1.4	4.6	8.3	7.4	-8.3	9.9	7.6
4.0	3.33	-16.4	13.0	5.5	2.2	-7.4	5.4	0.7	-1.7	-3.2	8.4
8.0	6.67	23.8	10.3	-12.6	4.3	18.8	3.1	-13.9	32.1	9.9	34.8

Table 4-5 - Error between max Newmark displacement and double integration displacement ($f_{cut} = 2.0$ Hz)

f	f/f_{cut}	ALF	ALF	MDC	MDN	MDN	MRN	MRN	SRP	MODE	MODE
[Hz]		[%]	[%]								
0.3	0.15	96.9	97.5	97.7	96.8	96.3	93.6	95.3	94.2	97.1	97.4
0.6	0.30	93.0	94.7	92.5	93.4	94.2	93.9	96.4	94.6	95.7	93.2
1.0	0.50	80.5	78.8	80.3	88.0	91.0	84.1	88.8	82.7	90.0	89.2
1.37	0.68	73.1	73.4	71.8	72.2	77.8	62.2	75.7	69.7	80.5	76.8
2.0	1.00	39.4	56.1	34.4	33.5	26.7	38.4	47.2	37.2	49.5	30.9
4.0	2.00	17.1	30.1	13.0	5.3	5.2	-4.6	2.0	4.3	1.4	10.8
8.0	4.00	43.2	21.7	33.8	8.4	21.9	-8.0	1.3	36.4	4.2	53.9

In the next graphs, the dependence of the error on the ratio between frequency of the mode of vibration of the system and cutoff frequency is showed. In the graphs, red crosses represent the mean value of the group.

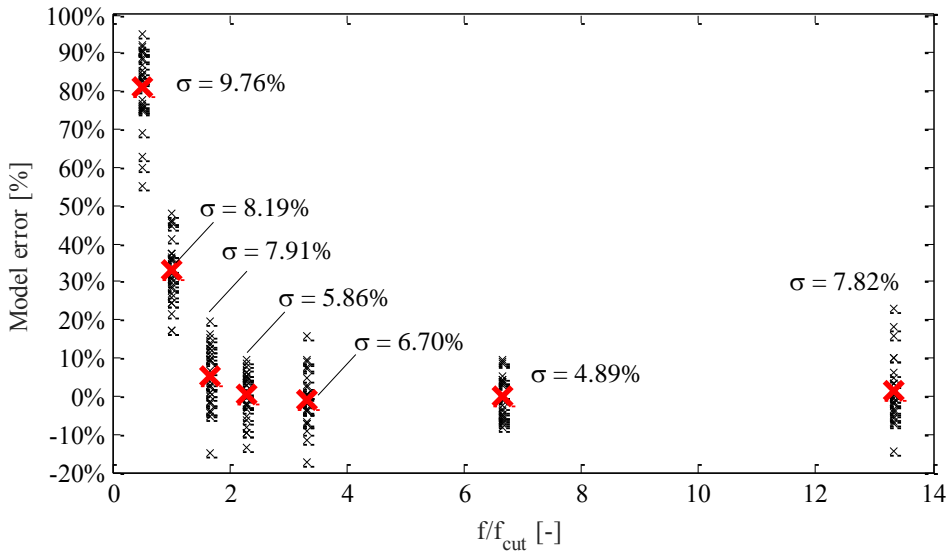


Figure 4-6 - Error between max Newmark displacement and double integration displacement ($f_{cut} = 0.6$ Hz)

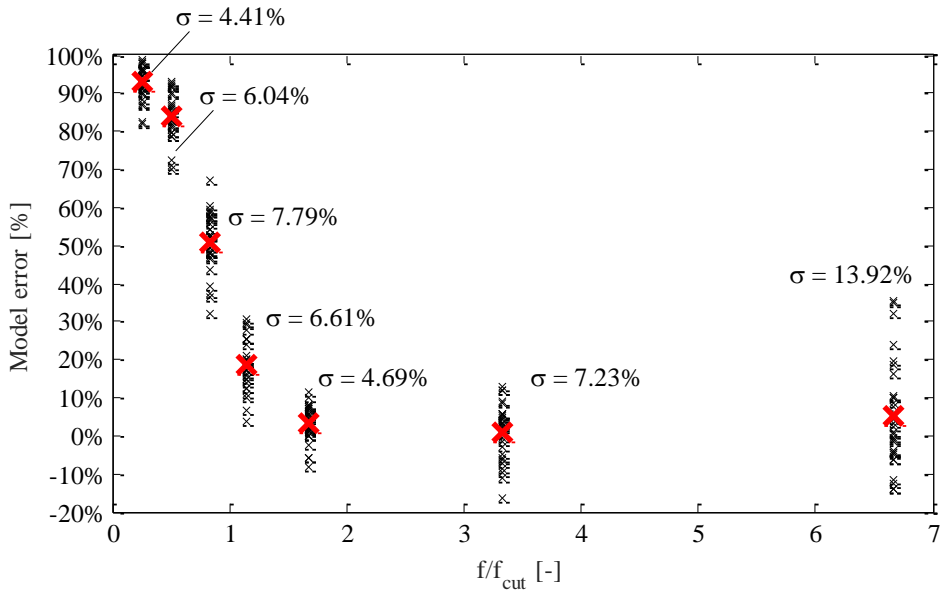


Figure 4-7 - Error between max Newmark displacement and double integration displacement ($f_{cut} = 1.2$ Hz)

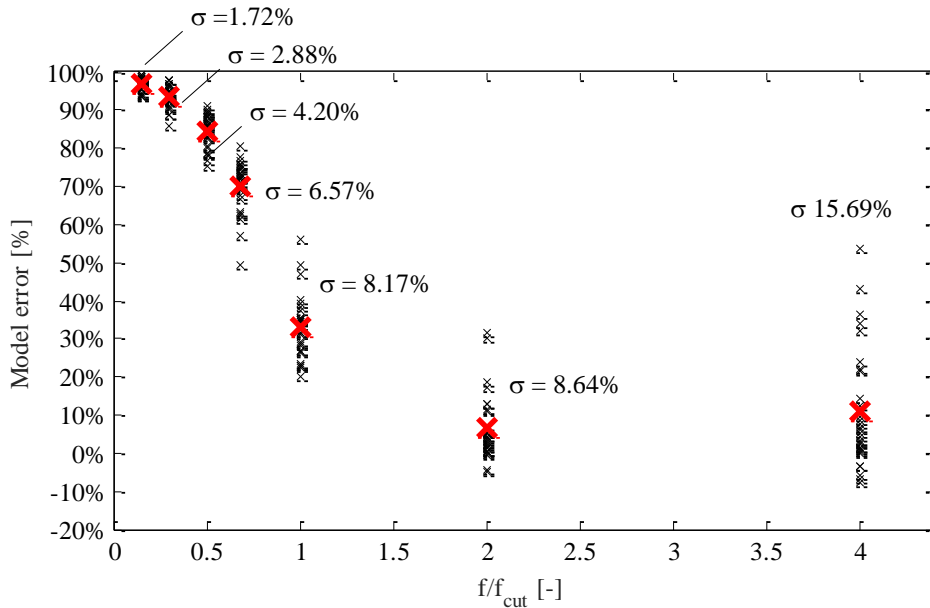


Figure 4-8 - Error between max Newmark displacement and double integration displacement ($f_{cut} = 2.0$ Hz)

It can be seen that:

- the error is basically independent on the frequency of the system (all the graphs present the same trend) while the dependence is strong on the ratio f/f_{cut} ;
- as expected, for f/f_{cut} close to 1 the mean error is around 30%. This is explained remembering that the cutoff frequency corresponds to a 70% reduction of the component in the signal at that frequency;
- the (mean) error is close to 0% when the ratio f/f_{cut} is about 2;
- a slightly higher error is observed for $f = 8$ Hz. This is explained by the fact that for higher frequencies, displacements are smaller. In this case, numerical error is predominant respect to the error due to the filter;
- standard deviation of the error seems to be independent to the f/f_{cut} ratio, being in the order of 7%. Higher values are obtained also in this case for $f = 8$ Hz. This seems to confirm the randomness of the numerical error.

4.5.5 Effect of residual displacements

Nonlinear system analysis is reported in this section. It was assumed an elastic-perfectly plastic force-displacement relation for simulating nonlinear system behaviour. The value of the horizontal yielding force which describes the elastic-perfectly plastic response was obtained by the following equation:

$$F_y = Ku_y \quad (4.30)$$

where the yielding displacement u_y was computed from the yielding rotation θ_y of base section:

$$u_y = h\theta_y \quad (4.31)$$

Yielding rotation was computed using the expression reported in UNI EN 1998 assuming the possibility of slippage of longitudinal reinforcement.

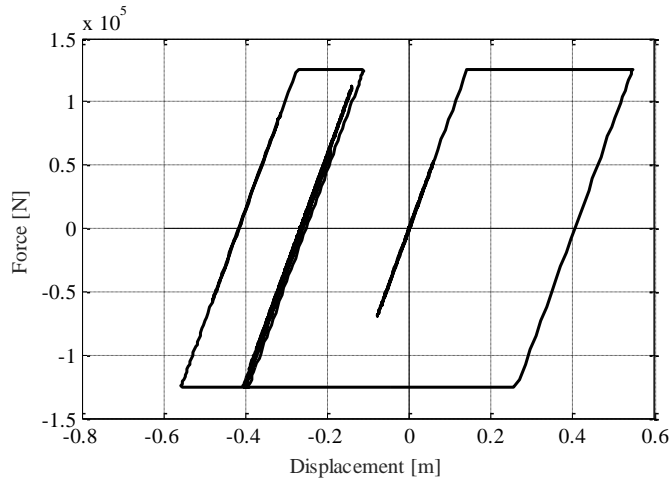


Figure 4-9 – Example of force-displacement time history

The column was subjected to increasing intensities of the ground accelerations recorded during the 2012 Emilia earthquake at different stations, multiplying recorded time histories by a factor k varying from 1 to 20. In this analysis it was selected a single value of the cut-off frequency f_{cut} of the Butterworth filter, fixed at 0.6 Hz. The dimension of the column was varied instead from 0.4 m to 0.7 m. The frequency of the system varies between 1.37 Hz and 4.20 Hz. A total of 1320 analysis was performed. In 117 cases yielding was reached.

In Figure 4-10 the error (black crosses) is showed against the residual displacement for the case of column 0.4x0.4 m. Similar results are obtained for other column dimensions. Neglecting the obviously unrealistic residual displacements up to 1.60 m, It can be seen that for residual equal to the displacement at yielding (about 0.14 m) the error is about 35% while for $f/f_{cut} = 2$ the expected value in the elastic system should be around 2%. Increasing residual hence ductility, the error tends to 60%.

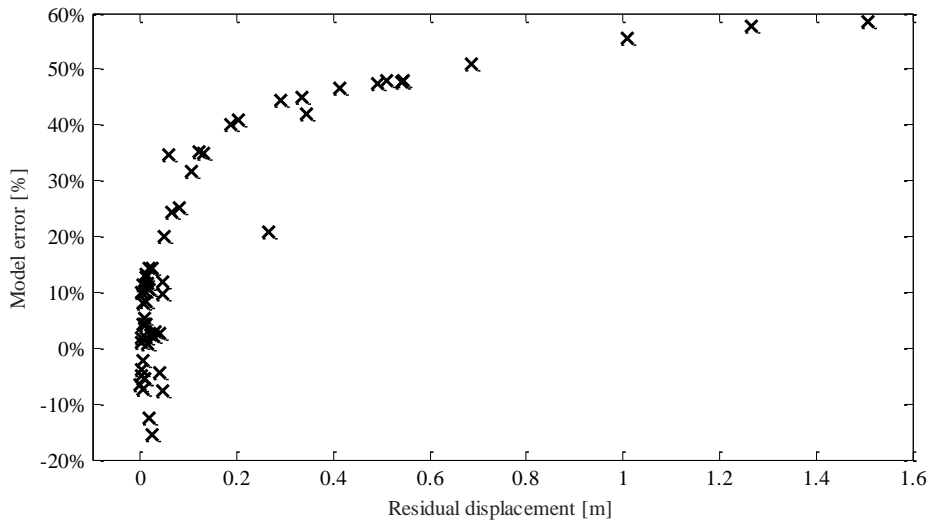


Figure 4-10 - Error between max Newmark displacement and double integration displacement varying at varying residual displacement

4.6 Conclusions

If a demand-capacity approach in terms of accuracy is used for the design of a monitoring system, the designer must check whether or not the accuracy of the information provided by the system satisfies the requirements. In this Chapter I discussed the problem of the estimation of the accuracy of the displacement response of a structure computed from acceleration data. I identified basically three sources of uncertainties which are namely: the instrumental uncertainties affecting acceleration measurements; the uncertainties introduced by the numerical double integration; the uncertainties due to the possible residual deformation of the monitored structure at the end of the motion.

The uncertainties belonging to the first group can be decreased choosing high-performance instrumentation and ensuring an installation compliant to the design drawings. In particular, errors in acceleration data due to erroneous calibration, environmental effects and misalignment reflect themselves in the displacement estimation, while noise seems to influence less the accuracy of the displacement estimation.

I computed the uncertainty in the displacement estimation for typical instruments in the range 3 - 5% plus the uncertainty due to instrument noise, which is expressed in length unit. For displacement less than 10 mm the influence of the noise is therefore predominant, and it decreases increasing the displacement. In other words, when the monitored structure is stiff, or very low thresholds value are desired in the assessment software, a particular attention must be paid in the choice of the accelerometer and to its noise.

It is worth remark, moreover, that I modeled noise as white noise. In some types of instruments (e.g. capacitive accelerometers) flicker noise (or pink noise) affecting low frequencies can be a relevant source of uncertainty when the implemented band-pass filter does not filter out these components.

I performed a parametric analysis to study the uncertainties of the model. In particular, I would know the influence of the numerical integration, of the filtering process, and of the residual displacements at the end of the motion on the overall accuracy. The parametric analysis was performed on linear and nonlinear sdof systems subjected to ground motion time histories downloaded from ITACA database. The error was computed comparing the “true” response of the systems, assumed as equal to the one obtained from Newmark’s integration method, and the “measured” response, obtained numerically integrating acceleration time histories.

The influence of the filtering process and of the numerical error on the overall uncertainty was studied on the linear system. It has been confirmed that the numerical error is random, characterized by a zero-mean value and a standard deviation around 7%. The error due to filtering process is instead systematic. Its mean value tends to zero for values of the ratio between frequency of the first mode of vibration and cutoff frequency higher than 2. This is very important in the definition of the cutoff frequency: estimating the frequency of the building prior to the monitoring system design is critical. It is also important to calculate the frequency of the degraded structures in order to avoid error increasing after possible yielding, taking into account that the stiffness of a column at yielding is about 30% of the elastic stiffness.

The effect of residual displacements at the end of the motion was also investigated in this Chapter. Simple non-linear analysis of an sdof subjected to increasing ground motion intensities were carried out assuming elastic-perfectly plastic force-displacement relation. In these analysis, the effect of filtering was neglected varying f/f_{cut} ratio between 2 and 4. The observed error is therefore due to numerical integration (which effect has already been studied above) and residual displacement.

I have found that also for residual displacement equal to the displacement at yielding, the error is higher than 30%, and tends at 60% increasing the value of residual displacement. The error tends to return to values of elastic analysis (i.e. the effect of residual displacement is strongly diminished tending to few percent) by simply adding the value of the residual displacement to the maximum displacement obtained from numerical integration.

5 MEMSCON EU Project

5.1 Introduction

In this Chapter I illustrate the MEMSCON EU research project, a project aiming to develop a reliable and cost effective monitoring system based on MEMS technology and wireless data transmission for the protection of reinforced concrete buildings against seismic events and settlements. In the second part of the Chapter I show MEMSCON prototypes from a civil engineer point of view, giving references where details about conception and design of the sensors can be found. Then, I focus my attention on the laboratory evaluation of MEMSCON technology in laboratory conditions. The first part of the experimental campaign consists of calibration tests and performance evaluation tests performed on small-scale specimens. The second part is the system evaluation on a full-scale 3D reinforced concrete frame tested dynamically in the laboratory inducing increasing structural damage to be correlated to the response of the monitoring system.

5.2 Description of MEMSCON EU Project

Memscon Project (www.memscon.com) was a research project co-founded by the European Community in the 7th Framework Programme, started in 2008 and concluded in 2012. The project

involved partners from 7 different countries, including private companies acting in the field of electronics, consultants and universities (Figure 5-1).

The aim of the research project was to develop a reliable and low-cost monitoring system for new reinforced concrete buildings, for their protection against seismic event and settlements, having recognized these as the most important sources of damage in RC buildings. The prototype monitoring systems consisted of a wireless network of sensors inside the building and a base station linking the building to a remote center for data analysis. The network of sensors included RFID (Radio Frequency Identification) MEMS (Micro-Electrical-Mechanical-Systems) sensors for the monitoring of accelerations and strains (Figure 5-2).

In Memsccon monitoring system, acceleration measurements during an earthquake are recorded by accelerometers attached at each floor of the building. In particular, two bi-axial accelerometers are placed at each floor in order to monitor translational and torsional motion, while one mono-axial accelerometer monitors acceleration along the direction of gravity.

Strain measurements are recorded at the interface between columns and foundations in order to estimate vertical loads in columns and to detect possible variations due to settlements. In particular, strain sensors were designed to be embedded into reinforcement concrete members and attached to steel reinforcing bars at the corners of the columns cross section. The software developed within the research project automatically estimates axial load at the bottom of the columns, and detects changes of its value highlighting differential settlements of the ground which can cause structural damage. Strain sensors are also used in the after-earthquake damage assessment of the monitored building highlighting possible inelastic deformation of the reinforcing bars at the end of the seismic motion.

The activities of the project was divided in three main tasks, being the first the development of the sensor network including the production of new instruments specifically designed for the application, the second the development of a software package for remote data processing, condition assessment and maintenance planning, and the third the evaluation of the performance of the whole system in laboratory conditions.

My activity into the project concerned experimental validation of Memsccon technology in laboratory conditions. Information on other activities of the project are available at the project's website (www.memsccon.com).

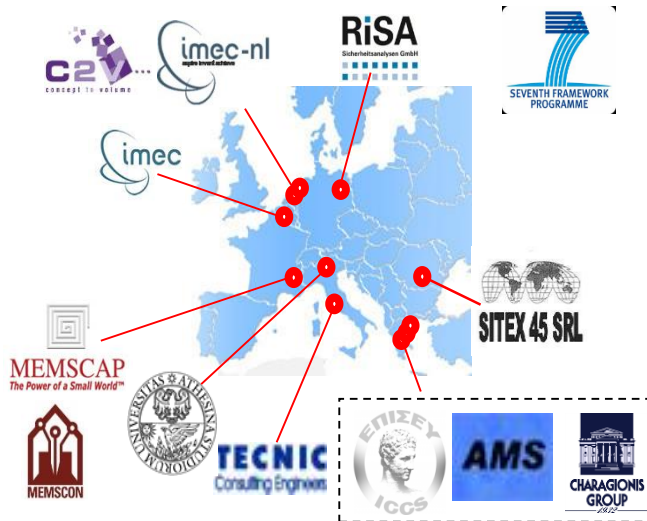


Figure 5-1 – Partners of MEMSCON EU project

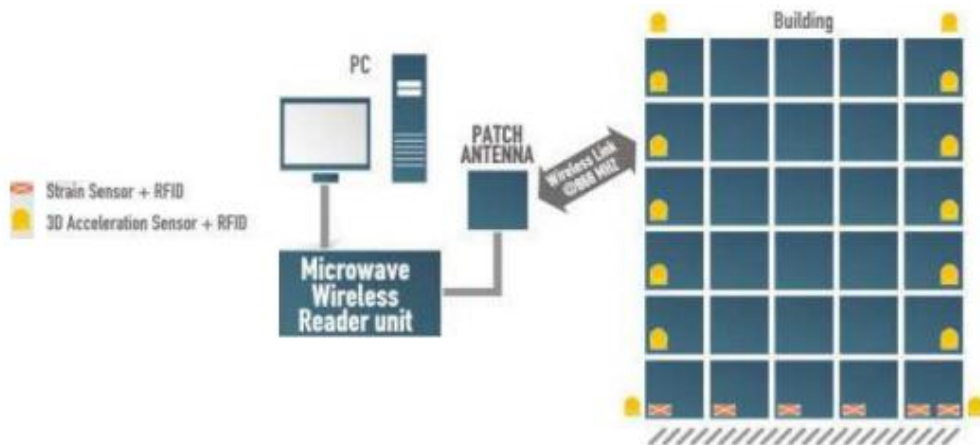


Figure 5-2 – Layout of the MEMSCON monitoring system: strain sensors are placed at the lowest level of the building while accelerometers are placed in pairs at each floor (from www.memsccon.com)

The methodology on which the system was developed within WP2. Details can be found in (DBA and TECNIC 2009). Here only a brief introduction is given.

The aim of Memscon project was to develop a seismic monitoring system for RC buildings compliant to seismic codes allowing for:

- (1) the localization of damaged members;
- (2) the estimation of the degree of local damage;
- (3) the detection of local and global failure mechanisms;
- (4) the decision for usability of the structure after the seismic event and for the application of immediate temporary measures;

- (5) the provision of the measures for structural repairing and rehabilitation and the estimation of the relevant costs.

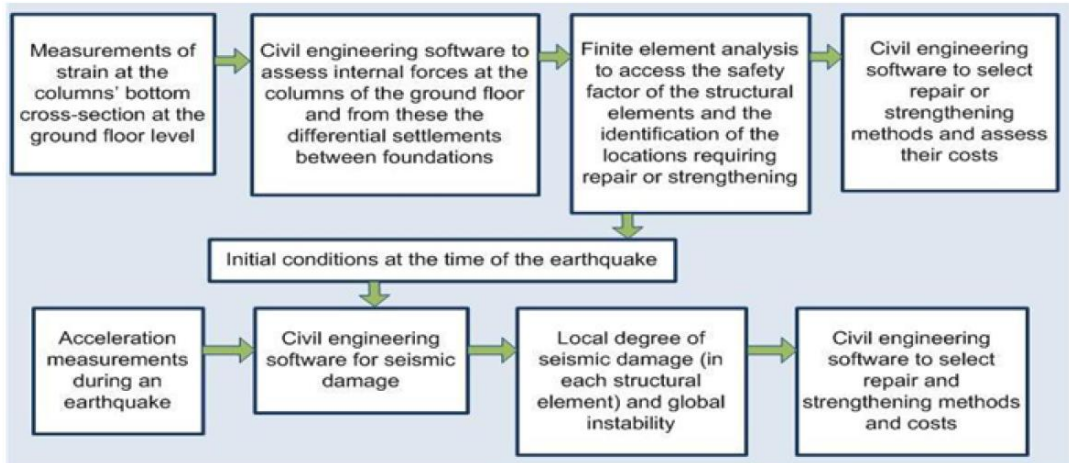


Figure 5-3 - Overview of the Memsccon methodology, from (RISA and TECNIC 2011)

The monitoring system consists of a network of tri-axial accelerometers. Two accelerometers are placed at each storey of the building, including the ground. A non-linear analysis of the building taking into account non linearity of steel and confined concrete and a hysteresis model is performed just after the seismic event using the acceleration measurements as input. The state of condition of the structure after the earthquake is based on the results of the analysis. In particular, displacement time histories are obtained from double numerical integration of acceleration measurements and imposed to each floor in the analysis. Moments and curvatures are calculated at each possible plastic hinge location at a modified Park-Ang damage index is computed for each cross section:

$$D = \frac{K_{s0} - (1 + \lambda\kappa) K_s}{K_{s0} - (1 + \lambda\kappa_u) K_{su}} \tag{5.1}$$

being the meaning of the symbols in the formula explained in Figure 5-4 and λ a constant.

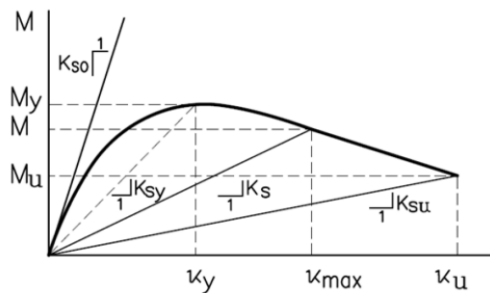


Figure 5-4 – Proposed sectional stiffness, from (DBA and TECNIC 2009)

For each member a damage state is estimated following the map between damage ratio and damage state reported in Table 5-1.

Table 5-1 – Proposed relation between damage ratio and damage states, adapted from (RISA and TECNIC 2011)

Damage Ratio	Damage state
$D < 0.2$	Light
$0.2 < D < 0.4$	Moderate
$0.4 < D < 0.6$	Severe
$D > 0.6$	Collapse

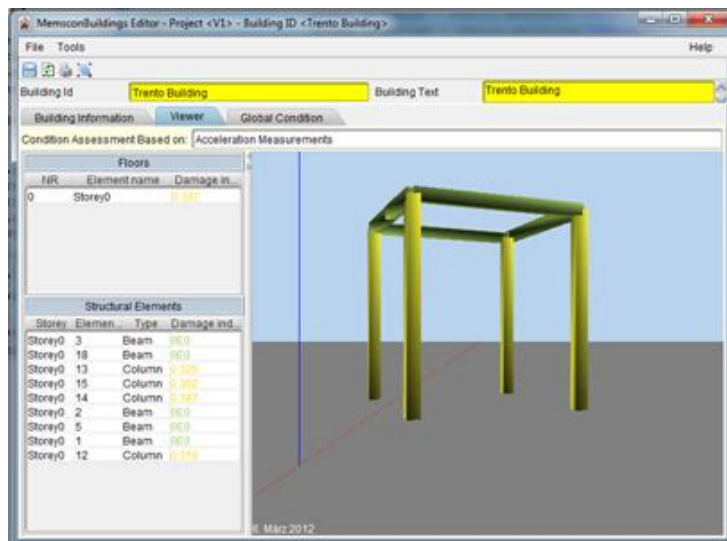


Figure 5-5 – Structural assessment result, from (RISA and TECNIC 2011)

5.3 Technology

Memcon technology was developed in two different phases. In the first phase, aiming to a feasibility study the instruments were developed assembling components available on the market in 2008. In the second phase aiming to the realization of the prototype the sensors were specifically designed for the application.

5.3.1 Phase I accelerometer

Each sensing is packaged in a plastic box of size 11x8x4cm, and has a 19cm antenna (Figure 5-6). The node weighs 150g, and contains a tri-axial accelerometer, with the following characteristics:

Table 5-2 – Phase I accelerometer characteristics

Characteristic	Value
Sampling rate	100 Hz
Resolution	18 mg
Range	± 2 g
Period of acquisition	up to 30 sec

Each accelerometer node measures, records and transmits over the wireless network 3-axis acceleration data, recorded by a MEMS-based sensor commercially available from Analog Devices Inc. A single base station (Figure 5-6), connected via USB to a standard PC, can acquire vibration data from many nodes at the same time within a range of dozens of meters, even inside a building. To reduce energy consumption, each sensing node is controlled by a hardware trigger that activates the node when a vibration threshold of 20 mg is exceeded. Below this level, the node remains asleep, saving batteries for a span of years. Once activated by a stronger vibration, the node acquires acceleration data for a maximum of 30 seconds, following the procedure reported in Figure 5-7 and described below. As a consequence, only if that amplitude is significant does the node consider the signal relevant and transmits it to the base station. The underlying idea is that together these hardware and software thresholds minimize power consumption of the node, avoiding the transmission of signals that are irrelevant for seismic analysis: so long network life can be expected.

When the hardware threshold is overcome and power is supplied to the node, acquisition starts and the first time window (lasting 5 seconds) is recorded by the device memory unit. Data acquisition is independent for the 3 axes, so that the same procedure is applied three times. The root mean square (RMS) is calculated by the computational chip, then it is compared with a threshold value THR (tunable by the programmer, and set at 15 mg during the tests). If the RMS value is higher than the THR, the measurements of the first window are considered as “relevant” for seismic analysis and are stored to be transmitted, while acquisition continues for another 5 seconds; otherwise the data so far are considered “irrelevant” and deleted, acquisition is interrupted and the device goes back to sleep mode.

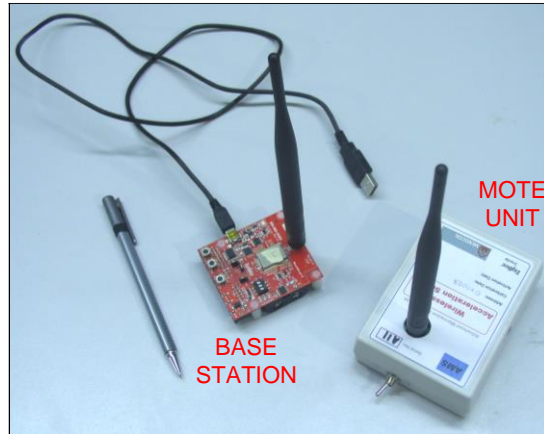


Figure 5-6 - Phase I base station and accelerometer

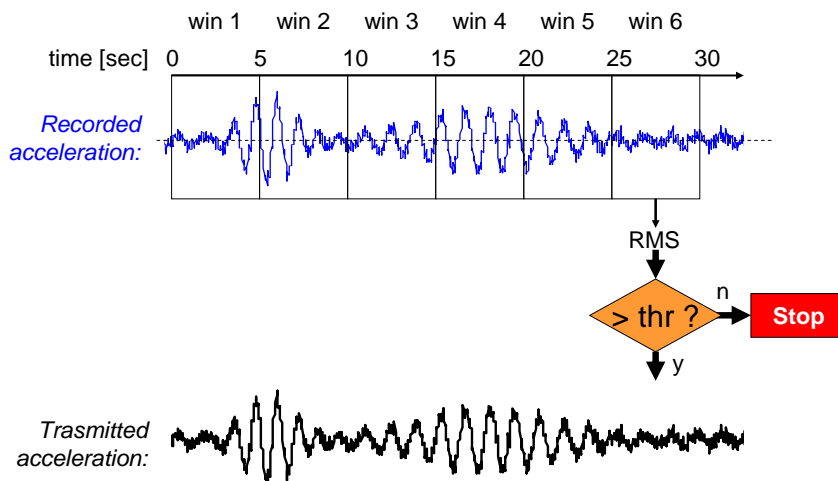


Figure 5-7 - Scheme of the software wake-up procedure

If data acquisition is still on (as $RMS > THR$ during the first time window), the same procedure is applied to the data recorded during the second 5-second time window, and so on. In other words, every 5 seconds the node decides whether to stop data acquisition and to cancel the last 5 seconds, because the vibration has become too small, or keep the acquisition on. In any case, when 30 seconds of acquisition have been acquired, the session is interrupted: if the vibration magnitude in the 6th window is relevant, the signal will last 30 seconds, otherwise it is limited to the first 25 seconds. Data are sent from the node to Base Station in hexadecimal format, to limit the amount transmitted. The Base Station is connected to a laboratory PC through USB cable. Data is acquired by of Microsoft Hyper-Terminal software.

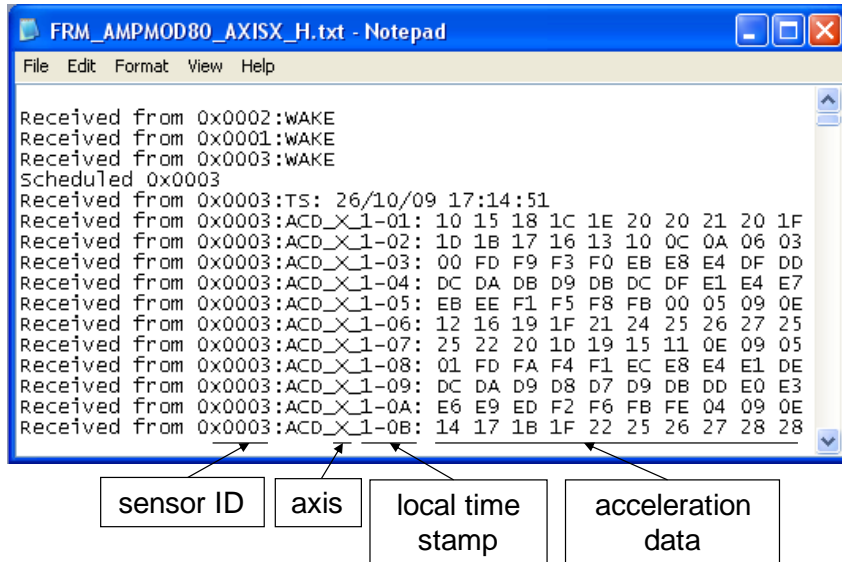


Figure 5-8 – Format of the transmitted data

The first lines of a sample file acquired by Hyper-Terminal contain the node wake-up messages and the global time stamp, identifying when the data transmission starts, according to the clock mounted on the node. The measurements are then local time-stamped, according to a time reference system from 0 to 30secs. To condense this local time with an efficient notation, the acquisition period (lasting up to 30 seconds) is divided into 6 packets of 5 seconds, these too divided into 50 sub-packets containing 10 acceleration values each.

5.3.2 Phase II.1 accelerometer

Phase II.1 accelerometer prototypes was developed for small-scale laboratory evaluation. It have been packaged in a temporary metal housing of size 10.5x7.5x3.5 cm and has a 7 cm long antenna. The weight of the node is about 165 g. The node is showed in the following figures.

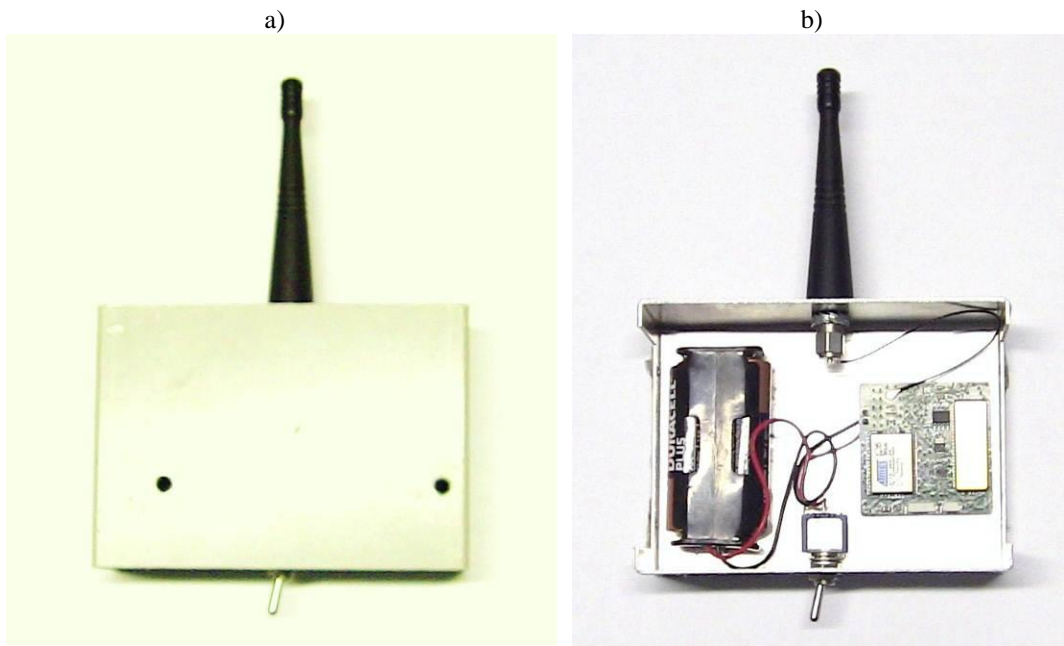


Figure 5-9 – The Phase II.1 accelerometer: outside (a) and inside (b)

Each node is able to measure accelerations in 3 dimensions, with three mechanically independent proof masses used to measure the acceleration in the 3 directions. The power is provided by two alkaline AA batteries.

Table 5-3 – Phase 2 accelerometer characteristics

Characteristic	Value
Sampling rate	200 Hz
Resolution	16 bit
Range	± 2 g
Max Voltage	± 1.25 V
Period of acquisition	up to 54 sec

The Phase II base station is implemented on a commercial available Meshbean module from Meshnetics. The connection to the PC is done using a standard USB connection with a micro-USB connector. The coordinator can acquire vibration data from many associated nodes within a range of dozens of meters, even inside a building. Moreover, at the same time it can acquire also strain measurements from wireless strain modules. The first time the coordinator is connected to the PC using the USB cable, the drivers for the SiLabs USB to serial bridge need to be installed. Before starting the MEMSCON viewer application, developed by IMEC, also CVI runtime (freely downloadable from the National Instruments website), needs to be installed. The viewer automatically finds the coordinator and shows the COM port number in the bottom status box. If no devices are

associated to the coordinator, the viewer displays “Number of associated devices: 0”. Turning the power on in the sensor modules one by one, each device is associated to the coordinator, and this is reported by the viewer software. It is possible to check the communication to each device by selecting the module number and clicking the “Ping device” button. The displayed frame in the status box contains the LQI (link quality indicator) which shows the quality of the wireless link (from 0 to 255, which means a perfect link).

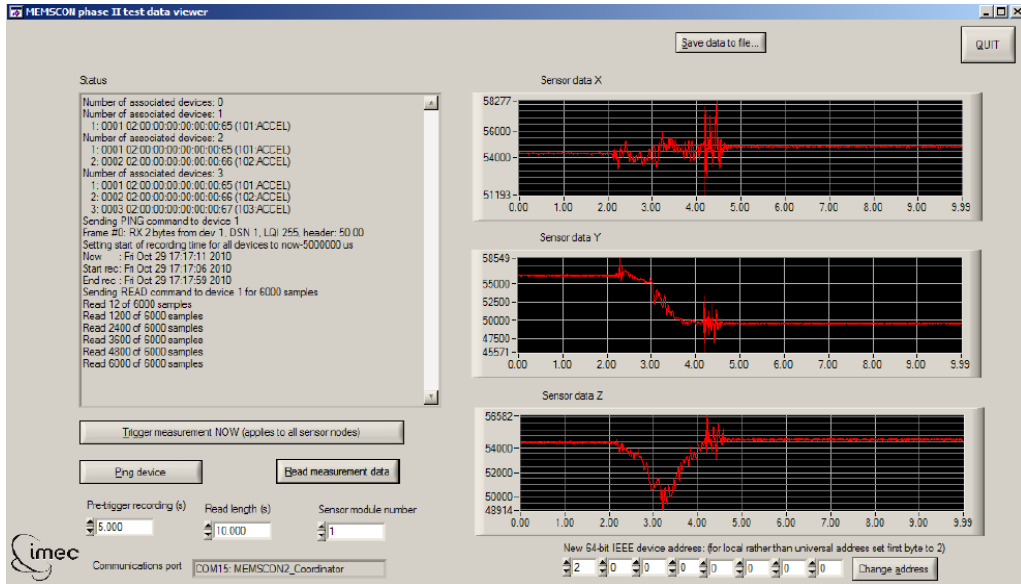


Figure 5-10 – Screenshot of viewer software and data acquisition process

A measurement is triggered, for all associated modules, by clicking the “Trigger measurement now” button. Before doing this, it is possible to select the desired pre-trigger recording time, between 0 and 50 seconds. In fact, sensors are always recording measurements, but they transmit data only when specified by the user. After the measurement is triggered, all associated sensor modules light up their orange LED indicating they are recording. The LED goes off and the recording ends 53 seconds after the start of the recording time. After waiting until the desired recording time has passed, it is necessary to select the desired readout length (maximum 53 seconds) and the desired sensor module. Reading out the recorded data wirelessly is possible by clicking the “Read measurement data” button. Readout progress is reported in the status box. When readout is finished, the data are visualized on the graphs on the right of the screen. Data can be saved to a CSV file with the button above the graphs. For the following analysis is possible to use Microsoft Excel and Matlab. Into each row of the data file, first column is the time, the second is the number of counts of the DAC on X axis, the third is the number of counts on Y axis and the fourth is the number of counts on the Z axis. To convert the number of counts to voltages, it is necessary to apply the ADC to Volts parameter to the counts, which is obtained dividing the maximum voltage range by the resolution (16 bit). It is important to note that a global

time stamp is not provided by the acquisition software. This is surely a limitation for the in-field application, doing the manual synchronization of the devices essential.

It is important to notice that reading out is possible for only one module at a time: this makes the reading out procedure very long if a great number of sensors is associated to the coordinator. . Moreover, I observed a glitch in the acquisition system (probably in the coordinator) which causes the frequent fail of the reading out. It has been noticed, during our tests, that the glitch occurs when more than one module is associated to the coordinator, whereas it doesn't occur when only one module is associated. When the glitch occurs, it is necessary to re-start the readout process. In this case, data aren't lost; however this problem increases exponentially the needed time for the acquisition.

5.3.3 Phase II.2 accelerometer

Phase II.2 MEMSCON accelerometers prototypes have been packaged in a metal housing of size 12x6.5x4 cm, with the antenna embedded into the package and not visible from outside the device. These devices were used for the system evaluation on the full-scale reinforced concrete frame reported below in this Chapter. The three orthogonal axes of the MEMS accelerometers (yellow part in the Figure 5-11) are directed as follows: X channel is along the package maximum length in plant, Y channel is along the orthogonal direction in plant, Z channel is directed as the thick of the device. Most important feature of MEMSCON devices are sampling rate equal to 200 Hz, a 16 bit resolution, 2.5V range and a 54 seconds maximum period of acquisition. Accelerometers package permits an easy connection of the device to the structure. In particular the holes along the lateral side permits to screw the accelerometers to the monitored surface.



Figure 5-11 – Phase II.2 MEMSCON accelerometer

5.3.4 Phase II.2 strain gauges

Phase II.2 MEMSCON strain measurement system consists of two parts, a strain mote to be attached externally to the structure and a strain sensor directly bonded to the steel reinforcing bars, connected

via a cable to the mote. From the user point of view, the front-end sensor (Figure 5-12) has a carrier made of polyimide approximately 8 cm long and 1 cm wide. PDMS cover is 4 cm long and 5 mm thick. Cable connecting mote (Figure 5-13) and front-end sensor is 25 cm long. Most important technical properties of the wireless module are a 16 bit resolution and a 2.5 V range. Phase II.2 strain sensors, like the Phase II.1 ones, sample single axis strain measures at 512 Hz then average the measures to reduce noise. Minimum sampling period is today 10 seconds. On each module up to 3 front-end strain sensors can be connected.

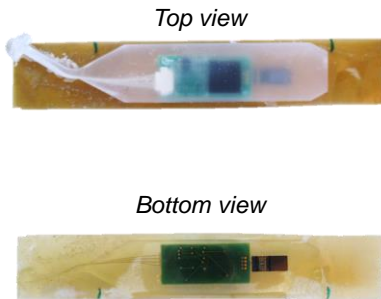


Figure 5-12 – Phase II.2 MEMSCON front-end strain sensor



Figure 5-13 – Phase II.2 MEMSCON wireless units for strain sensor

5.4 Laboratory evaluation of MEMSCON technology

5.4.1 Phase I accelerometer evaluation & calibration tests

Phase I accelerometers were tested comparing their response to dynamic excitation to the response of piezoelectric seismic accelerometers assumed as reference. The aim of the tests was to calibrate (that is to estimate their calibration parameters, in particular their sensitivity) MEMSCON devices, and evaluate their performance in terms of accuracy and precision compared to a reference sensor assumed as providing the “true” value of acceleration. Both types of sensors were placed on a dynamic shaking table (described also in Chapter 6) producing random and sinusoidal excitations of different frequency and amplitude. The testing scheme reflects the intent to acquire data independently and simultaneously from the reference and wireless sensors, subjected to the same excitation induced by the shaking table. The test set-up was arranged as follows:

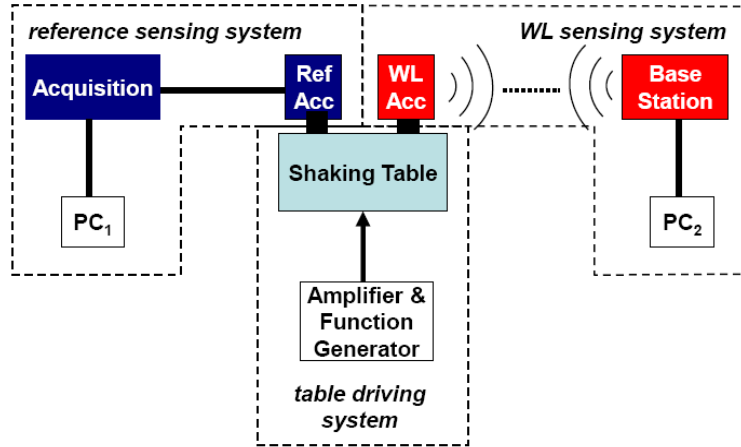


Figure 5-14 - Testing scheme

Three sub systems are evident: (i) the shaking table drive system, made up of the function generator (which generates the signal defined by the operator in terms of frequency), the amplifier (which amplifies the signal from the generator) and the shaking table, where the instruments are installed; (ii) the reference monitoring system, with the reference accelerometers (hereafter called “wired”), the acquisition board and a PC (labeled PC1) with a Labview application running; (iii) the MEMSCON monitoring system includes the wireless accelerometers, the base station and a PC (labeled PC2) with the MEMSCON application running.

Calibration was performed by using the “back to back” mounting scheme, by direct comparison between the reference accelerometer and the accelerometer under test. During the calibration tests, the shaking table was driven using a harmonic wave form defined by the operator using the function generator. For each direction of the sensors (X, Y, Z) tests at 1, 2, 4, 8, 16 Hz were carried out. Each test frequency was repeated twice at different wave amplitudes, with acceleration peaks of 1 m/s² and 4 m/s² (tests called “Low Amplitude” and “High Amplitude”, respectively). To sum up, 33 calibration tests were carried out. The accelerometers were connected to the shaking table in two different ways. The reference accelerometers were connected by steel studs to aluminum angle profiles, these in turn fastened to the shaking table by screws. The wireless accelerometers were fixed directly to the shaking table using thin double-sided tape.



Figure 5-15 - Sensor arrangement: (left) tests on X axis; (center) tests on Y axis; (right) tests on Z axis

In order to obtain the calibration parameters of the wireless sensors, it was necessary to make a pre-processing of data. In fact, the calibration parameters were given comparing the Fourier Transform (FFT) of the signals coming from the wireless sensors with the FFT of the signals coming from the corresponding reference accelerometer. To do this, it was necessary: (i) filtering the data, removing meaningless measurements; (ii) removing the offset (DC value) from the signals; (iii) synchronizing reference and wireless signals; (iv) finding the actual value of the wireless sensors sampling rate; (v) windowing both reference signals and wireless signals, in order to obtain a sample time period T_r that is an integer multiple of the fundamental period of the signal and avoid leakage (Ewins 2000).

Figure 5-16 reports the original time history of the test. In the graph, as in those below displaying time histories, the acceleration is plotted vs time. Three boxes are displayed, one for each pair of accelerometers: in the first the signals from B12-1 and WL1, in the second from B31 and WL2, and in the last from B12-2 and WL3. In each graph the black lines are the signals from the reference sensors, the red line refers to the signal from WL1 Phase I device, the blue refers to WL2 sensor and the green to WL3 sensor.

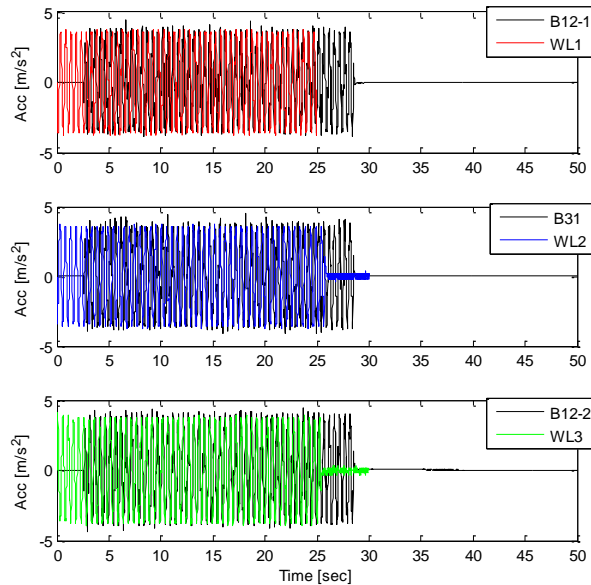


Figure 5-16 – Original time histories of the sample test

The first step in data pre-processing consists of deleting, from the acceleration measurements, data acquired when the shaking table is stopped, which are meaningless. For this purpose, a threshold was selected, large enough to be greater than the acceleration registered from the sensors under ambient noise only. This threshold value is set at 0.5 m/s². An algorithm deleting below-threshold data at the beginning and end of the signals was implemented in the Matlab code that pre-processes data acquired from the sensors. By implementing this procedure, the resulting signals refer to the table only when it is actually shaking. Specifically, the procedure obtains a signal that starts at a very low value of periodic vibration and also ends at a low value.

The offset of the signals was removed subtracting the mean value of the signals (over the total sample time period) to the signals. This operation will be repeated also after obtaining periodic signals. Reference signals start now from a time different from zero, this is due to the previous filtering procedure. Next step is to make reference signals starting from $t = 0$. To do this, the first value of the time vector has been subtracted to the entire vector.

The acquisition from reference and wireless sensors starts at different times. This is a direct consequence of the fact that the two acquisition systems are completely independent between them. Both temporal reference systems start from $t=0$ seconds, but they are not synchronized with each other.

Synchronization between the two systems has been performed manually, comparing for each tests the first peaks of the sin waves. Also the last peaks of the sin waves have been compared, in order to know whether sampling rate of Phase I devices was actually 100 Hz. Figure 5-17 shows that sampling rate is not 100 Hz, in fact time histories are not in sync with each other. Sampling rate of the Phase I devices was considered as a free parameter and changed until obtaining the best fitting. The actual sampling rate is reported in Table 5-4. After time scaling, wireless signals have been sampled again at exactly 100 Hz using the Matlab command *interp1q*.

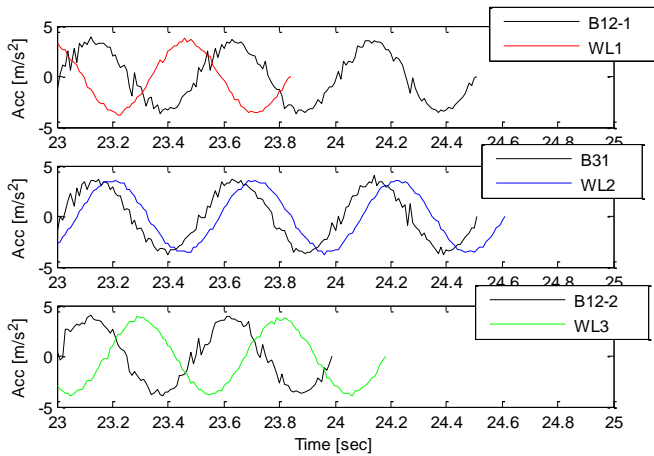


Figure 5-17 – Reference and wireless signals not in sync at $t = 25$ sec

Table 5-4 – Actual sampling rate of Phase I devices

Sensor	Sampling rate [Hz]
WL1	99.33
WL2	102.54
WL3	100.83

After synchronization and re-sampling, I obtained signals with 100 Hz sampling rate. Considering that the maximum frequency of interest contained in the signals is equal to 16 Hz, the sampling rate

is surely suitable to avoid amplitude ambiguities due to aliasing (Shannon’s sampling theorem (Ewins 2000)). Calculating the FFT, amplitude ambiguities (or leakage) also arise when the sampling period is not an integer multiple of the fundamental period of the signal. It can be demonstrated that the amplitude of periodic waveforms, as the signals I obtained during the tests, is accurately represented in the FFT when the sampling period $T_r = mT_1 = N/f_s$ where m is an integer, $T_1 (=1/f_1)$ is the fundamental period, N is the number of samples and f_s is the sampling rate. This implies that N must be equal to $m(f_s/f_1)$. After calculation of N for each signal, both reference and wireless signals have been therefore windowed by a rectangular window of magnitude equal to 1 and duration from $t = 0$ to $T_r = (N-1)*1/f_s$. In doing so, each window contains N samples and FFT can be calculated avoiding the leakage.

As mentioned above, calibration parameters of the wireless accelerometers was calculated directly comparing the FFTs of pre-processed reference and wireless signals. These signals had a sampling rate of 100 Hz and a number of samples N integer multiple of the fundamental period of both signals. The magnitude of the reference FFTs was in acceleration (m/s^2), the magnitude of the wireless FFTs was in counts. In Figure 5-18 and Figure 5-19 the spectra of the tests taken as example are showed. The spectra are reported in a semi-logarithmic chart, where the x-axis is the frequency domain (Hz) and the y-axis is the magnitude. In the figures, B12-1 and WL1 are plotted in red, B31 and WL2 are plotted in blue, B12-2 and WL3 are plotted in green. For each FFT (both reference and wireless), the peak of magnitude was then calculated. I plotted each reference-wireless pair in an acceleration-counts graph and I performed a linear regression to obtain the sensitivities of the devices.

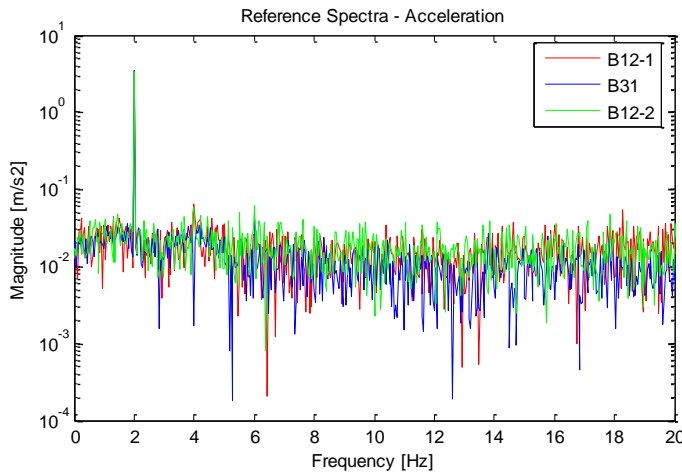


Figure 5-18 - Spectra of reference signals

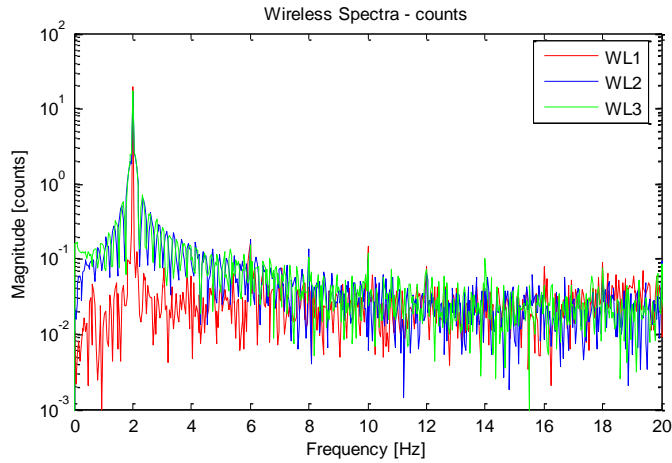


Figure 5-19 – Spectra of wireless signals

For each FFT (both reference and wireless), the peak of magnitude was then calculated. I plotted each reference-wireless pair in an acceleration-counts graph and I performed a linear regression to obtain the sensitivities of the devices. I noticed that not all data were meaningful, so some pairs have been discarded. Especially, all data obtained from tests at 16 Hz have been deleted because the scatter was too high. Calibration curves for X, Y and Z axes are reported in Figure 5-20, Figure 5-21 and Figure 5-22 respectively. Sensitivity values are reported in Table 5-5, Table 5-6 and Table 5-7.

Table 5-5 – Phase I accelerometer sensitivity (X Axis)

Sensor	S [counts/m/s ²]	R ²
WL1	5.6551	0.9994
WL2	5.8367	0.9899
WL3	5.5413	0.9954

Table 5-6 - Phase I accelerometer sensitivity (Y Axis)

Sensor	S [counts/m/s ²]	R ²
WL1	5.5145	0.9961
WL2	5.4720	0.9959
WL3	5.7699	0.9973

Table 5-7 - Phase I accelerometer sensitivity (Z Axis)

Sensor	S [counts/m/s ²]	R ²
WL1	5.5945	0.9976
WL2	5.6407	0.9979

WL3 5.5433 0.9990

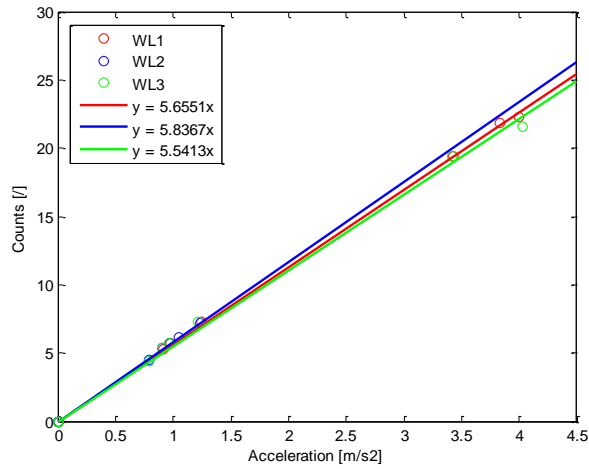


Figure 5-20 – Phase I calibration curves (X Axis)

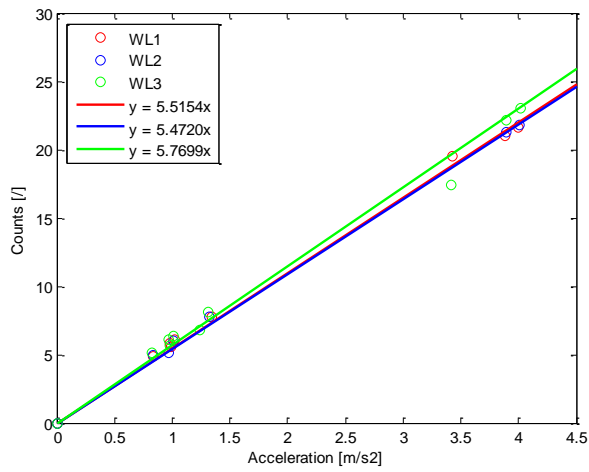


Figure 5-21 - Phase II calibration curves (Y Axis)

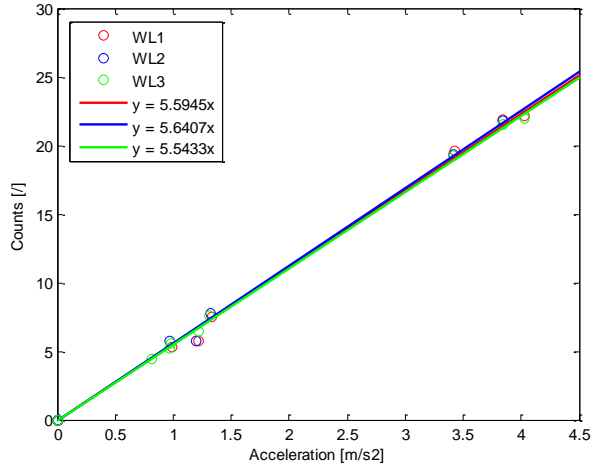


Figure 5-22 – Phase I calibration curves (Z Axis)

After the calibration of the MEMSCON Phase I wireless sensors, which means after having obtained their sensitivities, I have quantified the difference between the response of the calibrated wireless sensors and of the references. The committed errors are defined in terms of acceleration and are computed by analyzing the peaks in the wireless and reference signal spectra, applying the expression below:

$$E_{j,k} = 100 \times \left(\frac{M_{WL_{10i}} - M_{R_i}}{M_{R_i}} \right)_{j,k} \quad (5.2)$$

where subscripts identify the sensor ($i = 1,2,3$), frequency of the tests in Hz ($j = 1,2,4,8,16$) and acceleration amplitude ($k = L,H$), whereas M indicates the Magnitude (acceleration) of the peak of the spectra. We can esteem the resolution (in terms of acceleration) of the devices in about 0.17-0.18 m/s^2 (that is about 17-18 mg). The maximum scatter due to the resolution is therefore about 17% for low amplitude tests (that is when acceleration is around 1 m/s^2) and about 4% for high amplitude tests (when acceleration is around 4 m/s^2). In the following tables, errors in terms of acceleration for each test carried out are reported.

Table 5-8 - X Axis scatters (low amplitude tests)

f [Hz]	WL1 [%]	WL2 [%]	WL3 [%]
1	1.69	1.40	6.79
2	3.88	1.71	7.25
4	/	0.16	/
8	/	-3.35	-0.46
16	/	12.20	/

Table 5-9 - Y Axis scatters (low amplitude tests)

f [Hz]	WL1 [%]	WL2 [%]	WL3 [%]
1	2.71	0.04	12.50
2	6.50	/	13.01
4	4.93	1.33	12.68
8	0.06	0.41	3.90
16	-11.02	-22.65	-0.48

Table 5-10 - Z Axis scatters (low amplitude tests)

f [Hz]	WL1 [%]	WL2 [%]	WL3 [%]
1	/	-6.68	-2.25
2	/	/	-3.03
4	-37.6	-31.30	-25.60
8	-4.32	-1.51	1.93
16	-16.77	-16.84	-4.93

Table 5-11 - X Axis scatters (high amplitude tests)

f [Hz]	WL1 [%]	WL2 [%]	WL3 [%]
1	2.51	-1.19	7.96
2	0.03	/	2.59
4	0.78	/	/
8	-1.36	/	-3.39
16	-10.29	/	-18.82

Table 5-12 - Y Axis scatters (high amplitude tests)

f [Hz]	WL1 [%]	WL2 [%]	WL3 [%]
1	2.76	0.46	11-42
2	0.58	-15.89	-8.29
4	-4.07	-4.57	2.94
8	-4.44	-29.70	3.41
16	-15.21	-29.02	-12.37

Table 5-13 - Z Axis scatters (high amplitude tests)

f [Hz]	WL1 [%]	WL2 [%]	WL3 [%]
1	0.05	0.93	3.96
2	1.06	-2.57	1.50
4	0.74	-4.07	1.06
8	-2.81	-21.65	-1.85
16	-22.73	-31.27	-11.50

To obtain further information on the precision of the instruments tested, the standard deviation (STD) of acceleration errors were calculated, using fitted and synchronized time histories. A vector (i.e. a time history) of acceleration error is defined for each test as:

$$E_t = V_A(WL_i)_t - V_A(PCB_i)_t \quad (5.3)$$

where WL_i e PCB_i indicate the sensors “back to back” and t the time. Standard deviation of the acceleration error vector is defined by:

$$STD = \sqrt{\frac{1}{N} \sum_{t=1}^N (E_t - \overline{E_t})^2} \quad (5.4)$$

where $\overline{E_t}$ indicates the mean value. In the following Table 5-14 standard deviation values are reported for accelerometers WL1 WL2 and WL3 on the Y Axis. Values of the same order of magnitude were obtained for the X and Z Axis and are not here reported.

Table 5-14 – STD of acceleration error vector (Y Axis)

f [Hz]	A [m/s ²]	WL1 [m/s ²]	WL2 [m/s ²]	WL3 [m/s ²]
1	~ 1.00	0.24	0.23	0.19
2	~ 1.00	0.14	0.16	/
4	~ 1.00	0.13	0.13	0.17
8	~ 1.00	0.18	0.32	0.59
16	~ 1.00	0.23	0.44	0.70
1	~ 4.00	0.29	0.32	0.25
2	~ 4.00	0.40	0.43	0.35
4	~ 4.00	0.24	0.49	0.98
8	~ 4.00	0.57	0.61	1.06
16	~ 4.00	1.25	1.87	2.40

These values demonstrate good performance by the wireless sensors, as the errors are of same order of magnitude as the resolution (0,18 m/s²) for most of the tests. Nevertheless in high frequency tests (8-16 Hz) there is an increment in the errors recorded. This is probably due to the sampling rate (100 Hz) of the sensors used, inadequate to acquire data with sufficient precision at these frequencies. In any case this does not seem to be a problem: the sensors work well in the typical seismic range of frequencies (2-10 Hz)

5.4.2 Phase II.1 accelerometer evaluation & calibration tests

The procedure and the algorithms adopted for the calibration of Phase II.1 accelerometers are the same as the ones for calibration of Phase I instruments. In this set of tests, for each direction of the sensors (X, Y, Z) tests at 1, 2, 3, 4, 8, 10 Hz were carried out. The reference accelerometers are connected in the same way as in Phase I tests. The wireless accelerometers are fixed directly to the shaking table using double-sided tape during tests on Y axis, whereas during tests on X and Z axes they are connected to angle profiles by 2 stainless steel screws, screwed in the metal box of the devices. Like calibration of Phase I prototypes, also in this case the calibration was performed by using the “back to back” mounting scheme, directly comparing the outputs of the reference accelerometers and the accelerometers under test (Figure 5-23).



Figure 5-23 - Sensors arrangement (tests on X axis)

In order to obtain the calibration parameters of the wireless sensors, the same pre-processing as the one done on Phase I sensors has been performed.

In Figure 5-24 the original output, in voltage, from MEMSCON wireless sensors is plotted against the time. In this figure I observe that, probably due to a glitch in the software of the devices (or in the coordinator, or in both), there is a random axis shift in the readout. In fact, the shaking direction is always the Z direction but the devices record the shaking before on the Y Axis and then on the Z Axis. This glitch has not been represented a problem for the calibration because I knew *a priori* the direction of the shaking. It is obvious that during a future in-field operation, where shaking due to an earthquake is unpredictable, a glitch like this would be impossible to be fixed and so definitely unacceptable. Concerning the glitch, I have observed that the moment at which the data jump from an axis to another is always different among the tests, but all the sensors “jump” about at the same time. For this reason, the glitch were ascribed to the base station. The effect of the glitch was manually corrected before pre-processing the data.

Synchronization between reference accelerometers and accelerometers under tests proved that also Phase II.1 sensors exhibit an actual sampling rate which is different form the nominal value Table 5-15. Like Phase I accelerometers, Phase II.1 accelerometer therefore also show a defect in the clock. After synchronization of the signals, they have been re-sampled with a sampling rate equal to 200 Hz, using the Matlab command *interp1q*.

Table 5-15 – Actual sampling rate of Phase II.1 devices

Sensor	Sampling rate [Hz]
WL1	201.26
WL2	201.40
WL3	201.78

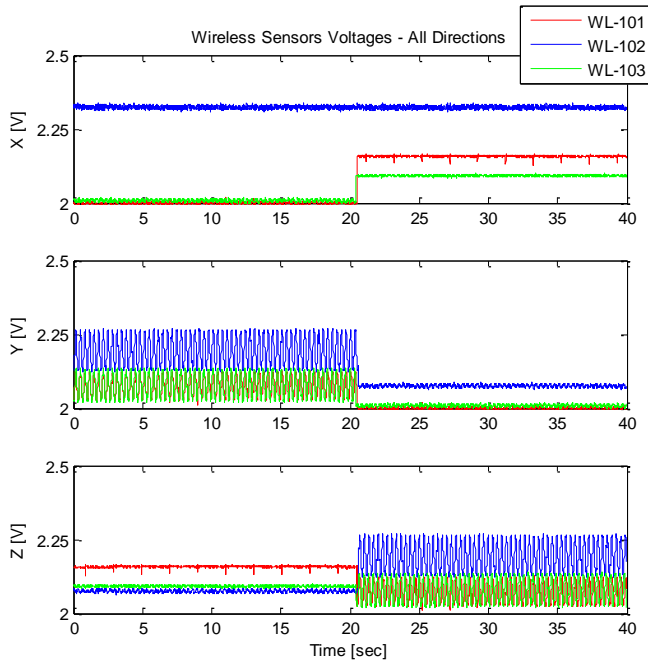


Figure 5-24 – Original output (Z direction, 3 Hz, High Amplitude test)

Calibration parameters of the wireless accelerometers were calculated directly comparing the FFTs of pre-processed reference and wireless signals. These signals had a sampling rate of 200 Hz and a number of samples N integer multiple of the fundamental period of the signal both after windowing. The magnitude of the reference FFTs was in acceleration (m/s^2), the magnitude of the wireless FFTs was in voltage (V). In Figure 5-25 and Figure 5-26 the spectra of the tests taken as example are showed. The spectra are reported in a semi-logarithmic chart, where the x-axis is the frequency domain (Hz) and the y-axis is the magnitude. In the figures, R1 and WL101 are plotted in red, R2 and WL102 are plotted in blue, R3 and WL103 are plotted in green. For each FFT, the peak of magnitude was then calculated. Simply dividing the peak in voltage by the peak in acceleration, the sensitivity S ($mV/m/s^2$) was obtained for each device, direction of shaking, frequency and amplitude. At the end of the analysis, regression lines of the pairs acceleration - voltage have been calculated. Their slope represents the sensitivity expressed in $[mV/g]$ of each wireless device.

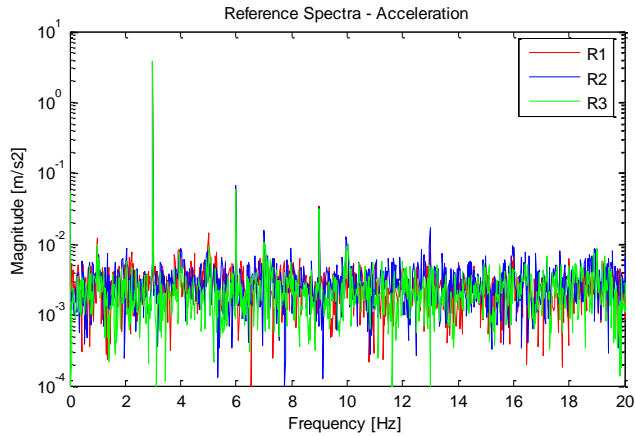


Figure 5-25 - Spectra of reference signals

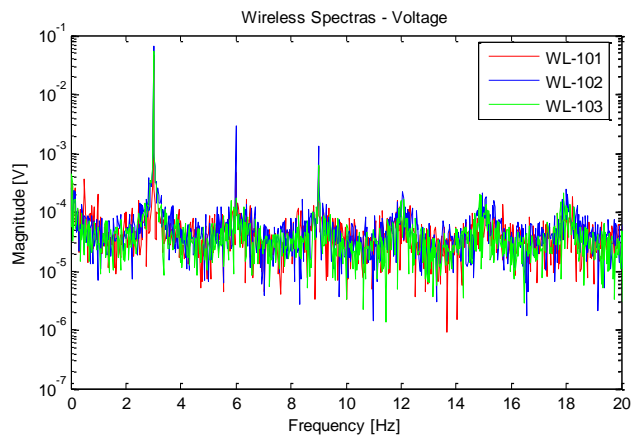


Figure 5-26 - Spectra of wireless signals

Table 5-16 – Sensitivity of Phase II.1 accelerometers (X Axis)

Sensor	S [mV/g]	R ²
WL1	110	0.9789
WL2	198	0.9999
WL3	216	0.9993

Table 5-17 - Sensitivity of Phase II.1 accelerometers (Y Axis)

Sensor	S [mV/g]	R ²
WL1	105	0.9818
WL2	383	0.9959
WL3	186	0.9996

Table 5-18 – Sensitivity of Phase II.1 accelerometers (Z Axis)

Sensor	S [mV/g]	R ²
WL1	120	0.9999
WL2	175	0.9997
WL3	141	0.9997

After the calibration of the MEMSCON wireless sensors, meaning after having obtained their sensitivities, I have quantified the difference between the response of the calibrated wireless sensors and of the references. The committed errors are defined in terms of acceleration and are computed by analysing the peaks in the wireless and reference signal spectra, applying Eq. (5.2). It is possible to esteem the resolution in acceleration of the devices simply by dividing their resolution in voltage (2.5 V / 65536) by their sensitivity. It can be said that the resolution in acceleration of Phase II.1 MEMSCON accelerometers is between 2 and 4 mm/s² (0.002-0.004 m/s²). The maximum error due to the resolution is therefore about the 0.4% for low amplitude tests (when acceleration is around 1 m/s²) and about the 0.1% for high amplitude tests (when acceleration is around 4 m/s²). In the following tables, errors in terms of acceleration for each test carried out are shown.

Table 5-19 - X Axis scatters (low amplitude tests)

f [Hz]	WL1 [%]	WL2 [%]	WL3 [%]
1	18.81	-2.63	-2.29
2	14.03	1.31	-2.93
3	8.31	-0.89	-2.26
4	1.87	1.89	-2.14
8	-4.92	-4.20	-0.86
10	-9.31	2.75	-0.40

Table 5-20 - Y Axis scatters (low amplitude tests)

f [Hz]	WL1 [%]	WL2 [%]	WL3 [%]
1	17.52	0.00	4.27
2	6.68	0.23	2.13
3	-8.96	-0.22	2.91
4	-16.63	-0.19	4.14
8	-23.13	-0.15	4.13
10	-31.82	1.03	3.14

Table 5-21 - Z Axis scatters (low amplitude tests)

f [Hz]	WL1 [%]	WL2 [%]	WL3 [%]
1	1.50	-0.91	0.00
2	-0.95	-2.68	-2.47
3	-1.04	-2.45	-1.91
4	-1.27	-1.64	-2.24
8	-1.62	-1.23	-0.93
10	-1.50	-2.11	-0.29

Table 5-22 - X Axis scatters (high amplitude tests)

f [Hz]	WL1 [%]	WL2 [%]	WL3 [%]
2	7.60	22.16	-1.40
3	3.78	8.78	-0.52
4	-3.81	7.39	0.14
8	-10.36	16.02	0.98
10	-13.03	16.15	1.21

Table 5-23 – Y Axis scatters (high amplitude tests)

f [Hz]	WL1 [%]	WL2 [%]	WL3 [%]
2	9.03	14.99	0.84
3	3.09	24.82	-0.59
4	-2.45	24.50	-0.46
8	-22.85	19.11	0.45
10	-29.77	18.18	-0.48

Table 5-24 – Z Axis scatters (high amplitude tests)

f [Hz]	WL1 [%]	WL2 [%]	WL3 [%]
2	-0.69	-1.43	-0.73
3	0.00	0.28	-0.38
4	0.13	0.57	0.30
8	-0.43	-0.03	0.79
10	-1.74	0.13	1.23

After calibration tests, additional tests were performed in order to determine the performance of the MEMSCON accelerometer. Besides tests on a metal frame, which will be explained below, sweep tests have been carried out also directly on the shaking table, keeping the same set-up used during calibration tests. Sweep tests were performed by setting the function generator so that it will produce

a vibration which changes in time. Especially, frequency of the shaking varies from 1 to 10 Hz along a period of 30 seconds, whereas the output of the function generator remains constant. Wireless signals were analyzed simply applying sensitivities and actual sampling rates, obtained both during calibration tests. Filtering has not been performed. Wireless and reference signals have been then synchronized with each other. Sweep tests were performed along all the three axis of the wireless accelerometers. Even so, only outcomes of tests along Z axis are in the following reported. In fact, as reported in the chapter concerning calibration, sensors WL101 and WL102 do not work well along X and Y axes (in particular sensor WL102 goes out of range) and the outcomes should not be meaningful for the characterization of the devices. For example, time histories of a sweep test performed along X axis is showed in Figure 5-27. Vibration was recorded so that at the beginning of the signals there are about 200 samples acquired while the shaker was not moving. I used these samples to determine the background noise of the signals, in terms of RMS. As mentioned above, error due to resolution is about 0.2-0.4 mg. The second cause of error is the background noise. It is clear that it cannot be calculated in a absolute sense but it can be related to the background noise of the reference PCB sensors. I noted that background noise of the MEMSCON device is higher than the one of the reference sensors. In particular, the values of the background noise are summarized in the following table.

Table 5-25 – Background noise of Memsccon and reference accelerometers

Sensor	Background noise [m/s ²]
WL101	0.1058
WL102	0.1169
WL103	0.1199
R1	0.0025
R2	0.0039
R3	0.0036

Reported data demonstrate that background noise on the wireless signals is about forty times the background noise of the reference signals (or the resolution). The actual limit of the devices is therefore not the resolution, but the background noise. This is confirmed by computing the STD value of the acceleration error vector. I observed that its value is about 0.15 m/s² which is of the same order of magnitude as the background noise, not as the resolution.

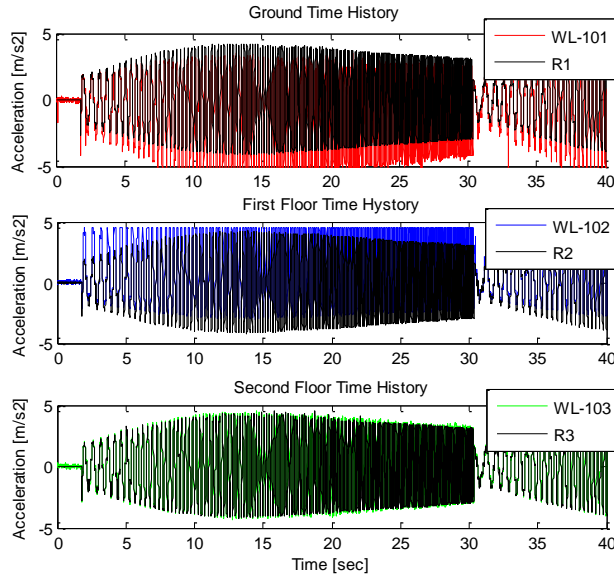


Figure 5-27 - High amplitude sweep test along X Axis time histories

5.4.3 Earthquake simulation on small-scale metal frame

For this type of tests a 2 storey steel/aluminum frame (Figure 5-28) was mounted on the shaking table. The frame has 4 steel columns between each floor, which are represented by aluminum slabs. This kind of tests allows also to estimate the mechanical properties of the structure employed in the tests (i.e. the metal frame) that corresponds to the building potentially damaged during an earthquake, e.g. via classical modal testing. By installing wireless and wired instruments back to back on the frame, three different time histories were induced: one on the table and two on the frame floors, correlated by the mechanical properties of the structure. On Phase II.1 sensors, 2 modulating frequency tests (“SWEEP TEST”) and 1 random input test were carried out.

Some physical properties of the frame are here reported. The weight of the structure was about 8 kg per floor slab. Natural frequencies were observed as equal to 2.1 Hz (first mode of vibration) and 5.2 Hz (second mode of vibration). Damping factor was estimated as about 1%.



Figure 5-28 – Steel/Aluminum frame

During the sweep test carried out on the metal frame the function generator was set so that frequency varies from 1 to 10 Hz along a period of 30 seconds. Moreover, the test was performed along Z axis only, since the bad performance of the wireless accelerometers along the other two axes. At least, it is important to note that only one test at low amplitude was performed, since the reference accelerometers can measure accelerations below about 0.6 g only. Recorded time histories, after conversion from voltage to acceleration, correction of the sampling rate and synchronization between the two acquisition systems are showed in the following figure. In the first box, the pair on the ground is reported, in the second the pair on the first floor and in the third the pair on the second floor. Lines and axes have the usual meaning: red line is sensor WL101, blue line is sensor WL102, green line is sensor WL103 and black lines are reference sensors.

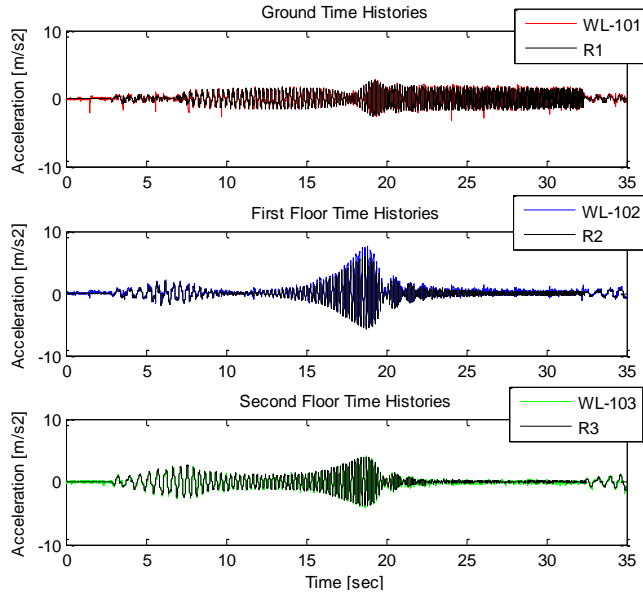


Figure 5-29 – Sweep test on frame time histories

It is interesting to determine the RMS values of the error committed by the MEMSCON devices, keeping in mind that the error due to resolution is about 0.1 mg. STD values obtained for this test are as follows:

Table 5-26 - STD error (sweep tests)

Sensor	STD [m/s ²]
Ground (WL101)	0.2618
1° Floor (WL102)	0.2077
2° Floor (WL103)	0.1468

As it can be noted from the table, STD value of the error is not of the same order of magnitude as the sensors resolution. However, it can be said the error is of the same order of magnitude as the background noise.

Last typology tests was the simulation of an earthquake, setting the function generator so that producing a random vibration like that occurring during an earthquake. For this purpose, the software supplied with the function generator was used. This software (Agilent Waveform Editor) permits to save into the function generator a vibration history decided by the user (also random) simply copying the amplitudes (voltages) in a table of the software. At the moment of the test, the vibration is defined by these amplitudes (in case multiplied by a factor) and by the period of the shaking. I set a random vibration like a real seismic event. The time history has been saved and so it is easily reproducible with the mentioned above software. Two tests were performed along Z axis only. Recorded time

histories of the first test, after conversion from voltage to acceleration, correction of the sampling rate and synchronization between the two acquisition systems are showed in the following figure.

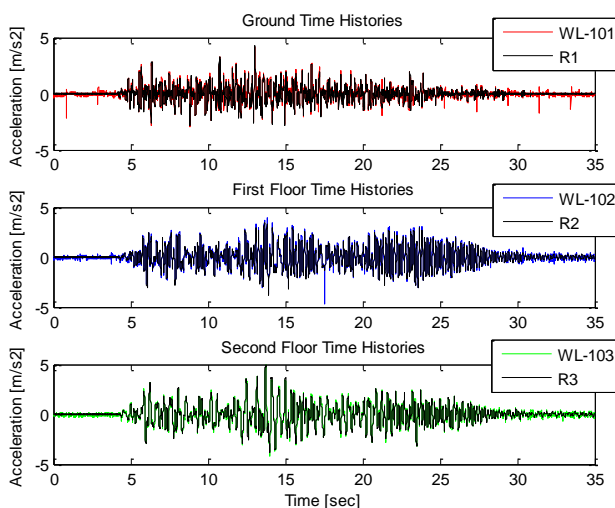


Figure 5-30 - Earthquake simulation test time histories

The STD values of the error were calculated also for this tests. They are reported in the following tables.

Table 5-27 – STD of earthquake simulation tests error

Sensor	STD [m/s ²]	STD [m/s ²]
	(test 1)	(test 2)
Ground (WL101)	0.1754	0.2095
1° Floor (WL102)	0.1317	0.1617
2° Floor (WL103)	0.1225	0.1464

Also in this case RMS values of the error are not of the same order of magnitude as the sensors resolution, but rather as the background noise.

5.4.4 Test on full-scale 3D frame

Introduction to the experimental validation

This validation campaign aimed at reproducing in laboratory conditions the possible extreme scenario which a real building monitored by MEMSCON monitoring system might encounter during its life cycle. In particular, during an earthquake the columns of a building can suffer extensive damage including concrete cracks, cover spalling, crushing and reinforcement yield. Moreover, these damages can be due also to foundations settlements. For this test, I considered only the damage occurring during an earthquake while ground settlements were neglected. Anyway, the frame was instrumented

also by Phase II.2 strain gauges, because they were expected to survive to the earthquake without loss of functionality. Strain gauges are in fact needed in the Memsccon methodology to provide a reliable input on the initial conditions at the start of the seismic event and to highlight possible inelastic deformations of the reinforcing steel.

The tests were carried out on a 9 square meters reinforced concrete specimen, consisting of four beam foundations in both longitudinal and transverse directions (being the longitudinal direction the direction parallel to the application of the force), four columns, four beams and a rigid slab. The strain sensors were bonded to the four corners of each frame column (16 sensors in total). The accelerometers were instead mounted above the concrete slab.

The frame was tested inducing progressive damage by the dynamic application of controlled displacement time histories at the top of the structure. Moreover, the frame was tested to collapse by static loading. The load forces and displacements applied to the test structure during the laboratory tests were selected in order to reproduce the behaviour of a standard building sited in a seismic zone. In particular, I selected a building dynamically characterized by a natural frequency of 1.5 Hz and applied loads compatible with laboratory equipment. Test protocol is fully illustrated in the following of this Chapter.

The simulated building

The considered construction (Figure 5-31 and Figure 5-32) consists of two buildings, intended for public use, linked one to the other in terms of resistance to the earthquake. In particular building A is a concrete building with dimensions in plane 12.3 x 12.3 meters whereas building B is made of precast concrete elements with dimensions in plane 26.9 x 12.5 meters. Building A is considered the only one resisting to lateral forces, whereas Building B lateral stiffness is assumed equal to zero. The lateral stiffness of the global construction is therefore given by the one of the concrete building only. Distribution of the resisting elements of building B is not of interest: building B is considered only in terms of mass in order to define the model for seismic analysis. Concerning Building A, the columns in plan are pitched at dimensions 3 x 3 meters and are parts of frames connected by concrete beams 30 x 50 in Y direction and 30 x 40 in X direction. The building has two floors out of the ground. The vertical floor pitch is 3.20 meters so the columns have a net height of 2.7 meters. The three-dimensional frame tested in laboratory is extracted by Building A (yellow square indicated in Figure 5-32).

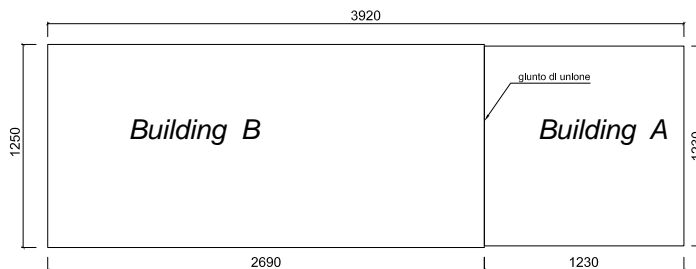


Figure 5-31 – Scheme of the construction

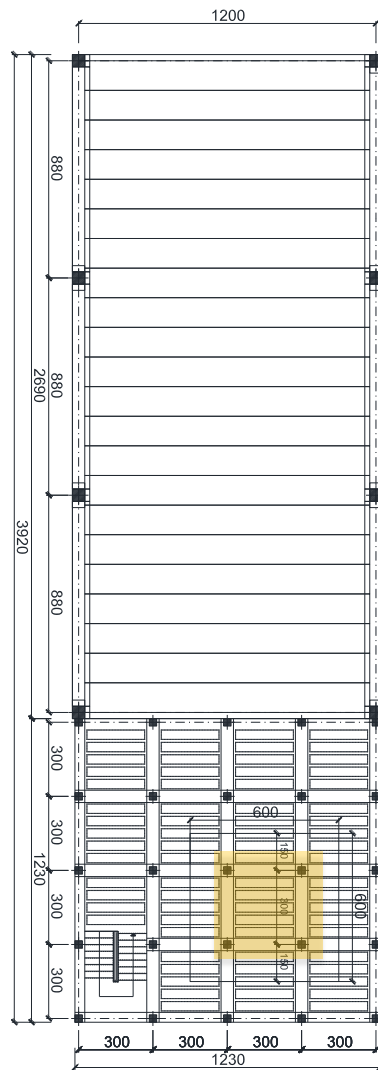


Figure 5-32 - Plane view of the construction

In terms of resistance to the earthquake, the construction (Buildings A and B) was schematized as follows:

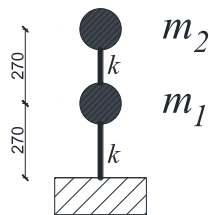


Figure 5-33 – Model for seismic analysis

In Figure 5-33 K is the sum of the columns stiffness (25 times the single column stiffness k). The masses m_1 and m_2 are instead equal to 4685 kN and 3515 kN respectively. Considering the mass and the stiffness, the eigenvalues of the systems with two degrees of freedom are evaluated as (Chopra 2011):

$$\lambda_{1,2} = \frac{m_1 k_2 + m_2 k_1 + m_2 k_2 \pm \sqrt{(m_1 k_2 + m_2 k_1 + m_2 k_2)^2 - 4m_1 m_2 k_1 k_2}}{2m_1 m_2} \tag{5.5}$$

Specimen design

Geometry of the structure to be designed is illustrated in the following figures:

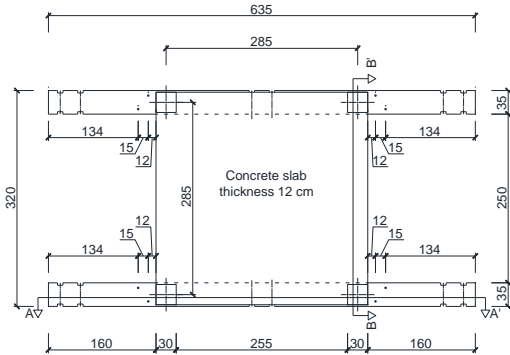


Figure 5-34 - 3D frame - Plane view

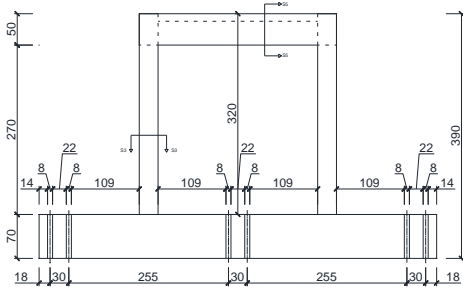


Figure 5-35 - 3D frame - Lateral view

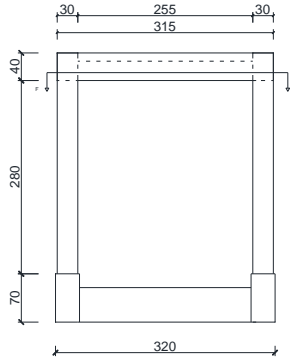


Figure 5-36 - 3D frame - Front View

The reference standard used for the specimen design is the European standard UNI EN 1992:2005 and Italian standard “Norme Tecniche per le Costruzioni 2008”. Here, only the results of the design process are reported. The interested reader can find the details of the design of the specimen in (Trapani et al. 2012; Cigognetti 2012; Coato 2012).

The column was designed with section 300 x 300 mm, reinforced longitudinally with 4 ribbed steel bars type B450C of diameter 20 mm (Figure 5-37).

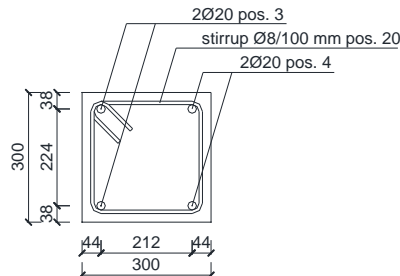


Figure 5-37 – Column cross section

The resistant bending moment M_{Rd} for the section when at the column head there is an axial compression force of 150 kN is therefore 93 kNm. To determine the maximum shear force in the column, which forms the plastic hinge at the column base, I divided the resistant moment by the half length of the column, obtaining $V_{Ed} = 65$ kN. To provide the column ductile behavior and to avoid shear failure, stirrups with diameter of 8 mm and pitch equal to 100 mm inside and to 200 mm outside the plastic region were provided.

The foundation of the 3D frame has the main function of anchoring the specimen to the ground and of guaranteeing the cantilever restraints at the bottom extremity of the column. The foundation strength must therefore be higher than the one of the column. Moreover, in order to assure the planned column behavior, the foundation was designed with the first cracking moment greater than the resistant moment of the column. This in order to realize a foundation beam very rigid and so to limit the rotation that can occurs around the plastic hinge. The column transmits to the foundation a shear

force and a bending moment. The shear is transferred directly to the laboratory strong floor by friction, without creating additional bending stresses in the beam. The bending moment instead reaches the ground by means of the bars embedded into the foundation beam. The longitudinal foundation cross section is showed below:

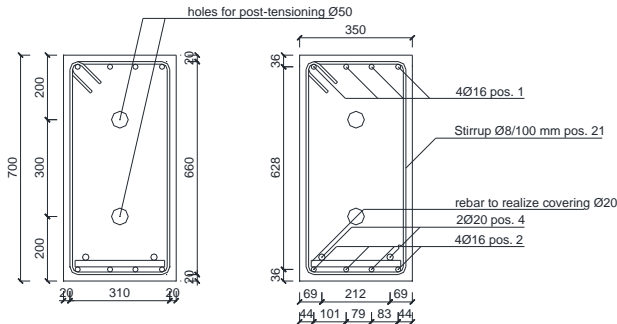


Figure 5-38 – Longitudinal foundation beams cross section

The longitudinal reinforcement is assumed as 4+4Ø16. The foundation beam is also pre-stressed with a force of 1400 kN in order to increase the first cracking bending moment. The resulting bending moment of first cracking M_{cr} is equal to 220 kNm and resisting bending moment M_{Rd} of the section is equal to 450 kNm

Since the constraint of the frame to the ground is given by the anchors embedded into the primary foundation beam, transverse secondary beams of the foundation does not have a specific structural function during the test, having also the direction orthogonal to the application of horizontal force. These beams, however, assume considerable importance during the carriage of the frame in the laboratory, providing to the frame (together with the longitudinal beams of the foundation) a closed ring with high stiffness, which contributes to avoid cracking of the structure.

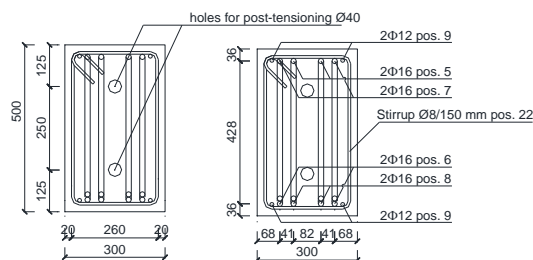


Figure 5-39 - Transverse foundation beams cross section

In the case of upper beams it is required that the value of their resisting moment is higher than the one of the columns, because I want the formation of plastic hinges only in the columns. The structural scheme of the beam can be assumed as a doubly framed element with moments applied at the ends equal to the resisting moment of the columns and distributed load equal to the own weight plus the weight of the concrete slab. The beam geometry is represented in the figure below:

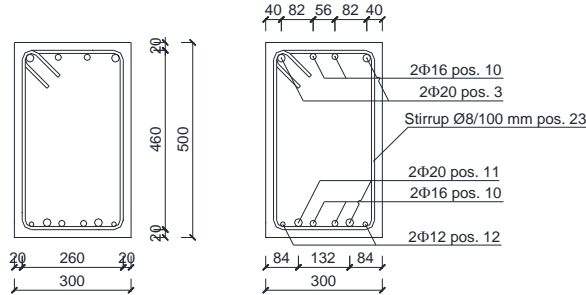


Figure 5-40 – Beam at the top cross section

As the secondary foundation beams, secondary beams in elevation also have no structural function during the experimental test, but are particularly important during the carriage of the frame. The geometry of the secondary upper beam is showed in the figure below:

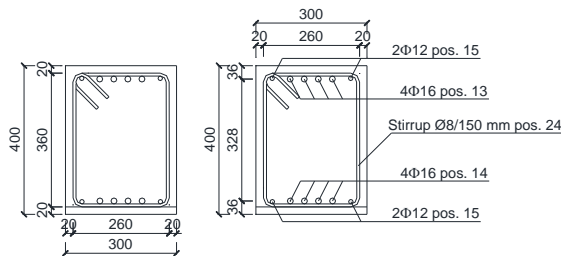


Figure 5-41 - Transvers beam at the top cross section

Designing the concrete slab I take into account both vertical (given by the own weight) and horizontal (given by the actuator) loads. I considered the following slab geometry:

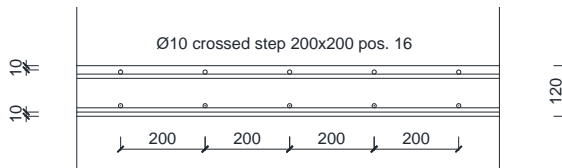


Figure 5-42 – Concrete slab cross section

Test setup

In order to avoid slipping and overturning of the frame during dynamic test, the frame was fastened to the strong floor of the laboratory. Considering the horizontal load was about 500 kN and the friction factor was assumed as 0.1, I placed at the end and in the middle of each foundation three steel plates type S235 of size 500*1400 mm and thickness 80 mm (Figure 5-43). The plates were fastened to the strong floor with 2 Diwidag bars of nominal diameter 36mm each. The post-tension in each bar is 500 kN (70% of the maximum strength). To apply vertical and horizontal load to the frame, two dynamic actuators were used at the same time. Vertical load was set in order to simulate vertical load into the columns at the ground floor of the building. Horizontal displacement instead was set to simulate the response of the building to the target earthquake. The horizontal actuator was operating in

displacement control and imparting to the slab the fast displacement corresponding to the design ground acceleration. It was a MTS 244.51 dynamic actuator with a 500 mm stroke, a 1000 kN capacity and a 680 litres per minute 3 stages servovalve. The vertical actuator, in force control, was connected to a steel distribution frame transferring the vertical seismic load to the centreline at the top of concrete columns. It was a MTS 243.60 static actuator with an asymmetric cylinder, a 500 mm stroke, a 1000 kN nominal capacity in compression, 660 kN in tension and a 60 litres per minute 2 stages servovalve.



Figure 5-43 – Anchorage of the frame to the strong floor

Both the actuators were connected to the same manifold MTS 293.32, which is a nitrogen filled accumulator connected between the actuators and the pumps intercepting the oil flow and allowing the operator to apply a zero, low (40 bar) and high (210 bar) oil pressure downstream, beside adsorbing any oil column shocks. The nominal oil flow is 943 litres per minute, theoretically sufficient to provide the optimal oil flow to both the actuators in extreme operating conditions. In fact this assumption was respected only for low amplitude of horizontal displacement tests: a reduction of the vertical force transmitted from the 243 actuator was detected in the central part of the tests, corresponding to the higher horizontal displacement and, in turn, to the oil demand peak. Horizontal and vertical actuators were controlled using a MTS FlexTest controller which provides high-speed closed-loop control, function generation, transducer conditioning and data acquisition for a full range of testing types, including real-time dynamic tests.

I designed two different load distribution systems, one for vertical load and the other for horizontal load. Vertical load was produced by MTS actuator code 243.60. As mentioned, vertical actuator was set to produce traction. A downward load was directly applied to a properly designed steel beam above the slab, as represented in Figure 5-44, through threaded bars crossing the slab. Steel beam connected to the vertical actuator was supported by two others steel beams supported they themselves by the columns. Using this vertical load system no loads were directly applied to the slab, which is totally unloaded. Horizontal load was produced by MTS actuator code 244.51. The actuator was dynamically controlled in displacement by the MTS controller, reproducing the response of the

structure to the target earthquake. In order to permit both traction and compression loads, the system I designed consists of two steel plates, attached to the transversal beams, rigidly connected by threaded bars. This “cap” was then connected to the horizontal actuator by others threaded bars. The load is therefore directly applied to the slab and not to the beams. Diaphragm behavior assumed for the slab ensures that horizontal displacement was equally transmitted to the head of the columns as requested.

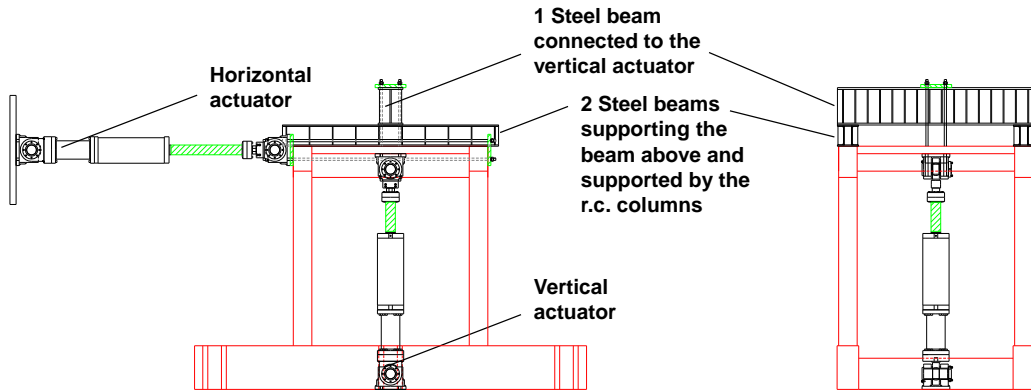


Figure 5-44 – Load distribution system

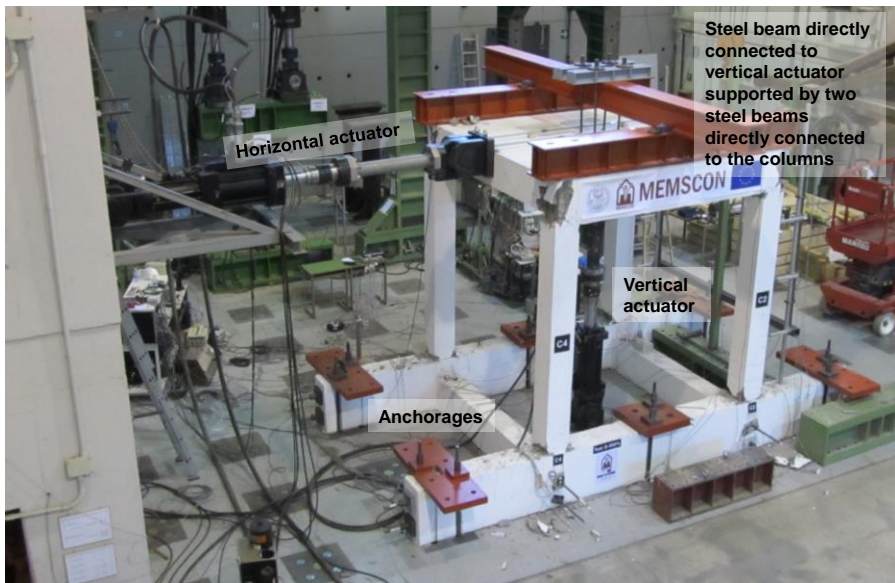


Figure 5-45 – Test setup

The instrumentation installed on the frame during the test includes:

- Memsccon strain gauges;
- HBM strain gauges;
- Memsccon accelerometers;
- PCB Piezotronics accelerometers;

- Gefran LVDTs;
- Cameras

I installed one MEMSCON strain sensor on each bar of the frame (16 sensors in total), all approximately at the interface level between foundation and columns, i.e. where position of the plastic hinges was expected. MEMSCON strain gauges were used above all to monitor strain during construction and concrete hardening (the system was turned on just after slab construction) and to verify the survival rate of the sensors after the simulated earthquake event. Sampling period (10 sec) was instead obviously unsuitable for monitoring during the simulated earthquake. HBM strain gauges were bonded on the longitudinal bars in the column in order to measure bar strain of the rebars both during construction and dynamic test. The strain gauges used were model HBM LY41-3/700. I installed 2 HBM strain gauges on each rebar, one at the same level of the MEMSCON strain gauge on the other side and one on the same side about 5 cm above. In any case, only 16 strain sensors were acquired during the tests, the ones on the same side of the MEMSCON sensors, because there weren't enough available channels in our acquisition devices. HBM strain gauges were used both for long term monitoring during construction of the frame and hardening of concrete and during dynamic tests. In particular, during construction we acquired strain data from all 16 HBM sensors by using a National Instruments Field Point system, consisting of FP2000 and 3 FPSG140. During dynamic tests I acquired instead 8 HBM sensors (embedded in columns 2 and 4) by using Field Point and the others 8 sensors (embedded in columns 1 and 3) by using HBM Spider 8. This because the limit of Field Point is the small settable sampling rate (1-2 Hz).

I installed 4 MEMSCON accelerometers above the frame slab, two above column C3 and two above column C2. The following figure represents the adopted configuration.



Figure 5-46 –Arrangement of the accelerometers above the slab

The reference accelerometers I installed above the frame close to the MEMSCON instruments were piezoelectric mono-axial high sensitivity accelerometers model 393C produced by PCB Piezotronics Inc. Acquisition module I used was model NI PXI 4472B produced by National Instruments.

To measure horizontal displacements during dynamic test along the columns I installed a set of Gefran LVDT displacement transducers at different heights. The steel structure supporting the instruments

was totally independent from the concrete frame, in order to avoid measurements uncertainties due to structure vibration. All displacement transducers were acquired from a MTS 494.75 board installed on MTS FlexiTest Controller.

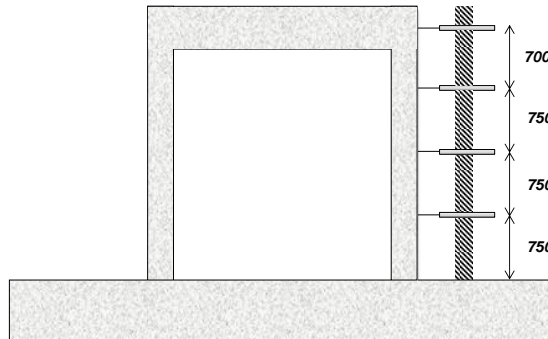


Figure 5-47 – LVDTs transducers coordinates

In the end, two cameras were installed in front of columns C1 and C3, in order to observe the evolution of cracking during the test. Another camera was installed on the side of column C3. During the tests, all the cameras recorded videos showing histories of displacements and the evolution of damage.

Load protocol

For the dynamic test I assumed as target earthquake a natural spectra-compatible earthquake in according to the Eurocode 8. To do this I used software REXEL (Iervolino, Galasso, and Cosenza 2009), having assumed a site class C and a topographic amplification factor equal to 1, and being the spectra parameters: $S = 1.15$; $T_B = 0.20$, $T_C = 0.6$, $T_D = 2.0$. The spectra-compatible earthquake found by the software is the Chenoua earthquake occurred on 29/10/1989 (Bounif et al. 2003).

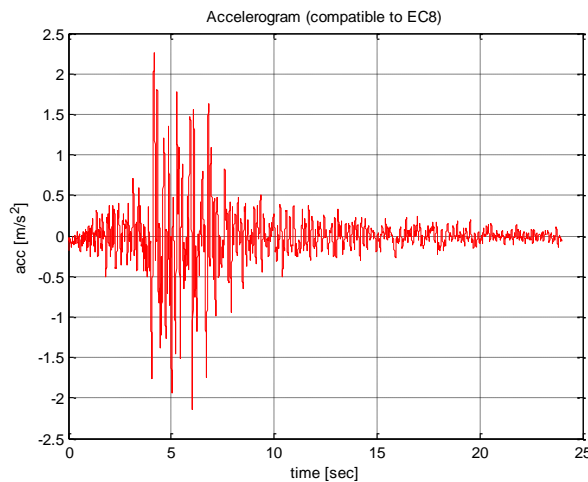


Figure 5-48 – Accelerogram of Chenoua earthquake

To obtain the history of displacements, I estimated the response of a single degree of freedom elastic system subjected to the ground acceleration, assuming a natural frequency of 1.5 Hz and damping ratio of 5%, applying the Newmark-beta method (Chopra 2011) to obtain the response of the model in terms of relative displacement respect to the ground.

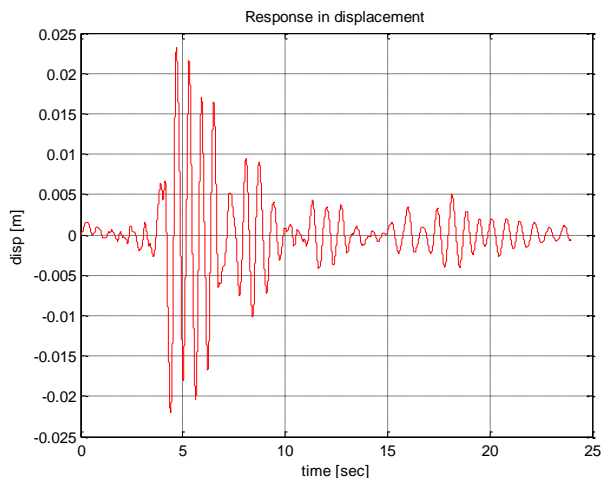


Figure 5-49 – Response in terms of displacement respect to the ground

This response in displacement was our reference during the dynamic test: I scaled it increasing maximum displacement produced by horizontal actuator, up to limit states as cracking, yielding and collapse.

I estimated from the double integration of the curvature along half the height of the column a displacement at first cracking equal to 1.2 mm. Displacement at yielding was instead estimated as 17 mm. I defined sequence of tests considering the value of displacement expected at first cracking of the frame d_{crack} and the value of displacement expected at yielding Δ_y as references. In particular I performed one tests with maximum displacement equal to the expected one of cracking and then I modulated the maximum displacement as reported in the following table.

Table 5-28 – Tests sequence

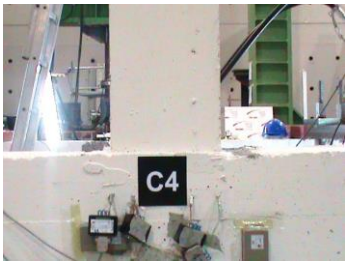
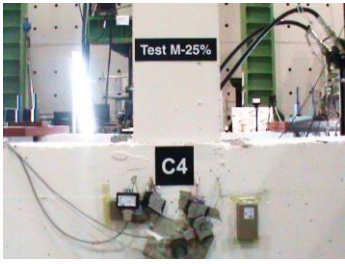
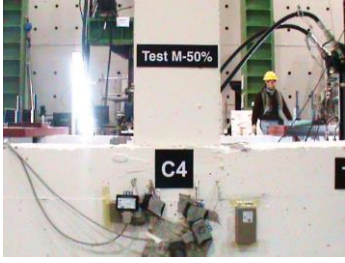
Test ID	Δ_{max} [mm]
I-crack	1.5
25% Δ_y	4.0
50% Δ_y	8.5
75% Δ_y	13.0
100% Δ_y	17.0
125% Δ_y	21.0
150% Δ_y	25.5

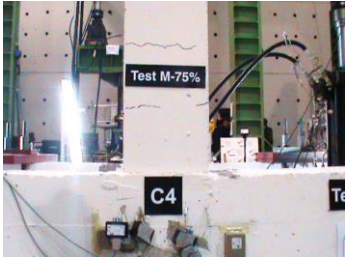
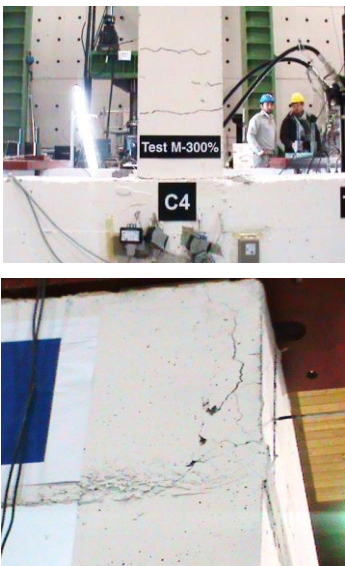
200% Δ_y	34.0
300% Δ_y	51.0
400% Δ_y	68.0
500% Δ_y	85.0

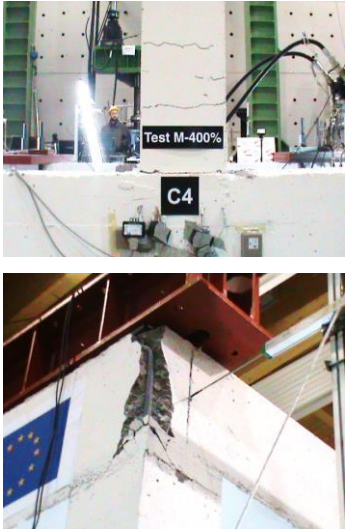
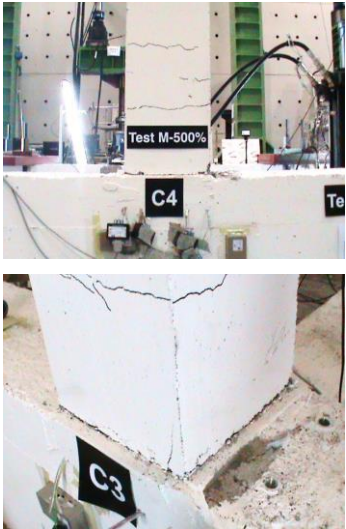
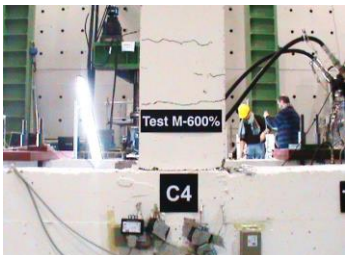
After each dynamic test, moreover, I induced also a static displacement history, with the same maximum displacement produced during the previous dynamic test, in order to assess frame stiffness to horizontal displacements and to check if the structure behavior was the same I expected during preliminary analysis.

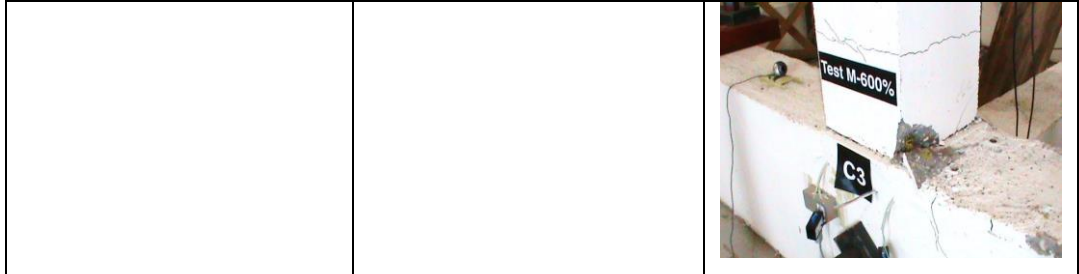
Test results

Below I report a table describing for each test the damage we observed after the seismic event. In the column reporting the picture, I selected to report the column C4 damage state or damage occurred in places different from columns.

Test	Damage Description	Damage Picture
Before the tests	No visual damage in the columns	No damage
Crack	No visual damage in the columns	
25% Δ_y	Cracking at the bottom of columns C1, C2, C3 and C4	
50% Δ_y	No further damage	

<p>75% Δy</p>	<p>Horizontal cracks in correspondence of stirrups in columns C1, C2, C3 and C4</p>	
<p>100% Δy</p>	<p>Cracking diffusion</p>	
<p>200% Δy</p>	<p>Cracking diffusion</p>	
<p>300% Δy</p>	<p>Cracking at the upper node</p>	

<p>400% Δy</p>	<p>Concrete spalling at the upper node</p>	 <p>The top photograph shows a wide view of the test setup for 'Test M-400%' with a label 'C4' in the foreground. The bottom photograph is a close-up of the upper node of column C4, showing significant concrete spalling and exposed reinforcement.</p>
<p>500 Δy</p>	<p>Concrete spalling at the bottom of columns C3 and C4</p>	 <p>The top photograph shows the test setup for 'Test M-500%' with labels 'C4' and 'Te'. The bottom photograph is a close-up of the base of column C3, showing concrete spalling and exposed reinforcement.</p>
<p>600% Δy</p>	<p>Diffusion of damage</p>	 <p>The photograph shows the test setup for 'Test M-600%' with a label 'C4'. It illustrates the progression of damage across the structure.</p>



After each dynamic test I performed also a static tests, in order to check if the structure behavior was the same I expected. In particular each static test consisted of a first step of vertical loading and of a following horizontal loading produced by horizontal actuator. Vertical actuator was controlled in force (producing the same force produced during each dynamic tests – about 600 kN) whereas horizontal actuator was controlled in displacements (producing the same maximum displacement produced during the last dynamic test, in both direction).

Below I report two figures showing the trend of displacements along columns C1 and C2 as measured by Gefran transducers:

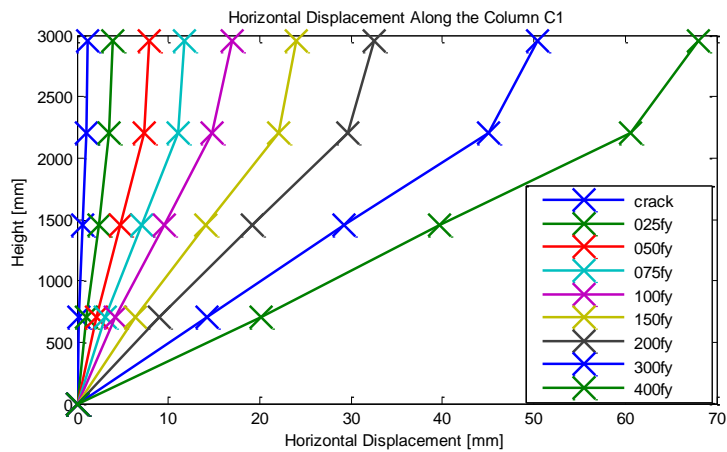


Figure 5-50 – Displacements profile - Column C1

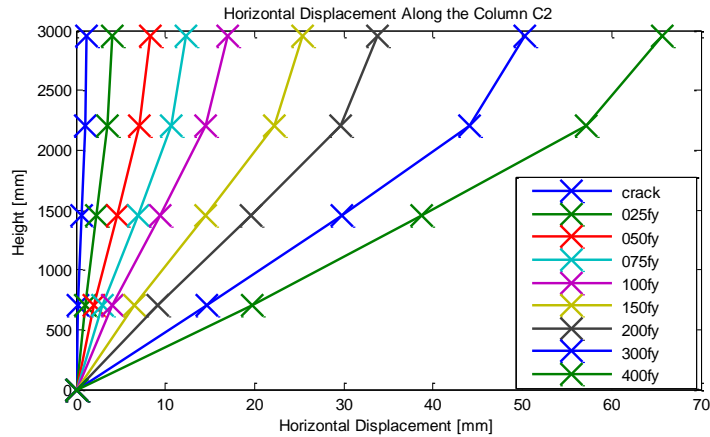


Figure 5-51 – Displacement profile – Column C2

Below I report the force-displacement relationship as registered by horizontal actuator (force) and mean value of Gefran transducers at the top of the frame (displacement). It can be seen that yielding actually occurs for a displacement which is three times (about 51 mm) the estimated displacement (17 mm, pink curve). In other words, yielding actually occurred during test named $300\Delta_y$.

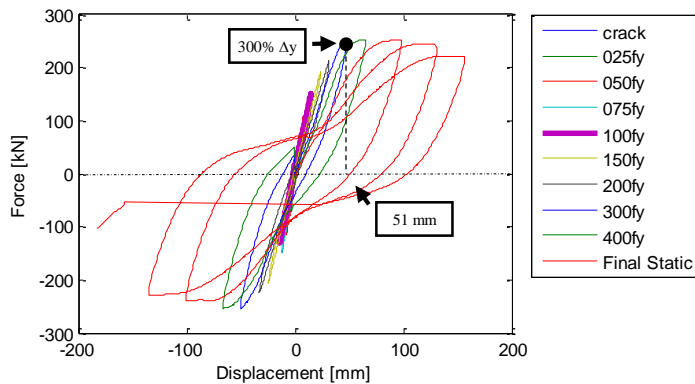


Figure 5-52 – Force – displacement Backbone curve

Below I report the comparison between the time histories of acceleration recorded by Memscion system and the reference one. Both Memscion and reference systems acquisitions were started by manual triggering at the respective DAQ units. Triggers was induced when the vertical actuator was producing about 75% of the maximum force (so about 5 seconds before the starting of the shaking). In the following I report the analysis related to the dynamic test performed inducing to the frame 100% of the expected displacement at yielding (17 mm), when at the top of the frame acceleration values of up to 0.4g were registered. Similar results were obtained analyzing data related to the other tests. As previously illustrated, to record the acceleration measured at the deck level during dynamic tests we installed four Memscion accelerometers above the frame slab, two above column C3 and two above column C2, mounting them back to back with reference accelerometers, placed in both

longitudinal and transversal directions. Memsccon accelerometers reliability was assessed simply comparing the response from each Memsccon device with that of the corresponding reference sensor. Below are the figures showing the comparison between signals from Memsccon and reference system, containing longitudinal accelerometers, and a focus where the optimum accordance between the two Memsccon sensors above column C3 is highlighted:

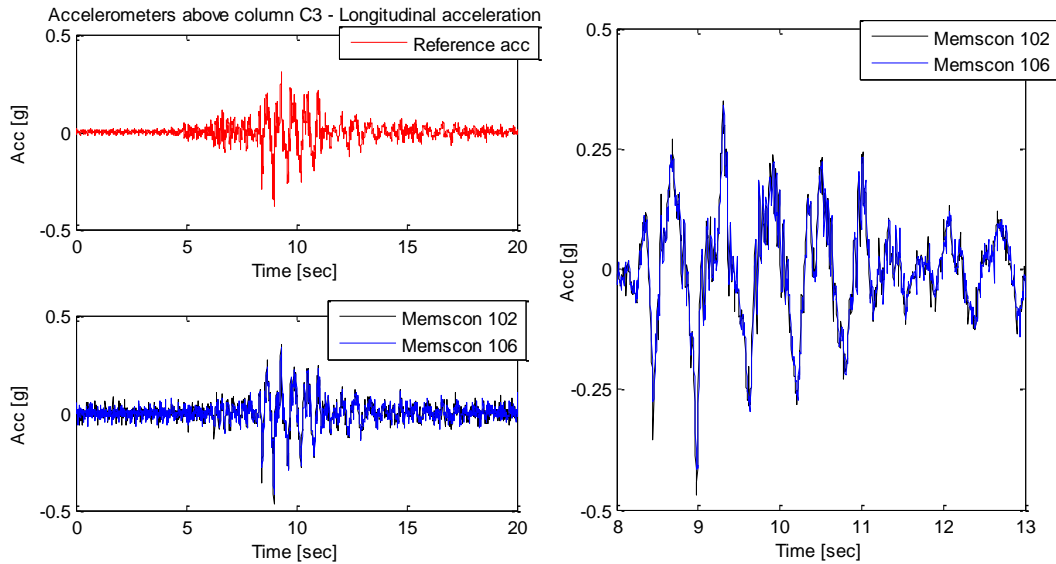


Figure 5-53 – Longitudinal acceleration at the top of column C3

I remark that to synchronize data from the two acquisition systems, we couldn't rely on time stamp provided by Memsccon devices (because on version of the software we used this feature was not implemented) but we were required to manually find the delay between the signals. Concerning accelerations on the transverse direction, related time histories are reported below:

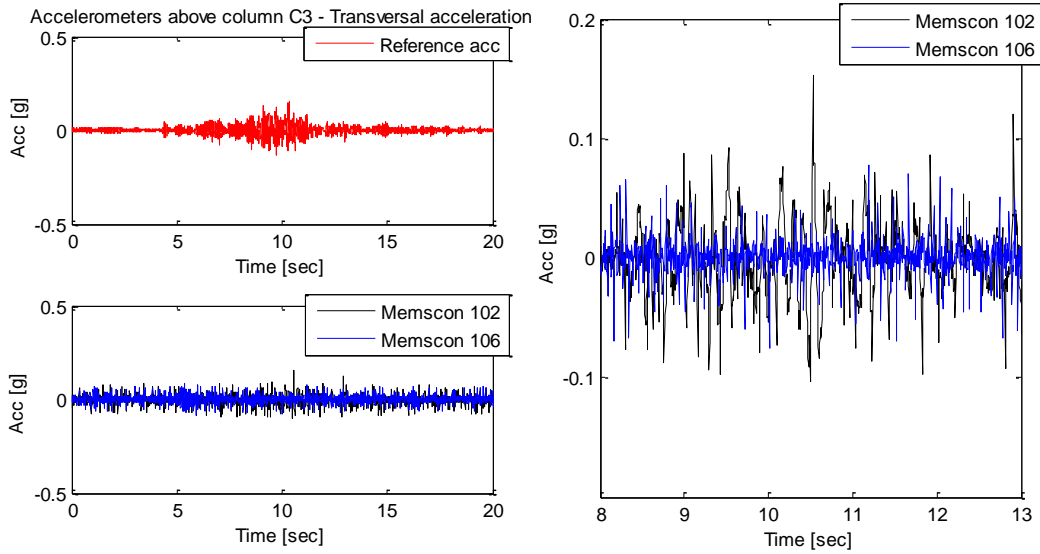


Figure 5-54 – Transverse acceleration at the top of column C3

The displacement time history induced to the frame by the horizontal actuator was estimated also using Memscon Accelerometers double integrating time histories of acceleration as recorded by the wireless devices. This response was compared to the displacement time history as produced by the actuator and recorded by the MTS system.

To do this, a high-pass filter was implemented, assuming that low frequency ($f < 1$ Hz) components into the signals (for example the dc value) induce error propagation and the not-convergence of the integration method. The filter is characterized by the following parameters:

- stop band frequency 0.2 Hz
- pass band frequency 1.2 Hz
- stop band attenuation 0.0001
- pass band ripple 0.0575
- density factor 20

In the following we I the results concerning test 100% Δ_y and accelerometers above column C3. The acceleration signals were filtered using the filter described above. Next, the velocity was obtained performing the first integration. Also time histories of velocity were filtered using the filter described above, next the displacement time histories were obtained performing the second integration.

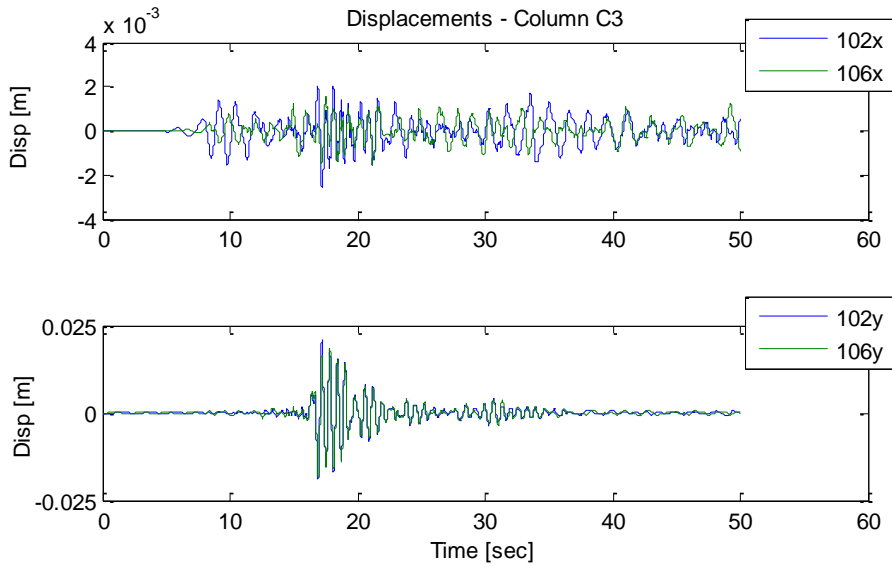


Figure 5-55 - Estimation of displacement time histories: transverse direction (top) and longitudinal direction (bottom)

Below I report the comparison between displacements as recorded by MTS system (displacement produced by the actuator) and displacements estimated by double integration. I observe a little asynchrony between the two systems, probably due to the fact that MTS system sampling rate is a little more than 100 Hz. In any case, the error committed estimating displacement using double integration is in the order of millimeter.

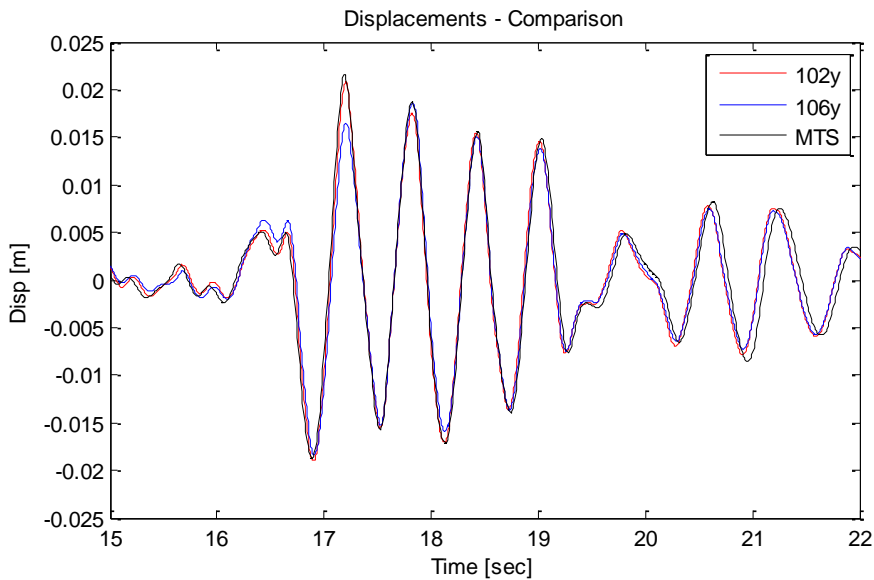


Figure 5-56 – Comparison between estimated displacements and displacements induced by the horizontal actuator

5.5 Discussion on laboratory evaluation

5.5.1 *Phase I accelerometers*

The nominal resolution of the wireless instruments was been previously estimated as 0.18 m/s^2 . The experimental campaign allowed us to estimate more accurately the sensitivity of the three wireless sensors tested, and then to apply the parameters to the measured values. I noted from the tests that device's sensitivity is very stable along all the three direction and equal to about 55 counts/g. Concerning the clocks of the MEMSCON devices, it is important to notice that reliable clocks are essential to determine frequencies and periods of the ground and structure vibration, these being primary considerations in seismic analysis. I estimated that WL1 clock was running faster than real time by about 0.6%, whereas WL2 and WL3 ran slower than real time by 3% and 1% respectively, so the sensors are not synchronized. I recognize that a reliable embedded clock is the first need of an ex-novo developed accelerometer. In my opinion the user must also be able to synchronize the mote clocks periodically, or the sensor should have the auto-sync functionality (for example pairing the instrument to a GPS unit). Instrument precision was defined as the error by the MEMSCON devices with respect to the references, in terms of error STD. After calibration, the vibration recorded by the prototypes presents frequency and amplitude components close to those acquired from reference accelerometers. The precision of the wireless instruments is of the same order of magnitude as the resolution (0.18 m/s^2) for most of the low frequency tests carried out. Larger errors are found in high frequency tests (16 Hz above all). This is reasonable because the 100 Hz sampling rate is not fully suited to such high frequency excitation. The wake-up procedure, which allows data transmission only if an acceleration $> 0.5 \text{ m/s}^2$ is recorded, is efficient even though during some tests some prototypes did not awake. This was probably due to the short time between one test and the next, and not to a procedure bug. During in-field application, this could be a problem if further seismic waves follow the main shock after 2-3 minutes. In this case, structure vibration would not be recorded by the system.

5.5.2 *Phase II accelerometers*

As explained above, I calculated sensitivity of Phase II.1 accelerometers directly comparing FFTs of reference and wireless signals, obtaining a set of voltage - acceleration pairs on which I performed a linear regression, with the hypothesis that the trend was linear. I obtained that sensitivity changes with sensor and direction on a range from 100 and 400 mV/g. Considering the maximum voltage range (from 0 to 2.5 V) and the 16 bit resolution of the sensors, I obtained that the resolution in mg is very high, about 0.1-0.4 mg. Concerning instruments clock, I observed during the campaign that the actual

sampling rate of the Phase II.1 devices is about 201.5 Hz and it slightly changes with the sensor. I obtained the accuracy of the system calculating the RMS value of the error committed by MEMSCON devices compared to reference ones. I obtained values about 20 mg for out of plane accelerations (i.e. on Z Axis) and significantly higher (worse performance) for in plane accelerations. Values about 20 mg are anyway 50-200 times the resolution. I blamed this error to a particularly high value of the background noise (about 10-20 mg) contained in the signals recorded by Phase II.1 accelerometers.

5.5.3 *System evaluation on full-scale 3D frame*

The comparison between Memsccon and reference recordings shows that Memsccon accelerometers are reliable to record acceleration data during an earthquake, with discrepancy between two systems in the order of 0.02g. The clock inside Memsccon devices appears to be stable; the sampling rate is about 202 Hz. In X direction (the direction orthogonal to the one of shaking) I observed a bandwidth noise in the order of 50 mg; this does not allow to recognize acceleration measured in this direction. This noise can be removed in order to increase the signal to noise ratio and to distinguish signal from noise applying to the signals a properly designed low-pass filter at about 20 Hz. High frequency response is in fact irrelevant for carrying out further damage detection analysis, and often carries spurious non-mechanical noise which deteriorate the quality of the analysis. The performance of the Memsccon accelerometers allows to estimate with good accuracy, in the order the few tenths of a millimeter, the displacement time history induced by the horizontal actuator to the concrete frame performing a double integration of acceleration measures, implementing a high-pass filter set to remove frequency components below 1Hz. It is worth pointing out, however, that such a good performance is related to a displacement time history of the concrete slab which is zero-mean, having the frame been restored to its initial equilibrium point at the end of each motion. The errors related to residual displacements investigated in Chapter 4 are therefore not taken into account.

Further considerations can be stated concerning the behavior of the monitored structure. I remind here that in this test the aim was to develop plastic hinges at the nodes between column and foundation and between column and beam. The value of displacement at yielding assumed as equal to 17 mm and computed twice the value resulting from the integration of curvatures along the height of the semi-column, taking into account the height of the plastic hinge at the base of the column and considering secant stiffness is equal to one third of the experimentally observed value. A better estimation, in any case still underestimating the observed value by 33%, can be obtained using the formula proposed in (Panagiotakos and Fardis 2001) for computing the value of chord rotation at yielding. The ratio between predicted and observed displacement at yielding is in any case well-matched with the dispersion reported in the previously cited work (COV = 36%).

5.6 Conclusions

In this Chapter I discussed the main aspects of the laboratory validation I performed on the MEMSCON monitoring system which is based on MEMS sensors and wireless data transmission and has the purpose to protect reinforced concrete buildings compliant to seismic codes against seismic events and settlements. The system consists basically on accelerometers placed at each floor of the building and strain gauges attached to reinforcing bars embedded into columns of the ground floor. The damage evaluation is performed remotely and not in real time, by means of a non-linear analysis on a preset model of the building, assuming data from sensors as input. In particular, acceleration data is used to estimate displacement time histories imposed dynamically to the model. The result of the analysis is a modified Park-Ang index representing the condition state of the building.

My task in the research project was the laboratory evaluation of the system on both small scale and full scale specimens, while unfortunately I had no access and responsibility on the evaluation of methodology on which software for damage assessment is based. It is obvious and also experimentally observed, however, that in this system the main source of uncertainty is epistemological, that is related to the knowledge on the building to be monitored, and in particular on its inelastic response (e.g. constitutive laws of materials, hysteretic behavior, ductility capacities and so on), being instrumental uncertainties basically secondary. Except the issues related to the clock inside the wireless nodes (e.g. nominal sampling rate different to actual sampling rate) and some glitch observed in node firmware, the observed performance of the system components are in fact satisfactory.

6 Case study: Seismic monitoring of precast buildings

6.1 Introduction

In this Chapter I apply the proposed framework for seismic structural health monitoring system and the method of structural drift estimation based on acceleration measurements only on a case study regarding the seismic monitoring of precast industrial buildings. In particular in this chapter I discuss the peculiarities of these buildings defining monitored limit states and monitoring strategy, which is different from the case of framed RC structures because commonly the assumption of diaphragm behaviour of the floor is not valid. Additional uncertainties related to the monitoring strategy and to the high dimensions in plane of this type of building are also studied. The monitoring system is then illustrated from the technological point of view, in particular system components and software are fully described. Results of the evaluation of the system in laboratory conditions are also reported in this Chapter.

6.2 Scope of application

Scope of application of the developed monitoring system is the monitoring of precast industrial buildings compliant to the most recent seismic codes (e.g. Eurocode 8).

In this thesis I adopt the fib definition of “precast industrial building” that is a building composed of precast elements that are joined together mechanically in the site, ensuring structural integrity of the whole structure and characterizing its response to the static and dynamic actions (fib 2008).

The term “industrial” allows to specify the class of buildings investigated to the ones with a single floor or with an intermediate floor.

A classification of Italian precast industrial buildings into typologies was performed by Reluis, DPC and ASSOBETON during triennial project 2005/08 (Bonfanti, Carabellese, and Toniolo 2008). For each typology, a brief description, geographical distribution and notes about seismic behavior are reported. In this document it is highlighted that most of the typologies of precast industrial building in Italy can provide a satisfactory response to seismic action when properly designed in particular regarding construction details and the application of the capacity design principle.

The experience of Emilia earthquake demonstrates how precast industrial buildings designed for gravity loads only (that is buildings into which a combination of inadequacy of detailing and brittle failure mechanisms exists) respond to a seismic event. Damage review in (Bournas, Negro, and Taucer 2013) indicates for example that about 75% of the industrial buildings presented damage and detachment of the claddings and about 25% of them presented partial or total collapse of the roof due to the loss of seating of the beams. The investigation demonstrates how most of the industrial buildings in the area struck by the 2012 earthquake had the following weaknesses:

- lack of effective beam-column joints able to transfer the seismic forces from the top floor, where the mass is concentrated, to the foundations: transferring mechanism totally rely on friction;
- low dimension of seating;
- inadequacy of transversal constraints for the beams (e.g. shear failure of the forks);
- insufficient capacity in terms of displacement and strength of the connections between claddings and structural elements;
- isolated foundations (e.g. concrete plinth without linking elements).



Figure 6-1 – Loss of seating of the beam and shear failure due to resultant reduced seating dimension (Savoia, Bacci, and Vincenzi 2012)



Figure 6-2 – Claddings collapse due to insufficient displacement capacity and strength of the connections between claddings and structural elements (Savoia, Bacci, and Vincenzi 2012)

Some buildings experiences also damage on columns. Basing on the performed in-field survey, observed damage on columns can be classified basically in two classes: (i) observed rotation at the base of the column due in turn to the rotation of the plinth or to failure of the plinth itself and (ii) flexural failure of the columns associated to the development of a plastic hinge at the column's base. Damage inspection proved moreover that often damage in columns occurred due to the impact of other structural elements or shelf contents and not directly to the seismic force.

In (Toniolo and Colombo 2012) there are reported the evidences of a similar damage inspection related to the L'Aquila earthquake. It was observed a general good behavior of precast building structures designed to resist seismic actions, but also in this case the collapse of a number of claddings, the collapse of roof elements due to insufficient detailing of shear connections, in some cases the buckling of longitudinal bars of columns due to excessive spacing of the stirrups, and cracking at the base of the columns. In any case, damage on precast facilities observed after L'Aquila earthquake is only a fraction of the damage occurred during the 2012 earthquake. The causes of the higher impact on the industrial facilities of the Emilia earthquake respect to the L'Aquila earthquake were justified not only by a better design of the structures in Abruzzo, but also by the low frequency content of the seismic waves of the former event (Bournas, Negro, and Taucer 2013).

As discussed in Chapter 3, nowadays there are no reliable technologies available for the monitoring of the actual condition state of a structure, including the monitoring of limit states related to brittle failure mechanisms such the ones experienced by buildings in Emilia.

On the contrary, when the expected failure mechanism is ductile, it is possible to find a relation linking structural exhibited performance levels and sustained structural damage to a state variable which can be achieved from instrumental monitoring. In this case, it is possible to assume as the state variable the value of the chord rotation at the end of the members or the value of the interstorey drift.

In this work, therefore, the typologies of buildings where the developed monitoring system can be installed are the ones without structural lacks regarding the seismic behavior, that is structures into which brittle failure mechanisms are prevented.

In other words, only structures that are new precast industrial buildings compliant to seismic codes or existing buildings retrofitted compliant to seismic codes can be monitored by this monitoring system. From a morphologic point of view, almost all the possible solutions present no detrimental lacks in terms of seismic behavior if structural lacks on connections between structural elements are abstained from design (Bonfanti, Carabellese, and Toniolo 2008). Structural lacks are here briefly reported again: (i) beam to column bearings or floor element to beam bearings based only on friction (ii) absence of transversal constraints for beams and floor elements (iii) shear failure of columns (iv) failure of the claddings. In this work, buildings into which these lacks are not prevented are not considered.

This means that beams are tied to the columns by means of shear connectors (dowel bars) designed compliant to capacity design. In particular, connections are overdesigned with respect to the concrete elements and the dissipation mechanism relies only on the development of plastic hinges at the base of the concrete columns, with the connections remaining elastic. This simplify the damage assessment based on structural monitoring of buildings struck by earthquakes, because brittle failure mechanisms which are difficult to predict are avoided and the (damage) state of the structures depends only on the performances of the laterally displaced ductile RC columns.

Whatever the typology of the superstructure, columns of the typical building investigated in this work act as vertical cantilevers ensuring in total the resistance of the building to lateral forces, including wind and seismic action.

6.3 Objectives

The objective of the developed monitoring system is to obtain the maximum response in terms of drift ratio (relative displacement between top and bottom divided by the member height) of each column of the monitored precast building. The value of the maximum displacement is compared to preset thresholds values representing different limit states. These values are assumed as deterministic.

In detail the functionalities of the system to be developed are:

- (1) Real-time continuous monitoring of accelerations and measurements recording activated automatically on trigger;
- (2) Automatic computation of displacements based on acceleration measurements;
- (3) Automatic computation of drift ratios sustained by structural members resisting to lateral actions;
- (4) Comparison between computed drift ratios and preset thresholds values;

- (5) Estimation of flexural limit states reached by each structural member resisting to lateral actions;
- (6) Email, sms, visual and acoustic alerting service.

6.4 Monitored limit state

As stated in the previous section, the monitored system is intended for precast industrial buildings compliant to the seismic codes. This means that the building is expected to dissipate input energy by means of the development of plastic hinges at the bottom of the concrete columns. The monitored limit state is therefore linked to these flexure-controlled components. The use of the information provided by the monitoring system is therefore the check of seismic demand in terms of lateral displacement (or drift ratio, or also chord rotation at the base) to thresholds values linked to deformation-related limit states. In principle, at least two points of the force-deformation response of the column should be known, namely the points related to yielding and ultimate condition.

However, the company which commissioned this research was interested to a monitoring system able to give as information the ratio between the maximum drift and the drift at yielding, assumed as deterministic, being the definition of threshold values representing different limit states responsibility of the final user.

A possible representation is showed in the next figure:

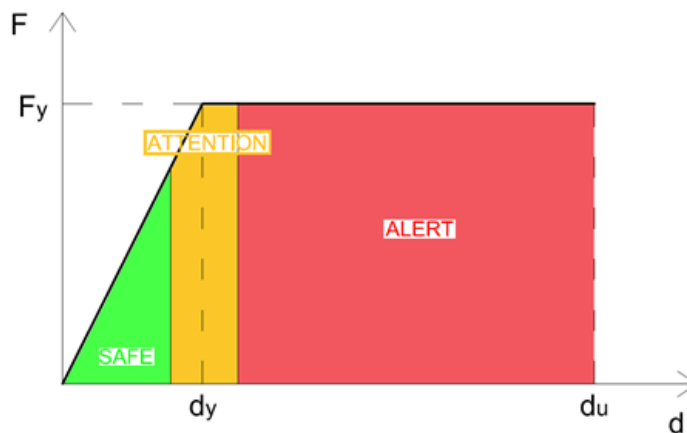


Figure 6-3 – Example of threshold values definition

Most of the studies available in the literature deal with columns characterized by shear span to depth ratio unsuited for precast industrial buildings. Recently, experimental tests performed within the project entitled “Seismic behavior of precast concrete structures with respect to Eurocode 8” and discussed in (Fischinger, Kramar, and Isaković 2008) had the goal to study deformation of slender reinforced concrete columns for the definition of seismic behavior of precast concrete columns. The tested specimen consisted of 6 columns 5 m high with a shear span ratio equal to 12.5, attached to the

ground by means of precast foundation sockets. The roof consisted of concrete I-beams, supporting double T panels on the top. The specimen were tested both with a series of pseudo dynamic tests and with an earthquake simulation. The results of the tests were as follows:

- yield drift about 2.8% (estimated approximating the response to a bilinear representation);
- stable response up to about 7.0%;
- 20% strength drop (assumed as collapse condition) at about 8%.

The study in (Fischinger, Kramar, and Isaković 2008) aimed also to find an expression for the prediction of drifts for slender precast columns matching the observed values. It was found that the yield drift can be predicted using the equation proposed in (Panagiotakos and Fardis 2001) which combines flexural, shear and bond-slip contributions:

$$\theta_y = \frac{\phi_y L_s}{3} + 0.00275 + \frac{a_{sl} \epsilon_y}{(d - d')} \frac{0.2 d_b f_y}{\sqrt{f_c'}} \quad (6.1)$$

where ϕ_y is the yield curvature, L_s is the shear span, a_{sl} is a zero-one coefficient indicating the presence (1) of absence (0) of slipping, $(d - d')$ is the distance between tension and compression reinforcement, ϵ_y is the yield strain of reinforcement, d_b is the diameter of the tension reinforcement, f_y is the mean yield stress of the longitudinal reinforcement and f_c' is the mean cylindrical compressive strength of the unconfined concrete.

6.5 Choice of the information provided by the system and target accuracy

The developed system shall provide the peak value PID of the chord rotation or drift ratio at the base of each column of the building.

$$PID = \max \left| \frac{\Delta_t(t) - \Delta_b(t)}{H} \right| \quad (6.2)$$

being $\Delta_t(t)$ the displacement time history at the top of the column and $\Delta_b(t)$ the displacement time history at the bottom of the column, and H the height of the column.

The target accuracy is expressed in terms of uncertainties (standard deviation):

$$u_D(PID) = 10\%$$

6.6 Choice of the physical quantity to be observed

The physical quantity to be observed is the acceleration measured at the top and at the bottom of a certain number of monitored columns. Acceleration measurements are sampled at a sampling frequency equal to 1000 Hz.

6.7 The inferring model

6.7.1 *Displacement time histories estimation*

At sensors locations, displacement time histories are computed from acceleration measurements through signal processing and numerical double integration, following the approach discussed in Section 4.3.

Displacement time histories of not-instrumented nodes are estimated by means of the following approach. Not assuming diaphragm behavior of the building's roof implies in principle that all columns are independent to each other and that all columns should be monitored at the base and at the top in two orthogonal directions in order to estimate the chord rotation or drift ratio at the bottom of the member. Being this economically impractical, defining the minimum number of sensors required to monitor building response with the desired accuracy defined in the previous step is critical. Reconstructing the response of a building given a limited number of measurements is possible assuming that the response of the structure remaining elastic can be approximated as a linear combination of the modes of vibration of the building. If the structure withstands a certain amount of inelastic demand, the same approximation can be seen a priori as the best fitting of the structural response.

Node displacement vector X_R of the structure can be expressed as (Chopra 2011):

$$X_R = [\Phi]\eta(t) \quad (6.3)$$

where $[\Phi]$ is the R (number of displacement of interest) x m (number of modes of vibration) modal matrix and $\eta(t)$ is the modal coordinates vector. Considering for simplicity 4 terms and 3 modes of vibration only, Equation (6.3) can be written in explicit form as:

$$\begin{bmatrix} X_{R1} \\ X_{R2} \\ X_{R3} \\ X_{R4} \end{bmatrix} = \begin{bmatrix} \Phi_{11} & \Phi_{12} & \Phi_{13} \\ \Phi_{21} & \Phi_{22} & \Phi_{23} \\ \Phi_{31} & \Phi_{32} & \Phi_{33} \\ \Phi_{41} & \Phi_{42} & \Phi_{43} \end{bmatrix} \begin{bmatrix} \eta_1 \\ \eta_2 \\ \eta_3 \end{bmatrix} \quad (6.4)$$

Equation (6.4) can be expressed as a system of independent linear equations:

$$X_{R1} = \Phi_{11}\eta_1 + \Phi_{12}\eta_2 + \Phi_{13}\eta_3 \quad (6.5)$$

$$X_{R2} = \Phi_{21}\eta_1 + \Phi_{22}\eta_2 + \Phi_{23}\eta_3$$

$$X_{R3} = \Phi_{31}\eta_1 + \Phi_{32}\eta_2 + \Phi_{33}\eta_3$$

$$X_{R4} = \Phi_{41}\eta_1 + \Phi_{42}\eta_2 + \Phi_{43}\eta_3$$

Being equations independent, the system of equations can be divided in two sub-systems, for example as:

$$\begin{bmatrix} X_{R1} \\ X_{R2} \end{bmatrix} = \begin{bmatrix} \Phi_{11} & \Phi_{12} & \Phi_{13} \\ \Phi_{21} & \Phi_{22} & \Phi_{23} \end{bmatrix} \begin{bmatrix} \eta_1 \\ \eta_2 \\ \eta_3 \end{bmatrix} \quad (6.6)$$

$$\begin{bmatrix} X_{R3} \\ X_{R4} \end{bmatrix} = \begin{bmatrix} \Phi_{31} & \Phi_{32} & \Phi_{33} \\ \Phi_{41} & \Phi_{42} & \Phi_{43} \end{bmatrix} \begin{bmatrix} \eta_1 \\ \eta_2 \\ \eta_3 \end{bmatrix} \quad (6.7)$$

Assuming a number m of measured node displacements and a number u of unmeasured (unknown) nodes displacements, Equation (6.4) can be rewritten as:

$$X_R = \begin{bmatrix} X_m(t) \\ X_u(t) \end{bmatrix} = \begin{bmatrix} [\Phi_{Xm}] \\ [\Phi_{Xu}] \end{bmatrix} \eta(t) \quad (6.8)$$

where $[\Phi_{Xm}]$ is the sub-matrix of $[\Phi]$ containing only rows related to measured node displacements and $[\Phi_{Xu}]$ is the sub-matrix of $[\Phi]$ containing only rows related to unknown node displacements. Equation (6.9) can be expressed as a system of two linear equations in two variables which are $X_u(t)$ and $\eta(t)$:

$$\begin{cases} X_m(t) = [\Phi_{Xm}] \eta(t) \\ X_u(t) = [\Phi_{Xu}] \eta(t) \end{cases} \quad (6.9)$$

From the first of it is possible to calculate $\eta(t)$ introducing pseudo-inverse matrix of $[\Phi_{Xm}]$ (which in general is not square):

$$\eta(t) = [\Phi_{Xm}]^{-1} X_m(t) = \left[[\Phi_{Xm}]^T [\Phi_{Xm}] \right]^{-1} [\Phi_{Xm}]^T X_m(t) \quad (6.10)$$

Substituting $\eta(t)$ in the second of (6.9) unknown nodes displacements can be estimated:

$$X_u = [\Phi_{Xu}] \left[[\Phi_{Xm}]^T [\Phi_{Xm}] \right]^{-1} [\Phi_{Xm}]^T X_m = [M] X_m \quad (6.11)$$

being $[M]$ the matrix relating unknown and measured node displacements. $[\Phi]$ matrix includes: (i) node displacements due to the ground motion, assuming the structure as perfectly rigid; (ii) node displacements related to mode of vibration, assuming the ground as rigid. More sophisticated

approach is possible introducing soil-structure interaction. In the following I assume that soil-structure interaction can be neglected. First columns of $[\Phi]$ matrix contain node displacements normalized by the maximum value due to ground motion assumed the building as perfectly rigid. The following columns contain node displacement due to modes of vibration (already normalized by definition).

6.7.2 Numerical example

The example structure in Figure 6-4 is a 4-columns RC building with foundations on rock and diaphragm behaviour on the roof. Measured node displacements are indicated in red in the figure. Possible movements of the building are:

- (1) rigid movement of the ground on X direction;
- (2) rigid movement of the ground on Y direction;
- (3) translational mode of vibration on X direction;
- (4) translational mode of vibration on Y direction;
- (5) torsional mode of vibration on both X and Y directions.

$[\Phi]$ matrix is:

Table 6-1 - $[\Phi]^T$ matrix for the example structure (in grey are the measured node displacements)

Displacement node	0	1	2	3	4	5	6	7	8	9	10	11	12	13	14	15
Ground X	1	1	1	1	1	1	1	1	0	0	0	0	0	0	0	0
Ground Y	0	0	0	0	0	0	0	0	1	1	1	1	1	1	1	1
1° Mode X	0	1	0	1	0	1	0	1	0	0	0	0	0	0	0	0
2° Mode Y	0	0	0	0	0	0	0	0	0	1	0	1	0	1	0	1
3° Mode (XY)	0	1	0	1	0	-1	0	-1	0	-1	0	1	0	1	0	-1

$[\Phi_{Xm}]$ reported in Table 6-2 is obtained extracting from $[\Phi]$ values related to measured node displacements (nodes displacements 0-1-7-8-9-11 in grey in Table 6-1) $[\Phi_{Xu}]$ while reported in Table 6-3 is built up from $[\Phi]$ values related to unmeasured node displacements (nodes displacements 2-3-4-5-6-10-12-13-14-15 in Table 6-1).

Table 6-2 - $[\Phi_{X_m}]^T$ matrix for the example structure

Displacement node	0	1	7	8	9	11
Ground X	1	1	1	0	0	0
Ground Y	0	0	0	1	1	1
1° Mode X	0	1	1	0	0	0
2° Mode Y	0	0	0	0	1	1
3° Mode (XY)	0	1	-1	0	-1	1

Table 6-3 - $[\Phi_{X_u}]^T$ matrix for the example structure

Displacement node	2	3	4	5	6	10	12	13	14	15
Ground X	1	1	1	1	1	0	0	0	0	0
Ground Y	0	0	0	0	0	1	1	1	1	1
1° Mode X	0	1	0	1	0	0	0	0	0	0
2° Mode Y	0	0	0	0	0	0	0	1	0	1
3° Mode (XY)	0	1	0	-1	0	0	0	1	0	-1

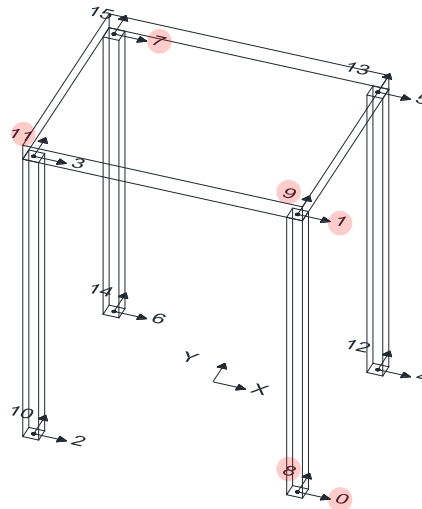


Figure 6-4 – Example structure (in red, measured node displacements; labels 0-8 displacements in the X direction, labels 9-15 displacements along Y direction; even labels displacements at the ground level, odd labels displacements at the roof level)

The pseudo-inverse matrix of $[\Phi_{x_m}]$ is calculated by:

$$[\Phi_{Xm}]^{-1} = \left[[\Phi_{Xm}]^T [\Phi_{Xm}] \right]^{-1} [\Phi_{Xm}]^T = \begin{bmatrix} 1.00 & 0.00 & 0.00 & 0.00 & 0.00 & 0.00 \\ 0.00 & 0.00 & 0.00 & 1.00 & 0.00 & 0.00 \\ -1.00 & 0.50 & 0.50 & 0.00 & 0.00 & 0.00 \\ 0.00 & 0.00 & 0.00 & -1.00 & 0.50 & 0.50 \\ 0.00 & 0.25 & -0.25 & 0.00 & -0.25 & 0.25 \end{bmatrix} \quad (6.12)$$

$[M]$ matrix which relates unknown node displacements to measured node displacements can be computed:

$$M = [\Phi_{Xu}]^{-1} [\Phi_{Xm}] = \begin{bmatrix} 1.00 & 0.00 & 0.00 & 0.00 & 0.00 & 0.00 \\ 0.00 & 0.75 & 0.25 & 0.00 & -0.25 & 0.25 \\ 1.00 & 0.00 & 0.00 & 0.00 & 0.00 & 0.00 \\ 0.00 & 0.25 & 0.75 & 0.00 & 0.25 & -0.25 \\ 1.00 & 0.00 & 0.00 & 0.00 & 0.00 & 0.00 \\ 0.00 & 0.00 & 0.00 & 1.00 & 0.00 & 0.00 \\ 0.00 & 0.00 & 0.00 & 1.00 & 0.00 & 0.00 \\ 0.00 & 0.25 & -0.25 & 0.00 & 0.25 & 0.75 \\ 0.00 & 0.00 & 0.00 & 1.00 & 0.00 & 0.00 \\ 0.00 & -0.25 & 0.25 & 0.00 & 0.75 & 0.25 \end{bmatrix} \quad (6.13)$$

$[M]$ matrix is an (u x m) matrix being u the number of non-instrumented locations and m the number of instrumented locations. Rows are related to node displacements 2-3-4-5-6-10-12-13-14-15. Columns are related to nodes displacements 0-1-7-8-9-11. The assumption of rigid motion without rotation of the ground implies that node displacements 2-4-6 can be estimated as the measured value of node displacement 0. Because the same assumption, node displacements 10-12-14 can be estimated as the measured value of node displacement 8. The assumption of rigid motion of the roof with possible rotation implies that for example node displacement 5 can be estimated as a linear combination of nodes displacements 1-7-9-11.

6.8 Analysis of uncertainties

6.8.1 Instrumental uncertainties

Instrumental uncertainties must be computed in accordance with the approach discussed in Section 4.4 basing on data sheets provided by manufacturers or determined experimentally.

6.8.2 Model uncertainties

Uncertainties of the model linking observations (accelerations) and information (chord rotation or drift ratio of each column) obtained directly without assumptions on the structural model must be computed in accordance with Section 4.5 or determined experimentally.

In this application there is a further source of model uncertainty, namely the model linking the displacements of monitored structural nodes and the displacements of not-monitored structural nodes (Section 6.7.1) which can be expressed by the formula:

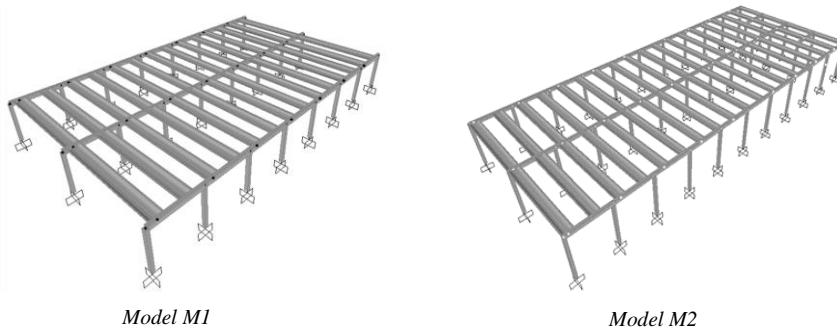
$$X_u = [\Phi_{Xu}] \left[[\Phi_{Xm}]^T [\Phi_{Xm}] \right]^{-1} [\Phi_{Xm}]^T X_m = [M] X_m \quad (6.14)$$

In particular it is evident that the uncertainty in the estimation of X_u depends on the number of modes included in $[\Phi]$ definition and on the number and location of monitored nodes m , in other terms on the arrangement of sensors.

To study this problem I performed a numerical analysis on 4 different precast building linear models showed in Figure 6-5. Columns were modelled as cantilevers at the bottom end being the beams pinned at the top of the columns and the roof elements pinned to the beams.

For each model, I performed a modal analysis generating the normalized modal matrix $[\Phi]$. Then, n different number of modes were taken into account, starting from a number sufficient to collectively account for at least 85% of the total mass in each direction. A set of different arrangements of the sensors was also considered and matrices $[\Phi_{Xu}]_{n,k}$ and $[\Phi_{Xm}]_{n,k}$ were generated for each arrangement. Then, a set of spectrum compatible accelerograms was generated and time-history analysis were performed using SAP 2000.

For each analysis and along both principal directions of the building, the maximum value of the displacement $X_{mod,i}$ at the top of the i -th column was determined.



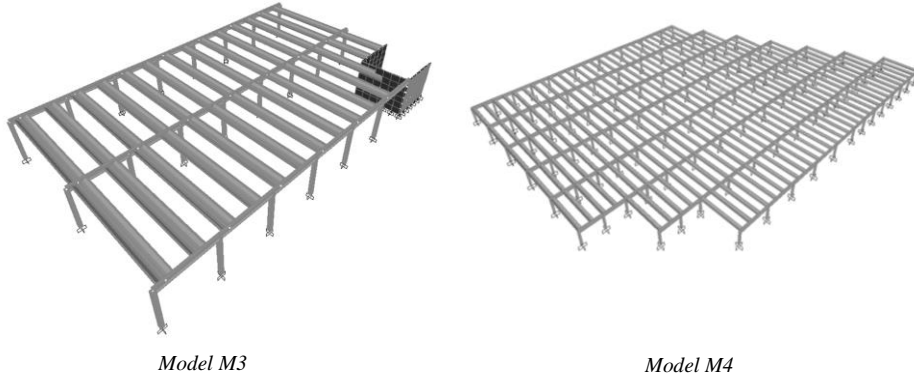


Figure 6-5 – Structural models used for the numerical analysis

For each sensor arrangement k , and number of modes taken into account n , the value of $X_{\text{mod},m,k}$ being m the sensors locations was used to apply Eq. (6.14) computing the value of $X_{u,n,k}$ which is the vector of the maximum displacements at not-measured location i estimated with the sensor arrangement k and taken into account the set n of modes:

$$X_{u,n,k} = [\Phi_{Xu}]_{n,k} \left[[\Phi_{Xm}]_{n,k}^T [\Phi_{Xm}]_{n,k} \right]^{-1} [\Phi_{Xm}]_{n,k}^T X_{\text{mod},m,k} = [M]_{n,k} X_{\text{mod},m,k} \quad (6.15)$$

Relating to each unmeasured node u and for each sensor arrangement k and set of vibration modes taken into account, the error due to the incompleteness of the measured field was expressed as the mean of the ratios of displacement calculated using Eq. (6.14) by the displacement obtained from the structural analysis:

$$e_{if,n,k} = \text{mean} \left(\left(\frac{X_{u,n,k}}{X_{\text{mod},u}} \times 100 \right) \right) \quad (6.16)$$

In the following results about the analysis performed on model M1 are provided. Similar results were obtained for models M2, M3 and M4.

In model M1 three modes were considered along longitudinal direction. The number of modes equal to the number of sensors taken into account along the transverse direction was varied between 3 (involving 93% of total mass) and 8 (involving 100% of total mass).

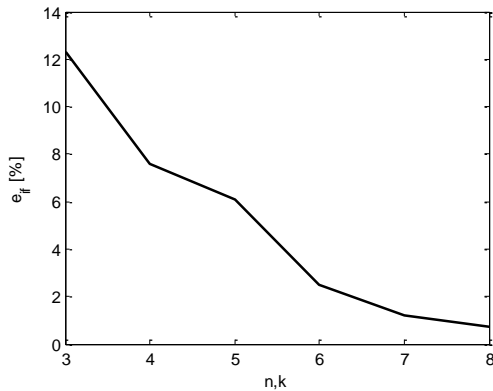


Figure 6-6 – Mean error against number of modes and sensors

It can be seen that arranging a number of sensors equal to $(n_l \times n_t)$ being n_l and n_t the number of columns along the two orthogonal directions, and taking into account all the modes of vibration the error tends to zero.

Another analysis was performed in order to study the influence of the number of modes. A number of modes equal to 3 in the transverse direction was considered, while the number of sensors was varied again between 3 and 8.

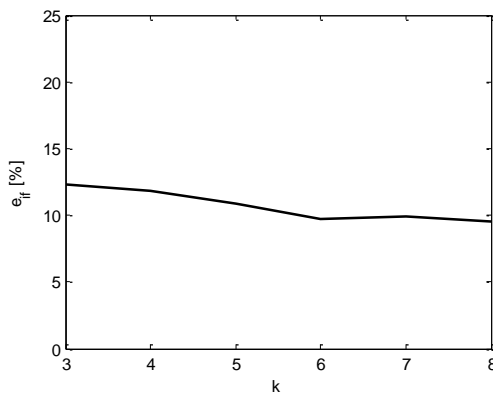


Figure 6-7 – Mean error against number of modes and sensors

It can be seen that the error is basically insensitive to the number of accelerometers when this is higher than the number of modes taken into account. This aspect was confirmed also from the analysis of the other models.

A principle can be therefore stated: the optimum number of sensors to be placed at the top of the columns is equal to $(n_l + n_t)$ being n_l and n_t the number of columns along the orthogonal directions. This number is also equal to the number of modes of vibration to be taken into account in the analysis.

Table 6-4 – Mean error against number of modes and sensors

n,k	$e_{if_{n,k}}$ [%]
3	12.3
4	7.6
5	6.1
6	2.5
7	1.2
8	0.7

Table 6-5 – Mean error against number of sensors ($m = 3$)

k	$e_{if_{n,k}}$ [%]
3	12.3
4	11.8
5	10.9
6	9.7
7	9.9
8	9.5

In this case, the further uncertainty due to the incompleteness of the field is about 1% and the total uncertainties of the displacement estimation of a not-measured node is:

$$u(x_u) = \sqrt{\sum_{i=1}^n u(x_m)_i^2} + 1\% \quad (6.17)$$

being n the number of measurement locations on which the not-measured node depends.

6.9 Description of the hardware

Hardware components of the designed monitoring system for seismic monitoring of industrial precast buildings are:

- a) accelerometers and cables;
- b) controller and acquisition units;
- c) power supply devices;
- d) host Pc;
- e) communication devices;

6.9.1 *Accelerometers and cables*

For the system performance characterization I decided to test two models of accelerometers, named S1 and S2 respectively, which are different to each other in terms of target, cost and specifications. Accelerometers named S1 are mono-axial capacitive accelerometers model 3711B112G produced by PCB Piezotronics. These accelerometers are high-profile instruments provided with a titanium enclosure which guarantees robustness and stability over time. The producer provides the customer a calibration sheet and a total life warranty. In measurement locations where measurements are required along two or three directions, two or three sensors are installed orthogonally inside a specifically designed package. Positive direction of the measurement is the one which exits by the upper surface in Figure 6-8. Specifications of the accelerometer are reported in Table 6-6. The accelerometer is supplied together to a 3 m blue cable with a male 4-pin circular connector at one end, which is necessary for the connection to the extension leads. These are needed to cover the distance (up to 100 m) between instrumented point locations, the acquisition units and power supplies. Extension leads are multipole shielded cables. They transmit both output signal and sensor supply voltage. At one end of an extension cable, the cable is divided in two different cables: one is connected to the acquisition unit, and the other to the power unit (Figure 6-10).

Accelerometers named S2 are also mono-axial capacitive accelerometers, model CXL04GP1 produced by Memsic. These accelerometers are general purpose instruments provided with a plastic

enclosure. The producer supplies a data sheet that reports only sensitivity value. This sensor is supplied together to a 2 m cable with a male 4-pin circular connector for the connection to the extension leads. Specifications of the accelerometer are reported in Table 6-7.



Figure 6-8 – Accelerometer model PCB 3711 (label S1)



Figure 6-9 – Accelerometer model CXL04GP1 (label S2)

Table 6-6 – S1 Sensor specifications

Physical quantity	[-]	Acceleration
Typology	[-]	Gas-damped MEMS
Measurement axis	[-]	1
Measurement range	[g]	±2
Sensitivity	[mV/g]	1000
Transverse sensitivity	[%]	≤ 3
Non linearity	[%]	≤ 1
Zero g drift (from 25 °C to T _{max})	[%FS]	± 2
Spectral noise (1 to 100 Hz)	[$\mu\text{g} / \sqrt{\text{Hz}}$]	22.9
Bandwidth	[Hz]	DC to 250
Operating temperature	[°C]	-54 to 121
Shock	[g]	3000
Supply voltage	[V]	6 to 30
Size	[cm]	1.14 x 2.16 x 2.16
Weight	[Kg]	0.016
Enclosure	[cm]	Titanium - Hermetic

Table 6-7 – S2 Sensor specifications

Physical quantity	[-]	Acceleration
Typology	[-]	Silicon MEMS
Measurement axis	[-]	1
Measurement range	[g]	±4
Sensitivity	[mV/g]	500 ± 15
Transverse sensitivity	[%]	± 5

Zero g drift (from 25 °C to T _{max})	[g]	± 0.1
Non linearity	[%FS]	± 0.2
Alignment error	[deg]	±2
Noise	[mg rms]	10
Bandwidth	[Hz]	DC to 100
Operating temperature	[°C]	-40 to 85
Shock	[g]	2000
Supply voltage	[V]	4.9 to 5.5
Size	[cm]	1.98 x 4.45 x 2.72
Weight	[Kg]	0.068
Enclosure	[cm]	Nylon

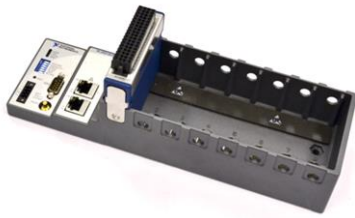


Figure 6-10 – Power unit for sensors

6.9.2 Controller and Data acquisition modules

Deterministic acquisition of measurements and their recording based on triggering is managed by National Instruments NI-RIO 9074 acquisition unit (in the following, Master Unit). Deterministic acquisition is performed by a software written using Labview FPGA module. Identification of seismic events, trigger algorithm and data recording is performed by a software written using Labview Real-Time module. The acquisition unit allow for the installation of up to 8 National Instruments C Series module. In case the distance between sensor locations and acquisition unit is higher than 100 m, one or more other acquisition units can be connected to the Master Unit. The expansion acquisition units are National Instruments NI-RIO 9148. The connection between Master Unit and Slave Unit can be done directly connecting them via RJ45 Ethernet cable or using an Ethernet Switch.

One or more National Instruments NI 9205 module is installed inside each unit. Cables transmitting data recorded by sensors are physically connected to these modules, which are in charge of A/D conversion. Each NI 9205 module can acquire up to 32 accelerometers.



(a)



(b)

Figure 6-11 - Master Unit (a) and Slave Unit (b)



Figure 6-12 – NI 9205 Module

6.9.3 Host Pc

The implemented Host Pc is fan-less Pc suitable for installation in harsh environment. Components of the Windows-based Host Pc are a 1.86GHz dual core Atom Processor, 4GB DDR3 RAM, 100 GB size Hard Disk, 1 VGA Port, 2-ports Gigabit Ethernet, 3 USB ports. The Host Pc is continuously connected to the Master Unit, allowing for real-time visualization of acceleration values, calculates displacements and drift ratios, and compares their values to previously defined thresholds values. The Host PC is then in charge of data transmission to building’s responsible engineers.

6.9.4 Communication devices

Communication between Master Unit, Slave Unit, and Host Pc is performed building a LAN Private Network using a multi-port Ethernet Switch. After a seismic event or on-demand, data is transmitted to in charge responsible engineers or companies using ADSL network of the building through the second Ethernet Port of the Host Pc. In case of absence of ADSL network (or in case of it is down following the seismic event), data are transmitted over GPRS.

6.9.5 Power supply device

Being critical the continuous operation of the monitoring system in particular in case of severe earthquakes, an Uninterruptible Power Supply (UPS) is associated to the monitoring system. The UPS must be able, in case of electric outage, to power all system electronic devices for a period of time big enough to complete all the expected tasks. Moreover, it must stabilize possible input voltage levels unsafe for the equipment. In this case, a 420 VA UPS was chosen, which is able to power the system for a period of time up to 15 minutes.

6.10 Description of the Software

The detailed explanation of the software I programmed falls outside the scopes of this thesis, but some basic principles are given in the following anyway.

6.10.1 Software modules

To develop the application I use Labview (www.ni.com/labview) which is a platform based on graphical language G and integrates measurement process and data processing in the same package. Concerning possibility of communication with hardware, Labview reaches its best performance with hardware by National Instruments, but in principle it works also with third party software.

Labview programs are called VIs (Virtual Instruments). Labview environment consists basically of a user interface (Front Panel) containing interactive controls and indicators, and a Block Diagram containing structures (e.g. loops, event structures and so on), nodes and terminals. The content of the Front Panel is based on the code developed in the Block Diagram. Code is developed in the Block Diagram basically connecting nodes with wires.

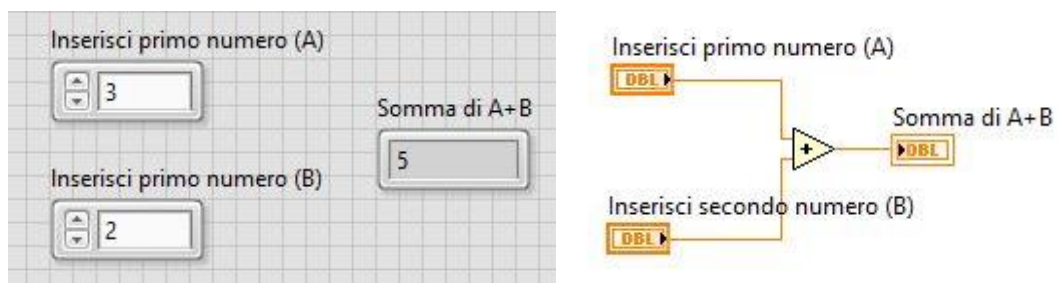


Figure 6-13 – Front Panel (left) and Block Diagram of a simple application producing the sum of two numbers

The basic concept of Labview programming is dataflow. The flow of data through nodes (functions, structures, controls and indicators, etc.) within the program determines the order of execution of the code. In other words, a node executes the code when all the required inputs are available, then it

produces output data that are passed to the next node in the flow path. This allows for creating block diagrams which execute different pieces of code simultaneously.

The monitoring system is based on a modular software consisting basically of three components:

1. A Real-Time application running on the cRIO controller which manages deterministic acceleration data acquisition, stores data on trigger and communicates data to the Host Pc;
2. An User Interface application running on the Host Pc which acquires data from cRIO, computes displacement time histories, computes maximum relative drifts for instrumented and not instrumented columns, compares value to thresholds, manage alerting services.
3. A pre-processor aiding the user to insert the input parameters.

The acquisition process runs on a CompactRIO controller. CompactRIO is an embedded system containing three components: a processor running a real-time operating system, a reconfigurable FPGA and I/O modules (Figure 6-14).

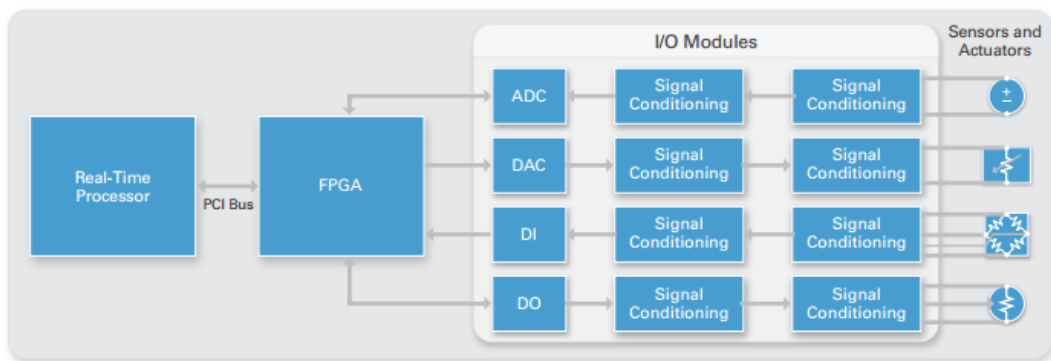


Figure 6-14 - CompactRIO architecture (from www.ni.com)

I selected this architecture because it is able to execute programs with specific timing requirements. In other words, it allows for deterministic software development. The application of seismic monitoring requires in fact a system always running without delays in the data acquisition.

Programming a deterministic application requires the division of the whole program in tasks: deterministic tasks, which are those which precise timing is fundamental, must run on the real-time device (e.g. the cRIO). Not deterministic tasks (such as Graphical User Interface, data analysis, File I/O, communication) must run on non-real-time devices, for example a typical desktop PC.

Sometimes deterministic and nondeterministic tasks are managed by the same target (e.g. a cRIO). In Labview, each task is identified as a loop or a sub-VI. Deterministic tasks must complete “on time, every time” and need for dedicated resources. The programmer of a target supposed to execute deterministic and nondeterministic tasks can assign priorities to different tasks using a Timed Loop or setting the priority of a sub-VI. For example, the dequeue of a FIFO at regular times is a process

to be run into a Timed Loop. Data storage is a nondeterministic task which must be run into a low-priority loop. A typical case is the producer-consumer architecture (Figure 6-15

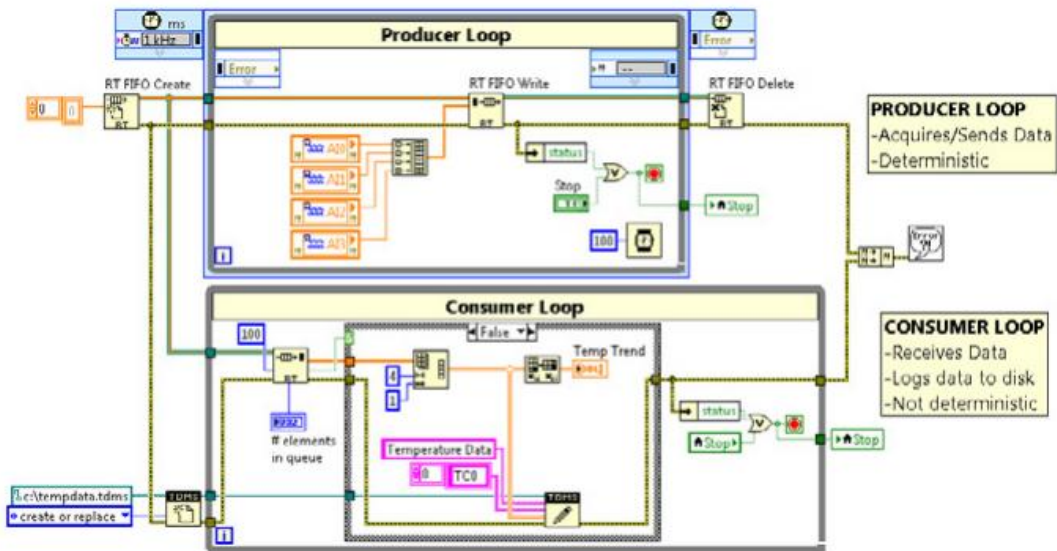


Figure 6-15 – Producer-Consumer architecture

6.10.2 RT Application

The structure of the RT application is basically a producer-consumer structure. In particular, the producer is a Timed Loop running at 1 kHz manages the dequeue of the FIFO into which data (in 4-20 mA) is queued by the FPGA, applies a low-pass filter, converts data in acceleration and queues data in a RT FIFO in case of trigger event. Moreover, another buffer permits to maintain in memory at each steps 10 seconds of data, in order to have the pre-event portion of the signal when a seismic event occurs. The consumer loop at lower priority perform dequeue of the RT FIFO and stores data in a binary file, which is transferred to the Client at the end of the motion.

As stated before, data is continuously recorded by accelerometers, but they are saved only for a trigger event, i.e. when an earthquake occurs. I implemented a simple algorithm which for seismic event detection, based on the following assumptions:

- the seismic event involves the whole building;
- the seismic event lasts at least several seconds;
- the seismic event causes accelerations higher than background noise.

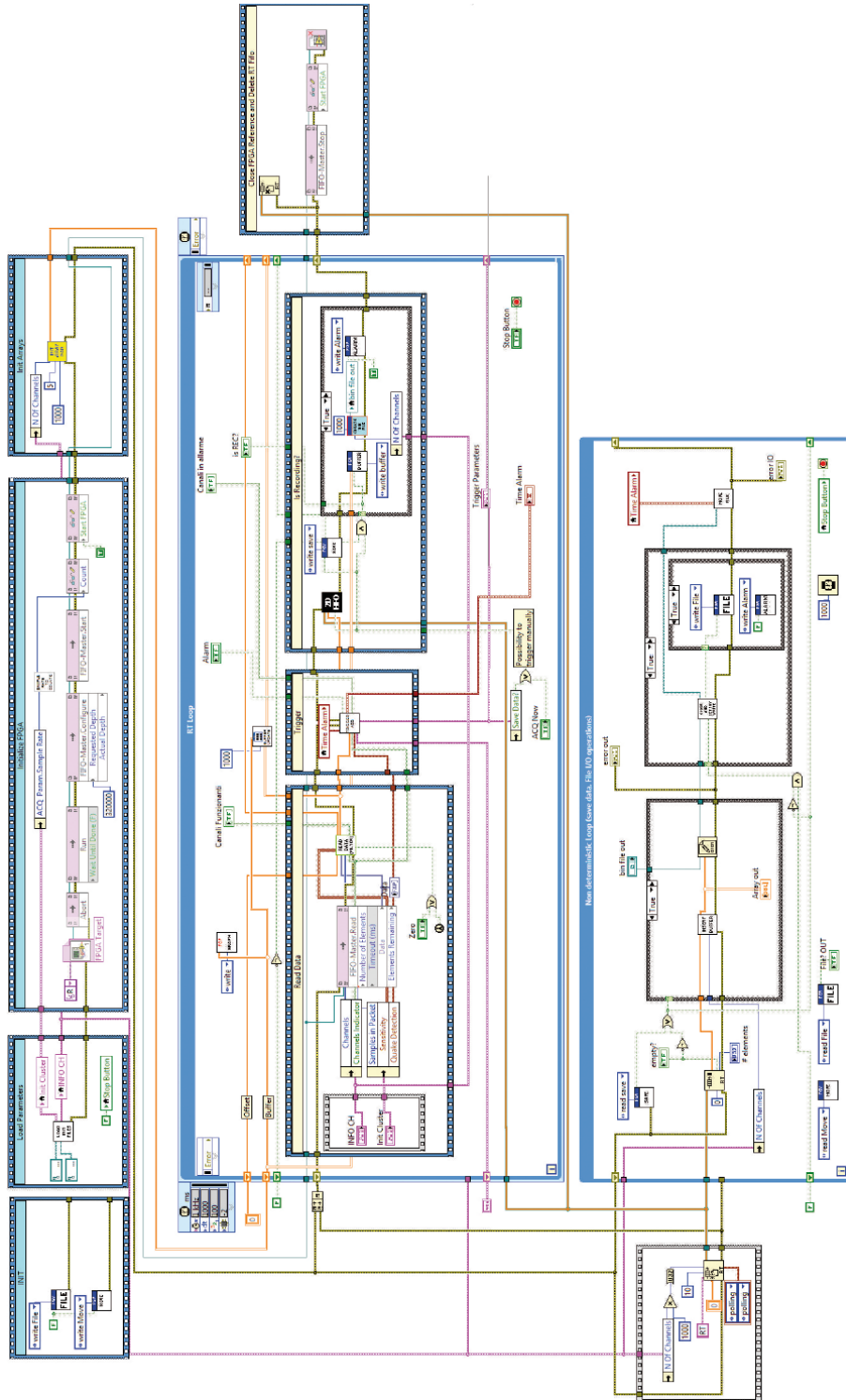


Figure 6-16 - RT App block diagram

An effective detection algorithm is fundamental because it reduces the probability of false alarms. For example, it is possible to avoid false alarms due to impacts in the proximity of sensor locations, or due to vibration caused by sources different from the earthquake.

The algorithm works as follows. To each cycle of the loop running at 1 kHz, a packet of 1000 values relative to each channel is analyzed. For each channel, the rms value or the peak value (depending on the quality of the signal) of the time window is computed and compared to a preset thresholds (e.g. 10 mg of acceleration). When the computed value is higher than the thresholds, the channel is set in a pre-alarm state. When the number of channels in pre-alarm state is higher than a thresholds, and the number of cycles in the pre-alarm state is also higher than another thresholds, the detected vibration is classified as due to an earthquake and data recording starts.

In order to avoid the separation of data relative to same event to different files, a further threshold is set to the minimum number of “negative” packets between two “positive” packets to be considered as separate events. I show an example in Figure 6-17. Here the threshold in terms of acceleration is set to 0.020 g (rms) and the minimum number of of “negative” packets is set to 3. With these values, also the third and the fourth packets are detected as positive.

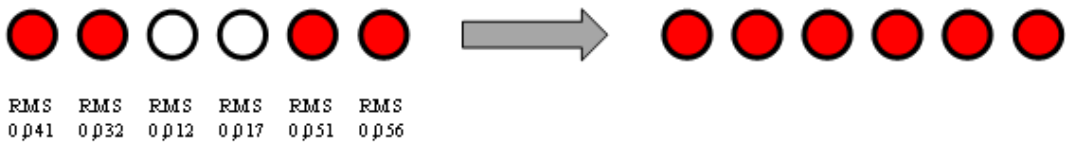


Figure 6-17 – Minimum number of “negative” packets to be considered as relative to the same event

6.10.3 Client Application

The Client Application running on a Pc connected to the cRIO over Ethernet shows at screen data recorded in real-time, computes displacements from acceleration data using the algorithms presented in the previous sections and stores data in memory. The application also tests the operation of the system and manages the remote communications via e-mail.

Data streaming between this application and application running on cRIO is ensured by using Functional Global Variables. When an earthquake occurs, the cRIO application stores data in a binary file, having chosen this format to limit resource usage. At the same time, the cRIO informs the Client that a file is available in its memory. The file is therefore transferred using FTP protocol and translated in txt format. The algorithm estimating displacements at measured and not measured points is applied. Displacements are stored in another txt file and transmitted by e-mail. At the same time, drift values are computed and compared to preset thresholds value in two scales, one relative to structural damage and one to danger for building occupants.

The main screen of the software is as follows (prototype user interface):

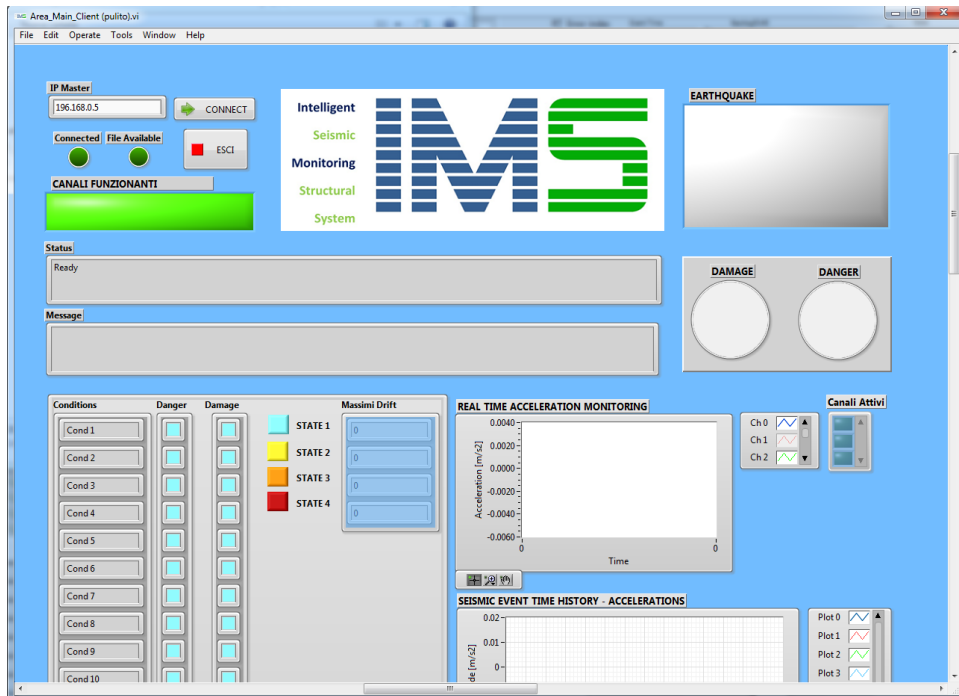


Figure 6-18 - Client application

6.10.4 Pre-processor

In order to simplify the setup of the monitoring system and to guide the user to insert data required for the methodology discussed in Section 6.7, I developed an executable pre-processor VI.

The monitoring system requires in fact the following information to work properly:

- $[M]$ matrix, which in turn depends on $[\Phi]$ matrix and on number and location of instrumented nodes;
- $[D]$ matrix, relating nodes between which the relative displacement values are computed;
- $[T]$ matrix, containing the threshold values;
- configuration parameters, including calibration parameters of the accelerometers.

The pre-processor is an application which computes automatically the $[M]$ matrix from $[\Phi]$ matrix and number and location of instrumented nodes. The main window of the pre-processor is showed in the following figure:



Figure 6-19 – Main window of the pre-processor

By clicking on “Carica File” (Load File) button, a dialog box asks for the location of the file .txt containing the $[\Phi]$ matrix, which has a number of rows equal to the number of nodes of the structural model and a number of columns equal to the number of modes of vibration taken into account plus the motion of the ground. After loading this file, the matrix appears at screen. The user is required now to turn on the led indicators corresponding to the monitored nodes (Figure 6-20)

	Modi				Monitorata?
GDL 1	1	0	0	0	<input type="checkbox"/>
GDL 2	1	0	1	0	<input checked="" type="checkbox"/>
GDL 3	1	0	0	0	<input type="checkbox"/>
GDL 4	1	0	1	0	<input type="checkbox"/>
GDL 5	1	0	0	0	<input type="checkbox"/>
GDL 6	1	0	1	0	<input type="checkbox"/>
GDL 7	1	0	0	0	<input type="checkbox"/>
GDL 8	1	0	1	0	<input type="checkbox"/>
GDL 9	1	0	0	0	<input type="checkbox"/>
GDL 10	1	0	1	0	<input type="checkbox"/>
GDL 11	1	0	0	0	<input type="checkbox"/>
GDL 12	1	0	1	0	<input type="checkbox"/>
GDL 13	1	0	0	0	<input type="checkbox"/>
GDL 14	1	0	1	0	<input checked="" type="checkbox"/>
GDL 15	1	0	0	0	<input type="checkbox"/>
GDL 16	1	0	1	0	<input type="checkbox"/>
GDL 17	1	0	0	0	<input type="checkbox"/>
GDL 18	1	0	1	0	<input type="checkbox"/>
GDL 19	1	0	0	0	<input checked="" type="checkbox"/>
GDL 20	1	0	1	0	<input type="checkbox"/>
GDL 21	0	1	0	0	<input type="checkbox"/>

Figure 6-20 - $[\Phi]$ matrix and led indicators of the monitored nodes

By clicking on “Calcola Coefficienti” (calculate coefficients) the software automatically computes the $[M]$ matrix. By clicking on “Salva su File” (save on file) the software saves it on a txt file in the appropriate path.

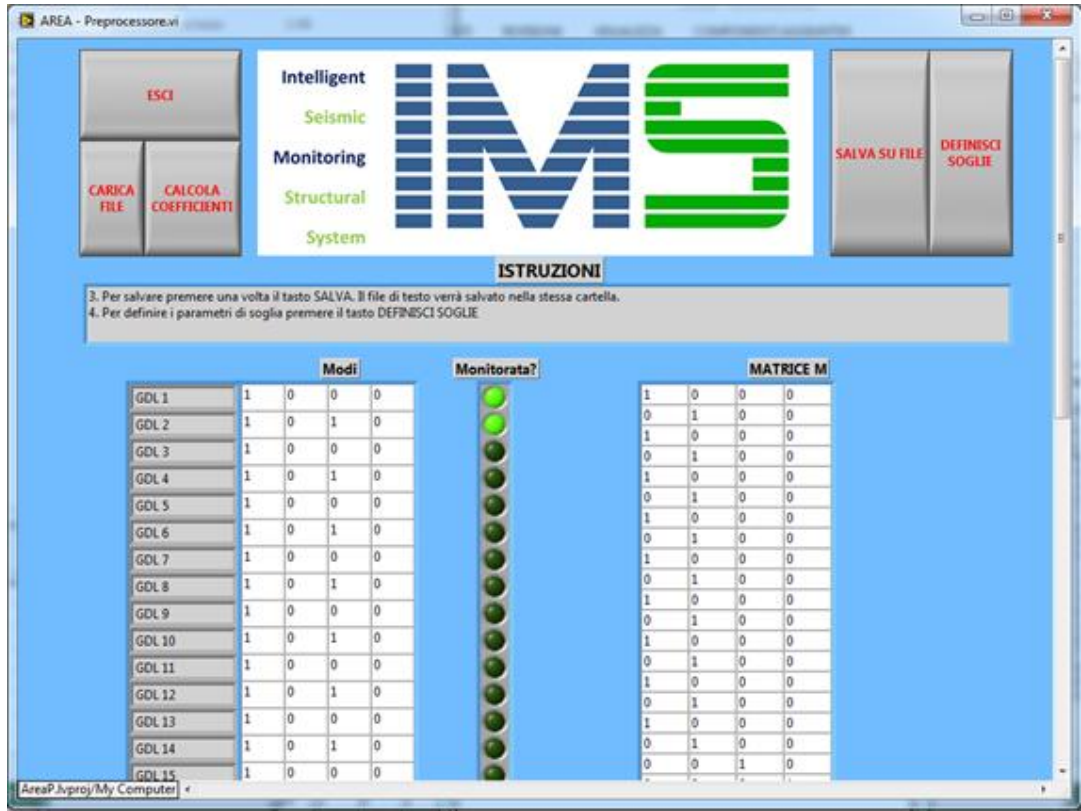


Figure 6-21 - $[\Phi]$ matrix, led indicators of the monitored nodes and $[M]$ matrix

By clicking on “Definisci soglie” (Define thresholds) another window appears on screen, which allows for the user-friendly definition of $[D]$ and $[T]$ matrices. The user has to input the number of limit conditions to be monitored (e.g. if the user wants to monitor the state of 10 columns the number of conditions is 20) and the number of threshold values (e.g. six).

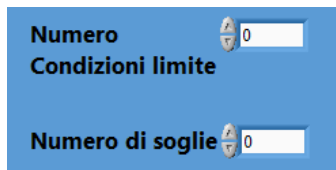


Figure 6-22 – Definition of the number of conditions to be monitored and of thresholds

By clicking “Genera Matrice” (Generate Matrix) a matrix having a number of rows equal to the number of conditions is shown at screen (Figure 6-23). The user has to insert into Columns C1 and C2 the IDs of the coordinates involved in the definition of the corresponding state condition, and in columns from S1 to S6 the threshold values. By clicking on “Completa Matrice” (Fill Matrix), the

values of the first row is copied to all the remaining. By clicking “Salva” (Save), $[D]$ and $[T]$ matrices are saved in the proper paths in txt files.

	C1	C2	S1	S2	S3	S4	S5	S6
Cond 1	0	1	2	5	10	4	10	30
Cond 2	2	3	2	5	10	4	10	30
Cond 3	4	5	2	5	10	4	10	30
Cond 4	6	7	2	5	10	4	10	30
Cond 5	8	9	2	5	10	4	10	30
Cond 6	10	11	2	5	10	4	10	30
Cond 7	12	13	2	5	10	4	10	30
Cond 8	14	15	2	5	10	4	10	30
Cond 9	16	17	2	5	10	4	10	30
Cond 10	18	19	2	5	10	4	10	30
Cond 11	20	21	2	5	10	4	10	30
Cond 12	22	23	2	5	10	4	10	30
Cond 13	24	25	2	5	10	4	10	30
Cond 14	26	27	2	5	10	4	10	30
Cond 15	28	29	2	5	10	4	10	30
Cond 16	30	31	2	5	10	4	10	30
Cond 17	32	33	2	5	10	4	10	30
Cond 18	34	35	2	5	10	4	10	30
Cond 19	36	37	2	5	10	4	10	30
Cond 20	38	39	2	5	10	4	10	30

Figure 6-23 – Generation of $[D]$ (cyan) and $[T]$ matrices

6.11 Evaluation of the system in laboratory conditions

6.11.1 List of experimental tests

The laboratory tests performed for the evaluation of the monitoring system for precast industrial buildings were:

- (1) calibration tests;
- (2) noise evaluation tests;
- (3) accuracy and precision evaluation tests, both in terms of acceleration and displacement;

6.11.2 Test equipment

Shaking table

The chosen shaking table is model 400 Electro-SEIS, made by APS Dynamics, Inc., suitable for testing and calibrating dynamic analysis instruments such as accelerometers. It is an electrodynamic force generator, and the displacement output is directly proportional to the voltage applied. Detailed information and a data sheet on the shaking table are available at www.apsdynamics.com/modal_shaking_overview.php.



Figure 6-24 – APS 400 Electro SEIS

The shaking table was used in horizontal “Fixed Body” mode (see table data sheet for detailed information on its operation). The table was placed over a table isolated from the ground in terms of vibrations.

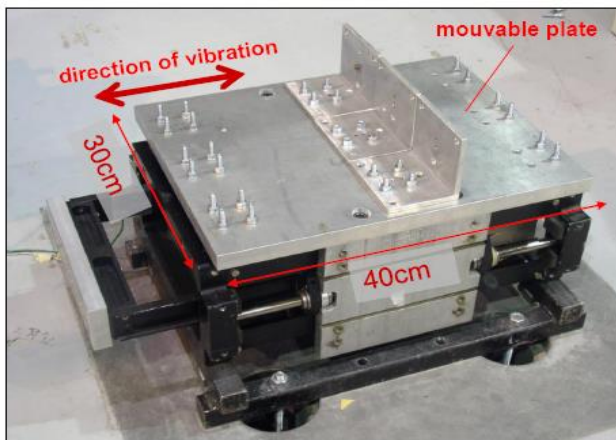


Figure 6-25 – Setup of the shaking table

Devices for input generation

To drive the table, two devices were used: a BRYSTON 7B-SST single channel amplifier which amplifies output voltage sourced by an AGILENT 33220A function generator. Function generator output can be sinewaves, ramps, sweep signals, white noise and arbitrary waves (e.g. earthquake waves) which can be inserted via MatLab software.



Figure 6-26 - Bryston 7b-SST (adapted from <http://bryston.com>)



Figure 6-27 - Agilent 33220Aw (adapted from <http://www.home.agilent.com>)

Information on the amplifier is available at http://bryston.com/7bsst_m.html while the data sheet, manuals and types of function generator can be downloaded from the site: <http://www.home.agilent.com/agilent/product.jsp?cc=US&lc=eng&nid=-536902257.536883183>.

Reference accelerometer

Sensors outputs were compared in terms of acceleration to a reference accelerometer. The reference accelerometer used in the tests is a piezoelectric mono-axial high sensitivity accelerometer model 393B31. The specifications of the sensors are available at the site:

http://www.pcb.com/products/browse_productlist.asp?RequestType=Filter&CategoryType=Product%20Type&CategoryId=316&app=941&tech=&config=&SearchCriteriaWithin=

The reference acquisition of acceleration data was performed by a software written in the Labview environment. The software allows to acquire data by command of the operator or by a trigger. The software automatically performs conversion to electrical unit (voltage) to acceleration and stores data on the hard disk. The system is based on a National Instruments PXI board, model 4472B. It has 8 channels, 24 bit A/D converter, $\pm 10V$ input range.

Reference displacement transducer

Estimated displacements from acceleration data were compared to a reference laser displacement sensor, model optoNCDT 1605 produced by Micro-Epsilon Messtechnik. The instruments consists of a part from which laser is sent and of a controller box. Displacement data was recorded using a modified version of the deployed software.



Figure 6-28 – Laser displacement transducer optoNCDT 1605

6.11.3 *Calibration tests*

Calibration of the sensors was performed both in the time domain and in the frequency domain by comparing the response of sensors S1 and S2 to the response of the reference sensor R. The scope of the experimental campaign was to define the sensitivity of the system, which is expected to be different from the one declared by producers. The difference between the two quantities can be ascribed not only to sensitivity variation, but also to not-nominal supply voltage, temperature variation and sensor's orientation error. The sensors were placed in "back to back" arrangement. Displacement time histories of different amplitude (0.05 – 040 g) and frequency (1 – 20 Hz) were produced using the shaking table. A total number of 48 tests was executed. The differences between actual sensitivity and sensitivity declared by the producers are reported in Table 6-8. The calibration curves are showed in Figure 6-29.

Table 6-8 – Difference between declared and actual sensitivity of the sensors

Sensor Label	Model	Declared Sensitivity [g/V]	Actual Sensitivity [g/V]	Variation [%]
S11	3711	1.007	0.973	3,37%
S12	3711	1.003	0.974	2,89%
S21	CXL04GP1	2.000	1.908	4,60%
S22	CXL04GP1	1.976	1.937	1,97%

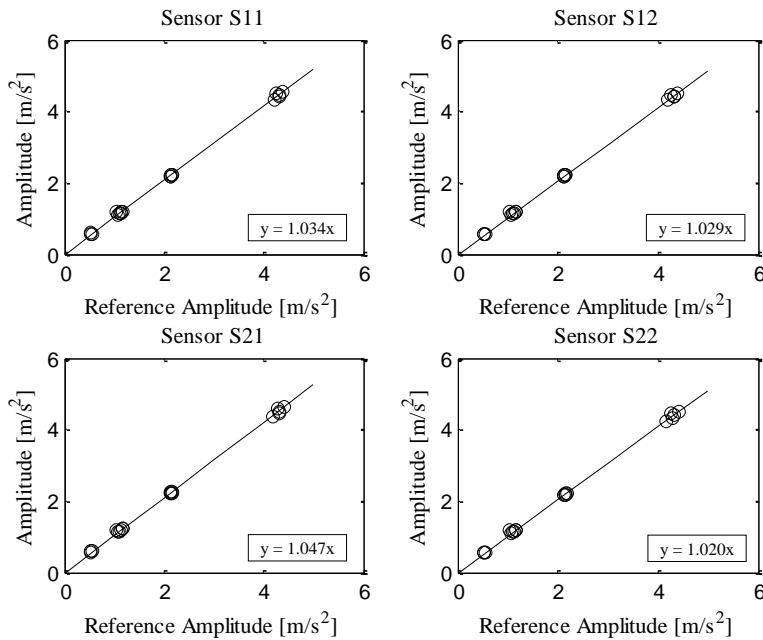


Figure 6-29 – Calibration curves of sensors S11, S12, S21, S22

The values of variation in Table 6-8 represent systematic errors affecting system’s accuracy. In principle, these errors can be removed by performing calibration test using the whole measurement chain in operative conditions. However, in practice often structural engineer uses nominal sensitivity values provided by the producers, and these errors should be taken into account.

6.11.4 Noise evaluation

Noise of a sensor affects its precision. For sensor-only characterization purposes, noise of the sensors should be evaluated using calibrated oscilloscopes or similar equipment in controlled ambient (e.g. temperature) conditions. For the purposes of the structural engineer, however, it is sufficient to study the performance of the whole measurement chain (sensor + cable + DAQ). The effects of low-frequency noise components in accelerometers signals and of cable lengths can be investigated in

laboratory recording measurements from sensors not subjected to mechanical vibrations, for example placing them over an isolated test-bed. The influence of different cables lengths was investigated, namely 5-25-50-75 m. Noise was expressed in terms of mg rms. In Table 6-9 the noise values are reported for the two types of sensors S1 and S2, both with and without the application of a low-pass 4-th order Butterworth filter with a corner frequency equal to 25 Hz (f superscript corresponds to the application of the filter). It can be seen from Table 6-9 that without the application of a low-pass filter the noise of the signals strongly increases with the increasing length of the cable. This is particularly pronounced for sensors S2, for which a rms noise higher than 200 mg is observed for cable length higher than 50 m. However, with the application of a 4-th order low-pass filter with a corner frequency of 25 Hz the noise level is around 5 mg for both the instruments, which are essentially equivalent in performance.

Table 6-9 - RMS noise values for different cable lengths with and without the application of a 4-th order Butterworth filter

Cable length [m]	S1 Noise [mg]	S1 ^f Noise [mg]	S2 Noise [mg]	S2 ^f Noise [mg]
5	0,5	0.2	3,0	0.9
5	0,5	0.2	3,0	0.8
25	3,8	1.7	9,1	0.5
25	4,0	1.8	9,3	0.5
50	8,1	1.9	205,5	0.7
50	8,2	2.0	205,5	0.6
50	8,2	1.9	206,0	0.7
75	16,8	3.8	260,7	5.7
75	16,9	3.7	259,4	5.8
75	16,8	3.7	259,2	5.8

Figure 6-30 reports an example of recorded signal by sensor S11 (cable length 75 m) both in the time domain and in the frequency domain. Background noise is uniformly distributed in the bandwidth 0-500 Hz. Noise can be classified as white noise with peak-peak amplitude of about 40 mg and rms noise of about 16 mg. Implementing a triggering algorithm for memory-save or energy-save purposes (for example saving data on memory or transmitting data only when necessary) and able to minimize number of false alarms requires the application of low-pass filters to the acceleration signals, increasing signal-to-noise ratio. Thresholds of these algorithms are in fact often close to the above values. The most used filter is Butterworth Filter because its linearity. After applying a low-pass 5-order Butterworth filter with 25 Hz cut-off frequency to the signal represented in Figure 6-30, the obtained filtered signal in time and frequency domains is represented in Figure 6-31. The filtered signal presents a reduced noise amplitude (8 mg peak-peak noise, 3.7 mg rms noise).

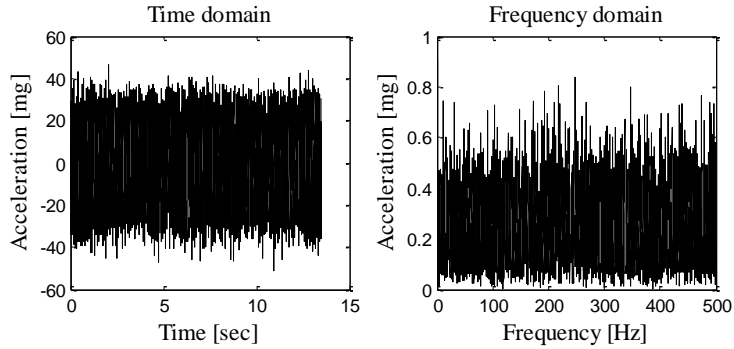


Figure 6-30 - Background noise: time domain (left) and frequency domain (right) relative to the unfiltered signal

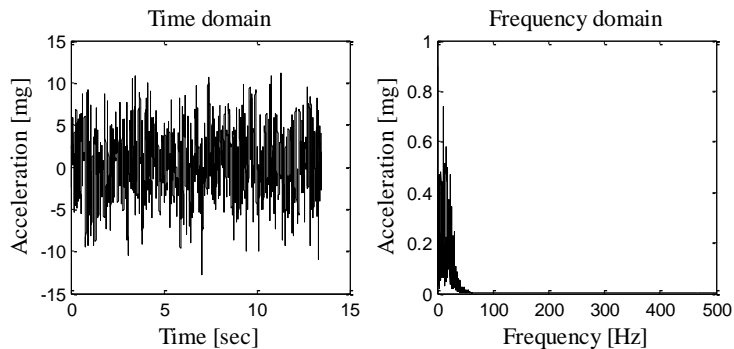


Figure 6-31 – Background noise: time domain (left) and frequency domain (right) relative to the filtered signal

Dividing the filtered signal in the frequency domain by the square of frequency, power spectra in terms of displacements is obtained. By the inverse Fourier Transform, the spurious displacement time history due to low-frequency noise content is obtained (Figure 6-32). The peak-peak spurious displacement amplitude is in the order of 1.5 cm. Hence, also the application of a high-pass filter is required, in order to remove low-frequency noise components.

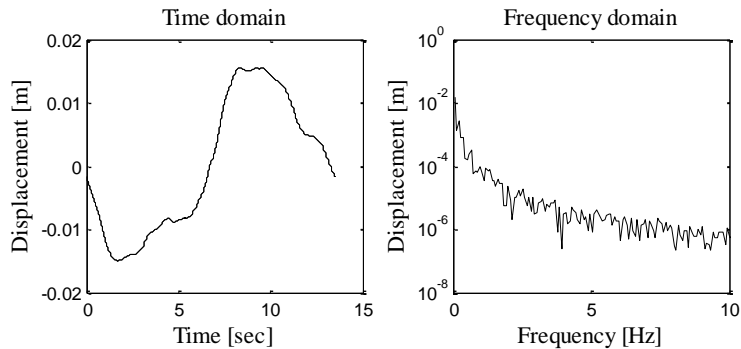


Figure 6-32 – Spurious displacements: time domain (left) and frequency domain (right)

6.11.5 Accuracy evaluation in terms of acceleration measurements

The accuracy of the system in terms of acceleration measurements was evaluated by comparing the response of the sensors to the response of reference accelerometer, in terms of effective value (rms) of the difference between the two signals. Only cable length equal to 5 m were evaluated in this stage. The comparison was performed giving as input to the shaking table sinusoidal displacement time histories and seismic-like time histories.

In Table 6-10 the effective value of the difference between sensors S1 and S2, and the reference accelerometer are reported for various sinusoidal time histories of different amplitude and frequency, both in case of original signals and in case of filtered signal. The filter used is again a 4-th order Butterworth filter with corner frequency equal to 25 Hz. The mean value of the effective value of the difference in the case of unfiltered signals is equal to 15.3 mg and 11.1 mg for sensors S1 and S2 respectively. In the case of filtered signals, mean values are 4.4 mg and 4.7 mg. The standard deviations are 9.2 mg and 5.4 mg in the case of unfiltered signals, and 2.9 mg and 3.7 mg in the case of filtered signals.

Table 6-10 – Effective value of the difference between response of sensors S1 and S2 and of reference accelerometers

Frequency [Hz]	Amplitude [mg]	$\Delta S1$ [mg]	$\Delta S1^f$ [mg]	$\Delta S2$ [mg]	$\Delta S2^f$ [mg]
1	52	19	3	13	2
1	105	28	3	19	2
2	52	13	1	8	1
2	106	16	4	12	4
2	212	25	7	18	6
2	425	41	11	20	17
4	56	6	1	5	2
4	113	11	2	12	3
4	216	19	4	13	4
4	439	25	5	18	4
8	115	6	2	5	3
8	208	13	4	9	5
8	424	14	4	16	10
16	115	6	3	5	2
16	212	8	1	5	5
16	418	12	9	11	8
20	111	5	3	4	3
20	218	9	8	5	4
20	431	16	9	14	6

4 time histories scaled from records obtained from ITACA database (Pacor et al. 2011) relative to Emilia Earthquake (records of Fivizzano, Mirandola in NS direction and Z direction, Copparo) were applied to the shaking table in order to evaluate the performance of the system, using sensor S1, in terms of acceleration measurements in seismic conditions. The comparison between the two sensors is reported from Figure 6-33 to Figure 6-36. In the figures, a value of 1 was added to the time histories of reference accelerometer for clarity. The whole time histories are on the left while an enlargement of 2 sec is on the right. Mean value μ and standard deviation σ of the difference between the response of sensor S1 and of reference accelerometer are reported in Table 6-11.

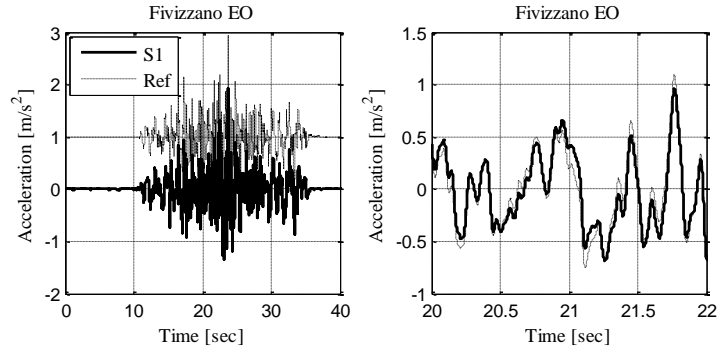


Figure 6-33 – Record of Fivizzano

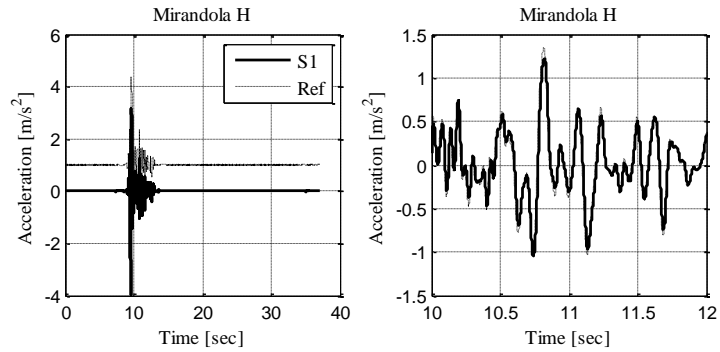


Figure 6-34 – Record of Mirandola in horizontal direction

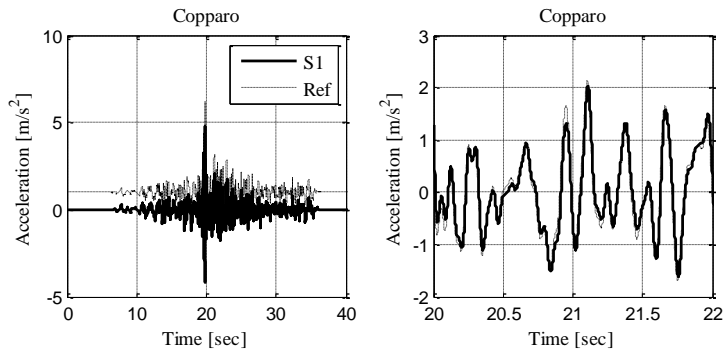


Figure 6-35 - Record of Copparo

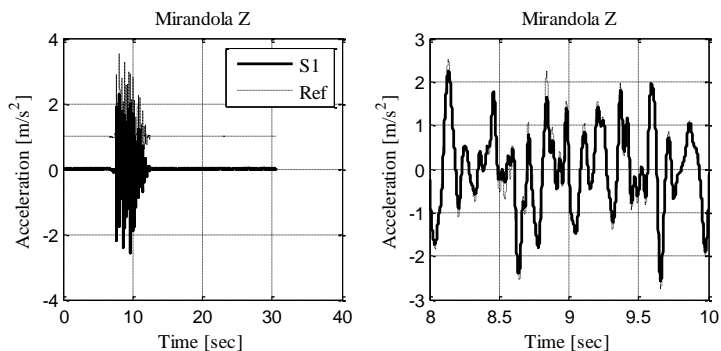


Figure 6-36 - Record of Mirandola in vertical direction

Table 6-11 – Mean and standard deviation of the difference between the response of sensor S1 and of reference accelerometer to 4 seismic events

Event	μ [mg]	σ [mg]
Fivizzano	0.03	8.86
Mirandola H	0.00	4.78
Copparo	0.00	9.11
Mirandola Z	0.00	4.37

6.11.6 Accuracy evaluation in terms of displacement

The accuracy of the system in terms of displacement measurements was evaluated by comparing the time histories of displacement obtained from acceleration data applying the algorithm presented in Chapter 4 to the displacements measured by a laser displacement transducer. Only sensor S1 and cable length equal to 5 m were evaluated in this stage. Three types of tests were performed: (a) single sinusoidal wave tests; (b) linear combination of sinusoidal waves tests; (c) seismic-like waves tests. The first type of test was conducted using sinusoidal waves of different amplitude (5-20 mm) and frequency (0.5-6 Hz). Figure 6-37 reports the records, corresponding to 3 peaks for each time history for clarity. For each time history (being these the estimated displacement time histories and the measured displacements), 5 peak values were extracted from a central portion of signal far enough from the beginning and from the end of the signal affected by the filter transient. In Table 6-12 only the mean value of the 5 peaks concerning frequencies equal to 0.5 Hz or 1.0 Hz, which are of major interest for the application of seismic monitoring of precast industrial buildings, are reported. It can be seen that for sine waves of frequency equal to 0.5 or 1.0 Hz and amplitude between 5 and 20 mm, the mean value of the difference between measured and estimated peak displacements is equal to 0.30 mm and its standard deviation is equal to 0.27 mm. Moreover, the observed maximum value is equal to 1.10 mm, relative to one of the peaks of test P5.

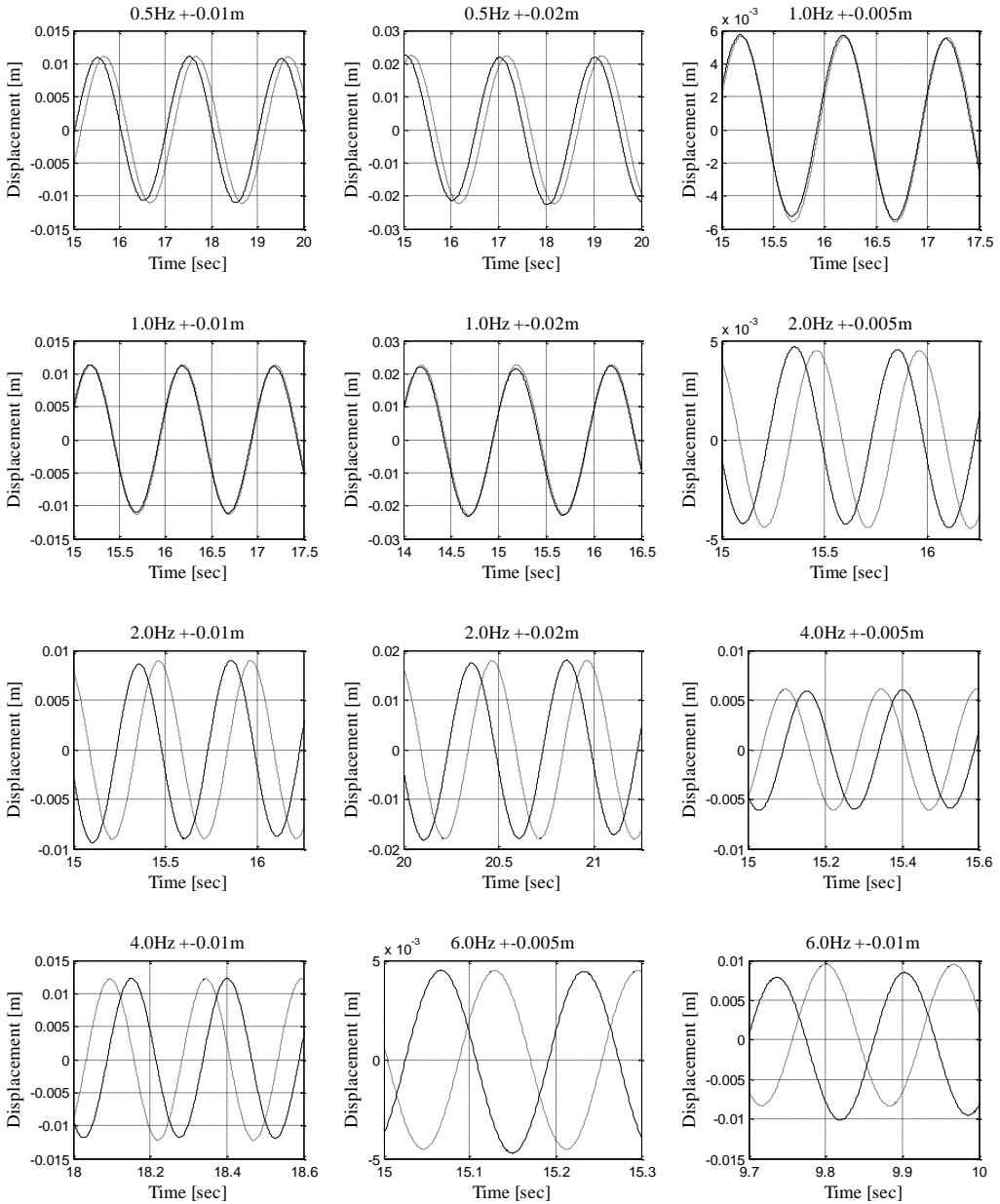


Figure 6-37 – Records using sinusoidal waves as input (estimated displacements are in continuous line; measured displacement are in dotted line)

It can be seen also that there is a dependency between mean value and standard deviation of the difference and the amplitude of the wave (Figure 6-38).

Table 6-12 – Difference between measured and estimated peak displacements (sine tests)

Test	Frequency [Hz]	Amplitude [mm]	Estimated Peak [mm]	Measured Peak [mm]	Error
P1	0.5	~10	10.82	11.07	2.26%
P2	0.5	~20	22.04	22.34	1.34%
P3	1.0	~5	5.46	5.58	2.15%
P4	1.0	~10	11.15	11.31	1.41%
P5	1.0	~20	22.74	22.50	-1.07%

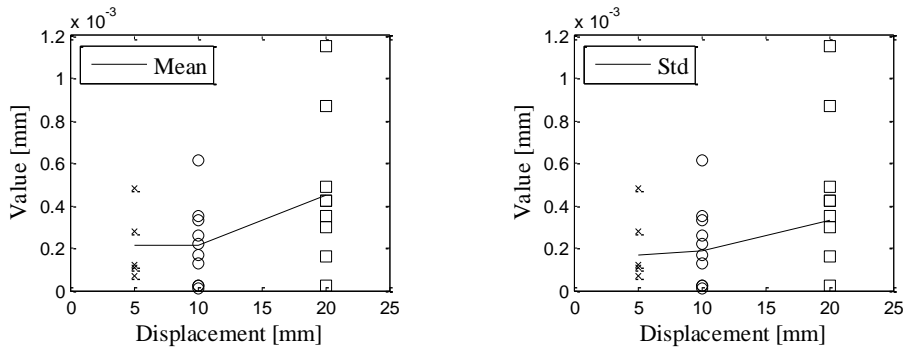


Figure 6-38 – Dependency of mean value and standard deviation on displacement amplitude

The second type of tests was conducted using linear combination of 2 or 3 sine waves as input for the shaking table. This series of tests had the scope of testing system performance to an intermediate level of wave complexity between simple sine waves and seismic waves. First input has 3 components at 1, 1.1, and 1.5 Hz (Figure 6-39); second input has 3 components at 2, 2.1, and 2.3 Hz (Figure 6-40); third input has 2 components at 2 and 3 Hz (Figure 6-41). Mean value and standard deviation of the difference in absolute value between measured and estimated displacement time histories, calculated after signal synchronization on a 10 seconds time window, are reported in Table 6-13.

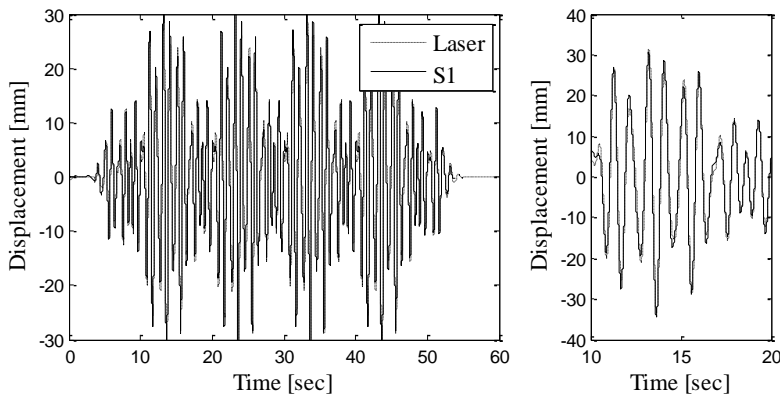


Figure 6-39 – Waves combination tests: 1, 1.1, and 1.5 Hz

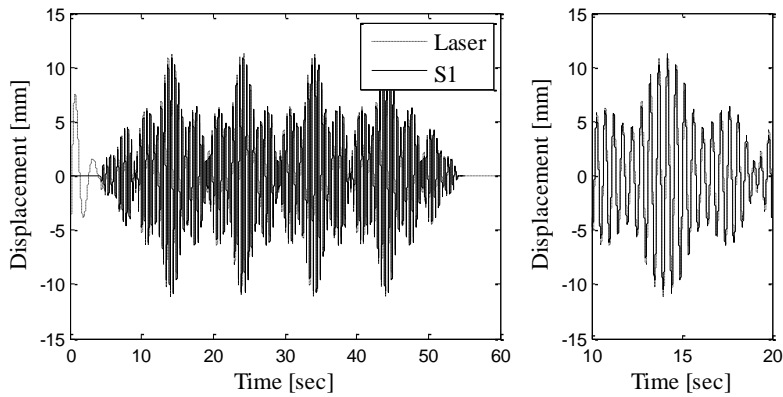


Figure 6-40: Waves combination tests: 2, 2.1, 2.3 Hz

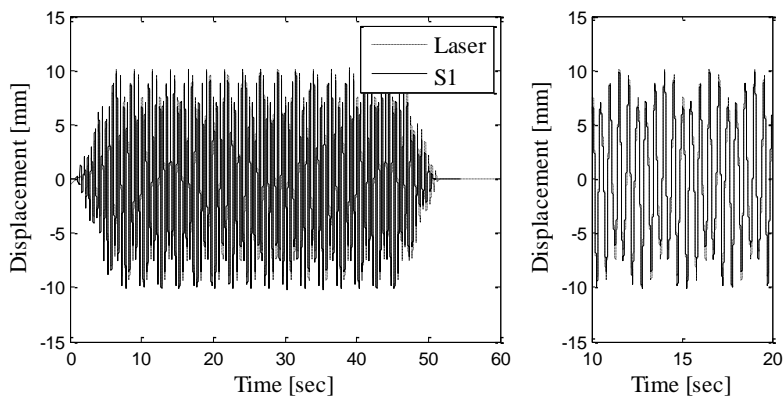


Figure 6-41 - Waves combination tests: 2, 2.1, 2.3 Hz

Table 6-13 - Difference between measured and estimated peak displacements (waves combination tests)

Input	Mean value [mm]	Standard Deviation [mm]
1, 1.1, 1.5 Hz	1.26	0.85
2, 2.1, 2.3 Hz	0.33	0.21
2, 3 Hz	0.52	0.35

The third series of tests was conducted giving to the shaking table time histories of displacements relative to real seismic events. I used 4 time histories downloaded from ITACA database (Pacor et al. 2011), two of them relative to events recorded in L'Aquila and the other two to data recorded in Fivizzano and Mirandola (Emilia Earthquake) The actual time history produced by the shaking table was obtained by scaling downloaded data in amplitude and in time. This series of tests had the scope of testing system performance to the real situation of seismic monitoring. The displacements recorded by the laser transducer was compared to the displacements estimated by the system from data

acceleration recorded by sensor S1. Figure 6-42 to Figure 6-45 show the results of this comparison, while Table 6-14 results of analysis of the difference between measured and estimated displacements.

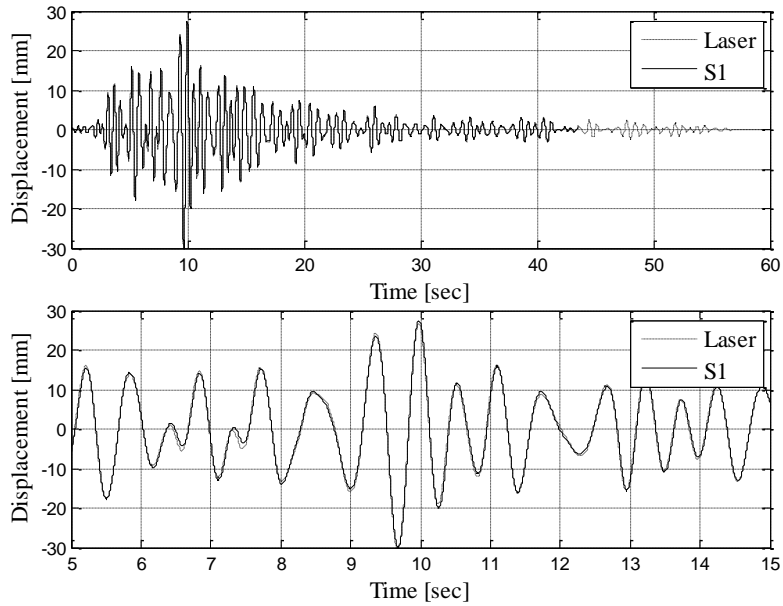


Figure 6-42 – Seismic wave tests: L'Aquila 1 record

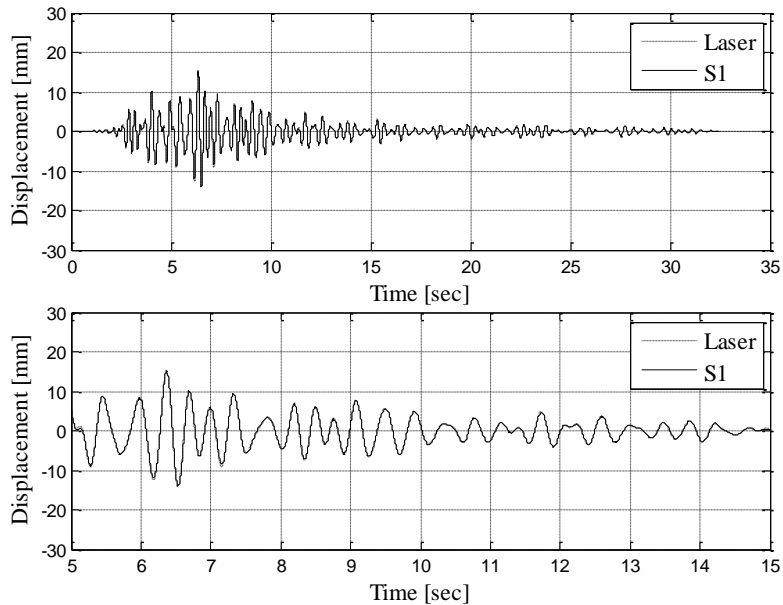


Figure 6-43 – Seismic waves tests: L'Aquila 2 record

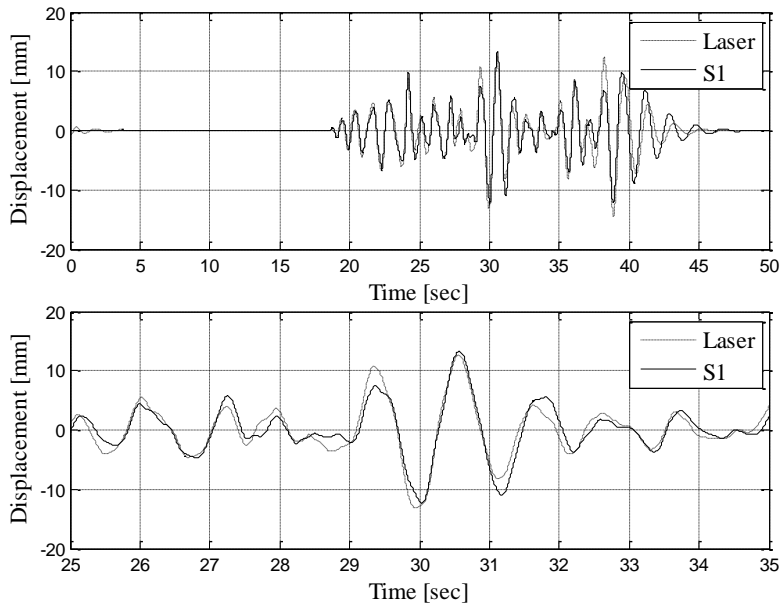


Figure 6-44 - Seismic waves tests: Fivizzano record

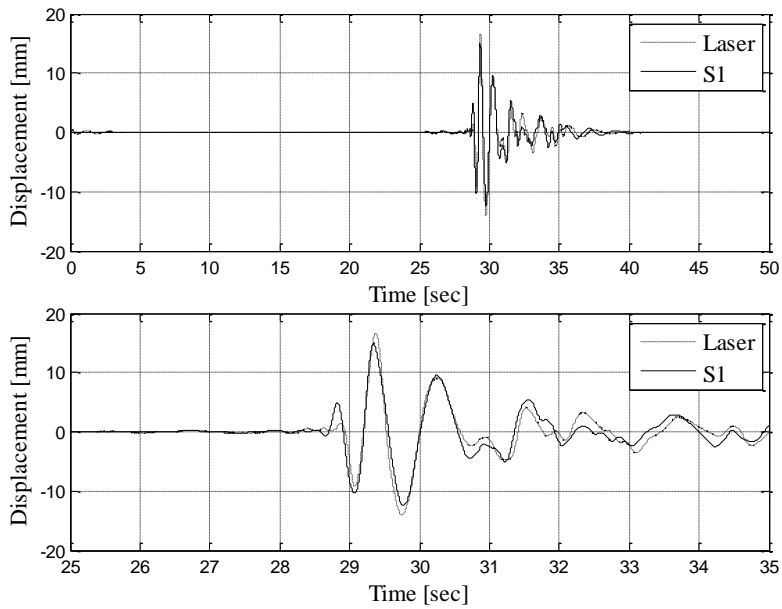


Figure 6-45 - Seismic waves tests: Mirandola record

Table 6-14 - Difference between measured and estimated peak displacements (seismic waves tests)

Input	Max [mm]	Mean [mm]	Std [mm]
L'Aquila 1	2.26	0.10	0.13
L'Aquila 2	0.89	0.41	0.39
Fivizzano	8.02	1.60	1.55
Mirandola	4.20	0.72	0.78

Table 6-15 – Maximum and minimum values of measured (Δ_M) and estimated (Δ_E) displacements

Input	Max Δ_M [mm]	Max Δ_E [mm]	Err	Min Δ_M [mm]	Min Δ_E [mm]	Err
L'Aquila 1	26.80	27.46	-2.46%	-30.33	-30.11	0.73%
L'Aquila 2	15.28	15.00	1.83%	-14.16	-14.19	-0.21%
Fivizzano	12.80	13.30	-3.91%	-14.60	-12.30	15.75%
Mirandola	16.70	14.90	10.78%	-14.10	-12.50	11.35%

6.12 Conclusions

In this chapter I analysed the problem of seismic structural health monitoring of precast buildings compliant to the most recent seismic codes. I highlighted that for this type of buildings, the dissipation seismic energy occurs by means of the development of plastic hinges at the bottom of the columns. The system must therefore monitor the flexure-controlled limit state of these components. The system I developed gives as information the drift ratio of the columns computed as the relative displacements between top and bottom of the member divided by the height. This information is compared to pre-set threshold value assumed as deterministic by the final user. An example of thresholds value are reported in the following figure:

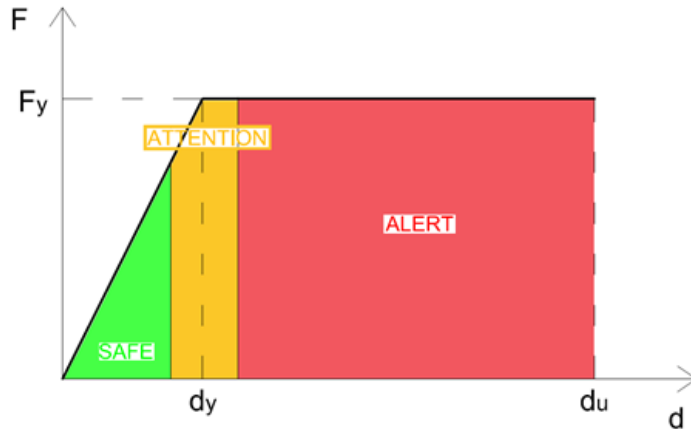


Figure 6-46 - Example of thresholds

Following the framework for the design a monitoring system proposed in Chapter 3, the target accuracy (design demand) is assumed as equal to 10% in terms of drift ratio.

When the assumption of rigid floor diaphragm is not valid, which is typical for Italian precast buildings, monitor the drift ratio of each column member would imply arranging sensors at the top of each column. Actually, it is possible to reduce the number of sensors decomposing seismic response to single modes of vibration, and estimate the displacement of not measured columns linearly combining a certain number of measured displacements. It has been found by means of numerical analysis that placing a number of sensors at the top of the columns equal to $(n_l + n_t)$ being n_l and n_t the number of columns along the orthogonal directions, applying the formula:

$$X_u = [\Phi_{X_u}] \left[[\Phi_{X_m}]^T [\Phi_{X_m}] \right]^{-1} [\Phi_{X_m}]^T X_m = [M] X_m$$

where X_u is the vector of not measured displacements and X_m is the vector of measured displacements, the uncertainty due to the incompleteness of the measured field is about 1%. The total uncertainty of not measured displacements is therefore:

$$u(x_u) = \sqrt{\sum_{i=1}^n u(x_m)_i^2} + 1\%$$

The designed monitoring systems consists of two capacitive accelerometers at the top of the monitored columns and two (or more when displacement variability is expected) pairs of accelerometers at the level of the ground. The controller of the system is a NI cRIO continuously acquiring data at 1 kHz sampling rate. Data is recorded only when earthquake actually occurs, having developed an algorithm for seismic event detection aiming to minimize the probability of false alarms. A host pc is connected to the cRIO performing analysis and user interface functions. The software of the system, based on different modules, was briefly described in this Chapter.

Instrumental uncertainties and the model uncertainties related to the double integration method were studied together testing in the laboratory the whole measuring chain instead of single components. Tests were performed placing accelerometers on a shaking table producing a set of waves, including seismic-like displacement time histories. Uncertainty was expressed as the error between the displacement obtained by double numerical integration and the displacement measured by a laser displacement transducer. It has been found that for single sine waves the estimation of the peak value has an uncertainty around 2%. This order of magnitude was confirmed using as input of the shaker combination of sine waves (uncertainty in the range 2-4%) and seismic-like time histories (2-5%).

It can be therefore assumed that the displacement provided by the system has an uncertainty around 5% concerning measured displacements, including instrumental uncertainty and uncertainty introduced by numerical double integration. This uncertainty must be combined to the uncertainty due to the incompleteness of the measured field using the equation reported above.

It is worth emphasising that further uncertainty are introduced when spatial variability of the ground displacement is expected. In this case, adding sensors at the ground level can reduce this uncertainty.

7 A monitoring method based on acceleration and tilt measurements

7.1 Introduction

In this Chapter I come back to the main sources of uncertainties in the estimation of displacement time histories from acceleration data only, which are the application of a band-pass filter needed to avoid drift in velocities and displacements and the residual displacement or interstory drift at end of the motion. Then, I propose a sensing bar consisting of a bar, hinged to the lower and upper floors of a story, instrumented with sensors. This arrangement permits to deploy different monitoring strategies. The first, not requiring any filtering, is the real-time monitoring of the tilt of the bar by means of measurements of inclination compensated to the effect of accelerations. The second, currently under test, is a monitoring method based on baseline correction approach driven by tilt measurements at the end of the motion which improves the accuracy of displacements estimation of the structure in case of plastic deformation. The third is a simplified approach which mitigate the effect of residual interstory drift on the overall uncertainty. A brief discussion on the installation of a prototype is also reported in this Chapter.

7.2 Motivation

In Chapter 4 concerning uncertainties related to the method of displacement (and hence interstory drift ratio) time histories estimation from acceleration measurements only I illustrated how this method suffers high uncertainties in particular when the structure sustains high inelastic deformation demands. In particular, one of the steps of the process of displacements estimation from acceleration data is the application of a band-pass filter which removes low-frequency components from the signals. It is clear that a structure sustaining inelastic deformation demands likely exhibits a residual displacement at the end of the seismic-induced motion. This information is totally deleted by the signal processing because a residual displacement implies a variation of the baseline and the high-pass part of the band-pass filter removes DC component from the signal.

In principle, as illustrated in Chapter 3, it is possible to relate seismic-induced structural damage to Peak Displacement (PD) value or Peak Interstory Drift (PID) value only, without taking into account Residual Displacement (RD) value or Residual Interstory Drift (RID) value. However, I demonstrated in Chapter 4 that the existence of a residual in displacement time histories implies higher uncertainties on the estimation of PD (or PID) values, being these uncertainties increasing with RD (or RID) value, decreasing the accuracy of the damage assessment methodology.

As an example, in Figure 7-1 I report in the upper part the interstory drift time history of a structure remaining elastic during the seismic motion ($PID \leq ID_y$) while in the lower part the interstory drift time history of a structure which sustained plastic deformation ($PID \geq ID_y$). It can be seen in the second case that the value of PID is underestimated. In other words, as demonstrated in Chapter 4, the accuracy of a monitoring system based on displacement estimation from acceleration data only decreases when the monitored structure sustains inelastic displacements.

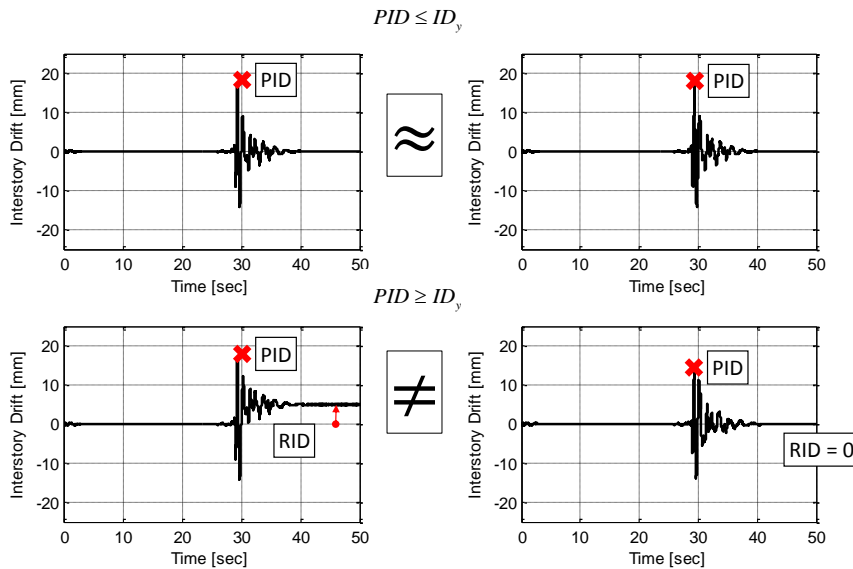


Figure 7-1 – Effect of Residual Interstory Drift (RID) on Peak Interstory Drift (PID) estimation from acceleration data only

7.3 The sensing bar

I show here a *sensing bar* which is suitable for the application on seismic structural health monitoring of framed RC buildings. In these buildings, damage assessment can be performed by monitoring in real-time the value of interstory drift ratio which is defined as the ratio of the relative displacement between two consecutive floors and the interstory height. Moreover, also the residual interstory drift, when present, can be considered as a clear indicator of structural damage.

The sensing bar consists of a hinged bar (for example an L or C steel section) instrumented with 2 bi-axial accelerometers measuring accelerations, one at each end of the beam and remaining parallel to the floors and one bi-axial inclinometer or accelerometer measuring the tilt of the beam (Figure 7-2). The accelerometers are fastened to steel cubic supports, in turns rigidly fixed to the floors by means of dowels. The beam is linked to the supports by means of mechanical hinges (e.g. one spherical hinge and one Cardan joint, or two Cardan joints). An inclinometer (or capacitive accelerometer) is fastened to a horizontal plate welded to any point of the beam (e.g. at the mid span).

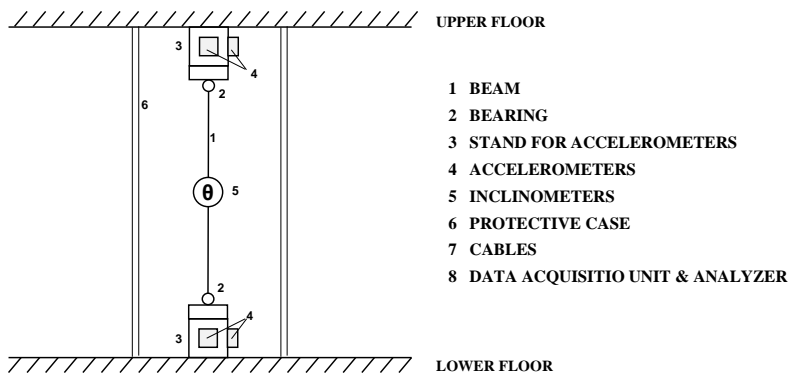


Figure 7-2 - Schema of the sensing beam (un-deformed configuration)

The rigid constraint between supports and floors ensures that accelerometers measure the horizontal accelerations of the floors. The mechanical hinges ensure that the beam is free to rotate during the seismic event and tilted of an angle equal to the ratio of the residual differential displacements between the floors and the distance between beam's ends (Figure 7-3).

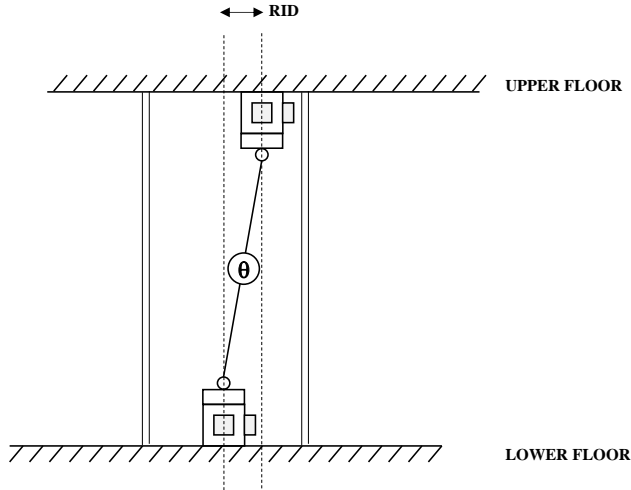


Figure 7-3 - Schema of the sensing beam (residual deformed configuration)

The schema of the sensing beam prototype is showed in the next figure.

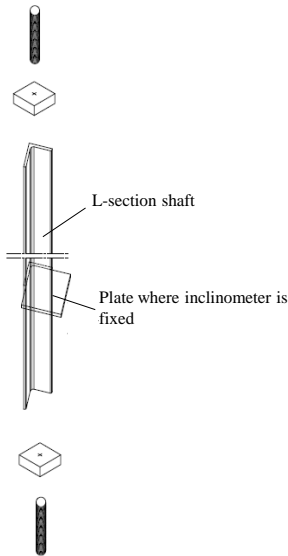


Figure 7-4 - Sensing beam (mechanical part)

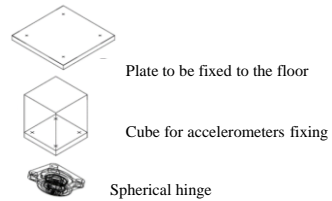


Figure 7-5 - Upper connection to the floor

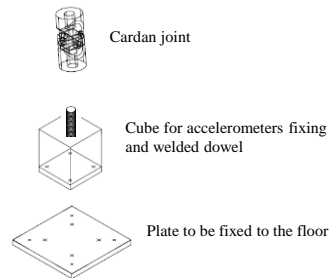


Figure 7-6 - Lower connection to the floor

The described sensing bar is suitable for the application of different algorithms which permit to overcome limitations of the PID estimation method based on double integration of acceleration measurements.

7.4 Real-time monitoring of tilt

In this Section, a possible use of the sensing bar described previously is discussed. It is the real-time monitoring of tilt, or inclination, of the sensing bar during the earthquake, respect to the original configuration. It is worth noting that MEMS inclinometers are practically accelerometers estimating pitch and roll angles from acceleration measurements. For this reason, when the inclinometer is acquired dynamically, acceleration experienced by the inclinometer must be compensated.

7.4.1 Arrangement with two accelerometers and one inclinometer

The inclinometer subjected to an acceleration $a(t)$ and tilted by an angle θ respect to the direction of gravity can be modeled as a mass m fixed by means of a spring subjected to the inertial force $ma(t)$ and to the gravity (Figure 7-7).

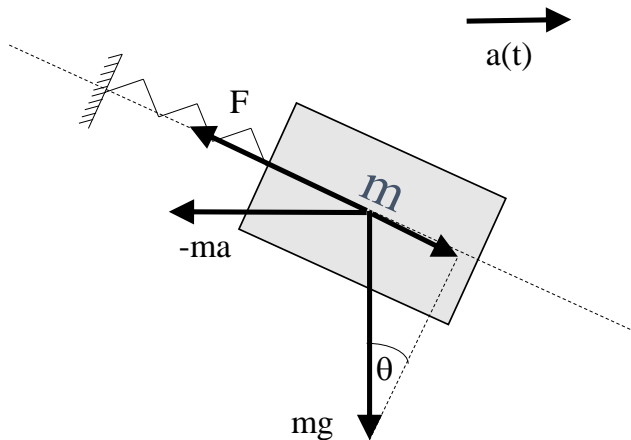


Figure 7-7 - Forces applied to the inclinometer

The equation of motion is:

$$F = mg \sin \theta - ma \cos \theta \tag{7.1}$$

The equation of motion of the inclinometer only tilted by an angle α respect to the direction of gravity is instead:

$$F = mg \sin \alpha \tag{7.2}$$

The effect of the dynamically imposed acceleration is therefore that the inclinometer measures a “fake” angle α_m which includes the effect of imposed acceleration and the actual tilt of the instrument θ :

$$mg \sin \theta - ma \cos \theta = mg \sin \alpha_m \tag{7.3}$$

which leads to:

$$\sin \theta = \sin \alpha_m + \frac{a}{g} \cos \theta \quad (7.4)$$

This equation can be solved numerically respect to angle θ , knowing the measurement of the inclinometer, $\alpha_m(t)$, and the acceleration to which it is subjected, a .

The acceleration a can be evaluated assuming that the field of acceleration is linear between the ends of the bar. In this case:

$$a = a_u + (a_l - a_u) \frac{(H - H_\theta)}{H} \quad (7.5)$$

where a_u and a_l are the accelerations at the upper and lower floor respectively, and H_θ is the height of the inclinometer from the lower floor. It is clear therefore that the scope of the accelerometers are to estimate the field of acceleration.

Analysis of uncertainty on θ can be carried out in first approximation by the linearization of Eq. (7.4) considering only the first order term of the Taylor expansion. It is obtained:

$$\theta = \sin \alpha_m + \frac{a_\theta}{g} \quad (7.6)$$

being sources of uncertainty the measurement of the inclinometer, α_m , and the acceleration to which the inclinometer is subjected, a_θ :

$$\sigma^2(\theta) = (\cos \alpha_m)^2 \sigma^2(\alpha_m) + \left(\frac{1}{g}\right)^2 \sigma^2(a_\theta) \quad (7.7)$$

The maximum value of the variance on θ is:

$$\sigma^2(\theta) \leq \sigma^2(\alpha_m) + \left(\frac{1}{g}\right)^2 \sigma^2(a_\theta) \quad (7.8)$$

Assuming that the inclinometer is fixed at the mid span of the bar, from Eq. (7.5), the acceleration a_θ is the mean value of the accelerations of the upper and lower floor:

$$a_\theta = \frac{a_l + a_u}{2} \quad (7.9)$$

The variance of a_θ is obtained from the rule of errors propagation:

$$\sigma^2(a_\theta) = \left(\frac{1}{2}\right)^2 \sigma^2(a_l) + \left(\frac{1}{2}\right)^2 \sigma^2(a_u) \quad (7.10)$$

Assuming equal the variances, it is obtained that:

$$\sigma^2(a_\theta) = \frac{\sigma^2(a_l)}{2} = \frac{\sigma^2(a_u)}{2} \quad (7.11)$$

The variance on θ is therefore:

$$\sigma^2(\theta) \leq \sigma^2(\alpha_m) + \left(\frac{1}{g}\right)^2 \frac{\sigma^2(a_u)}{2} \quad (7.12)$$

7.4.2 Arrangement with three inclinometers

A variation of the proposed setup consists of using 3 inclinometers instead of 1 inclinometers and 2 accelerometers. In this case, the equation of motion of one inclinometer fixed to a horizontal floor subjected to an unknown acceleration a_l (or a_u) is simply:

$$F = ma = mg \sin \alpha_l \quad (7.13)$$

where α_l is the “fake” angle recorded by an inclinometer fixed to a floor. The accelerations at lower and upper floors are therefore:

$$\begin{aligned} a_l &= g \sin \alpha_l \\ a_u &= g \sin \alpha_u \end{aligned} \quad (7.14)$$

Assuming that the inclinometer is fixed at the mid span of the bar, the acceleration a_θ is:

$$a_\theta = \frac{g}{2} (\sin \alpha_l + \sin \alpha_u) \quad (7.15)$$

and its variance is:

$$\sigma^2(a_\theta) = \frac{g^2}{4} \left[(\cos \alpha_l)^2 \sigma^2(\alpha_l) + (\cos \alpha_u)^2 \sigma^2(\alpha_u) \right] \leq \frac{g^2}{2} \sigma^2(\alpha_l) \quad (7.16)$$

The maximum value of the variance on θ is therefore, from Eq. (7.8):

$$\sigma^2(\theta) \leq \sigma^2(\alpha_m) + \frac{1}{2} \sigma^2(\alpha_l) = \frac{3}{2} \sigma^2(\alpha_m) \quad (7.17)$$

The maximum value of the variance depends therefore only on the performance of the inclinometers.

7.4.3 Preliminary tests

Preliminary tests on the performance of the method was carried out in laboratory by means of this latest setup. In particular:

- the prototype sensing bar was fixed to the shaking table already discussed in Section 6.11.2 at the bottom end and at the upper floor or the laboratory at the other end;
- one inclinometer was fixed to the shaking table;
- one inclinometer was fixed at the mid span of the bar;
- one inclinometer was fixed to the ground , simulating the top floor at rest;

All inclinometers were initialized to zero value while at rest on a horizontal plane before mounting them.

The standard deviation of the angle measurements recorded by the three inclinometers was observed equal to 0.0032, 0.0026, and 0.0029 rad (0.18, 0.15 and 0.17 rad°). An additional low-pass butterworth filter was therefore implemented ($f_{cut} = 5$ Hz). The standard deviations of the filtered signals were 0.31 0.34 and 0.22 mrad. A standard deviation of 0.35 mrad was assumed in the analysis. The expected standard deviation of the measurement of θ angle is therefore:

$$\sigma(\theta) = \sqrt{\frac{3}{2}}\sigma(\alpha_m) = 0.43 \text{ mrad}$$

The distance between the hinges of the bar was measured as 2995 mm. The position of the inclinometer fixed to the bar was measured as 1639 mm. The expected standard deviation of the estimated horizontal displacement is:

$$\sigma(\delta) = H\sigma(\theta) = 1,28 \text{ mm}$$

The shaking table was driven to produce sine waves at 0.5 Hz and 1.0 Hz. The reason of such a limited range investigated is that the available inclinometer offered an on-board low-pass filter with cut-off frequency equal to 2 Hz.

The angles measured by the inclinometers are plotted in Figure 7-8 and Figure 7-9 while estimated displacements are plotted in Figure 7-9 and Figure 7-11. In these plots, red dotted lines represent the mean value of the portion of shaking, equal to -3.5 mm and -5.4 mm for tests at 0.5 Hz and 1.0 Hz respectively.

It can be seen that at the beginning of the test the bar was actually tilted of an angle θ_0 , this implying also an initial displacement between the joint of the bar to the moving table and its joint to the roof. From Figure 7-9 it can be seen also an asymmetry of the displacement time history between -30 mm and 20 mm. This apparently strange behaviour can be explained by:

- the fact that at the beginning of the test the table was in a position different to its equilibrium position, defined by its electro-mechanical components;

- the fact that the table driven by a sine wave input shakes around its equilibrium position and not around initial condition.

It can be observed that:

- respect to the mean value of the shaking portion (-3.5 mm) the peak-peak value of the displacement is ± 25 mm as expected, with a standard deviation of 1.16 mm;
- the final displacement is basically equal to the equilibrium position of the table.

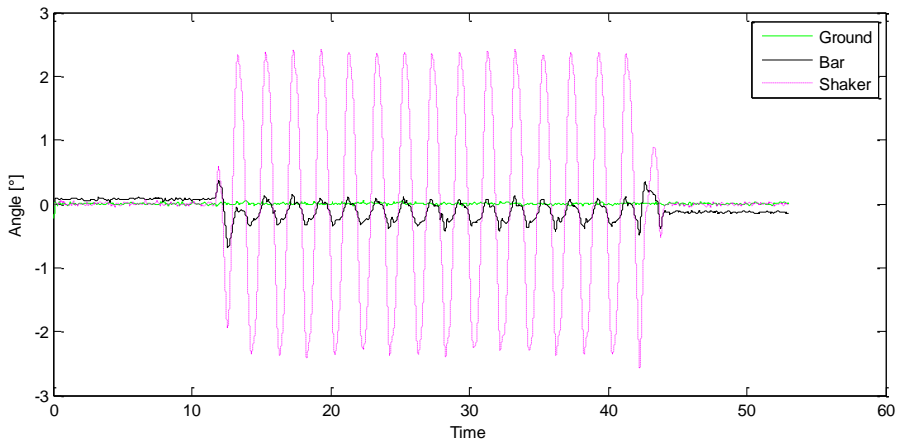


Figure 7-8 – Measured angles (test 0.5 Hz)

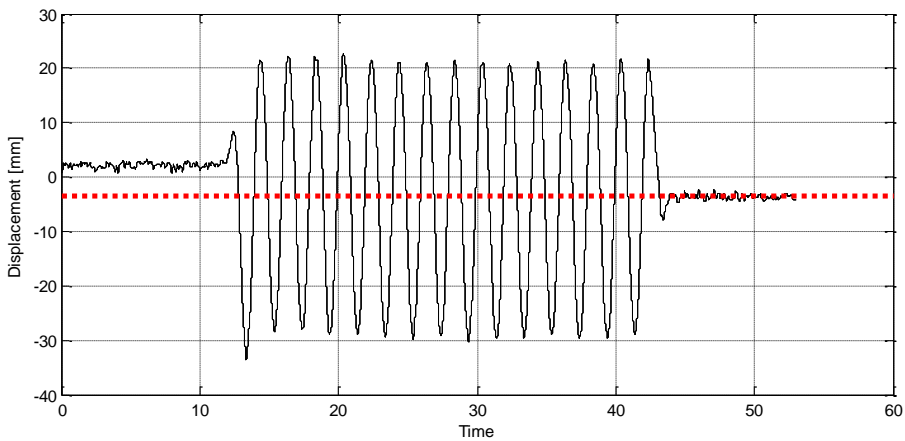


Figure 7-9 – Displacements (test 0.5 Hz)

The final condition of test at 0.5 Hz is the initial condition of test at 1.0 Hz. It can be seen in Figure 7-11 that:

- respect to the mean value of the shaking portion (-5.4 mm) the peak-peak value of the displacement is ± 25 mm as expected, with a standard deviation of 1.08 mm;

- the final displacement is basically equal to the equilibrium position of the table and to the initial displacement.

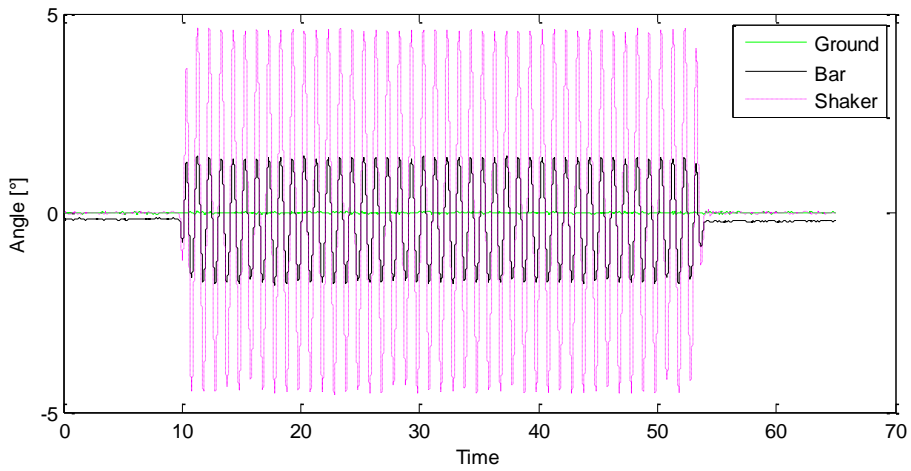


Figure 7-10 - Measured angles (test 1.0 Hz)

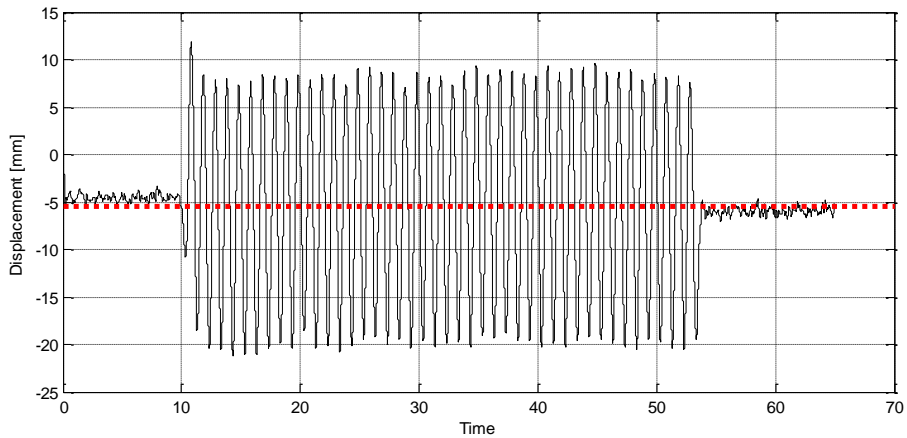


Figure 7-11 – Displacements (test 1.0 Hz)

7.5 Iterative baseline correction method

I propose here an iterative method for the estimation of interstory drift time histories based on the baseline correction of acceleration time histories driven by direct measurement of residual interstory drift after the seismic event. The evaluation of the performance of method is currently ongoing. The aim of this method is increasing the accuracy of Peak Interstory Drift (PID) estimation respect to the method based on double integration of band-pass filtered accelerations, obtaining at the same time

also information on Residual Interstory Drift (RID) which can be used in the damage assessment procedure.

7.5.1 *Theoretical background*

Signal processing consisting mainly in the application of a band-pass filter to the accelerometer time histories (and often to the velocity and displacement time histories) is necessary to remove from acceleration traces low-frequency components before double numerical integration to estimate displacements. The source of low frequency components was investigated by many authors in the last years, in particular within researches aiming to study low-frequency components of the ground motion. In (Iwan 1985) the source of baseline variation is ascribed to mechanical and electrical hysteresis of the transducer, having the Author observed that the instrument used to monitor ground motion presented a baseline shift when acceleration exceeded the value of 0.5 m/s^2 . Another source of baseline shift in acceleration time histories is identified in (Todorovska 1998) as the cross-axis sensitivity error of the transducer and the misalignment error. In (David M. Boore 2003) the effect of analog-to-digital conversion of acceleration data on displacement time histories estimation is investigated and it is concluded that the ADC process produces time-varying offsets in the baseline of acceleration time series which leads to drift in displacements. Another possible source of baseline shift is considered in (David M. Boore 2001), which is the mechanical tilt of the instrument during the motion. It is worth emphasizing that these cited works and others related have as goal the study of ground motion and in particular the estimation of displacement response spectra from strong motion records. The methods adopted in these works were applied to accelerograph transducers instead of accelerometer transducer. Here I try to extend these methods to accelerometer transducers and in particular to structural monitoring instead of ground monitoring.

In refer in the following to the works of David M. Boore and in particular to (David M. Boore 2001; D. M. Boore 2005; David M. Boore and Bommer 2005; Akkar and Boore 2009) which in turns refer to the research reported in (Iwan 1985).

In these works a method of baseline correction of the acceleration time histories is proposed in order to retrieve permanent ground displacements and displacement response spectra from acceleration data recorded by digital accelerographs of strong motion arrays. The baseline correction method is an alternative method to the method consisting in high-pass filtering the acceleration data before numerical double integration to estimate displacements. The baseline correction method consists of neglecting the source of the baseline shift in the recorded acceleration data (so no models for the source of this shift are needed) and introducing a simplified model of the baseline shift which is subtracted to acceleration time histories (obtained the so called “corrected time histories”) before double numerical integration.

The baseline shift is in general not evident in acceleration data while it manifests itself in velocity time histories as one or more linear trends and in displacement time histories as a drift increasing quadratically over time (Figure 7-12). In (David M. Boore 2001) it is observed that the linear trend in

velocity can be addressed to one or more changes of the baseline of the acceleration which occur after the strong shaking. The proposed baseline correction method assumes that two baseline variations have to be removed (David M. Boore 2001). The first between times t_1 and t_2 with baseline value a_m (representing the more or less complicated baseline shift that can occurs during the strong shaking), and the second from times t_2 to the end of the record with baseline value a_f . The level of a_f is determined from the slope of a linear fit to the portion of the velocity time history following the strong shaking:

$$v_f(t) = v_0 + a_f t \tag{7.18}$$

The level of a_m is computed with the requirement that the corrected velocity time history must be obviously zero-mean. This is true if the velocity of the baseline correction at the end of the $t_1 - t_2$ interval is equal to the velocity of the fitting line of at time t_2 obtained from Eq. (7.18), that is (David M. Boore 2001):

$$a_m = \frac{v_f(t_2)}{t_2 - t_1} \tag{7.19}$$

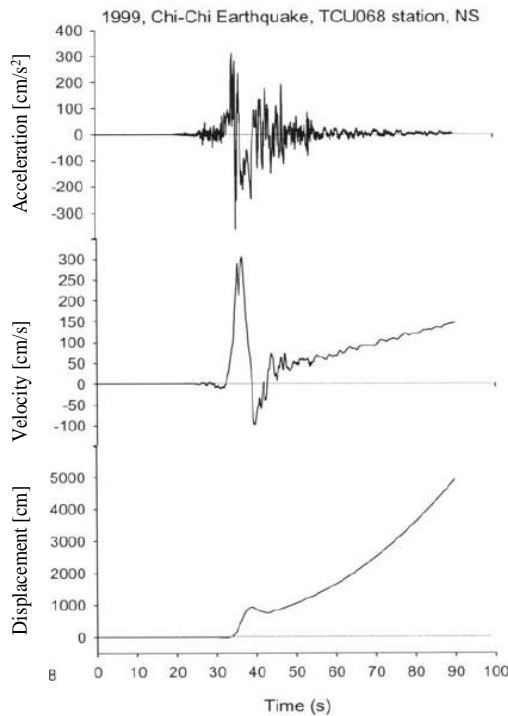


Figure 7-12 – Acceleration, velocity and displacement time histories recorded by TCU068 station in the NS direction during the 1999, Chi-Chi Earthquake, adapted from (Akkar and Boore 2009)

The free parameters of the model are therefore the times t_1 and t_2 only.

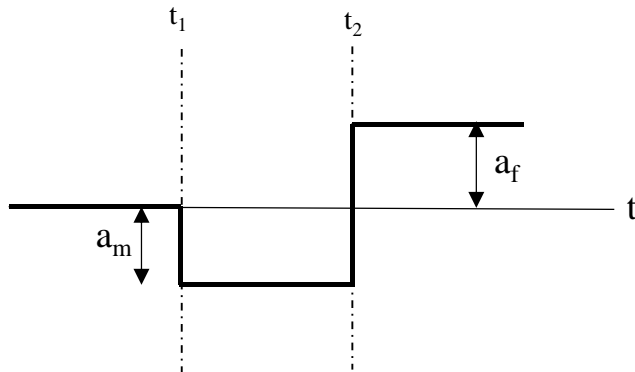


Figure 7-13 – Parameters of the model for baseline correction, adapted from (Akkar and Boore 2009)

A parametric study on the method was also reported in (David M. Boore 2001) applying baseline correction on several records of the 1999, Chi-Chi earthquake. Displacement time histories obtained by double integration of the corrected acceleration time histories are reported in Figure 7-14. In the same plots, also permanent ground displacements recorded by GPS stations few km far from accelerographs are reported.

This baseline correction method was further investigated and expanded in (Akkar and Boore 2009). Here, a Monte Carlo simulation is performed for several models of the acceleration baseline variations, determining the parameters describing the models in a random manner assuming a normal distribution of the random variable.

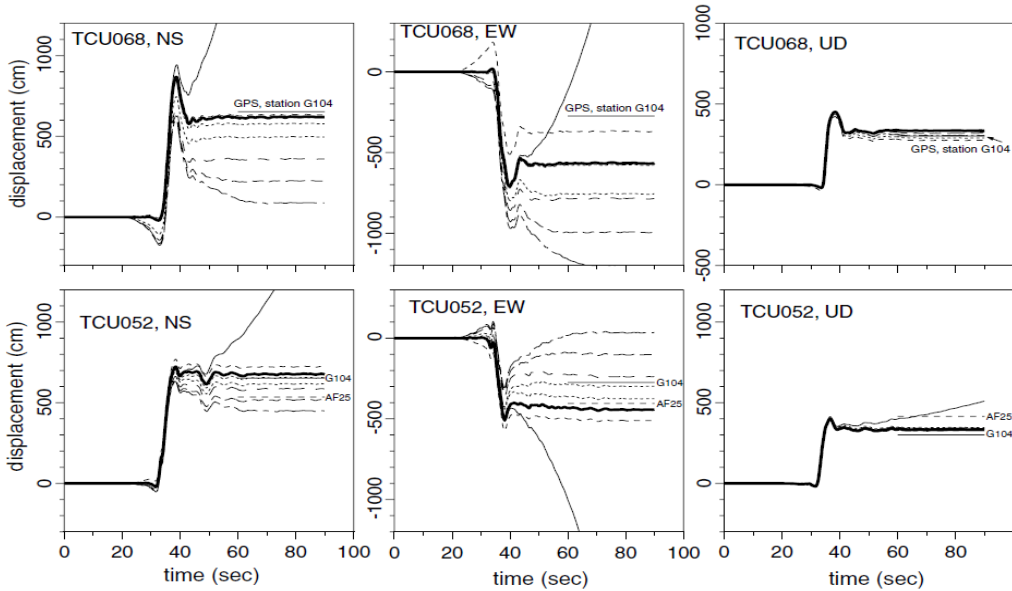


Figure 7-14 - . Displacement time histories obtained by double integration of the corrected acceleration time histories. Different curves correspond to different t_2 values (assuming $t_1 = 20$ sec just before strong shaking). From (David M. Boore 2001)

As stated before, in the previously cited papers a comparison between the displacement time histories obtained from double integration of baseline corrected accelerations and GPS station records demonstrates a good agreement. The Authors ascertain that it is in principle impossible to determine the model parameters without the displacement measurements of a GPS station, being however useless the application of the baseline correction method when these measurements are actually available. This is true for the estimation of permanent displacement of the ground, which is the topic of the previously cited works.

7.5.2 Algorithm of the method

The algorithm allows for the estimation of the time history of relative displacement between point 1 and 2 being measured the accelerations $a_1(t)$ and $a_2(t)$ at points 1 and 2 and the inclination respect to the gravity θ of a beam linking point 1 and 2.

1. Record acceleration time histories $a_1(t)$ and $a_2(t)$ on trigger, including pre-event accelerations $a_{p1}(t)$ and $a_{p2}(t)$ (I suggest as a minimum time of the pre-event portions of the time history a time equal to 5 sec and an optimum value equal to 10 sec);
2. Record the inclination θ of the beam respect to the gravity and compute the residual relative displacement Δ_R multiplying the inclination by the length of the beam.

3. Compute the mean values \bar{a}_{p1} and \bar{a}_{p2} of $a_{p1}(t)$ and $a_{p2}(t)$;
4. Subtract \bar{a}_p to the acceleration time histories $a_1(t)$ and $a_2(t)$ obtaining initial mean corrected accelerations $a_{zoc,1}(t)$ and $a_{zoc,2}(t)$;
5. Numerically integrate $a_{zoc,1}(t)$ and $a_{zoc,2}(t)$ to obtain velocities $v_{zoc,1}(t)$ and $v_{zoc,2}(t)$;
6. Choose a baseline model (e.g. the one showed in Figure 7-13) in function of the aspect of velocities, in particular verifying manually or automatically if they present one or more linear trends;
7. Choose a starting set of the model parameters (e.g. $t_{1,0}$ and $t_{2,0}$ for the model in Figure 7-13) for both corrected accelerations (4 total parameters in the example);
8. Subtract the values of the baseline model to mean corrected accelerations, obtaining first-tentative baseline corrected accelerations $a_{b1,0}(t)$ and $a_{b2,0}(t)$;
9. Double integrate baseline corrected accelerations obtaining $d_{1,0}(t)$ and $d_{2,0}(t)$ then compute the relative displacement time history $\Delta_0(t)$;
10. Compute the absolute difference $e = |\Delta_R - \Delta_0|$ and compare it to a predefined target value ϵ .
11. If it is higher, restart step 7 assuming a different set of parameters. On the contrary, compute the peak value of the relative displacement PID.

Actually the problem can have different solutions, in particular different sets of parameters can lead to the satisfaction of the condition $e = |\Delta_R - \Delta_0| \leq \epsilon$. In this case, it is possible to retrieve a distribution of PID values instead of a single value, to be expressed in terms of mean and standard deviation.

7.5.3 Simplified approach

During my discussion on the increment of uncertainty due to the residual displacement of the method of double integration of acceleration data only, I stated that underestimation of the peak value of the displacement increases with increasing the value of the residual displacement. This can be translated in terms of relative displacement stating that the error in the estimation of peak value of the relative displacement between upper and lower floors increases with increasing the value of relative residual displacement.

It can be demonstrated that the maximum value of this error (due to residual relative displacement only) is equal to the residual relative displacement.

A simplified approach consists therefore to correct the maximum value of relative displacement between points 1 and 2 obtained from double numerical integration of acceleration measurements (including band-pass filtering) by adding the value obtained from inclination measurement, that is:

$$PID = PID_{2int} + \theta H \quad (7.20)$$

being PID_{2int} the value obtained from accelerometers only and θ the inclination measurement. The error adding to the residual displacement to the maximum displacement obtained from double integration is plotted in Figure 7-15 as red crosses. It can be seen that, on average, the error tends to the value of the elastic case and it is in any case lower.

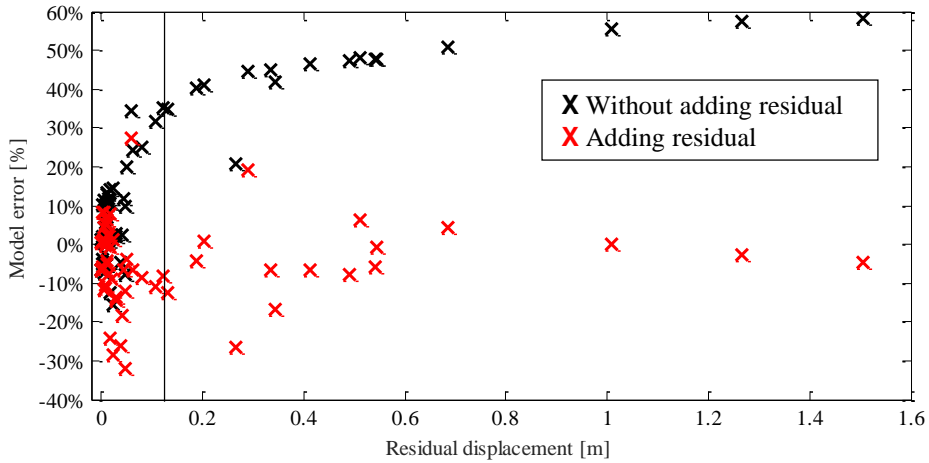


Figure 7-15 – Model error on PDI estimation adding RID value

7.6 Prototype of the system

The proposed sensing bar was applied in a prototype monitoring systems named SafeQuake developed by IKUBED, start-up of the University of Trento, and installed in the Elementary School in the town of Stenico, in Trentino.



Figure 7-16 – Stenico Elementary School

The need of the customer was monitoring in real-time the accelerations at the ground and at each of the two floors, detecting seismic events and estimating floor displacements to be compared to the results of a preliminary seismic vulnerability assessment.

A total of 4 sensing bars was installed, two at the first floor and two at the second. Each sensing bar was instrumented with 2 bi-axial accelerometers and 1 bi-axial inclinometer.

The sensors transmit analog (4-20 mA) signals to a NI cRIO 9074 controller where A/D conversion is performed by two NI 9203 8-channel modules. The controller is in turn connected via LAN to a Pc running the data analyzer software. The following figure illustrate the components of the system.

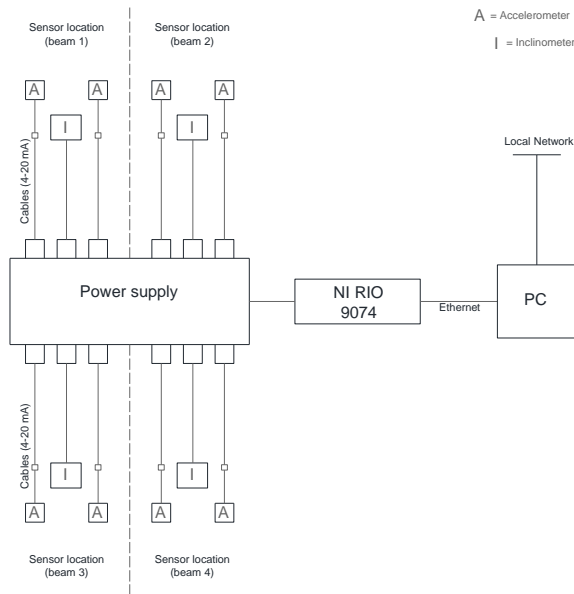


Figure 7-17 – Components of SafeQuake system

In principle, any accelerometer and inclinometer models can be used for sensing the motion of the beam. To test the effectiveness of the method, we selected low-cost sensors available in the market, namely the accelerometer AKE319T by Rion Technologies and the inclinometer IS2D90P24 by GEMAC. The same inclinometer model was used during tests discussed in section 7.4.3.



Figure 7-18 – GEMAC IS2D90P24 inclinometer



Figure 7-19 – RION AKE19T accelerometer

The designed system performs the following functions:

- real-time monitoring of floor accelerations;
- automatic event detection (the same principles discussed in section 6.10 were implemented);
- calculation of the time histories of displacement by means of simple double integration of acceleration measurements;
- measurement of the time histories of displacement by means of dynamic tilt measurements compensated to the effects of acceleration using the method discussed in 7.4 (beta);
- after-earthquake measurement of the residual interstory drift (RID) at the end of the motion from static tilt measurements;
- calculation of the time histories of displacement by means of double integration of acceleration measurements corrected by RID using algorithm discussed in 7.5.2 (beta);
- calculation of the maximum interstory drift (PID) using the simplified approach discussed in 7.5.3;

The front panel of the application, developed using the Labview platform, is showed below:

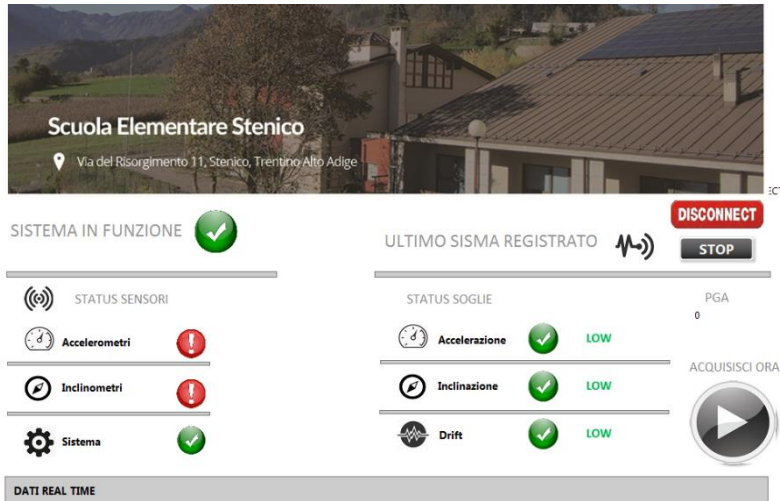


Figure 7-20 – Main screen of the application

In the following figures I show some picture of the installation.

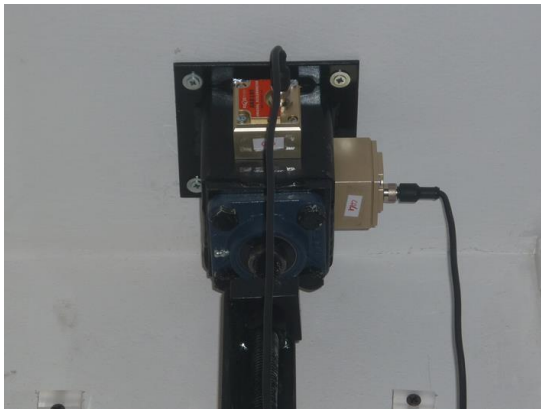


Figure 7-21 – Detail of the connection of the sensing beam to the 1° floor



Figure 7-22 - Rack



Figure 7-23 – Location of the beam at the first floor (behind a finishing)



Figure 7-24 – Sensing bema covered by the plastic protective involucro

7.7 Conclusions

After having remarked that the uncertainty in displacement estimation from acceleration data only is heavily increased in case of residual displacements at the end of the motion, a prototype of sensing bar is discussed in this Chapter. It consists of a bar instrumented with 2 bi-axial accelerometers and one bi-axial inclinometer. The accelerometers are fastened to steel cubic supports in turns rigidly fixed to the floors by means of dowels. The beam is linked to the supports by means of mechanical hinges (e.g. one spherical hinge and one Cardan joint, or two Cardan joints). The inclinometer (or a capacitive accelerometer) is fastened to a horizontal plate welded to the beam (e.g. at the mid span). The rigid constraint between supports and floors ensures that accelerometers measure the horizontal accelerations of the floors. The mechanical hinges ensure that the beam is free to rotate during the seismic event and tilted of an angle equal to the ratio of the residual differential displacements between the floors and the distance between beam's ends.

The sensing bar is suitable for the implementation of different monitoring methods. In addition to displacement time history estimation from double integration of floor accelerations, and to the measurement of the residual interstory drift at the end of the motion, 3 other methods were proposed in this Chapter.

The first consists on the real-time monitoring of sensing bar inclination, equal to the interstory drift ratio between the consecutive floors to which the bar is fixed. Different arrangements are possible (2 accelerometers + 1 inclinometer, 3 accelerometers, 3 inclinometers).

The arrangement with 3 inclinometers was tested in the laboratory fixing the bar to a shaking table to an end and to the roof to the other. The implemented method for acceleration compensation had as a result that with low-cost inclinometers it is possible to estimate displacement with a standard deviation of 1.2 mm when the interstory height is 3 m and when the time history is sinusoidal in the range 0.5-1.0 Hz. Residual displacement is correctly detected and no high-pass filters are needed.

Starting from the research of David Boore, I proposed a new monitoring method, currently under test, which is the baseline correction of acceleration time histories driven by the measurement of residual interstory drift. This method should allow for increasing the accuracy of the peak interstory drift estimation in case of residual displacements at the end of the seismic motion and, obviously, provides also the residual interstory drift, which can be an important indicator of structural damage.

The proposed method is basically an iterative baseline correction of the acceleration time histories driven by the residual interstory drift measured at the end of the motion. In particular, the baseline shift affecting the acceleration time history, which is the reason because a high-pass filter is required before integration, is modeled by a model characterized by a certain set of parameter. At each iteration, a set of parameters is used to correct the acceleration time histories, and integration is performed directly without filtering. A residual drift is commonly obtained at the end of the signal, which is compared to the one actually measured. The iterative process ends when the difference among the values is lower than a pre-set threshold.

A simplified approach which can be implemented when the system has reduced computational capabilities (e.g. a stand-alone wireless sensing beam) is also proposed in this Chapter. It consists of simply summing the peak interstory drift calculated by numerical integration of band-pass filtered accelerations and the residual interstory drift measured by the inclinometer. It has demonstrated in fact that the maximum error due to the residual interstory drift is the residual interstory drift itself.

8 Conclusions and future work

8.1 Conclusions

In this thesis the problem of after-earthquake damage assessment of RC buildings by means of seismic structural health monitoring (SHM) systems was investigated.

- The analysis of the state of the art about seismic SHM systems allows me to define it as a system which permits to obtain information on the monitored structure after an earthquake, by means of a backward analysis based on:
 - the collection of a set of observations;
 - a prior knowledge of the structure;
 - a model relating observations and information.

The obtained information can be related or not to the state of condition of the structure. If it is, the information is a state variable. If it is not, the information is a response parameter. Systems observing in real-time the seismic response of the structure extracting response parameters, and those comparing prior and posterior structural parameters (e.g. modal properties) both fall in the previous definition.

- Recognizing the lack of standards and guidelines for the design of SHM systems in general and of seismic SHM systems in particular, I proposed a logical framework for the design of these systems. Basically, I discussed how the design process can be driven by a demand-capacity approach, starting from the definition of the requested accuracy (demand) of the information to be provided (e.g. maximum lateral displacement with an uncertainty lower than ± 1 cm, or yielded/not yielded classification of a member with a probability of misclassification lower than 10^{-3}) and checking that the designed system, including the system components, sensors number and locations, models linking extracted information to observations, and so on, guarantees an accuracy (capacity) better than demand. This methodology implies the definition and quantification of all uncertainties involved, including ones related to the hardware (instrumental uncertainties) and to the inferring model (model uncertainties).
- Among all the information which can be correlated in some way to the state of condition of a building after an earthquake, I decided to study the interstory drift ratio (IDR). Many researches demonstrate in fact that damage on non-structural components such as partitions depends mainly on IDR, and that from IDR it is possible to compute easily the chord rotation demand to the ends of structural members (e.g. beams and columns), which in turns is well correlated to damage to these components. Moreover, also if not applied in this work, IDR is well suited to the use of a probabilistic approach, in particular of fragility functions.
- The most common monitoring method for IDR estimate is based on the double numerical integration of acceleration measurements. In this thesis I discussed in detail this method, describing the signal processing (in particular the application of an acausal band-pass filter) required to obtain reliable data and highlighting main sources of uncertainties.
- The main sources of uncertainty in the estimation of the peak of the interstory drift (PID):
 1. instrumental uncertainties;
 2. the filtering process;
 3. the possible residual displacement at the end of the motion.
- As a result of parametric analysis on SDOF systems excited by natural accelerograms, that the uncertainties pertaining to the model are predominant respect to the instrumental ones.
- Relating to the effect of filtering, it can be seen that:

CONCLUSIONS AND FURTHER WORKS

- the error is basically independent on the frequency of the system f up to 4 Hz, while the dependence is strong on the ratio f/f_{cut} .
- a dependence on f is observed for higher values: this is explained by the fact that for higher frequencies, displacements are smaller. In this case, numerical error is predominant respect to the error due to the filter;
- as expected, for f/f_{cut} close to 1 the mean error is around 30%. This is explained remembering that the cutoff frequency corresponds to a 70% reduction of the component in the signal at that frequency;
- the mean error is close to 0% when the ratio f/f_{cut} is about 2;
- standard deviation of the error seems to be independent to the f/f_{cut} ratio, being its mean value 7.13%. Highest values are obtained also in this case for $f = 8$ Hz. This seems to confirm the randomness of the numerical error.

f/f_{cut}	0.50	1.00	1.67	2.28	3.33	6.67	13.33
std	9.76%	8.19%	7.91%	5.86%	6.70%	4.89%	7.82%
mean	81.0%	33.2%	5.0%	0.2%	-0.8%	-0.2%	1.4%

- It can be concluded that when the system remains elastic:
 - a systematic error depending on the ratio between system natural frequency f and the cut-off frequency of the high-pass filter f_{cut} affects displacement estimation. This error tends to zero for f/f_{cut} higher than 2.
 - A random error due to numerical integration was also observed. This error is zero mean with standard deviation about 7%.
- Performing the same analysis on non-linear systems, assuming an elastic perfectly plastic force-displacement relationship, the error strongly increases. In case of residual displacement at the end of the motion, about 30% in case of a residual equal to the displacement at yielding and tending to 60% for higher residual deformation.
- On the contrary, instrumental uncertainties are in the range 3-6% (depending on instrument) when no information about the installed components are available (i.e. the uncertainty analysis is performed on data sheets only without any calibration) but can be strongly reduced by the calibration of the sensors and proper installation, down to 2.5%. In particular I estimated the uncertainty due to noise as less than 1 cm for cut-off frequency about 0.05 Hz. This implies that in principle also low-cost sensors can be effectively used, provided that each sensor is properly calibrated and installed. In case of flexible structures (namely structures in which natural frequency is lower than 1 Hz), a compromise between uncertainty due to noise and uncertainty due to filtering process is required. A possible approach, which

can be used when first mode of vibration is predominant and the contribution to displacement of higher modes is negligible, or when only first mode of vibration is affected by the high-pass filter, is applying to the obtained displacement time history a multiplicative safety factor depending on the f/f_{cut} ratio.

Error	Metric	performed	not performed
Calibration	%	1 - 2	0
Environmental	%	0.5 - 1	0.5 - 1
Ratiometricity	%	1 - 2	0.5
Mounting	%	2 - 3	1
Cross-axis sensitivity	%	2 - 3	2 - 3
Noise	cm	0.5	0.5
Instrumental uncertainty		3-6% ±	2.5% ±
		0.5 cm	0.5 cm

The importance of the study of uncertainties related to the model of interpretation of the observations is possibly higher in the case of seismic monitoring of precast industrial buildings, which is the case study I analyzed in detail in this work. For this type of facilities:

- the assumption of rigid behavior of the floor diaphragm is in general not valid. This implies that in principle each column, if considered as independent, should be monitored through two bi-axial accelerometers placed at its top and at its bottom;
- decomposing the global seismic response of the building as a summation of modes of vibration, I found by means of numerical analysis that placing only $N = n + m$ bi-axial accelerometers, being $n \times m$ the total number of columns, and considering N modes of vibrations assuming null the stiffness of the floor, it is possible to reduce the increase of uncertainty due to incompleteness of the measured field (i.e. the fact that only $N < n \times m$ columns are actually monitored) to less than 1%. In the following table, for example, the error trend due to the incompleteness of the measured field is showed for a building having 3 columns along the transversal direction and 5 along the longitudinal direction, varying number of sensors and modes in the range 3-8.

n	$e_{if_{n,k}}$ [%]
3	12.3
4	7.6
5	6.1
6	2.5
7	1.2
N=8	0.7

A prototype of sensing bar which is suitable for the application on seismic structural health monitoring is finally proposed in this thesis.

- The sensing bar consists of a bar instrumented with accelerometers and inclinometers. The accelerometers (or the inclinometers) are fastened to steel cubic supports in turns rigidly fixed to the floors by means of dowels. The beam is linked to the supports by means of mechanical hinges (e.g. one spherical hinge and one Cardan joint, or two Cardan joints). The inclinometer (or a capacitive accelerometer) is fastened to a horizontal plate welded to the beam (e.g. at the mid span).
- The sensing bar is suitable for the implementation of different monitoring methods. In addition to displacement time history estimation from double integration of floor accelerations, and to the measurement of the residual interstory drift at the end of the motion, 3 other methods were proposed.
- The first method consists on the real-time monitoring of sensing bar inclination, equal to the interstory drift ratio between the consecutive floors to which the bar is fixed. Different arrangements are possible (2 accelerometers + 1 inclinometer, 3 accelerometers, 3 inclinometers).
- The arrangement with 3 inclinometers was tested in the laboratory fixing the bar to a shaking table to an end and to the roof to the other. The implemented method for acceleration compensation had as a result that with low-cost inclinometers it is possible to estimate displacement with a standard deviation of 1.2 mm when the interstory height is 3 m and when the time history is sinusoidal in the range 0.5-1.0 Hz. Residual displacement is correctly detected and no high-pass filters are needed.
- The second method, currently under test, is basically an iterative baseline correction of the acceleration time histories driven by the residual interstory drift measured at the end of the motion. In particular, the baseline shift affecting the acceleration time history, which is the

reason because a high-pass filter is required before integration, is modeled by a model characterized by a certain set of parameter. At each iteration, a set of parameters is used to correct the acceleration time histories, and integration is performed directly without filtering. A residual drift will be obtained at the end of the signal, which is compared to the one actually measured. The iterative process ends when the difference among the values is lower than a pre-set threshold.

- A simplified approach is also provided in this work, which consists to simply summing the residual drift value to the peak drift value. This is particularly useful when the system has low computation capabilities or initial estimate of the peak drift value has to be provided, for example for immediate usability assessment.

Finally, the proposed sensing bar was applied in a prototype monitoring systems named SafeQuake developed by IKUBED, start-up of the University of Trento, and installed in the Elementary School in the town of Stenico, in Trentino. The designed monitoring system performs the following functions:

- real-time monitoring of floor accelerations;
- automatic event detection;
- calculation of the time histories of displacement by means of simple double integration of acceleration measurements;
- measurement of the time histories of displacement by means of dynamic tilt measurements compensated to the effects of acceleration;
- after-earthquake measurement of the residual interstory drift at the end of the motion from static tilt measurements;
- calculation of the time histories of displacement by means of double integration of acceleration measurements corrected by residual interstory drift measurement;

8.2 Future work

The natural continuation of this work is the implementation of the probabilistic approach in the estimation of the state of condition of a seismic monitored structure. In fact, in this thesis I focused mainly in the study of the physical parameter provided by the system (i.e. the displacement time history or the interstory drift ratio) rather than of the classification of the state of the building. It is clear that also assuming a deterministic value of the demand parameter, different structures can suffer different damages also considering the same nominal values of the structural parameters. In other words, a monitoring system should provide the probability of a certain level of damage, rather than the level of damage itself. A promising approach in this sense is the implementation of fragility curves, which basically give the probability of being in a certain state of condition, given the demand.

Concerning the method proposed in Chapter 7, the numerical study of its performance is currently on-going. The aim now is to develop a *sensing beam* as an industrial product, embedding very low cost sensors (accelerometers and inclinometers) into the beam itself, giving to the beam A/D conversion, memory, and wireless data transmission capabilities on-board.

References

- Akkar, S., and D. M. Boore. 2009. "On Baseline Corrections and Uncertainty in Response Spectra for Baseline Variations Commonly Encountered in Digital Accelerograph Records." *Bulletin of the Seismological Society of America* 99 (3): 1671–90. doi:10.1785/0120080206. <http://www.bssaonline.org/cgi/doi/10.1785/0120080206>.
- Anagnostopoulos, S., and M. Moretti. 2008. "Post-Earthquake Emergency Assessment of Building Damage, Safety and usability—Part 1: Technical Issues." *Soil Dynamics and Earthquake Engineering* 28 (3): 223–32. doi:10.1016/j.soildyn.2006.05.007. <http://www.scopus.com/inward/record.url?eid=2-s2.0-37249067615&partnerID=tZOtx3y1>.
- Applied Technology Council (ATC)-43. 1998. "Evaluation of Earthquake Damaged Concrete and Masonry Wall Buildings." FEMA 306.
- ASCE. 2000. *Prestandard and Commentary for the Seismic Rehabilitation of Buildings, Report No. FEMA-356*.
- ATC 20-1. 2005. *Field Manual: Postearthquake Building Safety Evaluation of Buildings*. California - USA.
- Baggio, Carlo, Alberto Bernardini, Riccardo Colozza, Livio Corazza, Marianna Della Bella, Giacomo Di Pasquale, Mauro Dolce, et al. 2009. *Manuale per La Compilazione Della Scheda*

Di 1° Livello Di Rilevamento Danno, Pronto Intervento E Agibilità per Edifici Ordinari Nell'emergenza Post-Sismica (AeDES). Roma: Editrice Italiani nel Mondo srl.

Balafas, Konstantinos, and Anne S. Kiremidjian. 2013. "Extension of the Rotation Algorithm for Earthquake Damage Estimation of Complex Structures." In *Proceedings of SPIE - The International Society for Optical Engineering*, edited by Jerome P. Lynch, Chung-Bang Yun, and Kon-Well Wang, 8692:86920S. doi:10.1117/12.2009877.
<http://www.scopus.com/inward/record.url?eid=2-s2.0-84878730033&partnerID=tZOtx3y1>.

———. 2014. "Reliability Assessment of the Rotation Algorithm for Earthquake Damage Estimation." *Structure and Infrastructure Engineering* 11 (1). Taylor and Francis Ltd.: 51–62. doi:10.1080/15732479.2013.879318. <http://www.scopus.com/inward/record.url?eid=2-s2.0-84908017223&partnerID=tZOtx3y1>.

Banon, Hooshang, and Daniele Veneziano. 1982. "Seismic Safety of Reinforced Concrete Members and Structures." *Earthquake Engineering & Structural Dynamics* 10 (2): 179–93.

Bindi, D., B. Petrovic, S. Karapetrou, M. Manakou, T. Boxberger, D. Raptakis, K. D. Ptilakis, and S. Parolai. 2014. "Seismic Response of an 8-Story RC-Building from Ambient Vibration Analysis." *Bulletin of Earthquake Engineering*, December. Kluwer Academic Publishers. doi:10.1007/s10518-014-9713-y. <http://www.scopus.com/inward/record.url?eid=2-s2.0-84917708565&partnerID=tZOtx3y1>.

Bonfanti, C, A Carabellese, and G Toniolo. 2008. "Strutture Prefabbricate - Catalogo Delle Tipologie Esistenti."

Boore, D. M. 2005. "On Pads and Filters: Processing Strong-Motion Data." *Bulletin of the Seismological Society of America* 95 (2): 745–50. doi:10.1785/0120040160.
<http://bssa.geoscienceworld.org/cgi/doi/10.1785/0120040160>.

Boore, D. M., A. Azari Sisi, and S. Akkar. 2012. "Using Pad-Stripped Acausally Filtered Strong-Motion Data." *Bulletin of the Seismological Society of America* 102 (2): 751–60. doi:10.1785/0120110222. <http://www.scopus.com/inward/record.url?eid=2-s2.0-84859123313&partnerID=tZOtx3y1>.

Boore, David M. 2001. "Effect of Baseline Corrections on Displacements and Response Spectra for Several Recordings of the 1999 Chi-Chi, Taiwan, Earthquake." *Bulletin of the Seismological Society of America* 91 (5): 1199–1211.

- . 2003. “Analog-to-Digital Conversion as a Source of Drifts in Displacements Derived from Digital Recordings of Ground Acceleration.” *Bulletin of the Seismological Society of America* 93 (5): 2017–24. <http://www.scopus.com/inward/record.url?eid=2-s2.0-0037652545&partnerID=tZOtx3y1>.
- Boore, David M., and Julian J. Bommer. 2005. “Processing of Strong-Motion Accelerograms: Needs, Options and Consequences.” *Soil Dynamics and Earthquake Engineering* 25 (2): 93–115. doi:10.1016/j.soildyn.2004.10.007. <http://www.scopus.com/inward/record.url?eid=2-s2.0-13644283118&partnerID=tZOtx3y1>.
- Bounif, A, M Bezzeghoud, L Dorbath, D Legrand, A Deschamps, L Rivera, and H Benhallou. 2003. “Seismic Source Study of the 1989, October 29, Chenoua (Algeria) Earthquake from Aftershocks, Broad-Band and Strong Ground Motion Records.” *Annals of Geophysics* 46: 625–46.
- Bournas, Dionysios A., Paolo Negro, and Fabio Taucer. 2013. “The Emilia Earthquakes: Report and Analysis on the Behavior of Precast Industrial Buildings from a Field Mission.” In *ECCOMAS Thematic Conference - COMPDYN 2013: 4th International Conference on Computational Methods in Structural Dynamics and Earthquake Engineering, Proceedings - An IACM Special Interest Conference*, 1600–1614. National Technical University of Athens. <http://www.scopus.com/inward/record.url?eid=2-s2.0-84898939620&partnerID=tZOtx3y1>.
- Building Research Institute. 2009. “Sensor Configuration - BRI Strong Motion Observation.” *Building Research Institute*. <http://smo.kenken.go.jp/smn/sensorconf>.
- Calvi, Gian Michele. 1999. “A Displacement-Based Approach for Vulnerability Evaluation of Classes of Buildings.” *Journal of Earthquake Engineering* 3 (3): 411–38. <http://www.scopus.com/inward/record.url?eid=2-s2.0-0033241831&partnerID=tZOtx3y1>.
- Celebi, M., A. Sanli, M. Sinclair, S. Gallant, and D. Radulescu. 2004. “Real-Time Seismic Monitoring Needs of a Building Owner—and the Solution: A Cooperative Effort.” *Earthquake Spectra* 20 (2): 333–46. doi:10.1193/1.1735987. <http://earthquakespectra.org/doi/abs/10.1193/1.1735987>.
- Celebi, Mehmet. 2007. “Developments in Seismic Monitoring for Risk Reduction.” *Journal of Risk Research* 10 (5): 715–27. doi:10.1080/13669870701447964. <http://www.tandfonline.com/doi/abs/10.1080/13669870701447964>.

- Celebi, Mehmet, and Ahmet Sanli. 2002. "GPS in Pioneering Dynamic Monitoring of Long-Period Structures." *Earthquake Spectra* 18 (1): 47–61. doi:10.1193/1.1461375.
<http://www.scopus.com/inward/record.url?eid=2-s2.0-0036478194&partnerID=tZOtx3y1>.
- Chan, W. S., Y. L. Xu, X. L. Ding, and W. J. Dai. 2006. "An Integrated GPS–accelerometer Data Processing Technique for Structural Deformation Monitoring." *Journal of Geodesy* 80 (12): 705–19. doi:10.1007/s00190-006-0092-2. <http://www.scopus.com/inward/record.url?eid=2-s2.0-37849188346&partnerID=tZOtx3y1>.
- Cheung, A, and AS Kiremidjian. 2013. "Development of a Rotation Algorithm for Earthquake Damage Diagnosis." *Earthquake Spectra*.
<http://earthquakespectra.org/doi/abs/10.1193/012212EQS016M>.
- Cheung, Allen, Garo Kiremidjian, Pooya Sarabandi, and Anne S Kiremidjian. 2014. "UNITED STATES PATENT: "US 2014/0012517 A1 - Structural Damage Estimation Based On Measurements of Rotations." United States.
- Chopra, Anil K. 2011. *Dynamics of Structures*. Edited by Prentice Hall. New Jersey.
- Cigognetti, Giacomo. 2012. "Wireless Sensors for Seismic Monitoring of Reinforced Concrete Buildings: Experimental Characterization and Application to a Full-Scale Framed Structure." University of Trento.
- Coato, Daniele. 2012. "Laboratory Validation of Memscan Technology for after-Earthquake Assessment of RC Buildings." University of Trento.
- Consortium of Organizations for Strong-Motion Observation Systems. 2009. "Strong-Motion Record Processing Guidelines."
- CSMIP. 2007. "System Requirements - Integrated Tri-Axial Accelerograph."
- DBA, and TECNIC. 2009. "Methodology for the Assessment of the Structural Condition of Monitored Damaged Reinforced Concrete Buildings and the Selection of Remedial Measures." Memscan Del. 2.1.
- Di Pasquale, Edmondo, and Ahmet Cakmak. 1987. "Detection and Assessment of Seismic Structural Damage." Buffalo.
- Dolce, Mauro. 2013. "Analogie E Differenze Nei Recenti Terremoti Italiani." In *Anidis*. Padova, Italy.

- DPC. 2014. "Osservatorio Sismico Delle Strutture."
<http://www.protezionecivile.gov.it/jcms/it/osservatorio.wp>.
- Dunn, Patrick F. 2010. *Measurement and Data Analysis for Engineering and Science*. Edited by CRC Press. Taylor and Francis Ltd.
- Duron, Ziyad H, William P Wiesmann, and Loland Alexander Pranger. 2004. "UNITED STATES PATENT: US 6,807,862 B2 - Device and Method for Determining and Detecting the Onset of Structural Collapse."
- Ewins, D.J. 2000. *Modal Testing, Theory, Practice, and Application*. 2nd ed. Philadelphia: Research Studies Pre.
- fib. 2008. *Structural Connections for Precast Concrete Buildings*. fib Bulletin.
- Fischinger, Matej, Miha Kramar, and Tatjana Isaković. 2008. "Cyclic Response of Slender RC Columns Typical of Precast Industrial Buildings." *Bulletin of Earthquake Engineering* 6 (3): 519–34. doi:10.1007/s10518-008-9064-7. <http://www.scopus.com/inward/record.url?eid=2-s2.0-47949085794&partnerID=tZOtx3y1>.
- Freescall Semiconductor. 2007. "Accelerometer Terminology Guide."
http://cache.freescall.com/files/sensors/doc/support_info/SENSORTERMSPG.pdf.
- Frishman, Fred. 1971. "On the Arithmetic Means and Variances of Products and Ratios of Random Variables." *National Technical Information Service*.
- Glisic, Branko, Daniele Inaudi, and Nicoletta Casanova. 2010. "<title>SHM Process as Perceived through 350 Projects</title>." In *Proceedings of SPIE - The International Society for Optical Engineering*, edited by Kara J. Peters, Wolfgang Ecke, and Theodore E. Matikas, 7648:76480P – 76480P – 14. doi:10.1117/12.852340.
<http://www.scopus.com/inward/record.url?eid=2-s2.0-77953486107&partnerID=tZOtx3y1>.
- Goel, Rakesh K. 2011. "Comparison of Base Shears Estimated from Floor Accelerations and Column Shears." *Earthquake Spectra* 27 (3): 939–46. doi:10.1193/1.3610247.
<http://www.scopus.com/inward/record.url?eid=2-s2.0-80052153310&partnerID=tZOtx3y1>.
- Günay, Selim, and Khalid M. Mosalam. 2013. "PEER Performance-Based Earthquake Engineering Methodology, Revisited." *Journal of Earthquake Engineering* 17 (6): 829–58.
doi:10.1080/13632469.2013.787377.
<http://www.tandfonline.com/doi/abs/10.1080/13632469.2013.787377>.

- Iervolino, I, C Galasso, and E. Cosenza. 2009. "REXEL: Computer Aided Record Selection for Code-Based Seismic Structural Analysis." *Bulletin of Earthquake Engineering* 8: 339–62.
- Im, Seok Been, Stefan Hurlebaus, and Young Jong Kang. 2013. "Summary Review of GPS Technology for Structural Health Monitoring." *Journal of Structural Engineering* 139 (10): 1653–64. doi:10.1061/(ASCE)ST.1943-541X.0000475.
<http://www.scopus.com/inward/record.url?eid=2-s2.0-84884998084&partnerID=tZOtx3y1>.
- Iwan, Wilfred D, Dan Constantin Radulescu, and Costin Radulescu. 2013. "UNITED STATES PATENT: US 8,538,734 B2 - Extreme Event Performance Evaluation Using Real Time Hysteresis Monitoring."
- Iwan, Wilfred D. 1985. "SOME OBSERVATIONS ON STRONG-MOTION EARTHQUAKE MEASUREMENT USING A DIGITAL ACCELEROGRAPH." *Bulletin of the Seismological Society of America* 75 (5): 1225–46. <http://www.scopus.com/inward/record.url?eid=2-s2.0-0022146402&partnerID=tZOtx3y1>.
- JCGM. 2008. *Evaluation of Measurement Data - Guide to the Expression of Uncertainty in Measurement*.
- JRC. 2007. "Field Manual for Post-Earthquake Damage and Safety Assessment and Short Terms Countermeasures." JRC Scientific and Technical Reports.
- Kamat, Vineet R., and Sherif El-Tawil. 2007. "Evaluation of Augmented Reality for Rapid Assessment of Earthquake-Induced Building Damage." *Journal of Computing in Civil Engineering* 21 (5): 303–10. doi:10.1061/(ASCE)0887-3801(2007)21:5(303).
<http://www.scopus.com/inward/record.url?eid=2-s2.0-34250680574&partnerID=tZOtx3y1>.
- Kaminosono, Takashi, Fumitoshi Kumazawa, and Yoshiaki Nakano. 2002. "Quick Inspection Manual for Damaged Reinforced Concrete Buildings due to Earthquakes."
- Kappos, A. 1997. "Seismic Damage Indices for RC Buildings: Evaluation of Concepts and Procedures." *Progress in Structural Engineering and Materials* 1 (1): 78–87.
- Kim, Junhee, Kiyong Kim, and Hoon Sohn. 2014. "Autonomous Dynamic Displacement Estimation from Data Fusion of Acceleration and Intermittent Displacement Measurements." *Mechanical Systems and Signal Processing* 42 (1-2). Elsevier: 194–205.
doi:10.1016/j.ymssp.2013.09.014.
<http://linkinghub.elsevier.com/retrieve/pii/S0888327013005013>.

- Kionix. 2007. "Accelerometer Errors." <http://www.kionix.com/sites/default/files/AN012AccelerometerErrors.pdf>.
- Lichtenwalner, Peter F, James P Dunne, Ronald S Becker, and Erwin W Baumann. 1999. "UNITED STATES PATENT: 6,006,163 - Active Damage Interrogation Method for Structural Health Monitoring."
- Limongelli, M.P. 2011. "The Interpolation Damage Detection Method for Frames under Seismic Excitation." *Journal of Sound and Vibration* 330 (22). Elsevier: 5474–89.
doi:10.1016/j.jsv.2011.06.012.
<http://linkinghub.elsevier.com/retrieve/pii/S0022460X11004895>.
- Lynch, J. P. 2006. "A Summary Review of Wireless Sensors and Sensor Networks for Structural Health Monitoring." *The Shock and Vibration Digest* 38 (2): 91–128.
doi:10.1177/0583102406061499.
<http://svd.sagepub.com/cgi/doi/10.1177/0583102406061499>.
- Lynch, Jerome P, Arvind Sundararajan, Kincho H Law, Ed Carryer, Hoon Sohn, and Charles R Farrar. 2003. "Field Validation of a Wireless Structural Monitoring System on the Alamosa Canyon Bridge." In *SPIE's 10th Annual International Symposium on Smart Structures and Materials*. San Diego, CA, USA.
- Mahin, Stephen A. 1998. "Lessons from Damage to Steel Buildings during the Northridge Earthquake." *Engineering Structures* 20 (4-6): 261–70.
<http://www.scopus.com/inward/record.url?eid=2-s2.0-0032055431&partnerID=tZOtx3y1>.
- McCormick, Jason, Hiroshi Aburano, Masahiro Ikenaga, and Masayoshi Nakashima. 2008. "Permissible Residual Deformation Levels for Building Structures Considering Both Safety and Human Elements." In *The 14th World Conference on Earthquake Engineering*. Beijing, China.
- Mitchell, H.B. 2010. *Multi-Sensor Data Fusion: An Introduction*. New York: Springer Berlin Heidelberg.
- Morris, A.S, and R Langari. 2011. *Measurement and Instrumentation Theory and Application*. Butterworth.
- MPampatsikos, V. 2008. "A Critical Review of the R.C. Frame Existing Building Assessment Procedure according to Eurocode 8 and Italian Seismic Code." University of Pavia.

- Naeim, Farzad, Scott Hagie, Arzhang Alimoradi, and Eduardo Miranda. 2005. "Automated Post-Earthquake Damage Assessment and Safety Evaluation of Instrumented Buildings." JAMA Report Number: 2005-10639. Los Angeles.
- Nakano, Yoshiaki, Hiroshi Kuramoto, and Masaya Murakami. 2004. "Guideline for Post-Earthquake Damage Evaluation and Rehabilitation of RC Buildings in Japan." In *13th World Conference on Earthquake Engineering*. Vancouver, Canada.
- New Zealand Society for Earthquake Engineering. 2009. "Building Safety Evaluation During a State of Emergency."
- Newmark, N, and E Rosenblueth. 1974. *Fundamentals of Earthquake Engineering*. Prentice Hall.
- Nickitopoulou, A., K. Protopsalti, and S. Stiros. 2006. "Monitoring Dynamic and Quasi-Static Deformations of Large Flexible Engineering Structures with GPS: Accuracy, Limitations and Promises." *Engineering Structures* 28 (10): 1471–82. doi:10.1016/j.engstruct.2006.02.001. <http://www.scopus.com/inward/record.url?eid=2-s2.0-33745030517&partnerID=tZOtx3y1>.
- Pacor, Francesca, Roberto Paolucci, Lucia Luzi, Fabio Sabetta, Andrea Spinelli, Antonella Gorini, Mario Nicoletti, Sandro Marcucci, Luisa Filippi, and Mauro Dolce. 2011. "Overview of the Italian Strong Motion Database ITACA 1.0." *Bulletin of Earthquake Engineering* 9 (6): 1723–39. doi:10.1007/s10518-011-9327-6. <http://www.scopus.com/inward/record.url?eid=2-s2.0-80855131516&partnerID=tZOtx3y1>.
- Panagiotakos, Telemachos B., and Michael N. Fardis. 2001. "Deformations of Reinforced Concrete Members at Yielding and Ultimate." *ACI Structural Journal* 98 (2): 135–48. <http://www.scopus.com/inward/record.url?eid=2-s2.0-0035297199&partnerID=tZOtx3y1>.
- Paolucci, R., F. Pacor, R. Puglia, G. Ameri, C. Cauzzi, and M. Massa. 2011. *Earthquake Data in Engineering Seismology*. Edited by Sinan Akkar, Polat Gülkan, and Torild van Eck. *Geotechnical, Geological and Earthquake Engineering*. Vol. 14. Geotechnical, Geological, and Earthquake Engineering. Dordrecht: Springer Netherlands. doi:10.1007/978-94-007-0152-6. <http://www.scopus.com/inward/record.url?eid=2-s2.0-84874358224&partnerID=tZOtx3y1>.
- Park, Y J, and A H S Ang. 1985. "Mechanistic Seismic Damage Model for Reinforced Concrete." *Journal of Structural Engineering* 111 (4): 722–39. <http://www.scopus.com/inward/record.url?eid=2-s2.0-0022043291&partnerID=tZOtx3y1>.

- Pauley, T, and M.J.N Priestley. 1992. *Seismic Design of Reinforced Concrete and Masonry Buildings*. New York: John Wiley & Sons Ltd.
- Ponzo, F. C., R. Ditommaso, G. Auletta, and a. Mossucca. 2010. "A Fast Method for Structural Health Monitoring of Italian Reinforced Concrete Strategic Buildings." *Bulletin of Earthquake Engineering* 8 (6): 1421–34. doi:10.1007/s10518-010-9194-6. <http://link.springer.com/10.1007/s10518-010-9194-6>.
- Porter, Keith, Judith Mitrani-Reiser, and James L. Beck. 2006. "Near-Real-Time Loss Estimation for Instrumented Buildings." *The Structural Design of Tall and Special Buildings* 15 (1): 3–20. doi:10.1002/tal.340. <http://doi.wiley.com/10.1002/tal.340>.
- Priestley, Nigel, Gian Michele Calvi, and Mervyn Kowalsky. 2007. *Displacement-Based Seismic Damage of Structures*. Edited by IUSS Press. 1st editio. Pavia.
- Rainieri, C., and G. Fabbrocino. 2014. *Operational Modal Analysis of Civil Engineering Structures*. New York: Springer.
- Rainieri, C., G. Fabbrocino, and E. Cosenza. 2010. "Integrated Seismic Early Warning and Structural Health Monitoring of Critical Civil Infrastructures in Seismically Prone Areas." *Structural Health Monitoring* 10 (3): 291–308. doi:10.1177/1475921710373296. <http://www.scopus.com/inward/record.url?eid=2-s2.0-79955721946&partnerID=tZOtx3y1>.
- Ricci, P. 2010. "Seismic Vulnerability of Existing RC Buildings." University of Naples Federico II.
- RISA, and TECNIC. 2011. "The System Guide and User Manual." Memscn Del. 2.4.
- Roberts, Gethin Wyn, Xiaolin Meng, and Alan Henry Dodson. 2004. "Integrating a Global Positioning System and Accelerometers to Monitor the Deflection of Bridges." *Journal of Surveying Engineering* 130 (2): 65–72. doi:10.1061/(ASCE)0733-9453(2004)130:2(65). <http://www.scopus.com/inward/record.url?eid=2-s2.0-2342510243&partnerID=tZOtx3y1>.
- Roufaiel, Magdy S L, and Christian Meyer. 1987. "Analytical Modeling of Hysteretic Behavior of R/C Frames." *Journal of Structural Engineering New York, N.Y.* 113 (3): 429–44. <http://www.scopus.com/inward/record.url?eid=2-s2.0-0023305787&partnerID=tZOtx3y1>.
- Ruiz-Garcia, Jorge, and Eduardo Miranda. 2003. "Inelastic Displacement Ratios for Evaluation of Existing Structures." *Earthquake Engineering & Structural Dynamics* 32 (8): 1237–58. doi:10.1002/eqe.271. <http://doi.wiley.com/10.1002/eqe.271>.

- Salawu, O. S. 1997. "Detection of Structural Damage through Changes in Frequency: A Review." *Engineering Structures* 19 (9): 718–23. <http://www.scopus.com/inward/record.url?eid=2-s2.0-0031237412&partnerID=tZOtx3y1>.
- Salawu, O. S., and C. Williams. 1995. "Bridge Assessment Using Forced-Vibration Testing." *Journal of Structural Engineering - ASCE*. <http://www.scopus.com/inward/record.url?eid=2-s2.0-0028977274&partnerID=tZOtx3y1>.
- Savoia, Marco, Lorenzo Bacci, and Loris Vincenzi. 2012. "Rilievo Fotografico Durante Sopralluogo Del 23 E 28 Maggio 2012 (dopo La Prima Sequenza Sismica Del 20 Maggio 2012)." *Terremoto dell'Emilia - Danni E Crolli Nell'edilizia Industriale*.
- Shakal, Anthony, and Moh Huang. 2013. "Recent Developments and Status of the California Strong Motion Instrumentation Program." In *SMIP13 Seminar Proceedings*. http://consrv.ca.gov/cgs/smip/docs/seminar/SMIP13/Documents/P8_Paper_Shakal.pdf.
- Skolnik, DA, and JW Wallace. 2010. "Critical Assessment of Interstory Drift Measurements." *Journal of Structural Engineering*, no. December: 1574–84. [http://ascelibrary.org/doi/abs/10.1061/\(ASCE\)ST.1943-541X.0000255](http://ascelibrary.org/doi/abs/10.1061/(ASCE)ST.1943-541X.0000255).
- Skolnik, Derek A., Robert L. Nigbor, and John W. Wallace. 2011. "A Quantitative Basis for Building Instrumentation Specifications." *Earthquake Spectra* 27 (1): 133–52. doi:10.1193/1.3532840. <http://www.scopus.com/inward/record.url?eid=2-s2.0-79953155805&partnerID=tZOtx3y1>.
- Sohn, H, CR Farrar, and FM Hemez. 2004. *A Review of Structural Health Monitoring Literature: 1996-2001*. <http://library.lanl.gov/cgi-bin/getfile?00796820.pdf>.
- Stephens, Jerry E., and James T P Yao. 1987. "Damage Assessment Using Response Measurements." *Journal of Structural Engineering New York, N.Y.* 113 (4): 787–801. <http://www.scopus.com/inward/record.url?eid=2-s2.0-0023324532&partnerID=tZOtx3y1>.
- STMicroElectronics. "Tilt Measurement Using a Low-G 3-Axis Accelerometer." 2010. http://www.st.com/web/en/resource/technical/document/application_note/CD00268887.pdf.
- Straser, Erik G, Anne S Kiremidjian, and Teresa H Meng. 2001. "UNITED STATES PATENT: US 8,292,108 B1 - Modular, Wireless Damage Monitoring System for Structures." United States.
- Sullivan, T.J, M.J.N Priestley, and Gian Michele Calvi. 2012. *A Model Code for the Displacement-Based Seismic Design of Structures*. Pavia: IUSS Press.

- Taskin, B, K Guler, U.M Tugsal, M Gencoglu, M Celik, Z Hasgur, M Aydogan, and A.I Saygun. 2012. "A Novel Post-Earthquake Damage Survey Sheet: Part I-RC Buildings." In *15th World Conference on Earthquake Engineering*. Lisboa, Portugal.
- Todorovska, Maria I. 1998. "Cross-Axis Sensitivity of Accelerographs with Pendulum like Transducers—mathematical Model and the Inverse Problem." *Earthquake Engineering & Structural Dynamics* 27 (10). John Wiley & Sons Ltd: 1031–51. doi:10.1002/(SICI)1096-9845(199810)27:10<1031::AID-EQE766>3.0.CO;2-1.
<http://www.scopus.com/inward/record.url?eid=2-s2.0-0032193575&partnerID=tZOtx3y1>.
- Toniolo, Giandomenico, and Antonella Colombo. 2012. "Precast Concrete Structures: The Lessons Learned from the L'Aquila Earthquake." *Structural Concrete* 13 (2): 73–83.
 doi:10.1002/suco.201100052. <http://www.scopus.com/inward/record.url?eid=2-s2.0-84861801548&partnerID=tZOtx3y1>.
- Torfs, Tom, Tom Sterken, Steven Brebels, Juan Santana, Richard van den Hoven, Vincent Spiering, Nicolas Bertsch, Davide Trapani, and Daniele Zonta. 2013. "Low Power Wireless Sensor Network for Building Monitoring." *IEEE Sensors Journal* 13 (3): 909–15.
 doi:10.1109/JSEN.2012.2218680.
<http://ieeexplore.ieee.org/lpdocs/epic03/wrapper.htm?arnumber=6301674>.
- Trapani, Davide, Giacomo Cigognetti, Daniele Coato, Davide Dalbosco, Daniele Zonta, Marco Molinari, Stephanos Camarinopoulos, and Manos Bairaktaris. 2012. "MCS Del. 3.3 - Test on Full-Scale 3D Frame." Memsccon Deliverables.
- Ulusoy, Hasan S., Erol Kalkan, and Krishna Banga. 2013. "Real-Time Seismic Monitoring of Veterans Affairs Hospital Buildings." In *Proceedings of SPIE - The International Society for Optical Engineering*, edited by Jerome P. Lynch, Chung-Bang Yun, and Kon-Well Wang, 8692:86920I. doi:10.1117/12.2012236. <http://www.scopus.com/inward/record.url?eid=2-s2.0-84878682255&partnerID=tZOtx3y1>.
- USGS. 2005. "The UCLA Factor Building Seismic Array." <http://factor.gps.caltech.edu/node/61>.
- . 2014. "NSMP Station Map." <http://earthquake.usgs.gov/monitoring/nsmp/stations/map/>.
- Vidal, F, M Feriche, and A Ontiveros. 2009. "Basic Techniques for Quick and Rapid Post-Earthquake Assessment of Building Safety." In *8th International Workshop on Seismic Microzoning and Risk Reduction*. Almeria, Spain.

- Williams, Martin S., and Robert G. Sexsmith. 1995. "Seismic Damage Indices for Concrete Structures: A State of the Art Review." *Earthquake Spectra*. doi:10.1193/1.1585817.
- . 1997. "Seismic Assessment of Concrete Bridges Using Inelastic Damage Analysis." *Engineering Structures* 19 (3): 208–16. <http://www.scopus.com/inward/record.url?eid=2-s2.0-0031105995&partnerID=tZOtx3y1>.
- Zimmerman, Andrew T., Michihito Shiraishi, R. Andrew Swartz, and Jerome P. Lynch. 2008. "Automated Modal Parameter Estimation by Parallel Processing within Wireless Monitoring Systems." *Journal of Infrastructure Systems* 14 (1): 102–13. doi:10.1061/(ASCE)1076-0342(2008)14:1(102). <http://www.scopus.com/inward/record.url?eid=2-s2.0-39549121473&partnerID=tZOtx3y1>.
- Zonta, Daniele. 2014. "Sensor Data Analysis, Reduction and Fusion for Assessing and Monitoring Civil Infrastructures." In *Sensor Technologies for Civil Infrastructures*, edited by Ming L Wang, Jerome P Lynch, and Hoon Sohn, 33–66. Woodhead Publishing Limited. doi:10.1533/9780857099136.410. <http://www.sciencedirect.com/science/article/pii/B9780857094322500152>.